INVESTIGATING THE ROLE OF VIRUS-MEDIATED TUMOUR MODULATION IN T CELL CENTRIC CANCER IMMUNOTHERAPY

INVESTIGATING THE ROLE OF VIRUS-MEDIATED TUMOUR MODULATION IN T CELL CENTRIC CANCER IMMUNOTHERAPY

By
Omar Salem, M.Sc.

A Thesis
Submitted to the School of Graduate Studies
in Partial Fulfillment of the Requirements
of the Degree
Doctor of Philosophy

McMaster University

DOCTOR OF PHILOSOPHY (2022) McMaster University
(Medical Sciences) Hamilton, Ontario

Title :	Investigating the Role of Virus-Mediated Tumour Modulation in T Cell Centric Cancer Immunotherapy
Author:	Omar Salem, M.Sc.
Supervisor:	Yonghong Wan, MD
Pages:	xvii, 237

Abstract

Cancer immunotherapy continues to be at the forefront of cancer treatment modalities delivering unprecedented outcomes. In this thesis we have investigated the combination of Oncolytic Viral Vaccines (OVVs) and Adoptive T Cell Therapy (ACT) for treating solid tumours. We used animal models, flow cytometry and high throughput transcriptomic analyses to characterize the therapeutic outcomes of such combination and understand the mechanisms behind its success on cellular and molecular levels. We focused on comparing the behaviour of different viruses, Vesicular Stomatitis Virus (VSV), and Vaccinia Virus (VacV), and showed that the choice of viral backbone indeed shapes the therapy outcome. While both viruses can achieve complete tumour regression when combined with ACT, VSV-treated tumours relapse shortly after remission. Additionally, we studied the effect of the virus route of administration and observed that intratumoural (IT) delivery leads to better overall survival of mice compared to intravenous (IV) delivery regardless of the viral backbone. Furthermore, we evaluated the necessity of virus replication in different tumour models. Our results show that virus replication, despite being dispensable for immunogenic tumour models, is necessary for durable outcomes in immunosuppressive models. Importantly, the reprogramming of the tumour microenvironment (TME) by OVVs was shown to be crucial for therapy success. Specifically, we show that unlike VSV, VacV is able to induce more inflammatory pathways, block metabolic pathways, cell cycle pathways and DNA repair pathways. We highlighted the role of inhibiting DNA repair pathways in preventing antigen loss and immune escape. Lastly, we examined the effect of the transcriptomic signature induced by VacV on the prognosis and survival of Skin Cutaneous Melanoma (SKCM) patients using a public dataset derived from the Cancer Genome Atlas (TCGA). Our analysis demonstrates that VacV transcriptomic signature correlates with favorable disease prognosis and better overall patient survival. In conclusion, the research described in this thesis reveals important insights pertaining to the choice of viral backbone, route of administration and unveils additional mechanisms by which OVVs complement the $CD8^+$ T cell mediated elimination of tumour cells.

Acknowledgments

First and foremost, I must express my gratitude to my supervisor, Dr. Yonghong Wan for this amazing opportunity to conduct such cutting edge research. While there were some struggles and challenges in optimizing a lot of the protocols used in this thesis, I am thankful that you continued to have faith that we could develop this project. I would also like to also thank my supervisory committee members, Dr. Ali Ashkar and Dr. Karen Mossman for their insightful inputs during my committee meetings and for always looking out for my success.

I must thank all past and present members of the Wan lab for their exceptional support during my graduate studies. You have all helped create a collaborative and fun work environment that really made graduate school a smoother experience. I also wish to specifically thank Dr. Scott Walsh for his mentorship and support throughout my PhD. Thanks Scott for all you have done for me and I cannot wait to congratulate you on starting the Walsh lab.

I would like to also acknowledge my collaborators in other labs across MIRC as well as the fantastic staff in the Central Animal Facility (CAF) for taking care of our experimental animals. I would also like to thank the Canadian Institutes of Health Research (CIHR) and the Terry Fox Foundation for funding the research described in this thesis.

Last but not least, I owe a huge thank you to my amazing family, my parents, siblings, wife and daughter who have had unwavering support for me throughout my graduate studies. Thank you all for your continued optimism and love throughout this endeavor. You have contributed as much as I did to the success of this thesis and for everything that preceded graduate school and everything that will follow and for this I will be forever grateful.

Table of Contents

Chapter 1 — Introduction 1

1.1. Cancer 2

1.2. The immune system and Cancer 3

1.2.1. Immune checkpoint therapy 4

1.2.2. Adoptive T cell Therapy 8

1.2.3. Cancer Vaccines 11

1.3. Oncolytic viruses 12

1.3.1. Mechanisms of action of OVs 14

1.3.2. Vesicular Stomatitis Virus (VSV) 15

1.3.3. Vaccinia Virus (VacV) 17

1.4. Route of administration 21

1.5. ACT + OVV: synergy at its best 22

1.6. Aims of the work 26

Chapter 2 — Materials and Methods 28

2.1. Mice 29

2.2. Cell lines 29

2.3. *In vivo* tumour models 30

2.4. Tumour growth monitoring 30

2.5. Adoptive T cell transfer 30

2.6. Viruses 30

2.7. Organ processing 31

2.7.1. Blood processing 31

2.7.2. Spleen Processing 31

2.7.3. Lymph nodes processing....31
2.7.4. Tumour processing....31
2.8. Surface and intracellular staining and Flow cytometry 32
2.9. Intracellular cytokine staining 32
2.10. *In vivo* T cell proliferation assay.... 33
2.11. Clariom S Assay 33
2.12. Clariom S data analysis 33
2.13. Patient gene signature analysis 34
2.14. *In silico* cytometry and survival correlation analysis 34
2.15. In vivo depletion 34
2.16. Heat inactivation 35
2.17. Psoralen Long Wavelength Ultraviolet Inactivation.... 35
2.18. X-gal staining protocol 35
2.19. Immunofluorescence (performed by Sreedevi Kesavan) 35
2.20. Data wrangling, visualization, and statistical analysis 36

Chapter 3 — Studying the effect of the viral backbone on the Efficacy of ACT + OVV 37

3.1. Introduction 38
3.2. Results 39
3.2.1. Triple combination of IL-15, IL-21, and Rapamycin yield memory-like $CD8^+$ T cells with strong proliferative capacity....39
3.2.2. Boosting ACT with oncolytic viral vaccines results in T cell expansion and tumour regression 42
3.2.3. Using Vaccinia virus-based OVV improves overall survival with less incidence of relapse....45

3.2.4. VacV and VSV lead to different systemic immune landscapes 49

Chapter 4 — Evaluating the effect of OVV route of administration on the efficacy of ACT + OVV..... 58

4.1. Introduction 59

4.2. Results 60

4.2.1. Intratumoural injection of OVVs leads to better tumour control and improves the overall mice survival with less incidence of relapse 60

4.2.2. Intratumoural analysis reveals no difference in tumour infiltrating immune cells following IT and IV delivery of OVVs 65

4.2.3. Intravenous and Intratumoural delivery of vaccinia virus result in T cell proliferation in different anatomical locations 70

4.2.4. LacZ staining shows wider viral spread across IT-treated tumours vs. IV-treated ones (in collaboration with Scott Walsh).....73

Chapter 5 — Evaluating the Contribution of Oncolysis in the Efficacy of ACT + OVV 78

5.1. Introduction 79

5.2. Results 81

5.2.1. Heat-inactivated VacVgp33 failed to boost P14 transferred cells leading to poor survival of the treated mice 81

5.2.2. Psoralen and Long Wavelength Ultraviolet (PLWUV) kills the replication capacity of VacV while preserving its ability to infect target cells and express its early genes. 85

5.2.3. PLWUV-inactivated VacV can boost transferred T cells and cause initial tumour regression but fail to induce durable cure in B16gp33 tumour model 92

5.2.4. Increasing the dose and/or frequency of PLWUV-inactivated VacV administration or transferred P14 T cells does not improve the efficacy 95

5.2.5. Combining PLWUV-inactivated VacVgp33 with replicating VacV-GFP restores the durable tumour control phenotype.....98

5.2.6. Microarray analysis reveals changes in inflammation, apoptosis and cell cycle/ DNA repair pathway signatures despite a scarcity of individual differentially expressed

genes in the TME following P14 + VacVgp33 or P14 + UV-VacVgp33 99
5.2.7. PLWUV-inactivated VacV is sufficient to induce cure in MC38 tumour model .109

Chapter 6 — Investigating the differential effects of VSV and VacV on altering the cellular and transcriptomic landscapes in the TME 112

6.1. Introduction 113

6.2. Results 114

6.2.1. Intratumoural immune analysis over a time course reveals no significant differences in cellular recruitment profile between P14 + VacVgp33 IT and P14 + VSVgp33 IT treatments. 114

6.2.2. *In vivo* depletion of NK1.1^{+} cells or Ly6G^{+} cells does not affect the efficacy of P14 + VacVgp33 treatment 120

6.2.3. Microarray analysis reveals distinct inflammatory profiles in the TME following VacV or VSV treatment 123

6.2.4. VacV causes the enrichment of immune processes and the downregulation of cell proliferation and metabolic processes within the TME 137

6.2.5. VacV causes the shutdown of DNA repair pathways eliminating the chance of antigen loss and immune escape.....144

Chapter 7 — Investigating the effects of cellular and molecular signatures observed in ACT + VacV treated tumours on the disease progression/outcome in human patients. 150

7.1. Introduction 151

7.2. Results 152

7.2.1. Infiltration of CD8^{+} T cells and M1 Macrophages in Skin Cutaneous Melanoma (SKCM) correlates with better overall survival 152

7.2.2. Hallmark pathways differentially regulated by ACT + VacV are predictive of positive prognosis in SKCM patients 161

Chapter 8 — Discussion 172

8.1. Studying the effect of the viral backbone on the Efficacy of ACT + OVV 173

8.2. Evaluating the effect of OVV route of administration on the efficacy of ACT + OVV 174

8.3. Evaluating the Contribution of Oncolysis in the Efficacy of ACT + OVV 176

8.4. Investigating the differential effects of VSV and VacV on altering the cellular and transcriptomic landscapes in the TME 180

8.5. Investigating the effects of cellular and molecular signatures observed in ACT + VacV treated tumours on the disease progression/outcome in human patients. 184

8.6. Concluding Remarks 186

List of Figures

Figure 1.1 | Illustration showing the working model of ACT + OVV therapy 25

Figure 3.1 | Triple combination of IL-15, IL-21 and Rapamycin yield memory-like CD8+ T cells with strong proliferative capacity 41

Figure 3.2 | Boosting ACT with oncolytic viral vaccines results in T cell expansion and tumour regression 44

Figure 3.3 | Using Vaccinia virus-based OVV improves overall survival with less incidence of relapse 48

Figure 3.4 | Lymphocyte analysis in blood and spleen following P14 + VacVgp33, P14 + VSVgp33 or PBS treatment. 53

Figure 4.1 | Intratumoural injection of OVVs leads to better tumour control and improves the overall mice survival with less incidence of relapse.....64

Figure 4.2 | Intratumoural analysis reveals no difference in tumour infiltrating immune cells following IT or IV delivery of OVVs 68

Figure 4.3 | Intravenous and Intratumoural delivery of vaccinia virus result in T cell proliferation in different anatomical locations 72

Figure 4.4 | GFP expression and LacZ staining showing tissue distribution of VacV following IT and IV infection 76

Figure 5.1 | Heat-inactivated VacVgp33 failed to boost P14 transferred cells leading to poor survival of the treated mice.....84

Figure 5.2 | Psoralen and Long Wavelength Ultraviolet (PLWUV) kills the replication capacity of VacV while preserving its ability to infect target cells and express its early genes.....88

Figure 5.3 | PLWUV-inactivated VacV can boost transferred T cells and cause initial tumour regression but fail to induce durable cure in B16gp33 tumour model.....91

Figure 5.4 | Increasing the dose and/or frequency of PLWUV-inactivated VacV administration or transferred P14 T cells does not improve the efficacy 94

Figure 5.5 | Combining PLWUV-inactivated VacVgp33 with replicating VacV-GFP restores the durable tumour control phenotype 97

Figure 5.6 | Principal component analysis and clustering of tumour samples yield three different clusters corresponding to different treatment conditions 101

Figure 5.7 | Microarray analysis reveals no DEGs between P14 + VacVgp33 and P14 + UV-VacVgp33 treatments 104

Figure 5.8 | GSEA reveals a higher magnitude of inflammation associated with P14 + UV-VacVgp33 compared to P14 + VacVgp33 107

Figure 5.9 | PLWUV-inactivated VacV is sufficient to induce cure in MC38 tumour model 111

Figure 6.1 | Intratumoural immune analysis over a time course reveals no significant differences between P14 + VacVgp33 IT and P14 + VSVgp33 IT treatments 118

Figure 6.2 | In vivo depletion of $NK1.1^+$ cells or $Ly6G^+$ cells does not affect the efficacy of P14 + VacVgp33 treatment 122

Figure 6.3 | Principal component analysis and clustering of tumour samples yield three different clusters corresponding to different treatment conditions 125

Figure 6.4 | Microarray analysis reveals transcriptomic differences among P14 + VacVgp33, P14 + VSVgp33 and P14 treatments 129

Figure 6.5 | GO enrichment analysis reveals over-representation of similar BP terms between P14 + VacVgp33 and P14 + VSVgp33 treatments.....136

Figure 6.6 | GSEA reveals differential pathway regulation between P14 + VacVgp33 and P14 + VSVgp33 treatments 143

Figure 6.7 | VacV causes the shutdown of DNA repair pathways eliminating the chance of antigen loss and immune escape (Data courtesy of Sreedevi Kesavan) 148

Figure 7.1 | Infiltration of $CD8^+$ T cells and M1 Macrophages in Skin Cutaneous Melanoma (SKCM) correlates with the upregulation of inflammatory pathways and better overall survival of patients 160

Figure 7.2 | Hallmark pathways activated by ACT + VacV correlate with better survival in SKCM patients 167

List of Tables

Table 3.1 | List of antibodies and their respective fluorescent channels used to stain blood and spleen samples 50

Table 3.2 | Time course showing the effect of different treatments on lymphocyte populations in peripheral blood of B16gp33 tumour-bearing mice. The data represents mean ± SEM 56

Table 3.3 | Time course showing the effect of different treatments on lymphocyte populations in spleen of B16gp33 tumour-bearing mice. The data represents mean ± SEM.....57

Table 4.1 | List of antibodies and their respective fluorescent channels used to stain tumour samples.....66

Table 4.2 | Frequency of cell populations in TME 4 days after treatment 66

Table 7.1 | Clusters of hallmark pathways resulting from hierarchical clustering analysis using Pearson correlation to estimate the distances between individual hallmark pathways.....168

Table 7.2 | Hazard ratio (HR) associated with each hallmark pathway calculated using univariate cox proportional hazard model 169

List of Abbreviations and Symbols

5-FC	5-Fluorocytosine
Ab(s)	Antibody(ies)
ACT	Adoptive T Cell Therapy
ADCC	Antibody-Dependent Cell-Mediated Cytotoxicity
APC(s)	Antigen-Presenting Cell(s)
BiTE(s)	Bispecific T Cell Engager(s)
BP	Biological Process
CAF(s)	Cancer-Associated Fibroblast(s)
CAR	Chimeric Antigen Receptor
CD	Cluster Of Differentiation
cDNA	Complementary DNA
CEN(s)	Cell-Associated Enveloped Virus(es)
Cop	Copenhagen
CPE	Cytopathic Effects
CSF	Colony Stimulating Factor
CTA(s)	Cancer–Testes Antigen(s)
CTL(s)	Cytotoxic T Lymphocyte(s)
CTLA-4	Cytotoxic T Lymphocyte Antigen-4 Cyclophosphamide
DAMP(s)	Danger Associated Molecular Pattern(s)
DC(s)	Dendretic Cell(s)
DEG(s)	Differentially Expressed Gene(S)
DLN(s)	Draining Lymph Node(s)
DMEM	Dulbecco's Modified Eagle Medium Deoxyribonucleic Acid
EEV(s)	Extracellular Enveloped Virus(es)
ER	Endoplasmic Reticulum
FACS	Fluorescence-Activated Cell Sorting
FASL	Fas Ligand
FBS	Fetal Bovine Serum
FDA	Food And Drug Administration
FLT3L	Fms-Related Tyrosine Kinase 3 Ligand
FOXP3	Forkhead Box P3
GFP	Green Fluorescent Protein
GM-CSF	Granulocyte/Monocyte Colony Stimulating Factor
GO	Gene Ontology
GSEA	Gene Set Enrichment Analysis
GSVA	Gene Set Variation Analysis

HDAC	Histone Deacetylase
HPMA	Hydroxypropyl]Methacrylamide
HSV	Herpes Simplex Virus
ICB	Immune Checkpoint Blockade
ICS	Intracellular Cytokine Staining
IDO	Indoleamine 2,3-Dioxygenase
IEV(s)	Intracellular Enveloped Virus(es)
IL	Interleukin
IMV(s)	Intracellular Mature Virus(es)
INF(s)	Interferon(s)
IRAEs	Immune-Related Adverse Events
IT	Intratumoural
IV	Intravenous
LCMV	Lymphocytic Choriomeningitis Virus
LDL	Low Density Lipoprotein
mAb	Monoclonal Antibody
MHC	Major Histocompatibility Complex
MOI	Multiplicity Of Infection
MPS	Mononuclear Phagocytic System
NDLNs	Non-Draining Lymph Nodes
NDV	Newcastle Disease Virus
NFκB	Nuclear Factor Kappa B
NK	Natural Killer Cell
NSCLC	Non-Small Cell Lung Cancer
ORA	Overrepresentation Analysis
OV	Oncolytic Viruses
OVT	Oncolytic Viral Therapy
OVVs	Oncolytic Viral Vaccines
PAMP(s)	Pathogen-Associated Molecular Patterns
PBMC(s)	Peripheral Blood Mononuclear Cell(s)
PBS	Phosphate Buffered Saline
PCA	Principal Component Analysis
PCR	Polymerase Chain Reaction
PD-1	Programmed Death 1
pDC(s)	Plasmacytoid Dendretic Cell(s)
PDL-1	Programmed Death Ligand 1
PEG	Polyethylene Glycol
PFS	Progression Free Survival

PFU	Plaque-Forming Unit
PLWUV	Psoralen And Long Wavelength Ultraviolet
PRR(s)	Pattern Recognition Receptor(s)
PVI	Post Virus Injection
RAG(1/2)	Recombination-Activating Genes (1/2)
RIP	Rat Insulin Promoter
RMA	Robust Multichip Average
RNA	Ribonucleic Acid
RNAseq	RNA Sequencing
S1P	Sphingosine 1- Phosphate
scFv	Single-Chain Variable Fragment
scRNAseq	Single Cell RNA Sequencing
SEM	Standard Error Of The Mean
SHP (1/2)	Src Homology Region 2 Domain-Containing Tyrosine Phosphatase (1/2)
SKCM	Skin Cutaneous Melanoma
TAA(s)	Tumour-Associated Antigen(s)
TCGA	The Cancer Genome Atlas
T_{CM}	Central Memory T Cells
TCR	T Cell Receptor
T_{EFF}	Effector T Cells
T_{EM}	T Effector Memory
TGN	Trans-Golgi Network
Th	T Helper
TIL(s)	Tumour-Infiltrating Lymphocyte(s)
TK	Thymidine Kinase
TME	Tumour Microenvironment
TNBC	Triple-Negative Breast Cancer
TNF	Tumour Necrosis Factor
TNFR (1/2)	Tumour Necrosis Factor Receptor (1/2)
TRAC	T-Cell Receptor A Constant
T_{reg}	Regulatory T Cells
T_{SCM}	T Stem Cell Memory
VacV	Vaccinia Virus
VEGF	Vascular Endothelial Growth Factor
VEGFR	Vascular Endothelial Growth Factor Receptor
VGF	Vaccinia Growth Factor
VSV	Vesicular Stomatitis Virus
vvDD	Double Deleted VacV

WR	Western Reserve
WT	Wild Type
Wy	Wyeth
ζ	Zeta
α	Alpha
β	Beta
γ	Gamma
μ	Micro

Declaration of Academic Achievement

The work presented in this thesis is the result of my research efforts as a graduate student at McMaster University since September 2016. The conceptualization and design of experiments described here was a collaborative effort between my supervisor, Dr. Yonghong Wan and myself. I was the primary researcher responsible for conducting all the described experiments and analyses. Data interpretation was done by myself in collaboration with Dr. Yonghong Wan and Dr. Scott Walsh. Collaborations with other lab members and data generated by colleagues are described below.

The experiment described in section 4.2.4 was conducted by Dr. Scott Walsh and the data was kindly provided to myself to include in my thesis since it strongly supports my line of work.

The experiments described in section 6.2.5 were an extension of my reported results and were conducted by Sreedevi Kesavan in collaboration with Dr. Scott Walsh and the data was kindly provided to myself.

Chapter 1 — Introduction

1.1. Cancer

Despite several advancements in cancer detection and treatment options, it remains the leading cause of death in Canada, and was responsible for 30% of all death in 2020 according to the Canadian Cancer Society[1]. An estimated number of 225,800 new cancer cases and 83,000 cancer deaths were expected in Canada in 2020. Thus, the need to develop more effective treatment regimens is higher than ever[1]. Our success in developing better therapies would indeed stem from the increased understanding of tumour biology, the strategies tumour cells use to interact with surrounding tissues, and the ways they are able to adapt, evolve, survive, and spread despite the tight regulatory mechanisms working against them. In 2000, Hanahan and Weinberg published a set of features, or hallmarks, that cells acquire on their way to becoming cancerous[2]. The functional capabilities acquired by cancer cells render them self-sufficient by driving their own replication, resisting apoptosis and anti-growth signals, creating their own blood supply by inducing angiogenesis, and breaking away from their original site and metastasizing to other body tissues[2]. As research progressed in the following decade, this list of features expanded, and was updated in 2011 to include the emerging hallmarks and enabling characteristics that cancer cells acquire in the process of carcinogenesis[3]. Two emerging features were highlighted, one involved the ability of cancer cells to induce metabolic changes that support their survival and proliferation. The second allows cancer cells to survive the immune attack mediated by T lymphocytes, Natural killer (NK) cells or other immune cells[3]. Genomic instability and mutability were also highlighted as an enabling feature that drive tumour progression[3]. Besides tumour cells, other types of non-cancerous cells e.g., fibroblasts, immune cells, and endothelial cells are present within the tumour microenvironment (TME) to varying degrees[4]. These cells provide a support niche that is critical to the continued growth of the cancer. For example, cancer-associated fibroblasts (CAFs) were reported to secret indoleamine 2,3-dioxygenase (IDO) which promotes resistance to both T cell- and NK-cell mediated anti-tumoural responses[5,6]. Alternatively, increased infiltration of $CD8^+$ T cells into the TME was shown to be strongly associated with improved patient outcomes[7,8].

Hence, the interaction of tumour cells with other cells in its local milieu play a key role in the disease progression.

1.2. The immune system and Cancer

Spontaneous regression of tumours following a bacterial skin infection was one of the first hints that a relationship exists between cancer and the immune state of the patient[9]. William Coley, who later became known as the "Father of Cancer Immunotherapy", confirmed the association between erypsipelas, a superficial bacterial skin infection, and the clinical outcome in patients with sarcoma[10]. This has led to trials of treating cancer patients with an extract from inactivated *Streptococcus pyogenes* and *Serratia marcescens*, an extract that was termed Coley's toxins, in an attempt to replicate the effects seen in natural infection cases[11]. In the twentieth century, Paul Ehrlich hypothesized that our bodies constantly generate neoplastic cells that are kept in check and eliminated by our immune system[10]. This hypothesis was mounted only 16 years after Coley's findings, but no connection was made by their contemporaries between the immune system and what Coley had reported. In 1957, Lewis Thomas and Sir Frank Burnet developed the cancer immunosurveillance theory which states that tumour associated antigens (TAAs) are identified and targeted by the cells of the immune system to prevent carcinogenesis in a manner similar to graft rejection[12]. In the last two decades, the Schreiber lab has made some efforts to reinstill some faith in the ability of the immune system to attack cancer cells. They proposed a new version of the cancer immunosurveillance hypothesis, which is now known as the cancer immunoediting hypothesis[13-15]. Their hypothesis was based on observing the different behavior of tumour growth between immunodeficient and immunocompetent hosts[13]. Two key observations were highlighted; the first is that immunodeficient mice that fail to produce mature T or B cells (RAG2-deficient mice) developed sarcomas more frequently and more rapidly compared to their immunocompetent counterparts[13]. This suggested that the immune system can resist the growth of developing tumours. Second, the tumours derived from the immunodeficient hosts were more immunogenic (later

referred to as “unedited”) compared to the ones derived from the immunocompetent ones[13]. The tentative explanation for this observation is that the immune attack on the developing tumours led to the elimination of subsets of cells expressing certain tumour rejection antigens while selecting for other subsets that can tolerate the immune system. Taken together, the cancer immunoediting hypothesis postulates a dual role for the immune system; by recognizing and attacking tumour-specific antigens, it protects the host by eliminating tumour cells. At the same time, it sculpts the developing tumours and selects for less immunogenic variants[14,15]. Three distinct phases of the immunoediting process were described: elimination, equilibrium, and escape[14,16]. Elimination is when the innate and adaptive immune systems detect a developing tumour and successfully destroy it. Equilibrium happens when tumour cells survive the elimination phase and enter a state of dormancy, in which the adaptive immune system prevents tumour outgrowth and sculpts the immunogenicity of the tumour cells. When tumour cells acquire the ability to circumvent the immune recognition, the escape phase begins. These findings were initially described in an unmanipulated immune system that is challenged by a developing tumour[14]. However, several reports later confirmed that immunoediting can also occur and, in some cases, is amplified when the established tumours are subjected to various forms of immunotherapy[17,18]. In the next sections we will focus on three different T cell – centric categories of immunotherapy.

1.2.1. Immune checkpoint therapy

The process of Naïve $CD8^+$ T cell activation relies on the receipt of three activation signals: the first is provided through the binding of the T cell receptor (TCR) to the target antigen presented on the Major Histocompatibility Complex class I (MHC I)[19,20]. The second, termed co-stimulation signal, is provided through the binding of CD28 on the T cell surface to one of its ligands e.g., B7-1 (CD80) or B7-2 (CD86) that are typically expressed on the surface of an antigen presenting cell (APC)[19-21]. The third and final signal is derived from the cytokine environment present during the T cell activation and is required for proper differentiation and development

of cellular effector functions[22,23]. Following successful activation, $CD8^+$ T cells proliferate and differentiate into effector T cells (T_{EFF}) that are primarily responsible for killing the target cells. After the clearance of the target antigen, cytokine withdrawal leads to the contraction phase, where the majority of $CD8^+$ T cells undergo apoptosis leaving a subset of memory T cells (T_{CM}) that are responsible for rapid recall responses in case of re-exposure to the same antigen[9]. In cases of repeated low-dose or low-affinity stimulation as seen in chronic infections and neoplastic disease, $CD8^+$ T cells acquire an exhausted phenotype state that is characterized by progressive loss of T cell function[9]. Exhausted T cells express an array of inhibitory molecules which collectively operate to negatively regulate the functional capacity of the T cells. In the natural course of an immune response, such inhibitory molecules act as "checkpoint molecules" that prevent the hyperactivation of the immune response and ensure immune homeostasis[9,24]. Two of the most well studied examples of checkpoint molecules are programmed cell death 1 (PD1), and Cytotoxic T lymphocyte antigen 4 (CTLA4). They exert their inhibitory functions at different anatomical locations and at different time-points during the T cell lifespan[24].

1.2.1.1. Cytotoxic T lymphocyte antigen 4 (CTLA4)

CTLA4 has a lot of structural and biochemical similarity to CD28 especially within the extracellular binding domain, and therefore, they both bind to the same ligands (B7-1 and B7-2)[25,26]. However, CTLA4 has greater affinity and avidity than CD28 for B7 ligands[27]. CD28 and CTLA4 have opposing immunoregulatory functions. Unlike CD28 that provides a co-stimulatory signal that is crucial for T cell activation, CTLA4 engagement restrains T cell activation by directly antagonizing CD28 function[28-30]. CTLA4 was shown to reorganize the T cell cytoskeleton and disturb the T cell – APC immunological synapse[31]. Additionally, it mediates the internalization of B7-1 and B7-2 ligands, thus preventing their binding to CD28[32,33]. Moreover, $CD4^+$ $CD25^+$ regulatory T cells (T_{reg}) were shown to have constitutive expression of CTLA4, and its expression was reported to be essential for the immunosuppressive functions of these cells[34]. James Allison

and his team were the first to demonstrate that blocking CTLA4 using neutralizing antibodies enhanced the anti-tumoural immunity in mouse models of colon carcinoma and fibrosarcoma[35]. CTLA4 success in preclinical studies was variable depending on the immunogenicity of model tested, the type of tissue targeted, and the tumour burden. Animal models of brain[36], bladder[37], ovarian[38], and colon[35] cancers showed benefit from anti-CTLA4 monotherapy, whereas less immunogenic models (e.g. B16 melanoma) did not respond as favorably[39]. Additionally, a greater tumour burden correlated with reduced responses to the anti-CTLA4 treatment[38]. Despite the mixed outcomes observed in preclinical models, anti-CTLA4 therapy was shown to be effective in clinical trials of melanoma, where potent tumour necrosis in melanoma patients was observed following treatment with Ipilimumab, a human anti-CTLA monoclonal antibody (mAb)[40,41]. As a result, Ipilimumab gained FDA approval in 2011 for non-resectable stage III/IV melanoma[9]. Trials in other tumour types including prostate cancer[42], small cell-lung cancer (SCLC)[43], non-small-cell lung cancer (NSCLC)[44], and renal cell carcinoma[45] were, however, not as impressive and no significant improvement in patient survival was reported. Multiple pleiotropic mechanisms were reported for anti-CTLA4 mediated tumour regression. One mechanism involves boosting effector T cell responses against tumour-associated neoantigens through enhanced clonal expansion[46,47]. Another mechanism associated with anti-CTLA4 is the local depletion of T_{reg} through antibody-dependent cell-mediated cytotoxicity (ADCC), which in turn enhances the T_{EFF} to T_{reg} ratio in the TME[48,49]. It is worth noting that these mechanisms rely on the presence of T cell responses, and depletion of T cells in animal models was shown to abolish any therapeutic tumouricidal activity associated with anti-CTLA4 treatment[50].

1.2.1.2. Programmed Death receptor 1 (PD1)

PD1 was first identified in 1992 as a mediator of apoptosis, and its role in the negative regulation of T cell activation became more evident in 1999 when the loss of mouse PD1 orthologue, *pdcd1*, was reported to cause autoimmunity[51]. PD1 was shown to restrain immune

responses primarily through delivering inhibitory intracellular signals that regulate the balance between T cell activation and tolerance[52]. Upon binding of PD1 to one of its ligands e.g., PDL1 (also known as B7-H1), PDL2 (also known as B7-H2), Src homology region 2 domain-containing tyrosine phosphatase 1 and 2 (SHP1 and SHP2) are recruited to the complex and mediate the dephosphorylation and inactivation of CD3 ζ subunit and its downstream adaptor proteins which is critical for TCR-mediated T cell activation[53]. Physiologically, PD1 activation is essential for controlling the activation and proliferation of differentiated effector T cells. As stated previously, PD1 engagement can lead to T cell apoptosis. Alternatively, it can induce a state of T cell dysfunction known as exhaustion[54,55]. What determines whether PD1 activation leads to apoptosis or exhaustion is still an active area of research[9]. In preclinical models, tumours were rejected in mice without functional PD1 whereas overexpression of PDL1 or PDL2 in cancer cell lines was found to limit the $CD8^+$ T cell responses[56,57]. Additionally, neutralizing PD1 axis using mAbs reversed the inhibitory effects and restored the T cells cytotoxicity towards tumour cells[56,58]. Besides its role in cancer treatment, PD1 axis proteins were shown to be useful biomarkers for tumour prognosis where multiple studies have shown a negative correlation between the expression of PD1 axis proteins and disease prognosis[59-61]. Following preclinical success, clinical trials were initiated to test the efficacy of mAbs designed to counteract negative immunoregulation by the PD1 axis[9,62]. In 2010, a phase I clinical trial using a single-agent anti-PD1 demonstrated the tolerability and clinical activity of PD1 blockade in patients with treatment-refractory solid tumours[63]. In 2014, anti-PD1 mAbs, pembrolizumab and nivolumab, gained FDA approval for use in refractory and unresectable melanoma[64]. This was based on the positive outcomes seen in KEYNOTE-001[65] and CheckMate 037[66] trials respectively. Pembrolizumab was then approved for the treatment of PDL1-expressing NSCLC because it provided a 4.3-month increase in progression-free survival (PFS) compared to chemotherapeutics[67,68]. The use of pembrolizumab and nivolumab has since been extended to other cancer types including head and neck squamous cell carcinoma[69,70], urothelial carcinoma[71,72], Hodgkin lymphoma[73,74] and others.

Targeting PDL1 by neutralizing antibodies has also proven to be an effective treatment in

different forms of cancer. In 2016, atezolizumab, the first PDL1-targeted humanized mAb, was approved for the treatment of urothelial carcinoma. The overall response rate to atezolizumab was only 15%, which was deemed as statistically significant[75]. Additionally, it was shown to be less toxic than traditional chemotherapy[76]. The following years have seen an expansion in the indications of atezolizumab to include NSCLC[77], triple-negative breast cancer (TNBC)[78] and SCLC[79]. Avelumab and durvalumab entered the market in 2017 as additional mAbs targeting PDL1 and were approved for different indications including Merkel cell carcinoma[80], urothelial carcinoma[81,82], advanced renal cell carcinoma[83] and NSCLC[84].

Despite the clinical success seen with immune-checkpoint blockade (ICB) therapy, several side effects have been reported. 15-90% of patients treated with ICB were reported to experience immune-related adverse events (IRAEs)[40]. Such events are mediated by the accumulation of overactive memory T cells that start infiltrating peripheral organs, such as the lungs and the gastrointestinal tract, causing inflammatory damage. Mucosal tissue appears to be susceptible as well since pruritis and mucositis occur in 68% and 40% of the patients respectively[85,86]. Nevertheless, such toxicities are generally better tolerated than toxicities associated with traditional chemotherapeutics[87]. Glucocorticoids are the mainstay for controlling IRAEs. However, Infliximab, an anti-TNF mAb, and other immunosuppressives can be used when glucocorticoids fail[9]. More importantly, only a subset of patients responds to ICB. The predictors of response are not yet fully characterized and remain an active area of research. Tumour-intrinsic and tumour-extrinsic response or resistance factors e.g., tumour mutational burden, neoantigen load, and gene expression signatures in the TME, are being investigated to build predictive models of ICB therapeutic response[88-90].

1.2.2. Adoptive T cell Therapy

Adoptive T cell therapy (ACT) involves infusing cancer patients with autologous or allogenic T cells[9]. It has shown considerable promise in the recent years. The concept was first

demonstrated in 1966 when a subset of patients experienced tumour regression following co-transplantation with patient derived leukocytes and autologous tumour cells[91]. In 1979, allogenic bone marrow transplantation was used to treat leukemia, and clinical improvement was shown to be mediated by a T cell graft versus tumour response[92]. In the late 1980s, ACT using tumour-infiltrating lymphocytes (TILs) for the treatment of metastatic melanoma was pioneered by Rosenberg and colleagues[93]. Over a period of 5+ years, 86 patients with metastatic melanoma were treated using autologous TILs plus high-dose intravenous bolus IL-2 with or without a single dose of cyclophosphamide[94]. The overall objective response to treatment was 34%, and the response duration was variable among patients. However, only 5/86 patients showed complete response[94]. A more rigorous lymphodepletion preparative regimen was introduced and another cohort of 93 patients with metastatic melanoma was treated with ACT and IL-2 following lymphodepletion with more success. 20/93 patients (22%) showed complete tumour regression and remained in complete remission 3 years after treatment[95]. Preparative lymphodepletion can be accomplished using chemotherapy or total-body irradiation or a combination of both, and was shown to enhance the persistence of the transferred T cells[96]. Several mechanisms have been speculated to account for the augmented efficacy of adoptively transferred T cells in the lymphopenic environment. One opinion suggests that lymphodepletion causes the elimination or reprogramming of immunosuppressive Myeloid derived suppressor cells (MDSCs), which are a heterogeneous population of $CD11b^{+}GR1^{+}$ cells that are found at high frequencies in tumours and in chronic infections and are thought to inhibit the function of T cells[97,98]. A second opinion claims that lymphodepletion reduces the competition between endogenous cells and transferred cells for the activating cytokines such as IL-7 and IL-15[99], and increases the functionality of antigen-presenting cells (APCs), which is mediated in part by the bacterial translocation that accompanies total-body irradiation[100]. Additionally, administration of the T cell growth factor IL-2 has been shown to be crucial for the success of ACT[101,102] . It is worth noting that the success of TIL-based ACT relies on the presence of healthy expandable populations of tumour specific $CD8^{+}$ T cells in the TME, a prerequisite that is not met in many types of cancer[9].

Engineering lymphocytes for ACT use was developed as an alternative method to address the challenges associated with isolating and/or expanding TILs *in vitro*. The technical ability to transduce lymphocytes with 80-90% efficiency using gamma retroviruses or lentiviruses provides an opportunity to genetically engineer lymphocytes with TCRs that recognize tumour antigens[103]. Genes encoding TCRs that recognize a wide variety of cancer antigens have been identified including melanoma–melanocyte differentiation antigens e.g., MART1, and gp100, and a variety of cancer–testes antigens (CTA) e.g., MAGE-A3, and NY-ESO-1 expressed on common epithelial cancers[95,104-106]. Additionally, engineering T cells with genes encoding molecules that improve the anti-tumour activity like IL-2 or IL-15 has been reported[107,108]. Since this method relies on the conventional TCRs, only tumour tissues presenting target antigens on specific MHC molecules are targeted by TCR-engineered lymphocytes. Despite offering a very flexible platform for targeting tumour antigens, there are disadvantages to using T cells with genetically engineered TCRs. Mispairing of the TCR α- and β-chains has been reported to occur resulting in diluted surface expression of the therapeutic TCR αβ[109,110]. Moreover, development of unexpected toxicities like "off-target" attack on unintended structures owing to cross-reactivity or antigenic mimicry has been associated with the use of genetically engineered T cells[109].

In 1989, Eshhar *et al.* developed a technique for engineering anti-tumour T cells based on the antigen binding specificity of antibodies, called chimeric antigen receptors (CAR)[111]. Antigen-recognizing regions of the heavy and light chains of antibodies are genetically linked to form a single-chain variable fragment (scFv) and attached to T cell signaling molecules, giving the lymphocytes the ability to recognize surface antigen and bypass the need for TCR-MHC interaction. First generation CARs contained CD3ζ alone as intracellular signaling domain[112], while second generation CARs incorporated a co-stimulatory domain e.g., CD28[113,114]. Multiple co-stimulatory signaling modules e.g., CD28, 4-1BB, and OX40 were added to the third generation CARs[115]. The addition of co-stimulatory signaling modules into CARs were hypothesized to recapitulate the natural co-stimulation associated with TCR activation and improve the persistence and potency of the engineered T cells[115]. Although retroviral transduction has been the typical method for

engineering T cells, CRISPR-Cas9 technology has been more recently used to direct the construct to the T-cell receptor a constant (TRAC) locus, resulting in uniform CAR expression and enhanced T cell potency[116]. The most successful application for CAR T cells has been the targeting of CD19 antigen in B-cell malignancies including non-Hodgkin lymphoma, acute lymphoblastic leukemia, and chronic lymphocytic leukemia[117-119]. Other examples include the targeting of GD2 antigen in neuroblastoma patients[120], and targeting of VEGFR2, which is overexpressed in tumour vasculature[121]. A limitation to the advancement of CAR T cell therapies is the requirement for the expression of tumour-restricted target antigens. The clinical success of CD19-specific CAR T cells is due, in part, to the high expression of CD19 in certain B cell malignancies and the lack of severe side effects when crossing over to normal $CD19^+$ B cells. Nevertheless, CD19 antigen loss is a common cause of treatment failure[9]. Additionally, toxicities arising from the CAR T cell therapy can be very severe affecting different organ systems. Cytokine release syndrome and neurotoxicity are among the side effect most commonly experienced by patients[122].

ACT represents a platform for personalized medicine, where patient-specific therapy design is usually required. The time required to generate the cells and the high cost of therapy can be prohibitive, and patient access is limited to these technologies at the time of writing. When compared to ICB therapy for example, the cost per patient in the case of ACT can be up to 10 times higher[9]. Moreover, only a few laboratories are certified to generate patient-grade injectable T cells, and a few tertiary care centers can administer the therapy[9]. While ACT carries much promise to cancer patients, key improvements in objective clinical responses, manufacturing and administration protocols, and toxicity profiles are indeed required for the technology to reach its maturity.

1.2.3. Cancer Vaccines

The aim of cancer vaccines is to actively stimulate the patient's adaptive immune system by eliciting an immune response against specific tumour antigens to regress the established

tumours and prevent further tumour growth[123]. The basic principles for successful implementations of therapeutic vaccines include: A) Delivery of large amounts of antigen to DCs, B) proper and optimal DC activation, C) Induction of strong and sustained $CD4^+$ and $CD8^+$ T cell responses, and D) Infiltration of the TME and reversing the immunosuppressive state within the TME[123]. The realization that cancer vaccines are not simply about replenishing the host with tumour-reactive T cells became evident after years of disappointing outcomes seen with different vaccination platforms. A series of phase III clinical trials of cancer vaccines using different target antigens e.g., MAGE-A3, MUC-1, telomerase, and others to treat different malignancies reported negative outcomes[124-129]. The only FDA-approved therapeutic cancer vaccine at the time of writing is Sipuleucel-T, which is a DC-based autologous cell vaccine, where autologous PBMCs, including APCs are activated *ex vivo* with a recombinant fusion protein (PA2024). PA2024 consists of a prostate antigen, prostatic acid phosphatase, that is fused to GM-CSF[130]. In a double-blind, placebo-controlled trial involving 512 patients with metastatic castration-resistant prostate cancer, men in the Sipuleucel-T group had a relative reduction in the risk of death of 22%, as compared with those in the placebo group which represented a 4.1-month improvement in median survival[130]. In hindsight, host, tumour, and environmental factors were not taken into consideration when designing such vaccines and the mechanisms governing immune exclusion or immune escape were not appreciated to have a direct effect on the tumour-specific immunity[131]. Consequently, these vaccines failed to generate enough numbers of healthy functional T cells that can infiltrate the TME and that persist long enough to elicit long-lasting immunity, making it evident that new strategies are required to overhaul the field's approach to vaccine therapy[123].

1.3. Oncolytic viruses

Oncolytic viruses (OVs) are naturally occurring or engineered replication competent viruses that selectively or preferentially propagate in tumour cells. Along the path of carcinogenesis, tumours evolve to evade immune recognition, and have weak or defective

antiviral programs, which make them an ideal environment for viral replication[132,133]. The use of viruses to treat cancer stemmed from the observation that, occasionally, cancer patients who contracted an infection disease like influenza went into transient periods of remission[134,135]. In the 1950s and 1960s, clinicians started using multiple wild type viruses e.g., Hepatitis, Epstein-Barr, West Nile, and yellow fever or even infected body fluids delivered through multiple routes to treat malignancies[136]. In immunocompetent patients, the immune system arrested the viruses, and no clinical benefit was seen in most cases. Immunocompromised patients, on the other hand, retained the infection and their tumours regressed, but they frequently became sick or even died when the infection spread to normal tissues[137]. In 1974, a study from Osaka university in Japan used mumps virus to treat terminal cancer patients and reported tumour regression in 37 out of 90 patients, which was particularly promising at the time[138]. Over the following two decades, the advancement of molecular biology and the increased capacity to engineer viruses contributed to enhancing the anti-tumour specificity of OVs. The first example was reported in 1991, when Martuza and colleagues engineered a thymidine kinase (TK) - negative Herpes Simplex Virus (HSV)[139]. TK-negative HSV was hypothesized to limit the viral replication to cells with high levels of TK, which is typically seen in cancer cells, and it indeed showed less neurovirulence and prolonged the survival of nude mice with intracranial U87 human gliomas[139]. The pace of OVs development accelerated dramatically over the following years, and viruses from at least ten different viral families entered the clinical arena[137,140]. Talimogene laherparepvec (T-Vec), an oncolytic HSV encoding granulocyte macrophage-colony stimulating factor (GM-CSF), was among the successful candidates that progressed in clinical trials. Intratumoural (IT) administration of T-Vec to patients with metastatic malignant melanoma led to complete regression in 8 out of 50 patients[141]. T-Vec gained FDA approval based on the improved durable response rate seen in a randomized phase III trial and is the only FDA approved OV at the time of writing[142].

1.3.1. Mechanisms of action of OVs

Although the fundamental premise of OVs had been their ability to infect and lyse tumour cells, clinical trials have not provided direct support that viral lysis of the infected cells is the main underlying mechanism for tumour destruction[140]. The field now accepts that curative viral oncolysis on its own can only happen when virus replication outpaces the antiviral immune response of patients[143]. Rigorous testing of multiple preclinical models suggests that the efficacy of many oncolytic viruses is, at least partly, due to the induction of anti-tumour immune responses[144,145]. Oncolytic *in situ* vaccination has been proposed as an important mechanism of action for OVs, where the viral lysis of tumour cells releases tumour-associated antigens (TAAs), pathogen-associated molecular patterns (PAMPs), danger-associated molecular patterns (DAMPs) into the TME. PAMPs and DAMPs aid in the maturation of DCs that capture TAAs and migrate to the lymph nodes where they present TAAs to T cells[146]. Furthermore, infection of tumour cells by OVs was reported to induce various inflammatory cytokines that recruit and activate immune effector cells[147]. Arming OVs by engineering them to express a variety of immunostimulatory transgenes has been pivotal to the development of OVs since it allowed researchers to target specific immune effector cells[143,148]. For example, GM-CSF, FMS-related tyrosine kinase 3 ligand (FLT3L), CCL3 or CCL5 have been shown to enhance the recruitment and differentiation of APCs[149-153]. IL-12, IL-15, and IL-18 are among the cytokines encoded by different OVs with the aim to activate T cells and NK cells[154-156]. Alternative strategies directed towards enhancing T cell activation by expressing co-stimulatory molecules on the surface of tumour cells have also demonstrated enhanced efficacy in preclinical models[157,158]. Other interesting examples of cargo loaded into OVs include bispecific T cell engagers (BiTEs) and immune checkpoint inhibitors[159-161]. Expression of BiTEs from an oncolytic Vaccinia virus (VacV) backbone resulted in bystander killing of uninfected tumour cells mediated by $CD8^+$ T cells[161]. Besides the lytic and immunostimulatory properties of OVs, disruption of tumour vasculature leading to tumour necrosis has been reported as a mechanism underlying OV efficacy[162]. While

OVs represent a truly unique platform with a multimodal mechanism of action, dissecting these mechanisms and understanding their contribution in achieving better clinical responses is critical for the advancement of the field. Additionally, the interaction between every viral backbone and the host immune system is unique and contributes to the outcome of the treatment. The Wan lab has focused its efforts on developing therapeutic regimens using Vesicular Stomatitis Virus (VSV) and Vaccinia Virus (VacV). In the next two sections we will briefly introduce these two viruses.

1.3.2. Vesicular Stomatitis Virus (VSV)

VSV is a prototypic non-segmented, negative-sense RNA virus (order *Mononegavirales*, family *Rhabdoviridae*)[163]. Pre-existing immunity to VSV in humans is generally very low and infections are mostly asymptomatic[163]. VSV virions are bullet-shaped and pack an 11 kb genome that comprises five genes encoding the nucleocapsid (N) protein, phosphoprotein (P), matrix (M) protein, glycoprotein (G) protein and large polymerase (L)[164]. The VSV G protein binds to the ubiquitously expressed low density lipoprotein (LDL) receptor, followed by receptor-mediated endocytosis and internalization into endosomes[165]. The viral envelope then fuses with the endosomal membrane following a conformational change in the G protein as a result of endosomal acidification, releasing the VSV ribonucleoprotein core into the cytoplasm[166]. VSV replicates in the cytoplasm resulting in the general shutdown of the host RNA and protein synthesis leading to cell death[165]. It has been postulated that defects in type I IFN signaling in tumour cells underlies VSV's tumour specificity[167]. This is due to the extreme sensitivity of VSV to the antiviral actions of type I IFN, where immunocompetent cells can launch an antiviral response quickly enough to inhibit viral replication before cell damage[165,167]. The M protein of VSV is responsible for many of the cytopathic effects and for the ability of the virus to inhibit the host type I IFN responses[168,169]. A variant with a single amino acid substitution or deletion at the methionine 51 in the M protein (VSV-M51R or VSV-ΔM51) has been developed for enhanced safety profile. Since this variant is defective in its ability to block the host gene expression, it was shown to stimulate the production

of type I IFN and induce a stronger virus mediated immune responses[170]. The experiments performed in this thesis were all done using the VSV-ΔM51 backbone.

Studies where VSV was employed as an oncolytic agent demonstrated the ability of VSV to induce a variety of immune responses including the induction of tumour-specific $CD8^+$ T cell responses[144], recruitment of neutrophils and NK cells[171,172], and the production of type III IFN (IL-28) in the TME[173]. Additionally, VSV was shown to activate and mature plasmacytoid DCs (pDCs) through TLR7. Upon TLR7 activation, pDCs upregulate the expression of MHC class II molecules, CD80, CD86 and produce high levels of type I IFN, leading to improved antigen presentation and priming of T cells[174-176]. The production of type I IFN by pDCs was shown to be critical for the accrual of virus-specific NK or $CD8^+$ T cells[177]. It is worth noting that the activation of innate and adaptive immune responses lead to the rapid clearance of VSV and have a counterproductive effect on the oncolytic capacity of the virus[165]. Nevertheless, the increased appreciation of the role of anti-tumour immune response and mobilizing immune cells to the TME pushed the field to engineer VSV variants that express a plethora of cytokines including IL-4[178], IL-12,[179] IL-15[156], IL-23[180], IL-28[173], FLT3L[181], and CD40L[182]. One of the examples that progressed to phase I clinical trials for the treatment of hepatocellular carcinoma (ClinicalTrials.gov Identifier: NCT01628640) include VSV expressing IFN-β encoding gene[183]. It has been hypothesized that the VSV-mediated expression of IFN-β would improve the safety of VSV by restricting its replication to IFN-resistant tumour cells. Additionally, it was shown to enhance the efficacy of oncolytic VSV therapy through the induction of $CD8^+$ T cell-mediated anti-tumour immune responses in mouse models of mesothelioma and NSCLC[184,185]. VSV has also been used as a vaccination platform due to its potent immunogenicity and its ability to generate strong humoral and cellular immune responses[186]. The Wan lab has pioneered the use of VSV as an anti-tumour therapeutic vaccine by engineering VSV to express a TAA and generate $CD8^+$ T cell responses against established tumours using a heterologous prime-boost vaccination platform[187]. We have also shown that the unique ability of VSV to boost $CD8^+$ T cells even during the acute phase of the primary response is due to their ability to infect follicular B cells in the spleen[188]. B cells act

as an antigen source for follicular DCs that capture and present the antigen to T_{CM} located within B cell follicles causing their expansion[188]. In this work, we continue to build upon our knowledge and expertise in using VSV as an oncolytic vaccine.

1.3.3. Vaccinia Virus (VacV)

Vaccinia virus (VacV) is a member of *Orthopoxvirus* genus of the subfamily *Chordopoxvirinae* of the poxviruses family. VacV virions are brick shaped and they pack a linear double-stranded DNA genome that is ~ 190Kb in length, encoding about 200 genes[189]. VacV was used worldwide as a vaccine against smallpox leading to the complete eradication of the disease by 1971[190]. The success of VacV as a smallpox vaccine was the first of its kind and remains unparalleled in the vaccinology field. VacV offers several advantages that make it an attractive choice for use as an oncolytic virus. The prolonged use of VacV for the last few decades has allowed for the extensive investigation of its biology and the long-term clinical observation of its safety and immunogenicity. This knowledge could be leveraged to create safe vectors with as little pathogenicity as possible for use in humans. Unlike other DNA viruses, the entire replication cycle of VacV happens in the cytoplasm, eliminating the need for viral genome entry into the nucleus and thus, eliminating the possibility of mutagenic integration in the host DNA[191]. This indeed adds to the safety profile of VacV. Additionally, the virus has a broad tissue tropism and can infect a wide range of mammalian cells making it suitable for testing in different experimental models[192]. This could be attributed to the lack of a specific cell surface receptor that is required for viral entry. Instead, the virus relies on several membrane fusion pathways[193,194]. Furthermore, its complex genome makes it less reliant on host proteins especially for processes involved in DNA replication and mRNA synthesis[195]. In addition, its large DNA genome can accommodate large sizes of transgenes up to 25 kb of foreign DNA making it an excellent platform for targeted gene therapy[196]. Moreover, the inherent immunogenicity of the virus which elicits an innate as well as an adaptive immune response could be harnessed and used to reprogram the immunosuppressive

TME and mount a tumour-specific immune response[197]. VacV encodes for several immune evasion proteins that interact with different key components and pathways of the host immune system[198]. Engineering these proteins can enable researchers to target the activation or the inhibition of specific immune pathways that are proven to play a role in eradicating or promoting certain kinds of neoplasia.

1.3.3.1. VacV Strains

Multiple strains of VacV exist, each with a different virulence profile and inherent oncolytic capabilities. Three strains: Wyeth (Wy), Western, Reserve (WR), and Copenhagen (Cop)[199] standout in the context of oncolytic therapy and are being investigated in this space[200]. The Wy strain is the least virulent of the oncolytic strains and was used extensively in North America as the smallpox vaccine. It has minimal inherent tumour selectivity, but it has been engineered to enhance its selectivity and oncolytic capacity[153,200]. The WR strain emerged as a primary laboratory strain derived from Wy after passage in mice and thus has minimal clinical use in humans. It has an inherent selectivity to cancer cells *in vitro* and a superior oncolytic activity[200,201]. The Cop strain was used in Northern Europe as a smallpox vaccine, but was withdrawn due to high levels of toxicity[200]. An attenuated version of Cop was latter engineered and used as a gene therapy platform to deliver the fusion suicide gene *FCU1* selectively to tumours to activate the prodrug 5-fluorocytosine (5-FC)[199].

1.3.3.2. Genetic modifications to VacV backbone

Early research efforts have been directed towards enhancing the safety and inherent cancer selectivity of the different VacV strains. The general approach of these efforts entails the genetic deletion or truncation of virulence genes to reduce its ability to proliferate in most normal cells while maintaining its ability to replicate in tumour cells. One of the most targeted genes to attenuate VacV is the thymidine kinase (*TK*) gene. VacV encodes for *TK* which ensures the

presence of enough supply of thymidine that is necessary for viral replication. The deletion of *TK* leads to the dependence of the virus on cellular *TK* expression[202,203]. In normal cells, cellular *TK* is regulated by the E2f transcription factors and is transiently expressed during the S phase of the cell cycle in proliferating cells. Tumour cells, on the other hand, often express high levels of *TK* constitutively regardless of their proliferation status[204]. VacV also expresses an EGF homologue (vaccinia growth factor; VGF) that binds EGFR[205]. When a host cell is infected, it starts secreting VGF which acts in autocrine and paracrine capacities to induce EGFR-mediated cell proliferation in both the infected and surrounding non-infected cells. VGF^- VacV has been demonstrated to replicate less efficiently in normal cell lines and display less pathogenicity in mice following *in vivo* infection[206]. VacV strains with deletions in both TK and VGF (known as double deleted VacV; vvDD) have been shown to selectively replicate in cancers with an activated EGFR pathway[201,207]. Deletion of other virulence genes including immunomodulatory genes (e.g. *B18R*)[208] and apoptosis inhibitors[209] has been reported to enhance the tumour selectivity and the safety profile of VacV vectors. By and large, those immunomodulatory virulence proteins function to shield the infected cells from pre-mature immune clearance and secure the production of more viral progeny. As such, it could be postulated that complex DNA viruses like VacV are not the best vaccination platforms since their diverse array of virulence proteins might lead to an attenuated immune response. However, the unparalleled success of VacV in the eradication of smallpox suggests otherwise. We believe that the redundancy of the immune system helps compensate for the effects of these virulence proteins and ultimately leads to a more refined immune response that strikes the right balance between inflammatory and anti-inflammatory pathways. The examples of genetic modifications to VacV presented here are not extensive and aim to provide a glimpse of the flexibility of VacV as a platform that can be tailored to specific and varied tumour phenotypes for optimal safety and efficacy. The experiments performed in this thesis were done using the TK^- WR strain backbone.

1.3.3.3. VacV replication cycle

Poxviruses coordinate the process of genome replication and virion assembly through temporal regulation of gene expression. Proteins involved in DNA replication[210-212], nucleotide biosynthesis[213], evasion of host defense[214-216] and other components needed for the process of early transcription are contained within the viral core along with the viral DNA. A DNA-dependent RNA polymerase is also contained within the viral core, leading to the synthesis of early messenger RNA, which upon translation yields early-stage proteins involved in the uncoating of viral DNA, DNA replication, and transactivation of intermediate mRNA[217]. The replication process takes place at discrete foci in endoplasmic reticulum (ER)-enclosed cytoplasmic mini-nuclei known as "poxvirus factories"[218]. Following genome replication, intermediate mRNA is then expressed through transcription factors encoded by early genes. Intermediate gene products then activate the transcription of late genes. Late gene products include proteins important for virion assembly and morphogenesis as well as enzymes and factors required for early gene transcription to be packaged inside progeny virions for use upon entry to a new host cell in the next cycle of infection[195,219]. This coupling of genome replication to the switch from early to late gene expression makes it possible to interrupt the infectious cycle through inhibition of DNA synthesis using either chemical inhibitors or mutations that block DNA replication resulting in the persistence of early gene transcription and inhibition of intermediate and subsequent late gene transcription[220]. Notably, the cytopathic effect of VacV is induced soon after viral entry due to the hijacking of the host translational machinery and the early viral enzymes that completely shut down host cell functions[221]. Upon completion of the replication cycle, VacV can produce four different types of infectious virions. The intracellular mature virus (IMV) is the most abundant form of virus and is retained within the infected cells. The IMV is released upon cell lysis and goes on to infect neighboring cells and start a new infection cycle[222]. The intracellular enveloped virus (IEV) is formed when an IMV is wrapped in a cell-derived lipid bilayer derived from the early endosomes or *trans*-Golgi network (TGN) and enables the virus migration along microtubules to

the cell membrane that fuses with the envelop and pushes the virion to the outer cell surface[223]. As such, virions are tethered to the outside of cells forming the cell-associated enveloped virus (CEV)[224]. The CEV can mediate the infection of neighboring cells by actin tail formation initiated by the infected cells[225]. This process is important for cell-to-cell spread of VacV. Alternatively, CEVs can be released from the cell surface as extracellular enveloped viruses (EVVs), that are responsible for long-range transmission of VacV *in* vivo[226].

1.4. Route of administration

The route of OV administration is an area of controversy in the field. Intratumoural (IT) delivery of OVs is used in ~50% of clinical trials, while intravenous (IV) delivery is used in ~35% of the trials[227]. Although numerous clinical trials have been emphasizing the importance of IT delivery of OVs, systemic delivery is required for metastatic disease. The argument for using IT delivery is that oncolysis is enhanced due to higher local concentrations of virions in the TME. Additionally, viral mediated modulation of inflammation within the TME is arguably maximized upon IT injection. On the other hand, the goal of systemic delivery is to inject enough virus beyond the viremic threshold so that the virus can reach the different metastatic sites and cause tumour destruction. In this case, the oncolysis as well as the local immune-mediated effects of OVs could be variable depending on the number of virions infiltrating each tumour site whereas systemic effects of the virus will be optimized. In a phase I clinical trial, intravenous (IV) administration of JX594 (an oncolytic VacV) resulted in recoverable virus from tumour biopsies only at viremic threshold of $> 10^9$ infectious units[228]. This indicates that extravasation of OVs to the TME is concentration-dependent and not a tropism-driven process. Virus sequestration in the liver and spleen by the mononuclear phagocytic system (MPS) represents a challenge for achieving high viremic concentration, and hence tumour infection, following IV delivery[137]. Additionally, soluble factors in the circulation e.g., antibodies, complement components, and coagulation factors coat the virus surface and facilitate the binding of virus particles to Fcγ receptors, complement

receptors or scavenger receptors on macrophages and endothelial cells leading to receptor-mediated phagocytosis and accelerated clearance from the circulation[229]. Strategies to minimize sequestration include chemically conjugating the viral coat proteins using biocompatible polymers e.g., polyethylene glycol (PEG), N-[2-hydroxypropyl]methacrylamide (HPMA)[230,231]. For example, PEGylated adenovirus 5 (Ad5) was shown to experience four-fold slower clearance than uncoated Ad5[232]. Similarly, HPMA-coated adenovirus was reported to have better shielding against neutralizing antibodies and thus have a prolonged circulatory half-life[233]. An alternative strategy to enhance the delivery of OVs to tumour sites after systemic injection is to hide them inside carrier cells[234]. In a preclinical study, dendritic cells and T cells were loaded with reovirus to shield the virus from systemic neutralization following IV administration[235]. The authors showed that pre-existing immunity to reovirus had a critical effect on determining the balance between anti-viral and anti-tumour immunity and proposed that DCs may be an appropriate vehicle for delivering reovirus to solid tumours[235]. In the current work we shed the light on the effect of OV route of administration on the anti-tumour immunity, tumour control and long-term efficacy.

1.5. ACT + OVV: synergy at its best

The Wan lab has previously reported on the use of heterologous prime-boost protocols to expand primed tumour antigen-specific T cells[187,236]. By engineering OV vectors to express TAAs, they gain an extra dimension of functionality by being able to engage and expand tumour-specific T cells turning them into oncolytic viral vaccines (OVVs)[187,236]. However, the use of a viral vector to prime the immune response is not ideal for various reasons. In the context of therapeutic vaccination, it could be costly to wait for the priming response before administering the booster dose. Pre-mature administration of the booster dose can result in suboptimal responses as the acute phase of the priming response could clear the antigen-loaded DCs and weaken the boosting responses. We have previously shown that VSV is able to get away from the acute phase clearance by infecting the follicular B cells in the spleen, which shields the antigen from the circulating

T cells[188]. While this property promotes the use of VSV as a booster vector it takes away the flexibility of the platform to accommodate other viral backbones. An alternative strategy to replace the priming phase of the therapy is to adoptively transfer primed central-memory-like T cells prior to using a boosting OVV. We highlighted the role of ACT as a standalone immunotherapeutic modality in an earlier section. Impediments to the efficient trafficking of the transferred cells to the TME represent a challenge to the success of ACT in solid tumours[237]. Additionally, the persistence of transferred cells has been a challenge to the ACT platform especially when using highly cytolytic terminally differentiated effector T cells. More rigorous investigation of different subsets of T cells along the continuum of differentiation demonstrated the superiority of less differentiated T cells to their more differentiated counterparts[238]. Reflecting on these two pieces of information, we can start to appreciate how OVVs are ideally suited to synergize with ACT. The model we envision is that upon transfer of CD62L-expressing T_{CM}, they would traffic to secondary lymphoid organs and be ready to expand through boosting with an OVV expressing the same antigen. Additionally, the inflammatory environment established upon OVV infection of the tumour would facilitate the recruitment of expanded T cells to the TME, a phenomenon that we refer to as "push-and-pull" (**Fig. 1.1**). Proof of concept that such therapeutic system works has been published by the Wan lab, where we demonstrate the robustness of the therapy as well as the flexibility of the system using different target antigens across different mouse strains[239-241].

As an additional layer of flexibility, we have established the utility of T_{CM} ACT cells in combination with a diversity of oncolytic virus vectors, including VSV and VacV. Previous studies in the lab have shown differences in autoimmune toxicity correlated with virus vector usage and associated modulation of the immune system. However, autoimmune toxicity caused the treated mice to reach endpoint early and observation of anti-tumour effect was truncated. Thus, we have yet to explore whether differences in viral vectors and their modulation of systemic immunity and the TME translates to differences in anti-tumour efficacy. In this thesis I will continue to develop this therapeutic platform, focusing on the role of the virus backbone in modulating the immune system and looking for distinct clinical outcomes that may arise due to this modulation. Not only

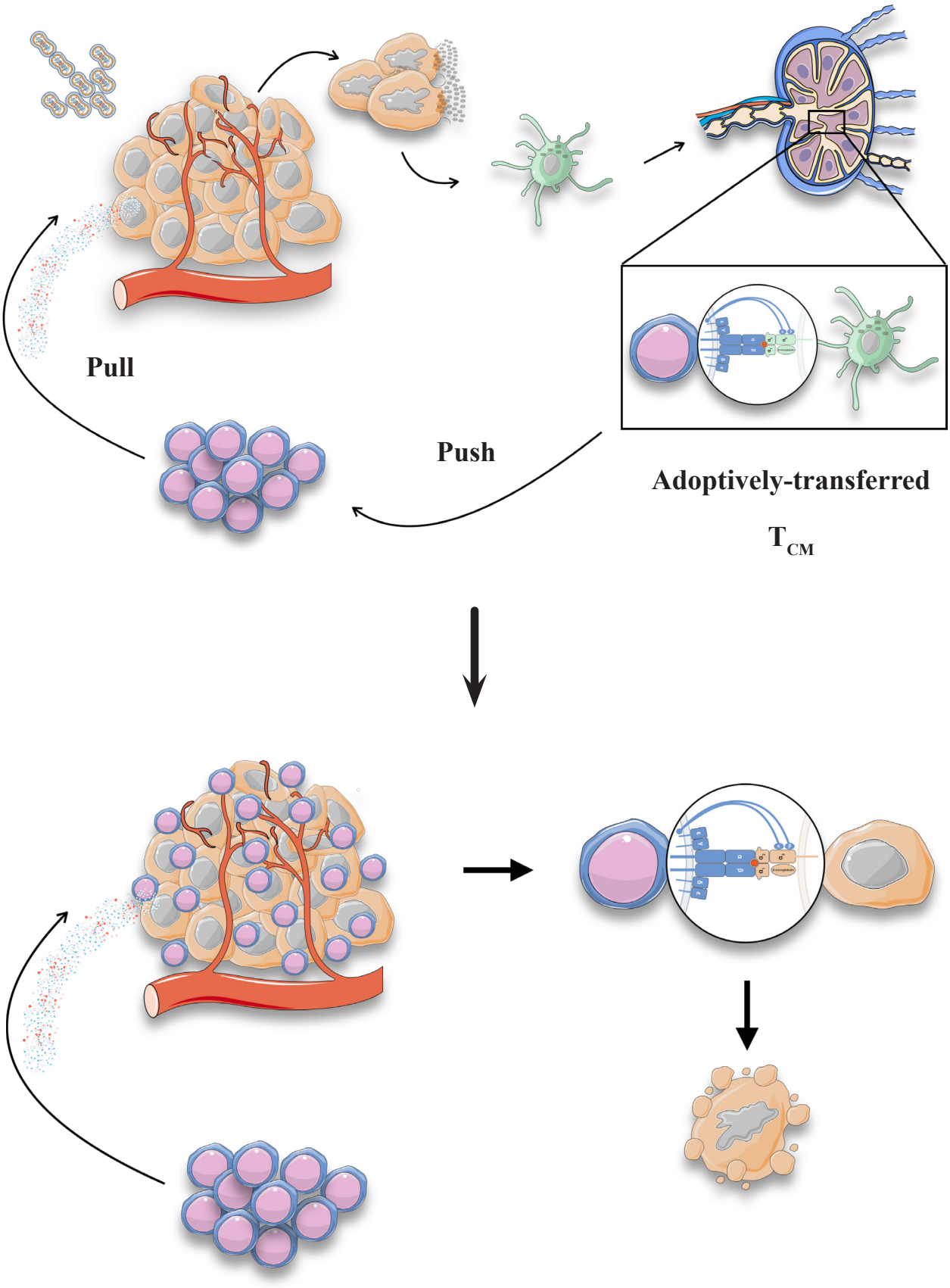
Pull
Push
Adoptively-transferred
T_{CM}

Figure 1.1 | Illustration showing the working model of ACT + OVV therapy

The attack of OVVs on the tumours cause the lysis of tumour cells and the expression of virus-encoded TAAs. APCs capture TAAs or become directly infected with OVVs and migrate to secondary lymphoid organs (e.g. a draining lymph node) where APCs meet T_{CM}-like T cells causing them to expand (push). The inflammation created in the TME by the viral infection recruits the expanded T cells to the TME (pull). The infiltrating T cells recognize tumour cells and attack them leading to tumour cell death.

will these studies allow us to determine the mechanisms by which virus vectors can modulate anti-tumour immunity but they will also help us implement this knowledge to develop our therapeutic platform and drive the cancer immunotherapy field forward.

1.6. Aims of the work

This thesis aims to investigate the specific aspects and mechanisms of the OVV and ACT combination therapy related to the choice of the OV backbone and its effect on the immune system and therapy induced anti-tumour immunity. With these studies and by building upon the previous work done at the Wan lab we will gain a better understanding of the determinants of success of such therapeutic platform. The broad aim of this work was to compare the therapeutic outcomes observed in treating the B16 melanoma model using ACT in combination with VacV or VSV. More specifically, we aim to address the following points:

1. Characterize the long-term anti-tumour efficacy of VSV- vs. VacV-based OVVs in combination with ACT in B16 tumour model.

   Hypothesis: ***VacV leads to less treatment-induced antigen loss due to its anti-inflammatory viral proteins that help balance the immune attack on the tumour***

2. Assess the effect of OV route of administration on the long-term efficacy of VSV- and VacV-based OVVs in combination with ACT.

   Hypothesis: ***IT injection enhances virion exposure and replication in the tumour, thereby augmenting viral-mediated immune modulation and facilitating anti-tumour immunity in the TME.***

3. Study the contribution of intratumoural virus replication in modifying the TME and achieving the desired clinical efficacy of ACT + OVV.

   Hypothesis: ***Oncolysis is necessary but insufficient to prevent immune escape and tumour relapse***

4. Study the effects of VSV and VacV-based OVVs in combination with ACT on altering the

cellular landscape and TME transcriptome.

Hypothesis: ***VacV leads to more drastic changes in the TME due to its complex genome and more extensive interaction with the host immune system allowing recruitment of more innate immune cells to complement CD8$^+$ T cell attack.***

5. Assess the effect of cellular and molecular signatures observed in ACT + VacV treated tumours in the disease progression/outcome in human patients.

   Hypothesis: ***Similar to was observed with VacV treated tumours, a more balanced / refined inflammatory signature correlates with positive prognosis and better overall survival in cancer patients***

Chapter 2 — Materials and Methods

2.1. Mice

C57BL/6 were purchased from Charles River Laboratories (Wilmington, MA). B6.PL-Thy1^{a}/CyJ (Thy1.1 congenic mice) were obtained from The Jackson Laboratory (Bar Harbor, ME). B6.Cg-Tcrat^{m1Mom}Tg(TcrLCMV)327Sdz (referred to as P14 mice) were initially purchased from Taconic Breeding Laboratories (Germantown, NY, USA), then a colony was established and bred in the Central Animal Facility (CAF) at McMaster University. Thy1.1^{+}P14 T cells were generated in the CAF at McMaster University by breeding P14 mice against Thy1.1^{+} congenic mice. All animal experimentation was approved by McMaster University's Animal Research Ethics Board (AREB) and complied with the Canadian Council on Animal Care guidelines.

2.2. Cell lines

Murine melanoma B16 cells or colon adenocarcinoma MC38 cells that are stably transduced to express gp_{33-41} epitope from the LCMV glycoprotein (referred to as B16gp33 and MC38gp33 respectively) were used to establish the *in vivo* tumour models[242,243]. B16gp33 cells were maintained in Dulbecco's modified Eagle's medium /Nutrient Mixture F-12 (DMEM/F12) supplemented with 5% fetal bovine serum (FBS), 1mM sodium pyruvate, 2mM L-glutamine, 0.1mM non-essential amino acids, 10mM HEPES, 55µM β-mercaptoethanol, 100 U/ml penicillin and 100µg/ml streptomycin (Thermo Fisher Scientific). To ensure the stable expression of gp_{33-41} construct, B16gp33 cells were further supplemented with 800µg/ml G418 (Sigma). MC38gp33 cells were maintained in DMEM medium supplemented with 5% fetal bovine serum (FBS), 1mM sodium pyruvate, 2mM L-glutamine, 0.1mM non-essential amino acids, 10mM HEPES, 100 U/ml penicillin and 100µg/ml streptomycin. For viral titration experiments, kidney CV-1 cells were maintained in Minimum Essential Medium (MEM) supplemented with 5% fetal bovine serum (FBS). All cell lines were grown at 37^{0}C in a 5% CO_2 – humidified incubator.

2.3. In vivo tumour models

To establish a treatable tumour, six- to eight-week-old C57BL/6 mice were injected intradermally with 2 x10^5 B16gp33 or MC38gp33. The cells were resuspended in 30 µL of PBS for injection. B16gp33 reached a treatable volume of 50 -100 mm^3 after 5-7 days, while MC38gp33 required 7-10 days to reach the same volume.

2.4. Tumour growth monitoring

Tumours were monitored by measuring their volume calculated as L*W*H using electronic calibers. 1000mm^3 was used as the endpoint as specified in the animal utilization protocol (AUP) in agreement with the CAF at McMaster University. Animals showing signs of sickness due to tumour ulceration and infection prior to endpoint were euthanized as per AREB guidelines.

2.5. Adoptive T cell transfer

Spleens from P14 or Thy1.1$^+$P14 mice we processed to a single cell suspension. Red blood cells were lysed using ACK lysis buffer. Bulk splenocytes from transgenic mice were cultured for 7 days in RPMI 1640 supplemented with 10% FBS, 100 U/ml penicillin, 100 ng/ml streptomycin, 2 mM L-glutamine, and 55µM β-mercaptoethanol. Splenocytes were stimulated with 100 ng/ml gp33 peptide (Biomer Technologies) in the presence of 10 ng/ml IL-15, 10 ng/ml IL-21 (BioLegend), and 20 ng/ml rapamycin (Sigma-Aldrich). Unless otherwise specified, 1x10^6 P14 or Thy1.1$^+$P14 cells were injected IV in B16gp33 tumour-bearing C57BL/6 mice.

2.6. Viruses

Recombinant Vesicular Stomatitis virus (VSV), and Vaccinia Virus (VacV) expressing the $CD8^+$ and $CD4^+$ T cell immunodominant epitopes of the lymphocytic choriomeningitis virus glycoprotein (LCMV-gp_{33-41} and LCMV-gp_{61-80}, respectively) in a minigene cassette were used for our studies (denoted as VSVgp33 and VacVgp33)[244,245]. Unless otherwise specified, VSVgp33 was

administered IV or IT at 2 x 10^8 PFU diluted to 200 µL or 50 µL in PBS respectively. VacVgp33 was administered IV or IT at 1 x 10^8 PDF diluted to 200 µL or 50 µL in PBS respectively.

2.7. Organ processing

2.7.1. Blood processing

100-200 µl of blood were collected from the periorbital sinus and red blood cells were lysed using ACK buffer. The resulting cell suspension were washed in PBS or FACS buffered and stained or stimulated as per the experimental design.

2.7.2. Spleen Processing

Spleens from euthanized mice we processed to a single cell suspension by breaking down the tissue using two microscope glass slides. Red blood cells were lysed using ACK lysis buffer. The resulting cell suspension was washed in FACS buffer and stained as indicated in each experiment.

2.7.3. Lymph nodes processing

Draining and/or non-draining lymph nodes from euthanized mice were processed to single cell suspensions by breaking down the tissue between two microscopic slides. The resulting cell suspension were washed in PBS or FACS buffered and stained or stimulated as per the experimental design.

2.7.4. Tumour processing

Using a scalpel and scissors, tumours were surgically removed and placed into a pre-weighed Eppendorf tube containing a small volume of RMPI-1640 with 10% FBS. Scissors were then used to cut the tumours into small pieces within the tube. The cut tumours were then incubated

in freshly prepared dissociation mixtures of collagenase type IV (0.5 mg/mL) and DNase I (0.2 mg/ mL) in RPMI-1640 media with 10% FBS and 5mM $CaCl_2$. 10 mL of dissociation mix were used per 0.1 mg of tumour. The tubes were placed into a temperature-controlled orbital shaker for 1h at 37°C with 200 rpm agitation. Two volumes of cold RPMI-1640 media with 10% FBS and 2mM EDTA were added to neutralize the collagenase activity and the tumours were refrigerated for 10 min. Finally, the tumours were passed through 70µm cell strainers, and the resulting cell suspension was washed in PBS or FACS. The resulting cells were stained as per the specific panel design of every experiment.

2.8. Surface and intracellular staining and Flow cytometry

Cell suspensions obtained from various processing protocols were washed using FACS buffer (PBS with 2% BSA and 2 mM EDTA). For surface staining, cells were treated with anti-CD16/ CD32 (Fc block) and surface stained with fluorescently conjugated antibodies against the specific cell surface markers (BD Biosciences). In case intracellular staining is specified, the cells were permeabilized and fixed with Cytofix/Cytoperm (BD Pharmingen) and stained using fluorescently conjugated antibodies against the specified intracellular targets. Data were acquired using LSRFortessa flow cytometer with FACSDiva software (BD Pharmingen) and analyzed with FlowJo Mac, version 10.7.1 software (BD Biosciences).

2.9. Intracellular cytokine staining

Peripheral blood mononuclear cell were collected and processed as described before. The cells were stimulated with gp_{33-41} peptide (1 µg/ml) in the presence of brefeldin A (GolgiPlug; BD Pharmingen, 1µg/ml added after 1 hour of incubation). After 5 hours of total incubation time, cells were stained and analyzed using flow cytometry as previously described.

2.10. In vivo T cell proliferation assay

B16gp33 tumour-bearing mice were treated with P14 T cells followed by VacVgp33 delivered IV or IT in the presence of FTY720 (4μg/g, Cayman Chemical, Michigan, USA). Mice were scarified at days 1, 2 and 3 following VacV administration and various lymphoid tissues were collected. The tissues were processed, stained and analyzed using flow cytometry as previously described.

2.11. Clariom S Assay

B16gp33 tumour-bearing mice were treated with P14 T cells followed by VacVgp33 or VSVgp33 or PBS IT. 48 hours later, the mice were euthanized, and the tumours were collected and homogenized using a tissue homogenizer. Total RNA was extracted using RNeasy kit (Qiagen) according to the manufacturer's protocol. RNA was normalized to an input amount of 100 ng and was submitted to Dr. Pare Genetic and Molecular Epidemiology Laboratory for Affymetrix Clariom S mouse assay. RNA underwent reverse transcription. cDNA was purified using magnetic beads and fragmented using UDG. Fragmented samples were hybridized to the microarray chips at 45 °C overnight. Stained arrays are scanned to generate intensity data. All reagent kits and arrays were purchased from Thermo Fisher Scientific (Loughborough, United Kingdom).

2.12. Clariom S data analysis

CEL files were preprocessed using the oligo package that utilizes multichip average method (RMA) for normalization[246]. Differentially expressed genes (DEGs) between the different treatment conditions were estimated using the Limma package[247]. Genes were considered differentially expressed if at least 2-fold change is returned with an adjusted P value < 0.05. Biological Process (BP) domain of the Gene Ontology (GO) annotations was used to identify the overrepresented biological processes using clusterProfiler R package[248-250]. Gene Set Enrichment

Analysis (GSEA) was done using fGSEA R package[251,252]. Hallmark gene sets from the Molecular Signatures Database (MSigDB) were used for the GSEA analysis[253].

2.13. Patient gene signature analysis

A cohort of 469 patients with Skin Cutaneous Melanoma (SKCM) data generated by The Cancer Genome Atlas (TCGA) was used for the analysis. Clinical data of the patients was obtained from the cBio Cancer Genomics Portal (http://cbioportal.org)[254,255]. Gene set variation analysis (GSVA) was used to estimate sample-wise gene set enrichment score using the GSVA R package[256]. Fitting of univariate cox proportional hazard regression model was done using survival R package[257].

2.14. In silico cytometry and survival correlation analysis

RSEM-normalized RNASeq data for SKCM cohort of 469 patients were downloaded from the firebrowser (http://firebrowse.org). Estimation of the immune cell subsets in each sample was performed using CIBERSORTx with the LM22[258] gene set on the CIBERSORTx website (http://cibersortx.stanford.edu). Individual subtypes or phenotypes of each population was added together to simplify the analysis. The median value for each immune cell subset was used to classify patients into high and low groups. Clinical data of the patients was obtained from the cBioportal (http://cbioportal.org)[254,255]. The overall survival of patients with high and low infiltrates for each immune population was plotted using Kaplan-Meier method and log-rank test was used to calculate the statistical significance.

2.15. In vivo depletion

Antibodies were given intraperitoneally at an initial dose of 250 µg one day before virus injection and another dose of 250 µg one day after virus injection. Anti-CD8 (clone 2.43, Bio X Cell), and anti-NK1.1 (in house produced from hybridoma cell line) depletion were maintained by

giving a weekly injection of 250 µg. Anti-Ly6G (1A8 clone, Biolegend) was injected every 4th day at the same dose.

2.16. Heat inactivation

VacV was incubated at 55^{0}C for 1 hour using a heat block. The virus was then used directly for *in vitro* or *in vivo* experiments.

2.17. Psoralen Long Wavelength Ultraviolet Inactivation

VacV was incubated with 10 µg/ml Psoralen (Sigma) for 10 min in a 6-well plate. The virus was then exposed to 365nm UV light for 10 min using Longwave Ultraviolet Crosslinker (Cole-Parmer).

2.18. X-gal staining protocol

CV-1 cells were seeded in 6-well plates to form a monolayer. The cells were infected using VacV in different MOIs. 24h after infection, X-gal Fixation buffer (0.1M phosphate buffer (pH 7.3) supplemented with 5 mM EGTA (Sigma), pH 7.3, 2 mM $MgCl_2$ and 0.2% glutareldahyde (Sigma) was added to the cells for 15 mins followed by 2 cycles of washing using the X-gal washing buffer (0.1M phosphate buffer (pH 7.3) supplemented with 2 mM $MgCl_2$). X-gal staining buffer containing 1 mg/ml X-gal was then added to the cells and left overnight at 37°C. Next day, the solution was aspirated off and the washing buffer was used to wash the cells.

2.19. Immunofluorescence (performed by Sreedevi Kesavan)

B16gp33 cells were plated onto 18x18mm glass cover slips and infected with VSV-gp33 and Vaccinia-gp33 for 6 hours or exposed to 20µM H_2O_2 for 1 hour. Cells were then harvested, fixed, and permeabilized using BD Transcription Factor Phospho Buffer Set (Catalog No. 563239) and then incubated in methanol overnight at -20^{0}C. Samples were then blocked with 10%BSA +

10%FBS in PBS for 1 hour before an overnight incubation with an anti-NBS1 antibody (NOVUS #7E4A2) in blocking buffer at 1:200 concentration. The next day, slides were incubated with Rabbit α Mouse Alexa488 secondary antibody at the 1:200 concentration. (Jackson #315-545-003) and counterstained with 10ug/mL of Hoechst dye. Cover slips were then inverted on glass slides and sandwiched with 80μL of Permount and sealed with nail polish.

2.20. Data wrangling, visualization, and statistical analysis

R studio was used for data analysis[259]. Data wrangling and processing was done using Tidyverse[260] and Tidyr[261] R packages. Data visualization was done using ggplot2 R package[262]. Heatmaps were created using ComplexHeatmap R package[263]. Enrichment networks were visualized using clusterProfiler R package[250]. Kaplan-Meier survival analysis was done using the survminer R package and log-rank test was used to calculate statistical significance[264]. Statistical analysis was done using rstatix R package[265]. Other packages used are specified in their relevant sections. Differences between means were considered significant at $p < 0.05$ and were indicated by *.

Chapter 3 — Studying the effect of the viral backbone on the Efficacy of ACT + OVV

3.1. Introduction

Previous work by the Wan lab demonstrated that Vesicular Stomatitis Virus (VSV)-based oncolytic viral vaccines (OVVs) can expand adoptively-transferred tumour-specific T cells (ACT) leading to complete tumour regression. Three different antigen-model systems based on B16 melanoma and CMS-5 fibrosarcoma tumours were tested to assess the robustness of the combination therapy. T cells with T cell receptors (TCRs) specific for a self-epitope, dopachrome tautomerase at residues 180 – 188 (DCT; 24H9R T cells), a foreign epitope derived from Lymphocytic Choriomeningitis Virus (LCMV) glycoprotein at residues 33-41 (gp33; P14 T cells), or a neo-epitope derived from a mutated ERK protein at residues 136 – 144 ($ErkM_{136-144}$; DUC18 T cells), were combined with VSV vectors encoding the relevant epitope. In all three models, initial tumour regression was observed. However, Walsh *et al.* observed that in case of targeting DCT, surviving mice developed vitiligo which indicates melanocyte damage, pointing to autoimmune pathology[239]. They extended the analysis to RIP-gp mouse model, in which LCMV glycoprotein is expressed under the control of rat insulin promoter (RIP) resulting in the expression of LCMV glycoprotein in pancreatic β-cells. Tumour bearing-mice treated with ACT + OVV developed diabetes concomitant with T cell-mediated tumour regression, indicating the treatment-mediated loss of insulin producing β-cells tied to therapeutic efficacy at the tumour. Interestingly, the use of Vaccinia Virus (VacV)-based OVV resulted in similar tumour regression in the absence of diabetes. Furthermore, induction of diabetes in VSV treated mice truncated the tumour regression observation as this represented an endpoint and mice had to be euthanized. The discrepancy in the outcome between both viruses promoted us to further investigate the different biological properties between both viruses and understand how their interaction with the host immune system can shape the outcome of ACT + OVV therapeutic protocol. In this chapter, we sought to study the effects of altering the backbone of OVV on the efficacy of ACT + OVV therapy. Our results demonstrate that despite the ability of both viruses to expand the antigen specific $CD8^+$ T cells, we observed that VacV leads to more durable tumour control and statistically significant

improvement in the overall survival of mice.

3.2. Results

3.2.1. Triple combination of IL-15, IL-21, and Rapamycin yield memory-like CD8$^+$ T cells with strong proliferative capacity

We have previously demonstrated the ability of rhabdoviruses expressing tumour-specific antigens to engage and expand tumour-specific T_{CM} in prime-boost models[187,188,266]. We had also shown their ability to expand T_{CM} derived from Lymphocytic Choriomeningitis virus (LCMV)-infected mice[241]. However, using a natural infection model is inefficient to generate T_{CM} cells in a timely manner with high enough yield for experimental use and is not a viable strategy for clinical implementation. Hence, we shifted to using transgenic LCMV P14 TCR mice where CD8$^+$ T cells express T cell receptor (TCR) specific for gp_{33-41} antigen (denoted as P14 T cells). Gattinoni *et al.* have previously shown that T central memory (T_{CM}) and T stem cell memory (T_{SCM}) cells are superior to T effector memory (T_{EM}) and T effector (T_{EFF}) cells in terms of their replication capacity and anti-tumour efficacy[267]. In order to maximize the expansion capacity of T cells following the OVV boosting, we developed a protocol to culture tumour-specific CD8$^+$ T cells *ex vivo* into a T_{CM} / T_{SCM} phenotype. Zeng *et al.* reported on the synergy of IL-21 and IL-15 in promoting CD44^{hi} memory CD8$^+$ T cells[268]. Additionally, He *et al.* demonstrated the ability of Rapamycin to generate long-lived memory CD8$^+$ T cells[269]. We tested the use of a combination of IL-15 and IL-21 in the presence or absence of Rapamycin to culture CD8$^+$ T cells. As a control, we cultured CD8$^+$ T cells in the presence of IL-2 which is known to drive the CD8$^+$ T cells into a terminally differentiated effector phenotype[270,271]. In all cases, 0.1 µg/ml of gp33 peptide was used to provide TCR stimulation for gp33-specific CD8$^+$ T cells. Flow cytometry was used to analyze the expression of CD62L and CD44 as a phenotypic readout to determine the identity of CD8$^+$ T cells. Using these markers, CD8$^+$ T cells may be subdivided into three different populations: T_{EM}

A

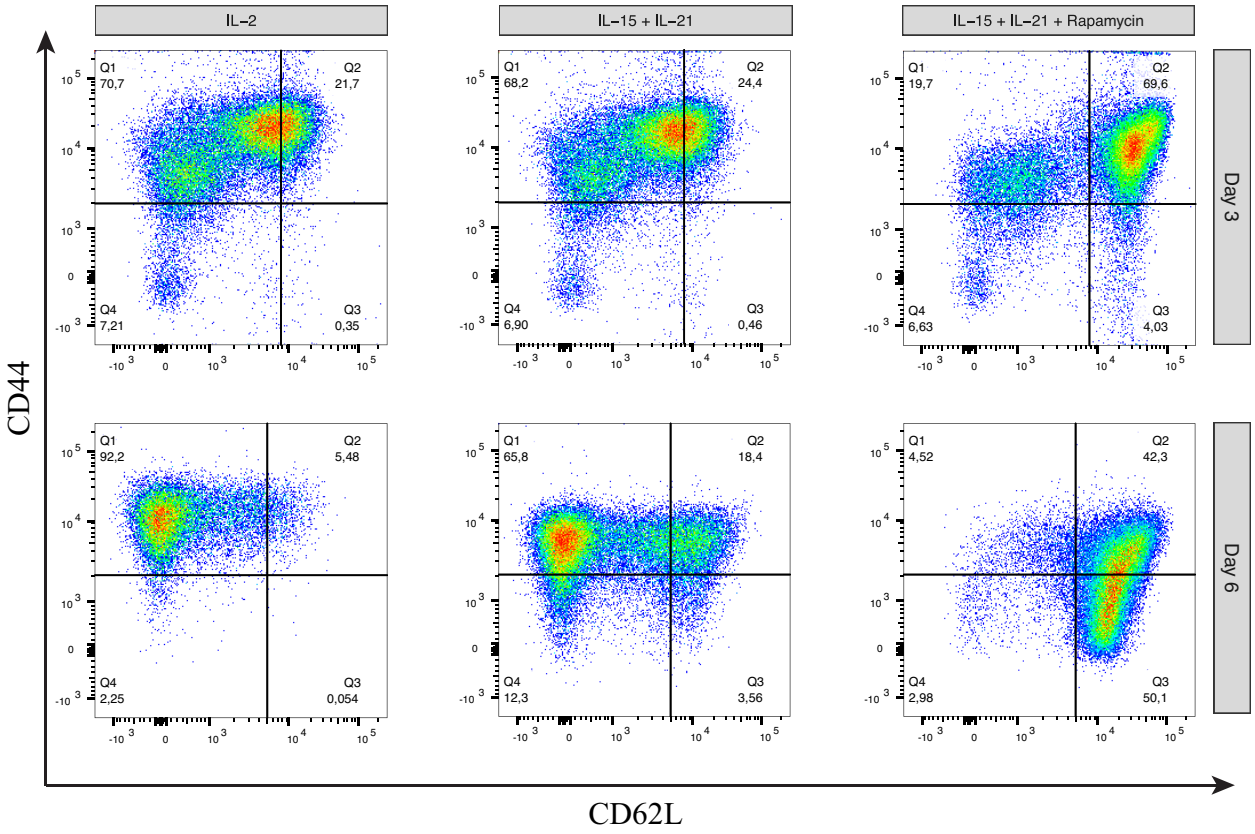
IL−2
IL−15 + IL−21
IL−15 + IL−21 + Rapamycin
Day 3
Day 6
Q1 70,7
Q2 21,7
Q4 7,21
Q3 0,35
Q1 68,2
Q2 24,4
Q4 6,90
Q3 0,46
Q1 19,7
Q2 69,6
Q4 6,63
Q3 4,03
Q1 92,2
Q2 5,48
Q4 2,25
Q3 0,054
Q1 65,8
Q2 18,4
Q4 12,3
Q3 3,56
Q1 4,52
Q2 42,3
Q4 2,98
Q3 50,1
CD44
CD62L

B

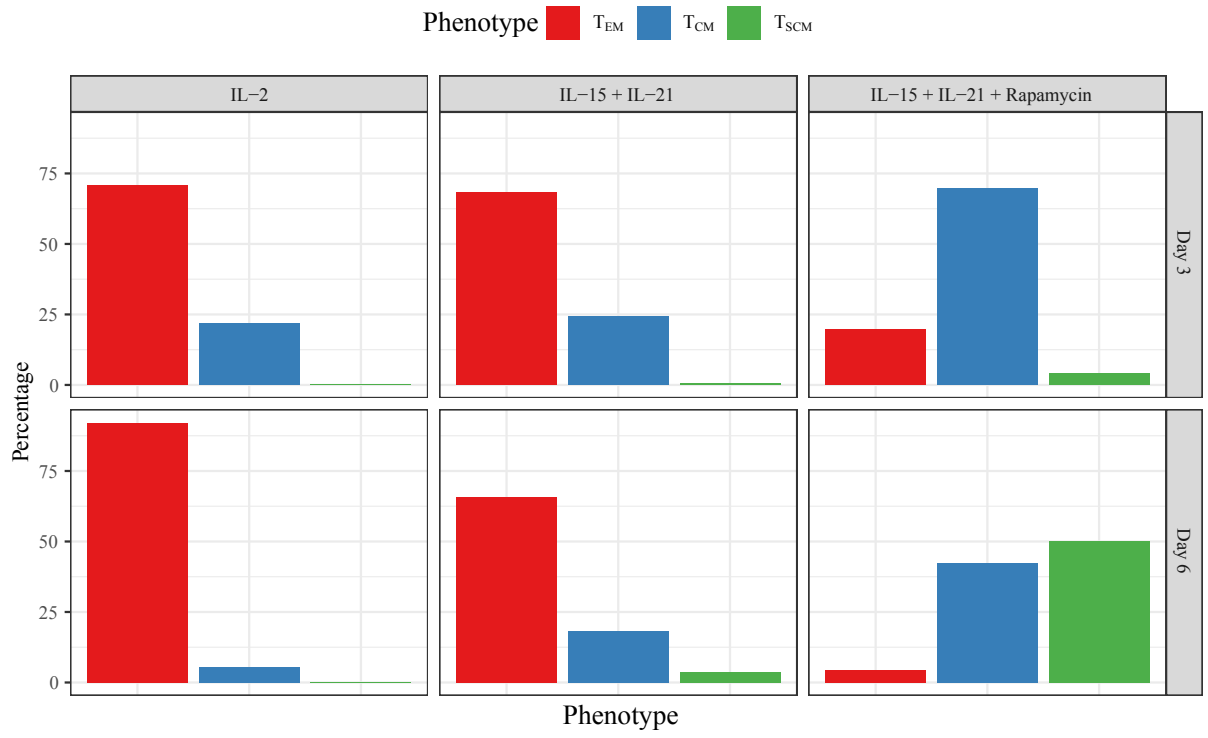
Phenotype
TEM
TCM
TSCM
IL−2
IL−15 + IL−21
IL−15 + IL−21 + Rapamycin
Day 3
Day 6
Percentage
0
25
50
75
Phenotype

Figure 3.1 | Triple combination of IL-15, IL-21 and Rapamycin yield memory-like CD8+ T cells with strong proliferative capacity

Spleens from P14 or Thy1.1^{+}P14 mice we processed to a single cell suspension. Red blood cells were lysed using ACK lysis buffer. Splenocytes were stimulated with gp33 peptide in the presence of IL-2 or IL-15 and IL-21 ± rapamycin. At day 3 and day 6 post culture initiation, the cells were collected, washed and stained for phenotype analysis using flow cytometry (A) Scatter plots showing the expression of CD44 and CD62L in different conditions (B) Summary of the phenotypic proportions resulting in each culture condition

($CD62L^{lo}CD44^{hi}$), T_{CM} ($CD62L^{hi}CD44^{hi}$), and T_{SCM} ($CD62L^{hi}CD44^{lo}$) [272,273]. On day 3 post culture seeding, we observed that in the presence of IL-2 or IL-15/IL-21, ~ 70 % of the cells showed a T_{EM} phenotype **(Fig. 3.1 A-B)**. The addition of Rapamycin to IL-15/IL-21 caused a shift in CD62L expression and resulted in ~ 70% of the cells being T_{CM} **(Fig. 3.1 A-B)**. On day 6, > 90% of the cells treated with IL-2 displayed a T_{EM} phenotype. IL-15/IL-21 - treated cells maintained the same phenotype as on day 3 with most cells (~70%) displaying T_{EM} phenotype and only ~ 20% of the cells showing T_{CM} phenotype. Interestingly, the presence of Rapamycin in culture pushed the cells away from T_{EM} phenotype and resulted in equal proportions of T_{CM} and T_{SCM} cells **(Fig. 3.1 A-B)**. In conclusion, the triple of combination of IL-15, IL-21 and Rapamycin resulted in a heterogenous population of T_{CM} and T_{SCM} cells, whereas IL-2 or IL-15 and IL-21 in the absence of Rapamycin resulted in mostly T_{EM} with some $T_{CM.}$ Moving forward we used the triple combination of IL-15, IL-21, and Rapamycin to culture $CD8^+$ T cells for ACT purposes.

3.2.2. Boosting ACT with oncolytic viral vaccines results in T cell expansion and tumour regression

In order to test the efficacy of combining ACT with OVV, we employed the B16gp33 melanoma tumour model, where B16 cells were stably transfection with gp_{33-41} epitope. C57BL/6 mice were intradermally implanted with 2×10^5 B16gp33 cells. Tumours were allowed to grow for 5 days to a size of ~ 50 - 100 mm^3 and were then treated using 10^6 P14 T_{CM} cells cultured as previously described or PBS, followed by 2×10^8 pfu of VSV engineered to expressed gp_{33-41} epitope (VSVgp33) or PBS 24 h later **(Fig. 3.2 A)**. Both P14 T_{CM} and VSVgp33 were delivered intravenously (IV) as earlier characterization had proven IV to be the superior route of delivering rhabdoviruses for achieving the maximum expansion of $CD8^+$ T cells[188]. Using flow cytometry-based intracellular cytokine staining (ICS), we quantified the gp33-specific $IFN\gamma^+$ $CD8^+$ T cells in the circulation at days 5 and 12 post virus injection (pvi). We observed that the combination of ACT + OVV boosted gp33-specific $CD8^+$ T cells to a mean of 12.9% ± 1.31% at

A

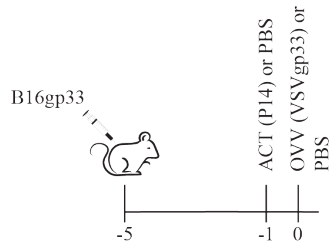
B16gp33
ACT (P14) or PBS
OVV (VSVgp33) or PBS
-5
-1
0

B

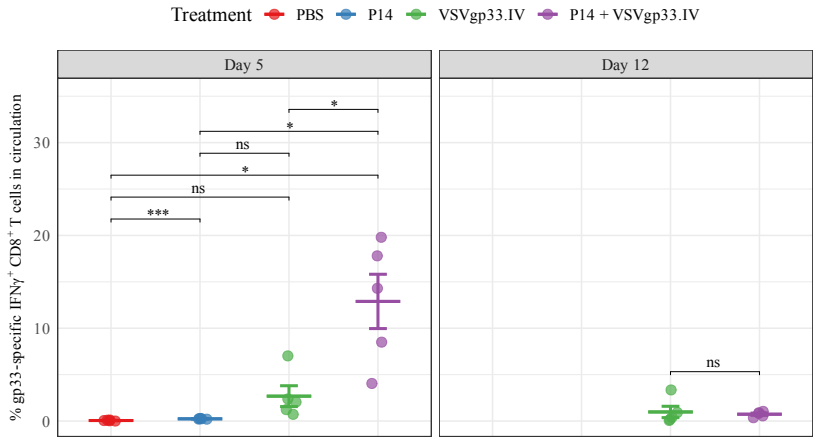
Treatment PBS P14 VSVgp33.IV P14 + VSVgp33.IV
Day 5
Day 12
% gp33-specific IFNγ+ CD8+ T cells in circulation
0
10
20
30
*
*
ns
*
ns
***
ns

C

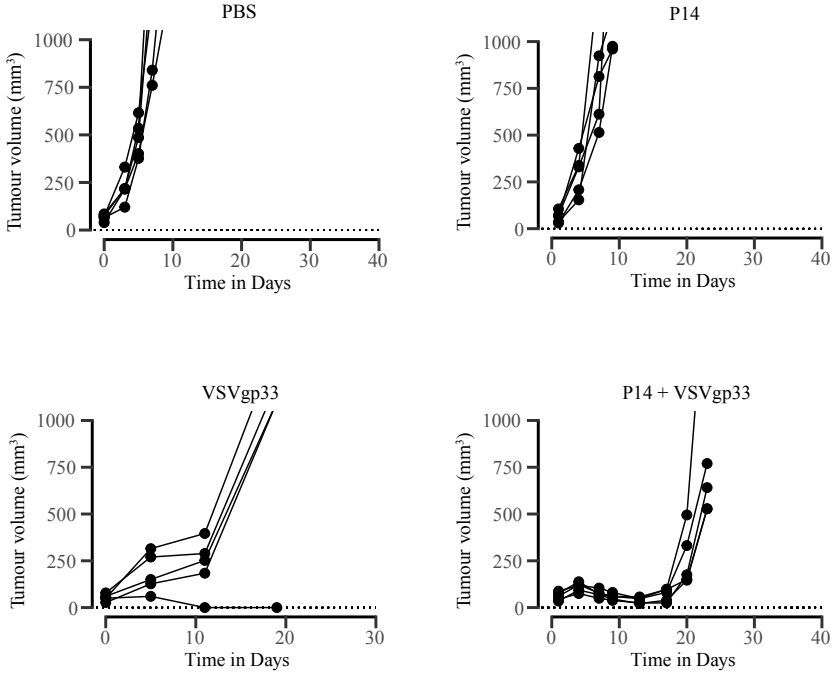
PBS
P14
VSVgp33
P14 + VSVgp33
Tumour volume (mm3)
0
250
500
750
1000
Time in Days
0
10
20
30
40

D

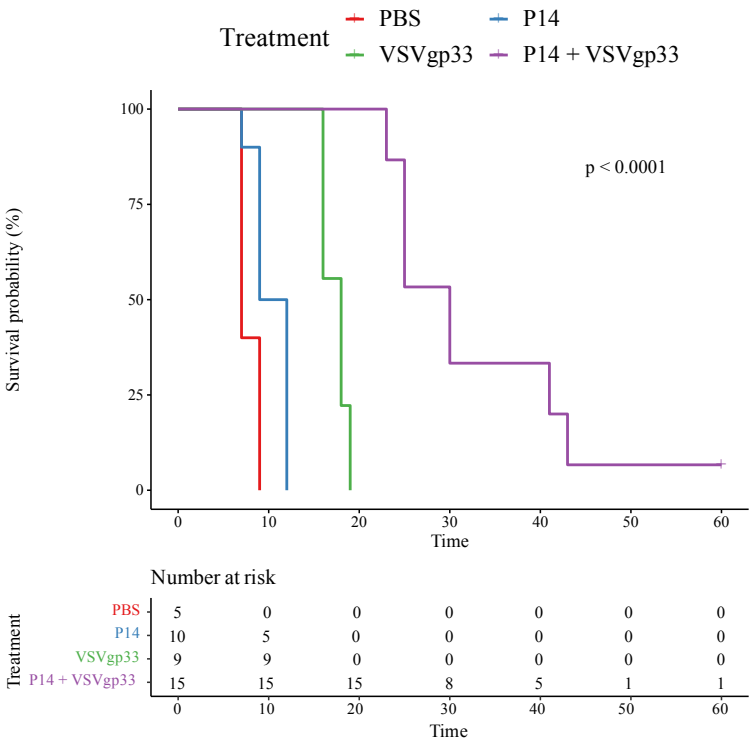

Figure 3.2 | Boosting ACT with oncolytic viral vaccines results in T cell expansion and tumour regression

(A) Schematic illustration showing the treatment protocol. (B) C57BL/6 mice (n=5) were intradermally implanted with $2x10^5$ B16gp33, and the 5-day old tumours were treated using $1x10^6$ adoptively transferred P14 T cells or PBS followed by either $1x10^8$ pfu VSVgp33 or PBS. At days 5 and 12 pvi, blood samples were collected, processed, stained for intracellular IFNγ and analyzed using flow cytometry. Data is presented as the percentage of $IFN\gamma^+$ gp33-specific $CD8^+$ T cells/total $CD8^+$ T cells in the peripheral circulation. Pairwise t-test with BH correction was performed to compare each pair of treatments at each time point independently. The horizontal bars represent means ± SEM (C) Tumour volumes were continuously measured every third day and are presented as length * width * height. (D) Overall survival was monitored for up to 60 days post tumour challenge. Mice from at least 2 independent experiments were pooled to calculate the survival statistics using log-rank test and create Kaplan-Meier plots. **p < 0.05, **p <0.01, ***p <0.001, ****p <0.0001*

day 5, while VSVgp33 alone treatment resulted in a mean of 2.68% ± 0.5%. ACT treatment with no OVV boosting led to undetectable responses **(Fig. 3.2 B)**. At day 12, the responses dropped to < 1% in all 3 conditions **(Fig. 3.2 B)**. The expansion of P14 T cells in ACT + OVV-treated mice correlated with remarkable tumour regression, where tumours were completely gone ~ 14 days pvi **(Fig. 3.2 C)**. On the other hand, ACT alone had no significant impact on tumour growth while VSVgp33 treatment slowed down tumour growth but caused no regression **(Fig. 3.2 C)**. This resulted in a statistically significant increase in overall mice survival (p value < 0.0001; log-rank test) **(Fig. 3.2 D)**. Unfortunately, the tumour regression observed in the P14 + VSVgp33-treated mice was short-lived and the mice developed relapsing tumours 10 days after remission.

3.2.3. Using Vaccinia virus-based OVV improves overall survival with less incidence of relapse

We next tested whether changing the OV backbone will have an influence on the therapeutic effect of ACT + OVV. Because of the initial data observed by Scott Walsh in the context of RIP-gp model, we elected to use Vaccinia virus (VacV) engineered to express gp_{33-41} epitope and assessed its efficacy in boosting P14 T cells and controlling B16gp33 tumours. To this end, B16gp33 tumours at a size of 50 – 100 mm^3 were treated using P14 T cells and VSVgp33 or VacVgp33 delivered IV **(Fig. 3.3 A)**. Although we did not observe a statistically significant difference in the levels of gp33-specific $IFN\gamma^+$ $CD8^+$ T cells in the circulation at days 5 and 12 pvi, there were some time-point-dependent disparities between the different virus treatments **(Fig. 3.3 B)**. P14 + VSVgp33 treatment resulted in a slightly higher levels of gp33-specific $IFN\gamma^+$ $CD8^+$ T cells at day 5 pvi with a mean of 12.3% ± 0.623% compared to a mean of 6.77% ± 0.327% in case of P14 + VacVgp33. At day 12 pvi, we observed higher levels of gp33-specific $IFN\gamma^+$ $CD8^+$ T cells in mice treated with P14 + VacVgp33 with a mean of 4.17% ± 0.523% compared to a mean of 1.32% ± 0.124%. Both viruses showed an equal ability to regress B16gp33 tumours in the initial phase of treatment **(Fig. 3.3 C)**. Despite the lack of significant differences in $CD8^+$ T cell

A

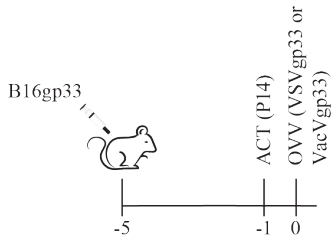
B16gp33
ACT (P14)
OVV (VSVgp33 or VacVgp33)
-5
-1
0

B

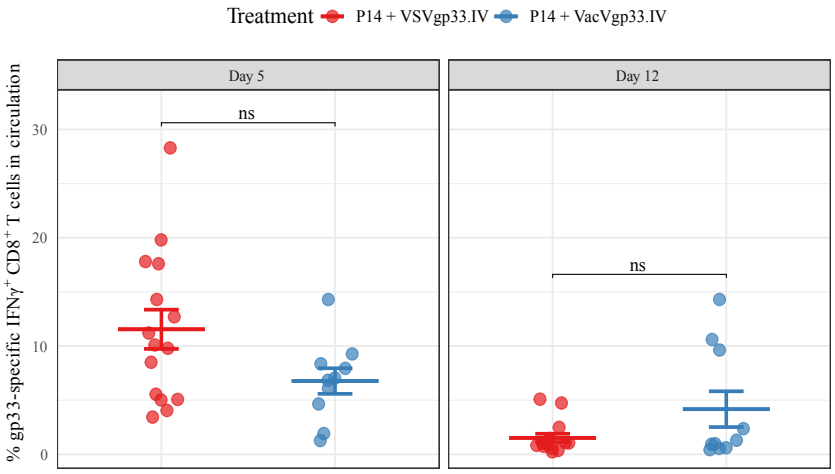
Treatment
P14 + VSVgp33.IV
P14 + VacVgp33.IV
Day 5
Day 12
ns
ns
% gp33-specific IFNγ+ CD8+ T cells in circulation
0
10
20
30

C

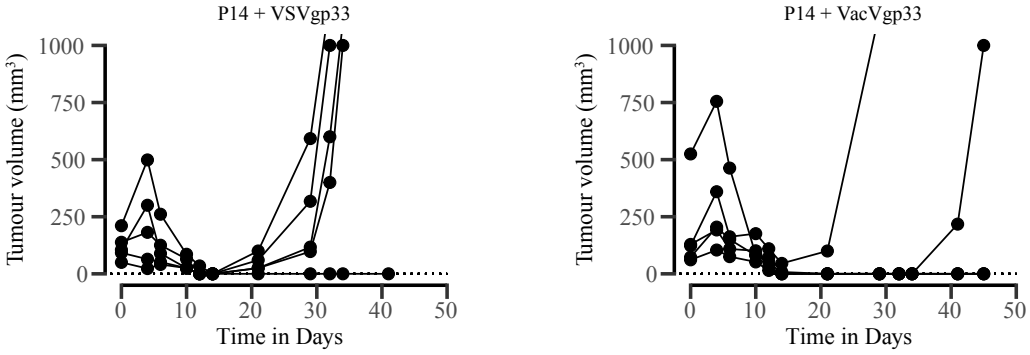
P14 + VSVgp33
P14 + VacVgp33
Tumour volume (mm3)
0
250
500
750
1000
0
10
20
30
40
50
Time in Days

D

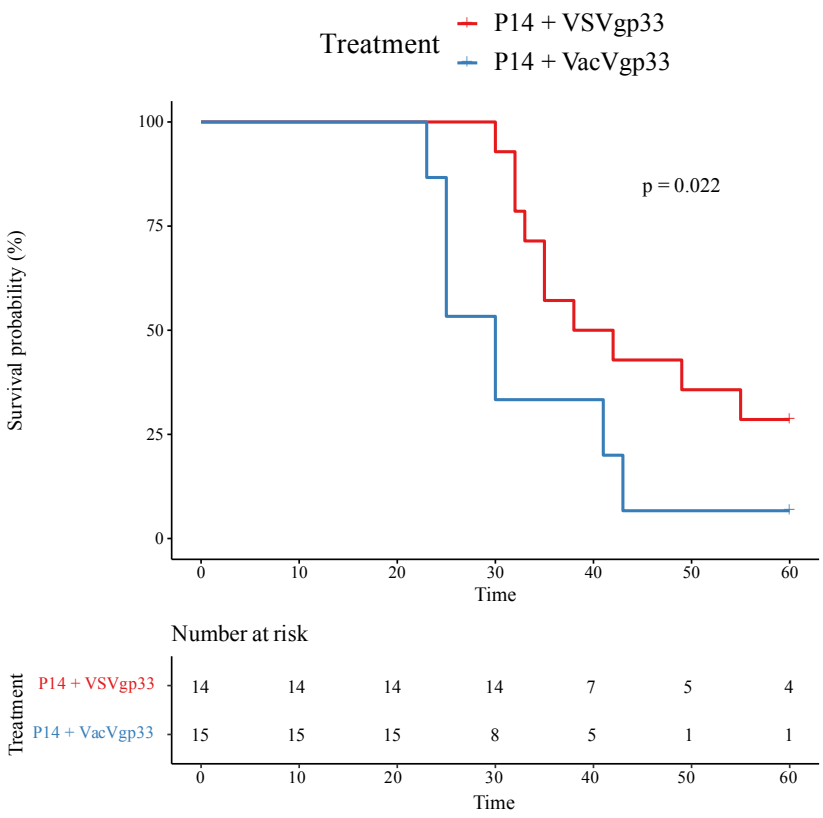
Treatment
P14 + VSVgp33
P14 + VacVgp33
Survival probability (%)
100
75
50
25
0
p = 0.022
0
10
20
30
40
50
60
Time
Number at risk
Treatment
P14 + VSVgp33
P14 + VacVgp33
14 14 14 14 7 5 4
15 15 15 8 5 1 1
0
10
20
30
40
50
60
Time

Figure 3.3 | Using Vaccinia virus-based OVV improves overall survival with less incidence of relapse

(A) Schematic illustration showing the treatment protocol. (B) C57BL/6 mice (n=5) were intradermally implanted with $2x10^5$ B16gp33, and the 5-day old tumours were treated using $1x10^6$ adoptively transferred P14 T cells followed by either $1x10^8$ pfu VSVgp33 or VacVgp33 delivered IV. At days 5 and 12 pvi, blood samples were collected, processed, stained for intracellular IFNγ and analyzed using flow cytometry. Data is presented as the percentage of $IFN\gamma^+$ gp33-specific $CD8^+$ T cells/total $CD8^+$ T cells in the peripheral circulation. Pairwise t-test with BH correction was performed to compare each pair of treatments at each time point independently. The horizontal bars represent means ± SEM (C) Tumour volumes were continuously measured every third day and are presented as length * width * height. (D) Overall survival was monitored for up to 60 days post tumour challenge. Mice from 3 independent experiments were pooled to calculate the survival statistics using log-rank test and create Kaplan-Meier plots. *$*p < 0.05$, **$p <0.01$, ***$p <0.001$, ****$p <0.0001$*

responses, mice treated with P14 + VacVgp33 showed a statistically significant improvement in overall survival with a median survival of 40 days in contrast to mice treated with P14 + VSVgp33 which had a median survival of 30 days (p value = 0.022; log-rank test) **(Fig. 3.3 D)**. Moreover, 4/14 mice (~ 28.57%) treated with P14 + VacVgp33 showed durable responses with no relapsing tumours. This is a clear improvement over the P14 + VSVgp33 treatment where only 1/15 mice (~ 6.67%) showed a durable response with no relapse.

3.2.4. VacV and VSV lead to different systemic immune landscapes

In order to get a better understanding of the effects of the different viral backbones on altering the immune populations in tumour-bearing mice, we treated B16gp33-bearing mice with either P14 + VSVgp33, P14 + VacVgp33, or PBS, followed by harvesting their blood, and spleens at days 1, 3 and 5 pvi. Organs for every 2 mice were pooled together into one sample to maximize the number of recovered immune cells. Table 3.1 summarizes the antibodies and their respective fluorescent channels used in this study. We analyzed $CD8^+$ T cells, $CD4^+$ T cells and NK cells. The frequency of these populations remained consistent at different times in the circulation of PBS treated mice **(Table 3.2, Fig. 3.4 A)**. P14 + VSVgp33 treatment led to an initial drop in the frequency of both $CD4^+$ and $CD8^+$ T cells in the circulation but not the NK cells at day 1 pvi. This drop in T cell frequency was transient and both $CD8^+$ and $CD4^+$ T cells recovered by day 3 pvi **(Table 3.2, Fig. 3.4 A)**. This is consistent with our collective observations in the Wan lab that VSV treatment causes transient lymphopenia. It is worth noting that the observed increase in the frequency of NK cells detected at day 1 pvi was not due to an increase in the numbers of NK cells. Rather, the drop in T cells resulted in the over-representation of NK cells. In P14 + VacVgp33-treated mice, we observed an increase in the total $CD8^+$ T cells at day 5 pvi (29.57% ± 2.42%) compared to both PBS and P14 + VSVgp33 treatments (19.43% ± 0.26% and 19.17% ± 0.63% respectively) **(Table 3.2, Fig. 3.4 A)**. Additionally, using ICS, we analyzed the frequency of gp33-specific $IFN\gamma^+$ $CD8^+$ T cells. At day 1 pvi, no detectable gp33-specific responses were detected

Table 3.1 | List of antibodies and their respective fluorescent channels used to stain blood and spleen samples

Marker	Fluorescent channel
CD3	BV605
CD8	BV711
CD4	PE-Cy7
NK1.1	APC
IFNg	PE
FOXP3	FITC
Thy1.1	APC-Cy7
Fixable viability dye	BV510

A

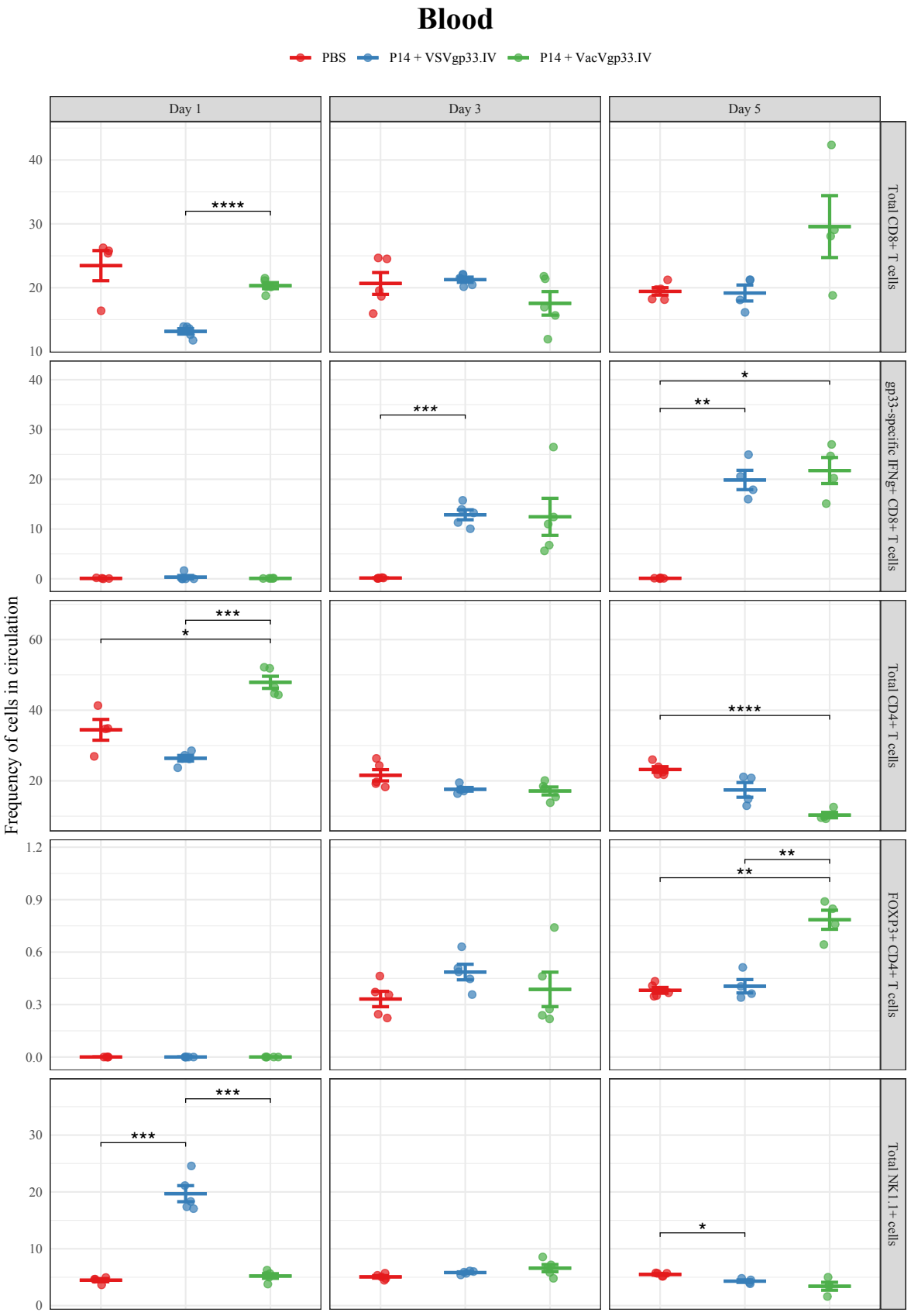
Blood
PBS
P14 + VSVgp33.IV
P14 + VacVgp33.IV
Day 1
Day 3
Day 5
Frequency of cells in circulation
Total CD8+ T cells
gp33-specific IFNg+ CD8+ T cells
Total CD4+ T cells
FOXP3+ CD4+ T cells
Total NK1.1+ cells

B

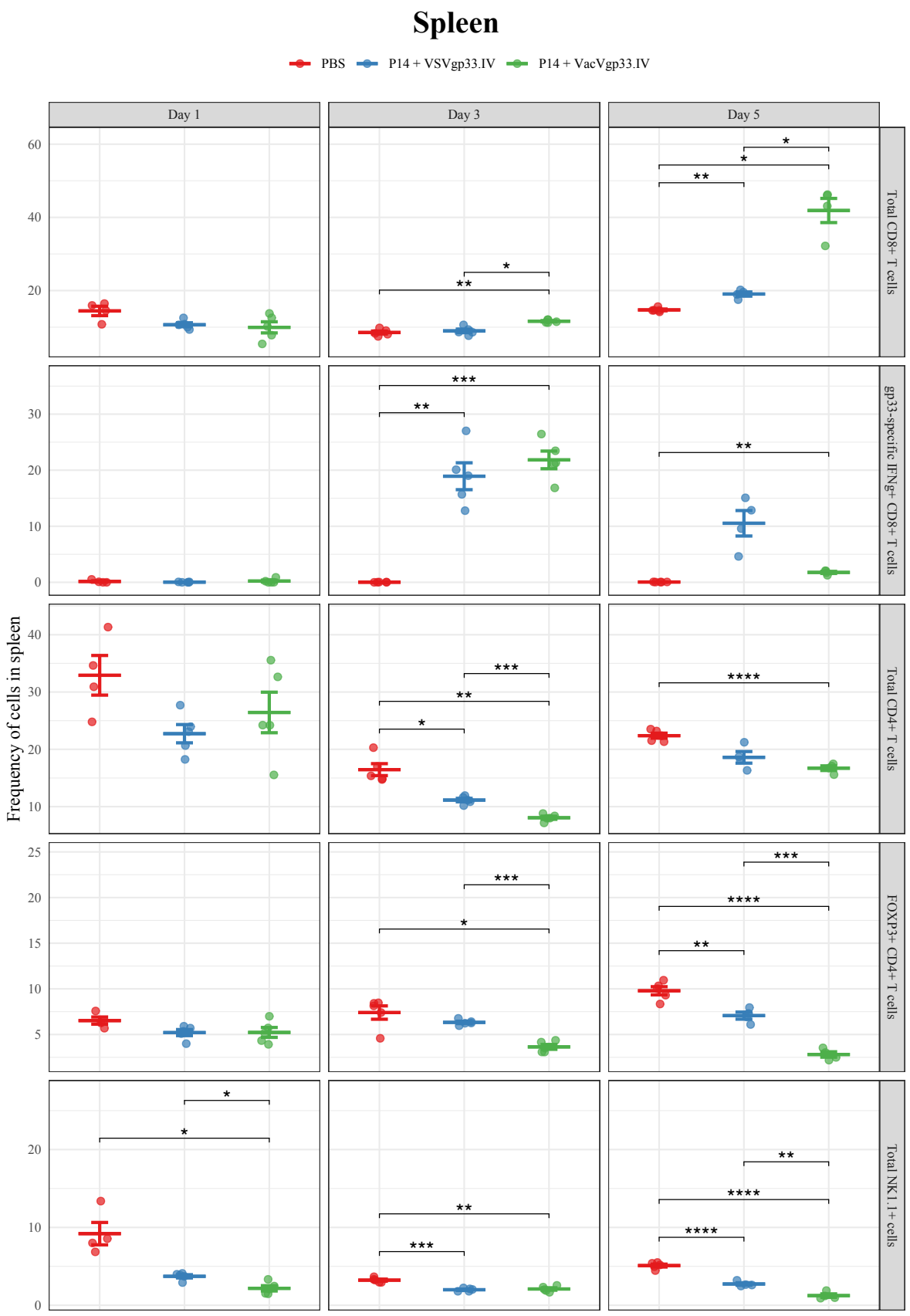
Spleen
PBS
P14 + VSVgp33.IV
P14 + VacVgp33.IV
Day 1
Day 3
Day 5
Frequency of cells in spleen
Total CD8+ T cells
gp33-specific IFNg+ CD8+ T cells
Total CD4+ T cells
FOXP3+ CD4+ T cells
Total NK1.1+ cells

Figure 3.4 | Lymphocyte analysis in blood and spleen following P14 + VacVgp33, P14 + VSVgp33 or PBS treatment.

C57BL/6 mice (n=10 / treatment / time point) were intradermally implanted with $2x10^5$ B16gp33 cells. 5 days later the mice were treated using $1x10^6$ adoptively transferred P14 T cells followed by 1 x 10^8 pfu VacVgp33 or VSVgp33 or PBS. At days 1, 3, and 5 post treatment, blood samples and spleens were collected, processed, stained for the shown surface and intracellular markers and analyzed using flow cytometry. Organs for every 2 mice were pooled together into one sample. Shown is the frequency of each cell population with respect to the total viable cells or the respective parent population in each organ. Pairwise t-test with BH correction was performed on each cell population at each time point independently. The horizontal bars represent means ± SEM. *$p < 0.05$, **$p < 0.01$, ***$p < 0.001$, ****$p < 0.0001$.

in the circulation. In both P14 + VSVgp33 and P14 + VacVgp33 treatments, we detected gp33-specific IFNγ$^+$ CD8$^+$ T cells at day 3 pvi at frequencies of 12.87% ± 0.45% and 12.45% ± 1.67% respectively. The responses peaked at day 5 pvi reaching 19.86% ± 0.97% and 21.75% ± 1.31% in P14 + VSVgp33 and P14 + VacVgp33 treatments respectively **(Table 3.2, Fig. 3.4 A)**. Consistent with what we had reported before, we observed no statistically significant difference in IFNγ$^+$ gp33-specific CD8$^+$ T cells between P14 + VacVgp33 and P14 + VSVgp33 treatment groups at any time point. Unlike P14 + VSVgp33 treatment, P14 + VacVgp33 led to a significant increase in the frequency of CD4$^+$ T cells in the circulation at day 1 pvi. This increase was transient and the frequency of CD4$^+$ T cells dropped as the frequency of CD8$^+$ T cells started to rise. Interestingly, P14 + VacVgp33 treatment led a statistically significant increase in the frequency of FOXP3$^+$ CD4$^+$ T cells (0.78% ± 0.03%) compared to both PBS (0.38% ± 0.01%) and P14 + VSVgp33 (0.4% ± 0.02%) groups. Nevertheless, the biological impact of such difference is questionable since the effect size is extremely small.

Consistent with what was observed in the circulation, P14 + VacVgp33 treatment led to an overall increase in the frequency of CD8$^+$ T cells day 5 pvi in the spleen **(Table 3.3, Fig. 3.4 B)**. The increase was statistically significant compared to both PBS and P14 + VSVgp33 groups (41.88% ± 1.65% vs. 14.72% ± 0.11% and 19.05% ± 0.29% respectively). At day 1 pvi, no IFNγ$^+$ gp33-specific CD8$^+$ T cells were detected. Interestingly, gp33-specific CD8$^+$ T cells in the spleen peaked at day 3 pvi in both P14 + VSVgp33 and P14 + VacVgp33 treatment groups (18.92% ± 1.07% and 21.83% ± 0.7% respectively). The observed drop in frequency at day 5 pvi could be due to the recruitment of cells out of the spleen to the tumour site. The frequency of both CD4$^+$ T cells and NK cells were lower in both P14 + VSVgp33 and P14 + VacVgp33 compared to PBS at all time-points **(Table 3.2, Fig. 3.4 A)**. Moreover, we observed a gradual increase in the frequency of FOXP3$^+$ CD4$^+$ T cells throughout the time course in PBS and P14 + VSVgp33 treatments. On the other hand, P14 + VacVgp33 treatment led to a gradual decrease in the frequency of the aforementioned cells **(Table 3.2, Fig. 3.4 A)**. At day 5 pvi, we detected a statistically significant difference in FOXP3$^+$ CD4$^+$ T cells between P14 + VacVgp33 treated mice

(2.81% ± 0.15%) and PBS (9.79% ± 0.2%) or P14 + VSVgp33 (7.07% ± 0.19%) treated mice. In summation, P14 + VacVgp33 treatment caused an increase in the overall $CD8^+$ T cell population in both the spleen and the peripheral circulation. It also resulted in reduced frequency of $NK1.1^+$ cells and $FOXP3^+$ $CD4^+$ T cells in the spleen compared to both PBS and P14 + VSVgp33 treated mice.

Table 3.2 | Time course showing the effect of different treatments on lymphocyte populations in peripheral blood of B16gp33 tumour-bearing mice. The data represents mean ± SEM

Treatment	Population	Day 1	Day 3	Day 5
PBS	Total $CD8^+$ T cells	23.46 % ± 1.18%	20.67% ± 0.76%	19.43% ± 0.26%
	gp33-specific $IFNg^+$ $CD8^+$ T cells	0.09% ± 0.02%	0.14% ± 0.01%	0.11% ± 0.01%
	Total $CD4^+$ T cells	34.45% ± 1.47%	21.58% ± 0.71%	23.2% ± 0.36%
	$FOXP3^+$ $CD4^+$ T cells	0% ± 0%	0.33% ± 0.02%	0.38% ± 0.01%
	Total $NK1.1^+$ cells	4.47% ± 0.14%	5.06% ± 0.1%	5.49% ± 0.06%
P14 + VSVgp33.IV	Total $CD8^+$ T cells	13.16% ± 0.19%	21.26% ± 0.18%	19.17% ± 0.63%
	gp33-specific $IFNg^+$ $CD8^+$ T cells	0.33% ± 0.15%	12.87% ± 0.45%	19.86% ± 0.97%
	Total $CD4^+$ T cells	26.4% ± 0.35%	17.61% ± 0.23%	17.44% ± 1.04%
	$FOXP3^+$ $CD4^+$ T cells	0% ± 0%	0.49% ± 0.02%	0.4% ± 0.02%
	Total $NK1.1^+$ cells	19.7% ± 0.63%	5.81% ± 0.06%	4.31% ± 0.11%
P14 + VacVgp33.IV	Total $CD8^+$ T cells	20.32% ± 0.21%	17.55% ± 0.83%	29.57% ± 2.42%
	gp33-specific $IFNg^+$ $CD8^+$ T cells	0.09% ± 0.01%	12.45% ± 1.67%	21.75% ± 1.31%
	Total $CD4^+$ T cells	47.9% ± 0.77%	17.14% ± 0.5%	10.31% ± 0.38%
	$FOXP3^+$ $CD4^+$ T cells	0% ± 0%	0.39% ± 0.04%	0.78% ± 0.03%
	Total $NK1.1^+$ cells	5.21% ± 0.18%	6.6% ± 0.28%	3.41% ± 0.35%

Table 3.3 | Time course showing the effect of different treatments on lymphocyte populations in spleen of B16gp33 tumour-bearing mice. The data represents mean ± SEM

Treatment	Population	Day 1	Day 3	Day 5
PBS	Total $CD8^+$ T cells	14.44% ± 0.64%	8.55% ± 0.18%	14.72% ± 0.11%
	gp33-specific $IFNg^+$ $CD8^+$ T cells	0.15% ± 0.06%	0.02% ± 0%	0.05% ± 0%
	Total $CD4^+$ T cells	32.92% ± 1.73%	16.46% ± 0.47%	22.39% ± 0.2%
	$FOXP3^+$ $CD4^+$ T cells	6.52% ± 0.2%	7.4% ± 0.33%	9.79% ± 0.2%
	Total $NK1.1^+$ cells	9.2% ± 0.72%	3.23% ± 0.06%	5.1% ± 0.08%
P14 + VSVgp33.IV	Total $CD8^+$ T cells	10.67% ± 0.24%	8.99% ± 0.22%	19.05% ± 0.29%
	gp33-specific $IFNg^+$ $CD8^+$ T cells	0.03% ± 0.01%	18.92% ± 1.07%	10.53% ± 1.14%
	Total $CD4^+$ T cells	22.73% ± 0.71%	11.14% ± 0.14%	18.6% ± 0.51%
	$FOXP3^+$ $CD4^+$ T cells	5.21% ± 0.15%	6.33% ± 0.06%	7.07% ± 0.19%
	Total $NK1.1^+$ cells	3.72% ± 0.09%	1.99% ± 0.04%	2.73% ± 0.08%
P14 + VacVgp33.IV	Total $CD8^+$ T cells	9.96% ± 0.68%	11.63% ± 0.08%	41.88% ± 1.65%
	gp33-specific $IFNg^+$ $CD8^+$ T cells	0.22% ± 0.08%	21.83% ± 0.7%	1.77% ± 0.09%
	Total $CD4^+$ T cells	26.43% ± 1.58%	8.06% ± 0.12%	16.71% ± 0.2%
	$FOXP3^+$ $CD4^+$ T cells	5.23% ± 0.24%	3.64% ± 0.12%	2.81% ± 0.15%
	Total $NK1.1^+$ cells	2.18% ± 0.15%	2.09% ± 0.07%	1.24% ± 0.11%

Chapter 4 — Evaluating the effect of OVV route of administration on the efficacy of ACT + OVV

4.1. Introduction

The route of OV administration is currently an area of debate in the field. Local vs. systemic delivery offers distinct set of benefits as well as some limitations. On one hand, local delivery of OVs using IT injection ensures the highest concentration of virions in the TME. On the other hand, inaccessible tumours or multiple metastatic tumours represent a challenge to IT delivery and systemic routes are better suited in these situations. The argument against IV delivery is the premature neutralization and clearance of OVs in the circulation reducing the total number of virions to arrive at the TME. In the context of ACT + OVV, choosing the optimum route of administration is complicated by the necessity to expand the transferred T cells in the periphery before recruiting them to the TME. As such, we believe that each virus is unique in its requirement for a specific route of administration to achieve the best outcomes. In the previous chapter, we demonstrated the synergy and complementarity between ACT and OVV. We also highlighted the difference in therapeutic efficacy when using different viral backbones. In this chapter we aim to address the effect of different routes of administration on the efficacy of ACT + OVV. Our results demonstrate that IT injection of VSV resulted in lower magnitude of T cell responses compared to IV injection. VacV on the other hand, led to T cell expansion to comparable levels following IV or IT injections. Despite the differences in T cell expansion profiles, IT delivery of both VSV and VacV following ACT showed a trend of better overall survival of mice. The effect on survival was statistically significant only in case of VacV. Additionally, we did not detect significant differences in the immune infiltrates in the TME following IT or IV administration of VSV or VacV. This data highlights the flexibility of VacV as a vaccine since both IT and IV routes result in comparable T cell expansion. Moreover, the significant improvement in the overall survival observed following VacV IT injection correlated with more virus infection and replication within the TME as detected by LacZ reporter staining.

4.2. Results

4.2.1. Intratumoural injection of OVVs leads to better tumour control and improves the overall mice survival with less incidence of relapse

While P14 + VacVgp33 treatment offered an incremental improvement over the P14 + VSVgp33 treatment, ~ 70% of the treated mice developed relapsing tumours. This prompted us to test whether the local presence of OVVs within the TME would lead to improved outcomes. Hence, we decided to deliver OVVs intratumourally rather than intravenously to maximize their presence in the TME. B16gp33 tumours at a size of 50 - 100 mm^3 were treated using P14 T cells and VSVgp33 or VacVgp33 delivered IT. We first compared IT and IV delivery of each virus to determine the effect of changing the route of delivery on T cell expansion, tumour control and overall survival. IT delivery of VSVgp33 led to a lower magnitude of gp33-specific $CD8^+$ T cell response (4.11% ± 0.121%), which is a statistically significant decrease compared to the IV route (*p* value = 0.0011, t test) **(Fig. 4.1 A)**. The inferior ability of VSVgp33 to boost P14 T cells when delivered IT is consistent with what was observed previously at the Wan lab[187,188]. Interestingly however, the lower magnitude of responses in the circulation did not correlate with worse tumour control nor with overall survival **(Fig 4.1 B-C)**. The median survival of mice treated with P14 + VSVgp33 IT was 32 days which is a slight increase over P14 + VSVgp33. IV treatment (30 days). Additionally, 4/20 mice (20%) were completely cured and showed no relapse, which is indeed an improvement over the outcome observed with P14 + VSVgp33.IV (6.67%). Despite the better trend seen with IT delivery of VSVgp33, the difference in survival, however, was not statistically significant. P14 + VacVg33 IT treatment led to the of expansion of P14 T cells at day 5 pvi to a magnitude of 12.3% ± 0.517% which is higher compared to P14 + VacVgp33.IV (6.77% ± 0.374%) **(Fig. 4.1 D)**. This points to the flexibility of VacV in boosting $CD8^+$ T cells through multiple routes of injection. Moreover, mice treated with P14 + VacVgp33 IT had a statistically significant increase in the overall survival where 17/25 mice or 68% were

A

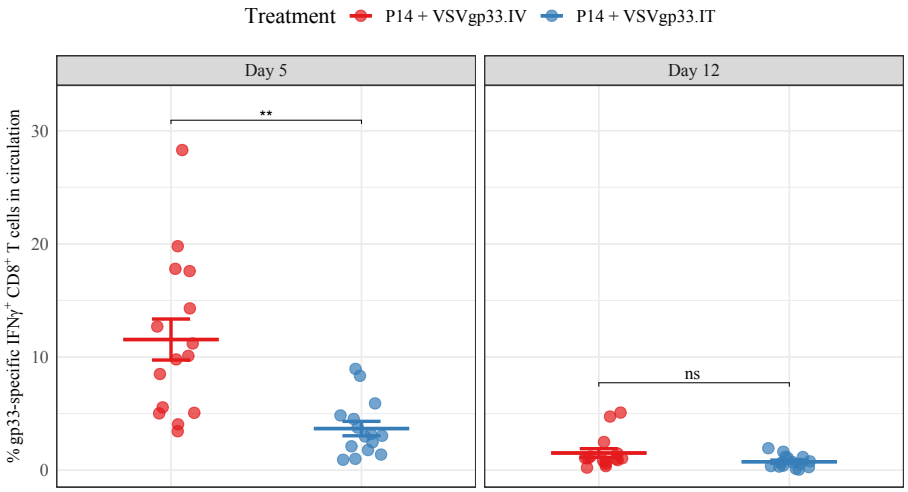
Treatment
P14 + VSVgp33.IV
P14 + VSVgp33.IT
Day 5
Day 12
**
ns
% gp33-specific IFNγ+ CD8+ T cells in circulation
0
10
20
30

B

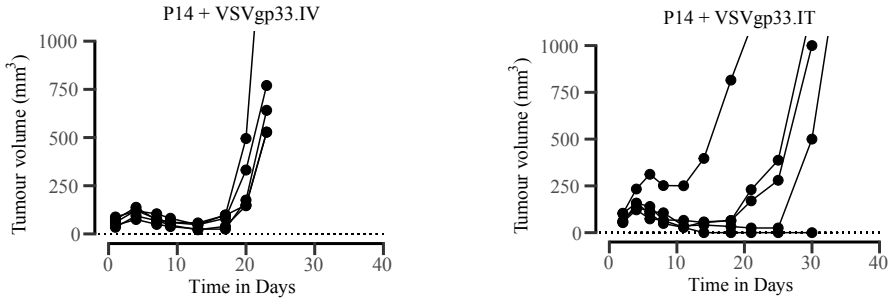
P14 + VSVgp33.IV
P14 + VSVgp33.IT
Tumour volume (mm3)
0
250
500
750
1000
0
10
20
30
40
Time in Days

C

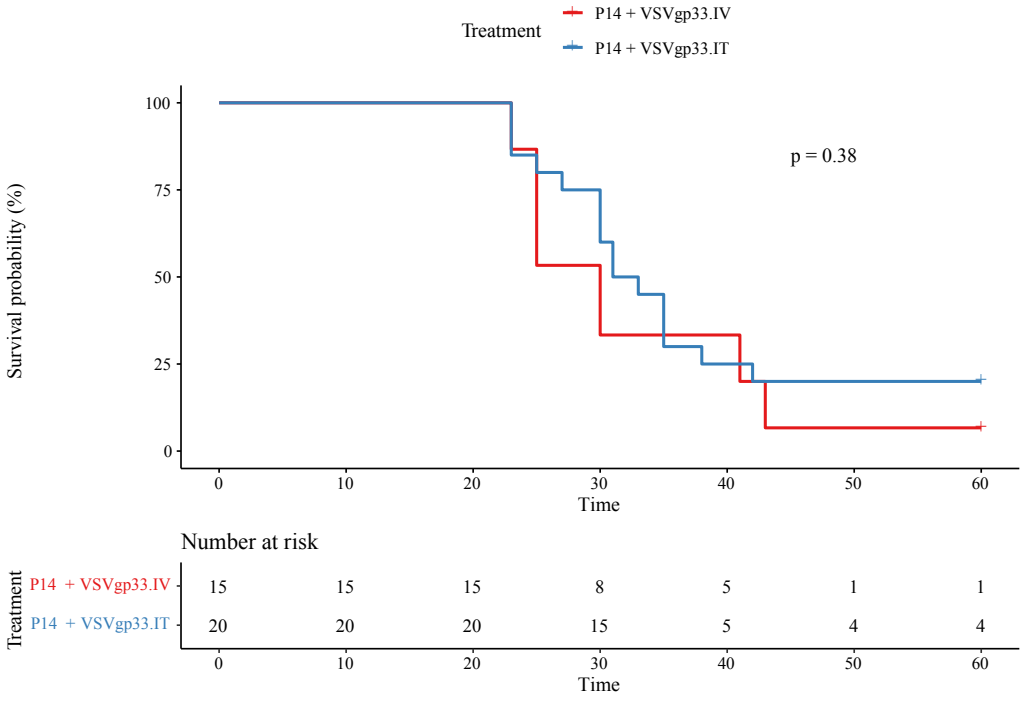
Treatment
P14 + VSVgp33.IV
P14 + VSVgp33.IT
Survival probability (%)
0
25
50
75
100
p = 0.38
0
10
20
30
40
50
60
Time
Number at risk
Treatment
P14 + VSVgp33.IV
P14 + VSVgp33.IT
15 15 15 8 5 1 1
20 20 20 15 5 4 4
0
10
20
30
40
50
60
Time

D

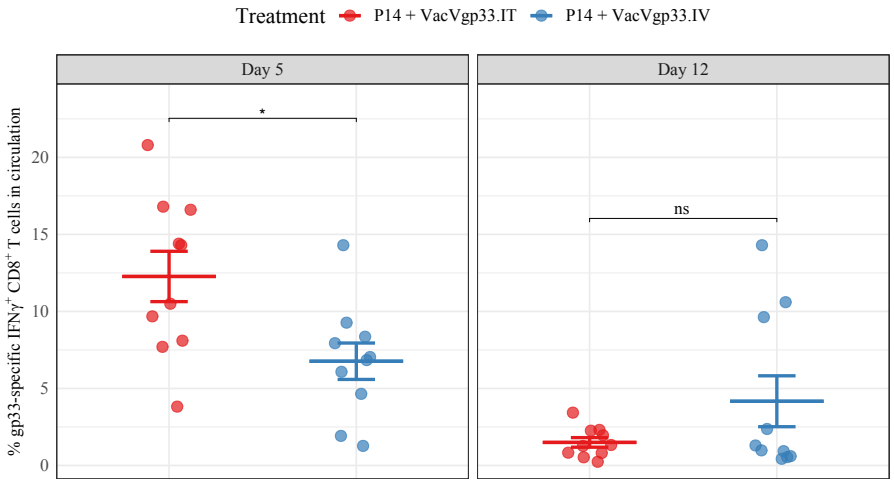
Treatment
P14 + VacVgp33.IT
P14 + VacVgp33.IV
Day 5
Day 12
% gp33-specific IFNγ+ CD8+ T cells in circulation
*
ns
0
5
10
15
20

E

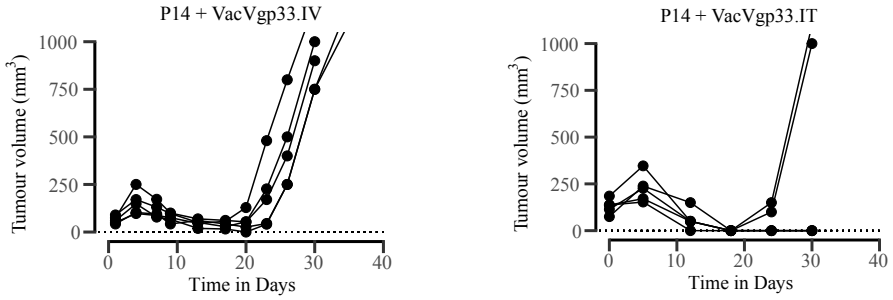
P14 + VacVgp33.IV
P14 + VacVgp33.IT
Tumour volume (mm3)
Time in Days
0
250
500
750
1000
0
10
20
30
40

F

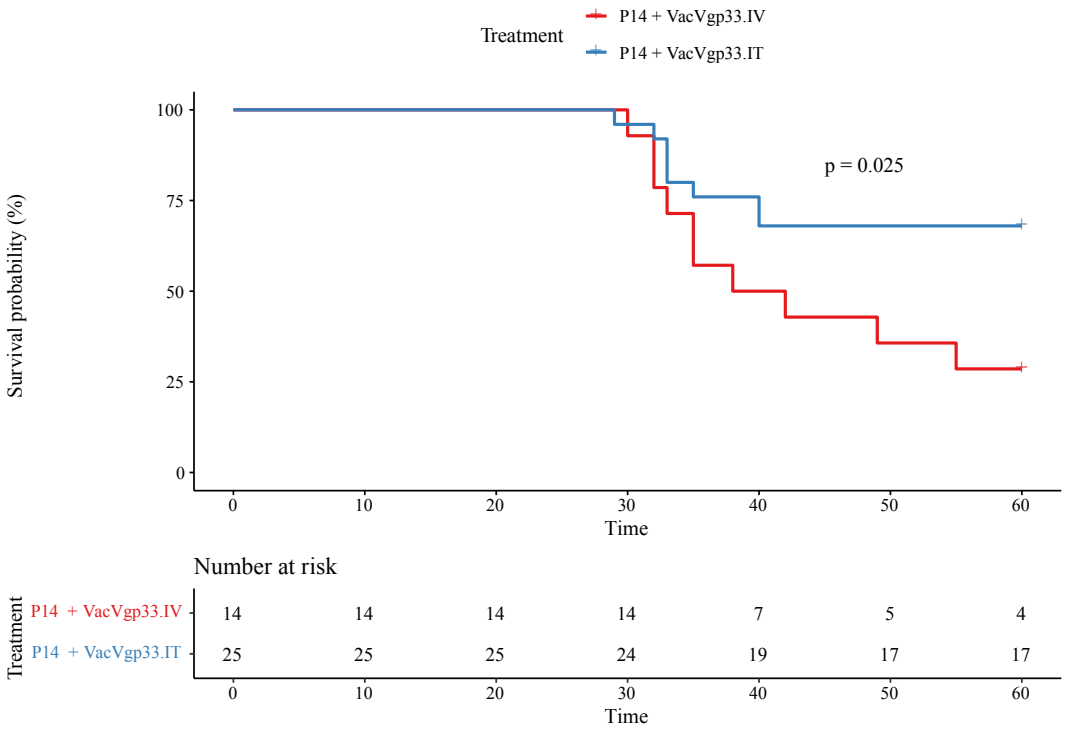
Treatment
P14 + VacVgp33.IV
P14 + VacVgp33.IT
Survival probability (%)
p = 0.025
Time
Number at risk
P14 + VacVgp33.IV 14 14 14 14 7 5 4
P14 + VacVgp33.IT 25 25 25 24 19 17 17
0
10
20
30
40
50
60
0
25
50
75
100

G

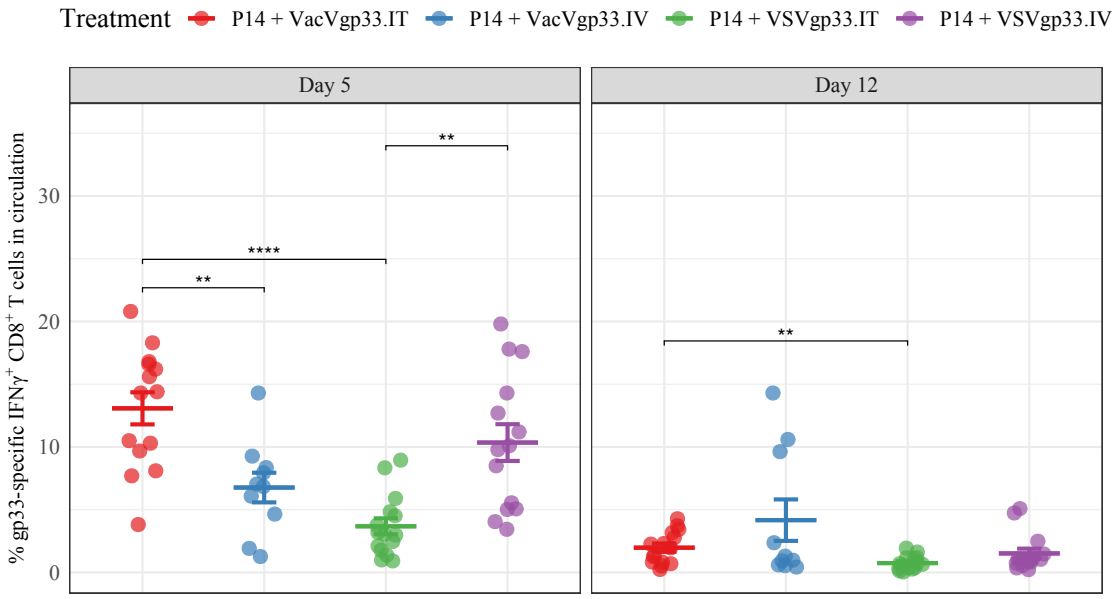
Treatment
P14 + VacVgp33.IT
P14 + VacVgp33.IV
P14 + VSVgp33.IT
P14 + VSVgp33.IV
Day 5
Day 12
% gp33-specific IFNγ+ CD8+ T cells in circulation
0
10
20
30
**
****
**
**

H

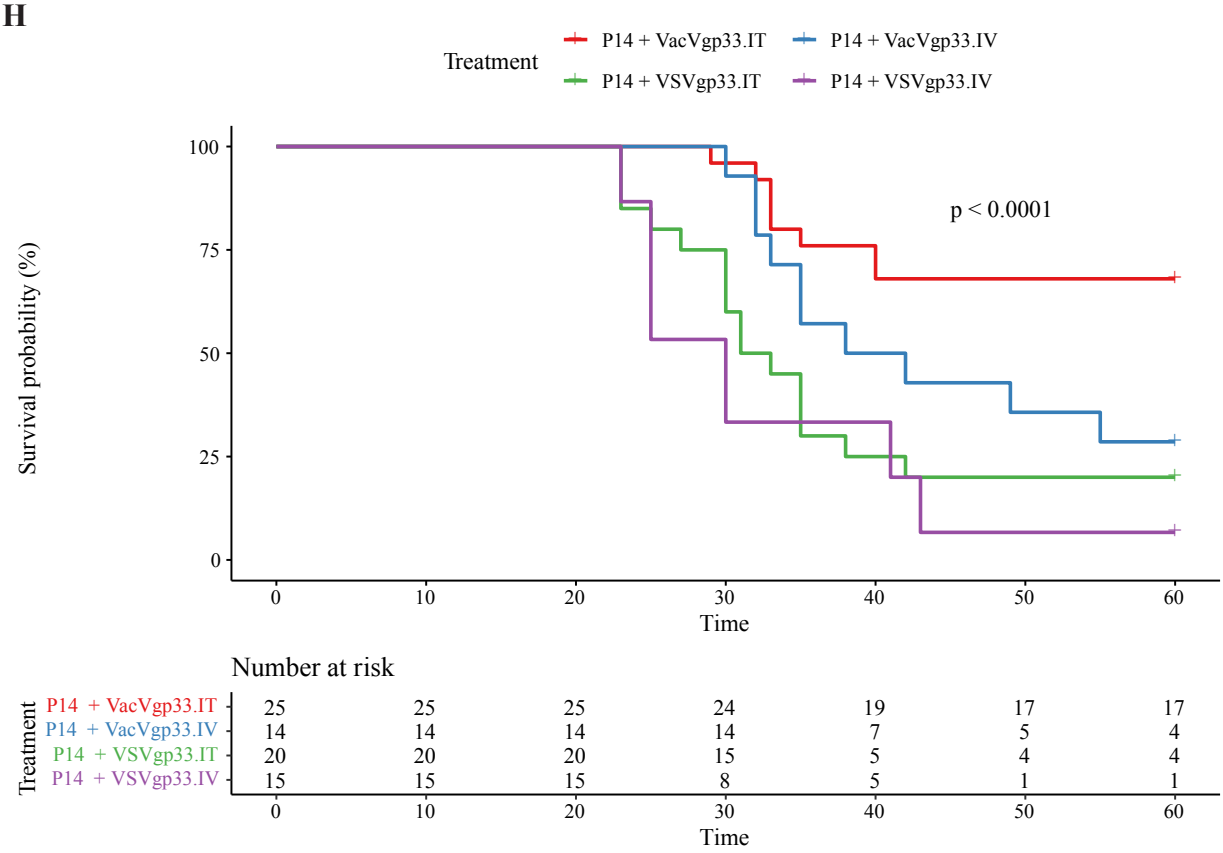
Treatment
P14 + VacVgp33.IT
P14 + VacVgp33.IV
P14 + VSVgp33.IT
P14 + VSVgp33.IV
Survival probability (%)
0
25
50
75
100
p < 0.0001
0
10
20
30
40
50
60
Time
Number at risk
Treatment
P14 + VacVgp33.IT 25 25 25 24 19 17 17
P14 + VacVgp33.IV 14 14 14 14 7 5 4
P14 + VSVgp33.IT 20 20 20 15 5 4 4
P14 + VSVgp33.IV 15 15 15 8 5 1 1
0 10 20 30 40 50 60
Time

Figure 4.1 | Intratumoural injection of OVVs leads to better tumour control and improves the overall mice survival with less incidence of relapse

C57BL/6 mice (n = 5) were intradermally implanted with $2x10^5$ B16gp33 cells. 5 days later the mice were treated using $1x10^6$ adoptively transferred P14 T cells followed by 1 x 10^8 pfu VacVgp33 or VSVgp33 delivered IT or IV. (A, D, G) At days 5 and 12 pvi, blood samples were collected, processed, stained for intracellular IFNγ and analyzed using flow cytometry. Data is presented as the percentage of $IFN\gamma^+$ gp33-specific $CD8^+$ T cells/total $CD8^+$ T cells in the peripheral circulation. Pairwise t-test with BH correction was performed to compare each pair of treatments at each time point independently. The horizontal bars represent means ± SEM (B,E) Tumour volumes were continuously measured every third day and are presented as length * width * height. (C, F, H) Overall survival was monitored for up to 60 days post tumour challenge. Mice from at least 3 independent experiments were pooled to calculate the survival statistics using log-rank test and create Kaplan-Meier plots. *$p < 0.05$, **$p < 0.01$, ***$p < 0.001$, ****$p < 0.0001$

cured and remained tumour free compared to only 28.57% in mice treated with P14 + VacVgp33. IV (p value = 0.025; log-rank test) **(Fig. 4.1 E-F)**. Finally, we compared IT and IV routes using both VSV and VacV backbones in terms of the magnitude of gp33-specific responses and overall mice survival. P14 + VacVgp33 IT was superior compared to both P14 + VacVgp33 IV and P14 + VSVgp33 IT with regards to the magnitude of gp33-specific responses at day 5 pvi **(Fig. 4.1 G)**. However, no statistically significant difference was found when comparing P14 + VacVgp33 IT to P14 + VSVgp33 IV. Moreover, P14 + VacVgp33 IT treated mice showed a statistically significant difference in overall survival compared to the three other treatment groups (p value <0.0001; log-rank test) **(Fig. 4.1 H)**. In conclusion, IT delivery of both VSV and VacV resulted in better tumour control and improved overall survival compared to IV delivery, but this difference was most obvious and only reached significance in the context of VacV treatment.

4.2.2. Intratumoural analysis reveals no difference in tumour infiltrating immune cells following IT and IV delivery of OVVs

In order to further characterize the differences between IT and IV delivery of OVVs, we sought to analyze the immune infiltrates in the TME following OVV delivery using both routes. To this end, B16gp33 tumour-bearing mice were treated using P14 T cells and VSVgp33 or VacVgp33 or PBS delivered IT or IV. 4 days later, the mice were euthanized, and the tumours were harvested for further analysis. We relied on a combination of mechanical breakdown of tumour tissue followed by enzymatic digestion to break down the extracellular matrix and release the infiltrating immune cells. Immune cells were then purified using a CD45 antibody magnetic selection kit, stained, and analyzed using flow cytometry. Table 3.4 shows a list of the antibodies used in this study. We first calculated the frequencies of different cellular populations relative to the total viable leukocytes recovered from each tumour **(Table 4.1 and Fig. 4.2 A)**. In PBS treated mice, we observed that $CD11b^+$ cells were the predominant population in the TME representing 12.9% ± 1.56%, $CD8^+$ T cells and $CD11c^+$ DCs followed at 8.24% ± 1.54% and 6.91% ± 1.53%

Table 4.1 | List of antibodies and their respective fluorescent channels used to stain tumour samples

Antibody	Fluorescent channel
CD3	BV605
CD8	BV711
CD4	APC-Cy7
NK1.1	APC
CD11b	PE
CD11c	BV421
Ly6G	PerCP-Cy5.5
Ly6C	FITC
FVS	BV510

Table 4.2 | Frequency of cell populations in TME 4 days after treatment

Treatment	$CD8^+$ T cells	Total $CD11b^+$ cells	$NK1.1^+$ cells	$CD4^+$ T cells	Total $CD11c^+$ cells
PBS	8.24% ± 1.54%	12.93% ± 1.56%	2.87% ± 0.48%	5.65% ± 1.07%	6.91% ± 1.53%
P14 + VacVgp33 IT	48.19% ± 0.71%	25.64% ± 1.62%	7.38% ± 0.54%	3.05% ± 0.33%	2.99% ± 0.16%
P14 + VacVgp33 IV	55.76% ± 1.57%	24.48% ± 1.85%	3.64% ± 0.31%	3.41% ± 0.17%	2.3% ± 0.1%
P14 + VSVgp33 IT	30.99% ± 2.38%	31.79% ± 0.34%	8.76% ± 0.92%	4.22% ± 0.59%	3.57 % ± 0.35%
P14 + VSVgp33 IV	35.57% ± 2.09%	34.04% ± 1.76%	7.33% ± 0.35%	3.71% ± 0.25%	4.56% ± 0.15%

A

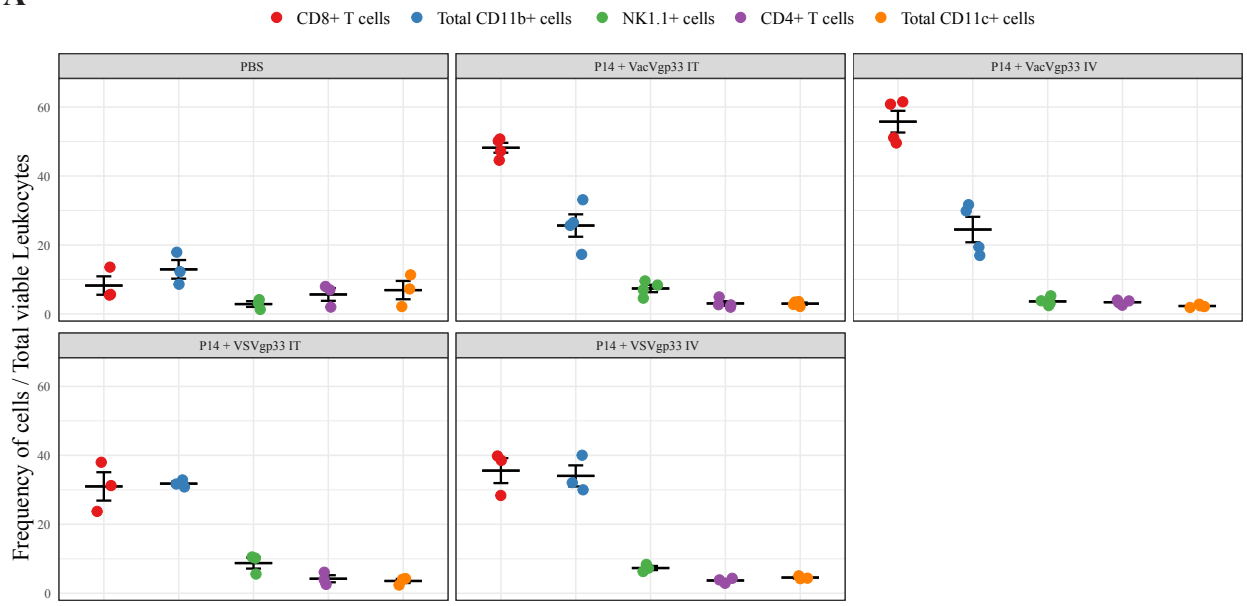
CD8+ T cells
Total CD11b+ cells
NK1.1+ cells
CD4+ T cells
Total CD11c+ cells
PBS
P14 + VacVgp33 IT
P14 + VacVgp33 IV
P14 + VSVgp33 IT
P14 + VSVgp33 IV
Frequency of cells / Total viable Leukocytes
0
20
40
60

B

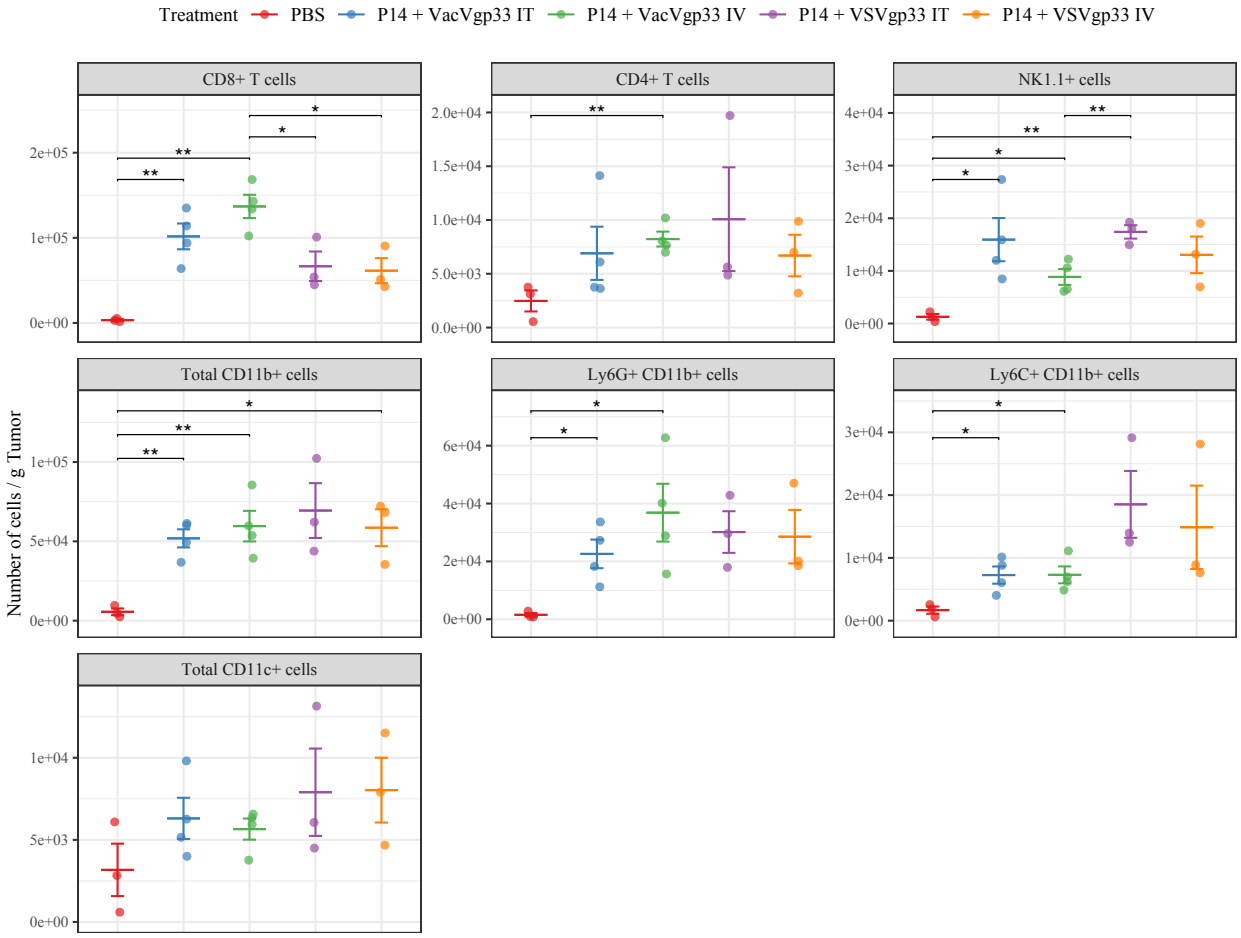
Treatment
PBS
P14 + VacVgp33 IT
P14 + VacVgp33 IV
P14 + VSVgp33 IT
P14 + VSVgp33 IV
CD8+ T cells
CD4+ T cells
NK1.1+ cells
Total CD11b+ cells
Ly6G+ CD11b+ cells
Ly6C+ CD11b+ cells
Total CD11c+ cells
Number of cells / g Tumor

Figure 4.2 | Intratumoural analysis reveals no difference in tumour infiltrating immune cells following IT or IV delivery of OVVs

C57BL/6 mice (n = 4) were intradermally implanted with $2x10^5$ B16gp33 cells. 5 days later the mice were treated using $1x10^6$ adoptively transferred P14 T cells followed by 1 x 10^8 pfu VacVgp33 (IT or IV) or VSVgp33 (IT or IV) or PBS (IT). At day 4 post treatment, the mice were euthanized and the tumours were collected, processed, stained for the shown surface markers and analyzed using flow cytometry. Shown is the frequency of each cell population with respect to the total viable cells recovered for every tumour (A) and the number of cells normalized to the respective weights of the tumours in g (B). Pairwise t-test with BH correction was performed on each cell population independently. The horizontal bars represent means ± SEM. *P < 0.05, **P<0.01, ***P<0.001, ****P<0.0001.

respectively. $CD4^+$ T cells and $NK1.1^+$ cells represented the two populations with least presence at 5.65% ± 1.07% and 2.87% ± 0.48% respectively. We were indeed excited to observe that ACT + OVV treatment altered the presence of different immune populations within the TME. Both VSV and VacV markedly increased the presence of $CD8^+$ T cells in the TME compared to PBS. Nevertheless, noticeable differences were observed among the two viruses. In mice treated with P14 + VacVgp33, $CD8^+$ T cells represented 48.19% ± 0.71% and 55.76 ± 1.57% of the total immune cells within the TME in case of IT and IV delivery respectively. P14 + VSVgp33 treated mice on the other hand had a lower frequency of $CD8^+$ T cells representing 30.99% ± 2.38% for IT delivery and 35.57% ± 2.09% for IV delivery. Alternatively, a higher frequency of $CD11b^+$ cells were detected in tumours treated with P14 + VSVgp33 (31.79% ± 0.34% for IT and 34.04% ± 1.76% for IV) compared to P14 + VacVgp33 (25.64% ± 1.62% for IT and 24.48% ± 1.85% for IV). To compare the changes in different populations of cells more accurately, we normalized the number of cells recovered from every tumour to its respective weight. In both VSV and VacV treatments, no statistically significant difference was found between IT and IV routes **(Fig 4.2 B)**. A higher number of $CD8^+$ T cells were recovered from tumours treated with P14 + VacVgp33. The difference was statistically significant when comparing P14 + VacVgp33 IV to P14 + VSVgp33 IT and P14 + VSVgp33 IV. $CD4^+$ T cells represented a smaller population of cells and showed no statistically significant differences between both viruses and routes. Interestingly, IT delivery of both viruses resulted in more $NK1.1^+$ cells infiltration in the TME. Nevertheless, the difference in $NK1.1^+$ frequency between routes was not statistically significant. With regards to myeloid populations in the TME, we did not observe a statistically significant difference between the two viruses in terms of the total $CD11b^+$ cells. Nevertheless, most myeloid cells recovered from P14 + VacVgp33 treated mice were $Ly6G^+$ $Ly6C^{int}$ cells (markers typically expressed by neutrophils or granulocytic-myeloid derived suppressor cells [G-MDSCs]). On the contrary, P14 + VSVgp33 resulted in the recruitment of equal proportions of $Ly6G^+$ $Ly6C^{int}$ and $Ly6G^-$ $Ly6C^{int/hi}$ cells (markers that are typically expressed by inflammatory monocytes and monocytic-myeloid derived suppressor cells [M-MDSCs]). In conclusion, it appears that the route of virus delivery

for both VacVgp33 and VSVgp33 had only minimal effects on the observed changes in cellular populations, making it difficult to reconcile differences in therapeutic outcome based on immune cell recruitment.

4.2.3. Intravenous and Intratumoural delivery of vaccinia virus result in T cell proliferation in different anatomical locations

We next studied the site(s) of antigen presentation and initial $CD8^+$ T cell proliferation to get a better understanding of how VacV drives the proliferation of $CD8^+$ T cells following different routes of delivery. We used Fingolimod (FTY720), a sphingosine 1- phosphate (S1P) receptor modulator, which blocks the S1P-dependent egress of lymphocytes from secondary lymphoid organs[274] to stop the circulation of P14 T cells. FTY720 caused the retention of the P14 T cells in the spleen and lymph nodes and allowed us to observe the anatomical locations where antigen presentation and initial $CD8^+$ T cell proliferation occur. B16gp33 tumour-bearing mice were treated with $Thy1.1^+$P14 T cells followed by VacVgp33 delivered IV or IT or PBS in the presence of FTY720. The frequency of P14 T cells was assessed in various lymphoid tissues (spleen, draining lymph nodes (DLNs), non-draining lymph nodes (NDLNs), and bone marrow) on days 1, 2, and 3 pvi. Using flow cytometry we quantified the number of P14 cells expressing Ki67, a nuclear protein associated with cell proliferation[275]. The earliest evidence of a proliferative response was observed at day 2 pvi **(Fig. 4.3 A)**. We calculated the fold change in $Ki67^+$ $Thy1.1^+$ P14 T cells from day 1 to day 2 and found that, in case of IV delivery, the spleen and bone marrow are the major sites of early T cell proliferation **(Fig. 4.3 B)**. Additionally, IV delivery of the VacV resulted in a relatively delayed (and a lower magnitude) proliferative response in DLNs and NDLNs, which was evident by the fold change in $Ki67^+$ $Thy1.1^+$ P14 T cells from day 1 to day 3 **(Fig. 4.3 B)**. IT delivery was found to induce a slower proliferative response, where no significant fold change in $Ki67^+$ $Thy1.1^+$ P14 T cells was observed from day 1 to day 2. At day 3 pvi, we detected 42 folds of increase in $Ki67^+$ $Thy1.1^+$ P14 T cells in the DLNs **(Fig. 4.3 B)**. Although

A

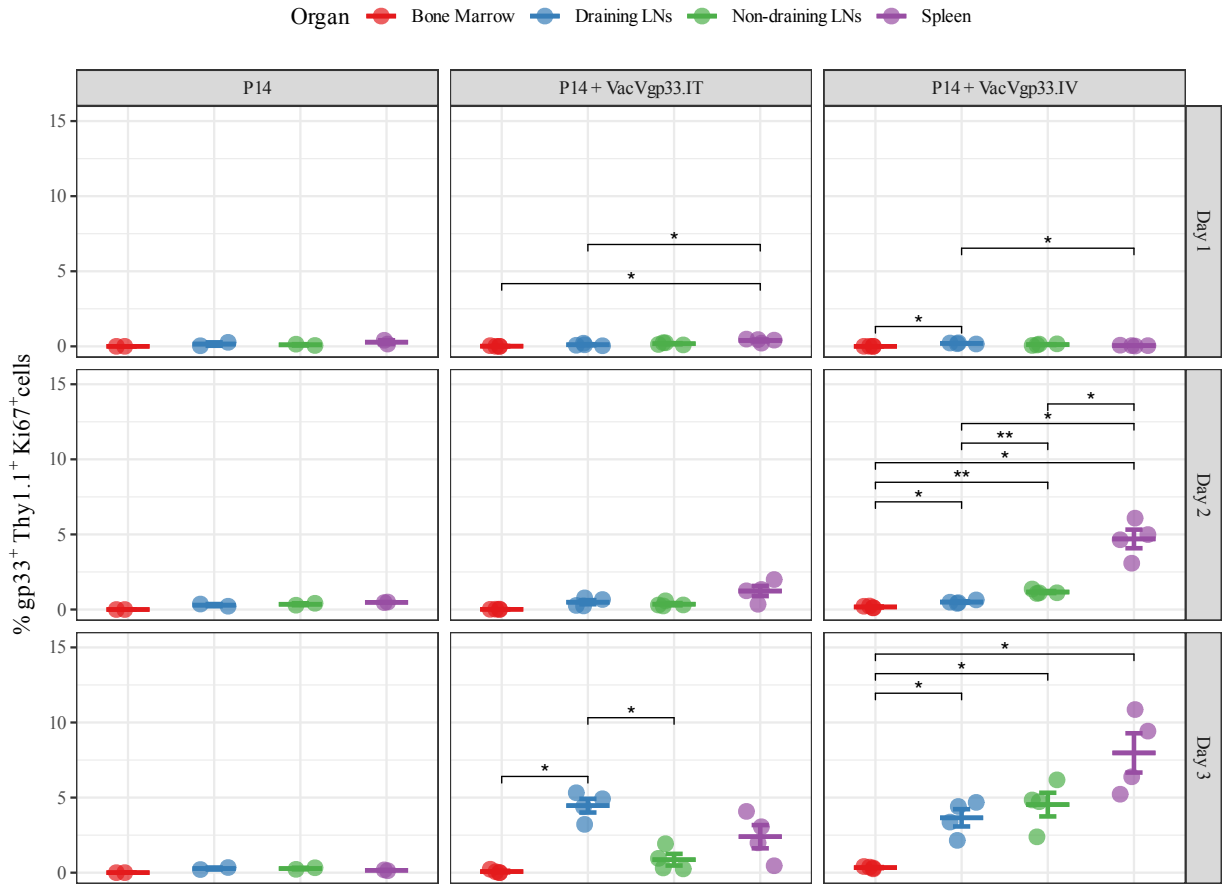
Organ
Bone Marrow
Draining LNs
Non-draining LNs
Spleen
P14
P14 + VacVgp33.IT
P14 + VacVgp33.IV
Day 1
Day 2
Day 3
% gp33+ Thy1.1+ Ki67+ cells
0
5
10
15
*
**

B

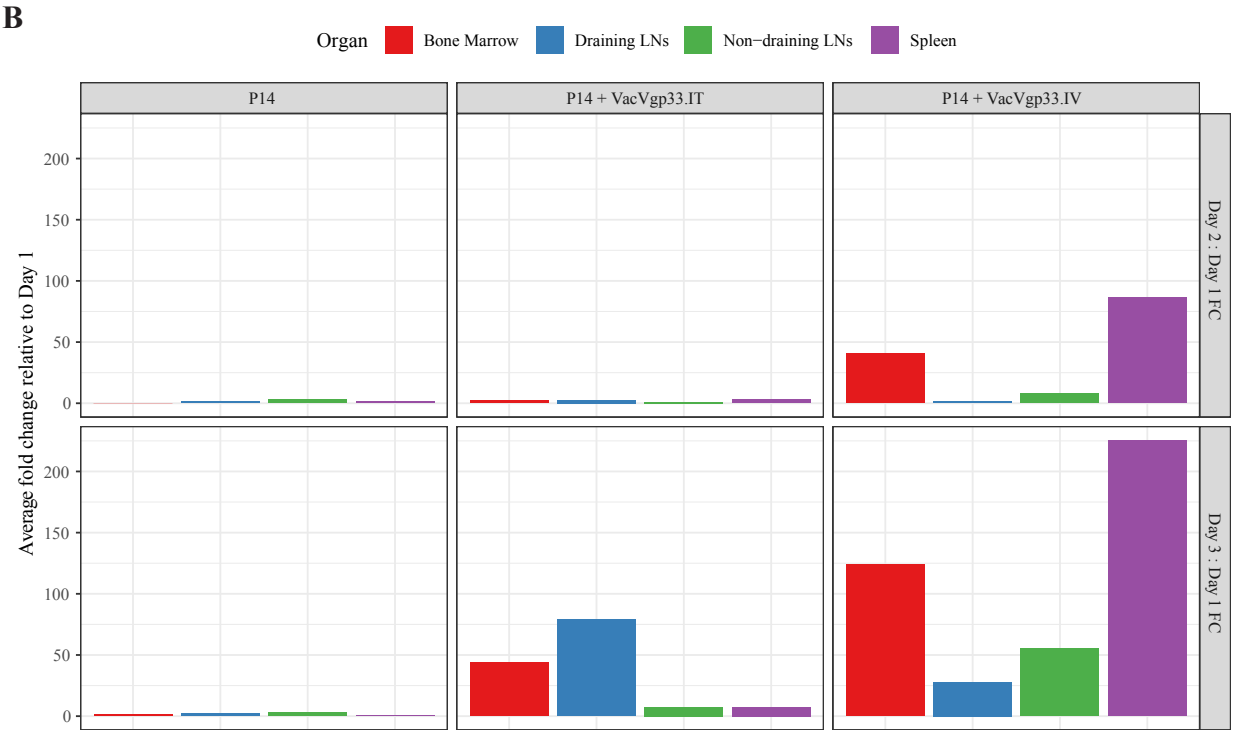
Organ
Bone Marrow
Draining LNs
Non−draining LNs
Spleen
P14
P14 + VacVgp33.IT
P14 + VacVgp33.IV
Day 2 : Day 1 FC
Day 3 : Day 1 FC
Average fold change relative to Day 1
0
50
100
150
200

Figure 4.3 | Intravenous and Intratumoural delivery of vaccinia virus result in T cell proliferation in different anatomical locations

C57BL/6 mice (n = 4) were intradermally implanted with $2x10^5$ B16gp33 cells. 5 days later the mice were treated using $3x10^6$ adoptively transferred P14 T cells followed by 1 x 10^8 pfu VacVgp33 (IT or IV) in the presence of FTY720 (4µg/g). The mice were euthanized at days 1,2, and 3 pvi and various lymphoid organs were collected, processed, stained for the intracellular expression of ki67, and analyzed using flow cytometry. Shown is the frequency of $Ki67^+$ $Thy1.1^+$ P14 T cells / total viable leukocytes (A). The fold change in $Ki67^+$ $Thy1.1^+$ P14 T cells was calculated by dividing the average frequency of every organ from day 2 by day 1 or from day 3 by day 1 (B). The horizontal bars represent means ± SEM. *P < 0.05, **P<0.01, ***P<0.001, ****P<0.0001.

some proliferation was also evident in the spleen and bone marrow on day 3, it was of much less extent compared to the DLNs. In conclusion, IV delivery of VacV causes a faster proliferative response of P14 T cells which takes place mainly in the spleen, whereas the IT delivery causes a slower proliferative response which takes place in the DLNs.

4.2.4. LacZ staining shows wider viral spread across IT-treated tumours vs. IV-treated ones (in collaboration with Scott Walsh)

Motivated by the injection route dependent difference in anatomical location of antigen presentation we wanted to further define viral distribution and the effect of viral replication/viral gene expression following IT or IV administration. For this work we relied on GFP and LacZ reporter genes included in the viral genome by previous modifications. GFP is expressed under an early promoter p7.5 while LacZ is expressed under a VacV late promoter p11. Since LacZ is expressed under a late promoter, its expression indicates the completion of viral replication. Notably, the gp33 transgene is expressed under a synthetic promoter representing a hybrid early/late promoter, so it is expressed throughout virus replication including tissues and cells in which GFP and LacZ expression is observed. As well, we chose to focus only on VacV for this analysis since these transgenes could be assessed concomitant with virus mediated gp33 antigen presentation and any ongoing immune response. We treated B16gp33-tumour bearing mice with P14 and VacVgp33 delivered either IT or IV. Mice were then sacrificed at different time-points with tissues frozen in OCT and resultant tissue slides stained with DAPI for GFP analysis or stained for LacZ according to *Gierut et al.*[276]. We detected GFP expression in the tumours following both IT and IV injection (**Fig. 4.4 A**). However, GFP was detectable at 6h pvi in case of IT injection, unlike IV injection, where GFP was detected at 24h pvi. Additionally, GFP was detected in the spleen only following IV injection. Interestingly, despite detecting GFP expression in the spleen following IV injection, no LacZ was observed at any time point indicating that the infection of spleen was non-productive (**Fig. 4.4 B**). As anticipated, we observed a greater viral load in the

A

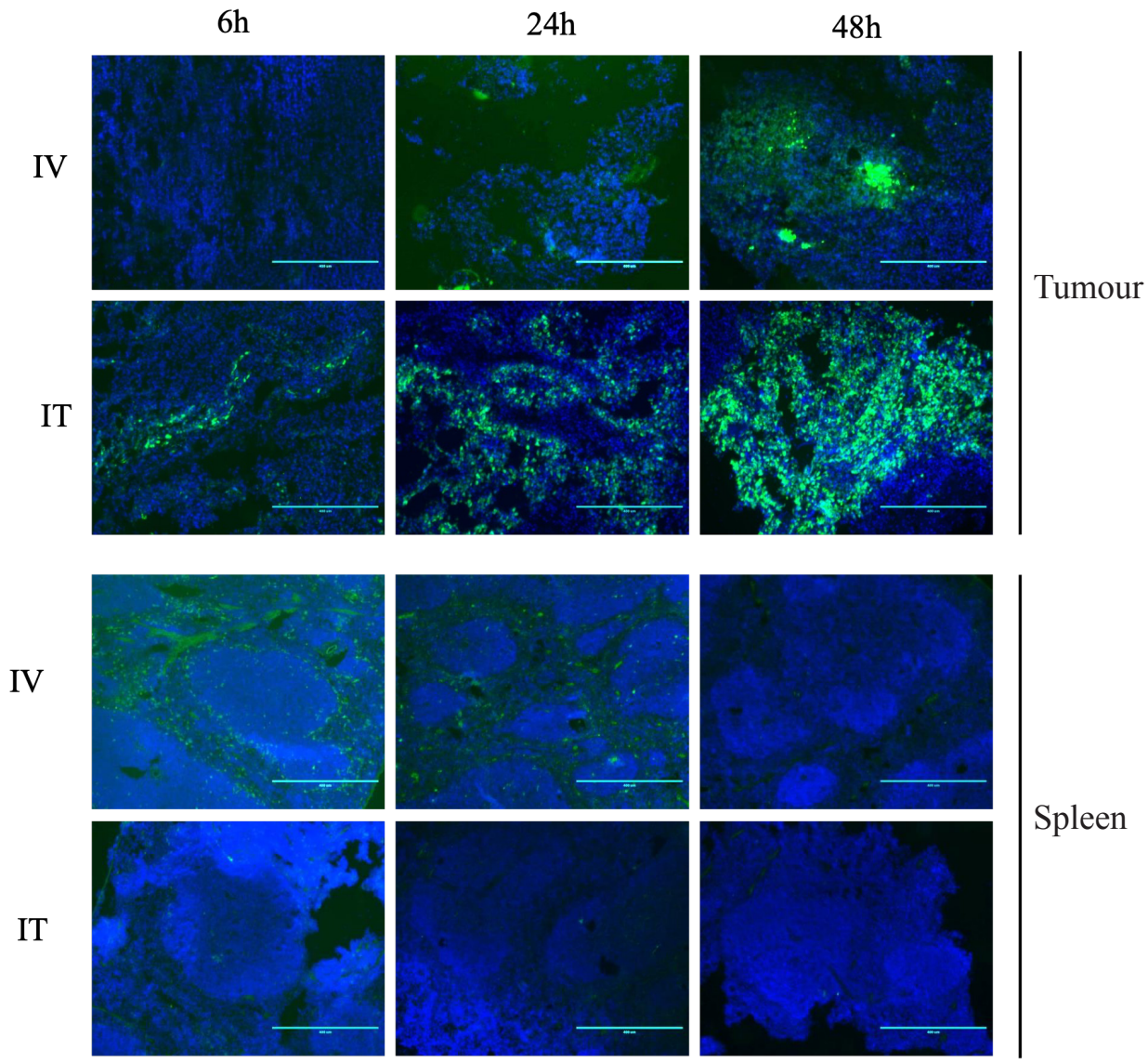

B

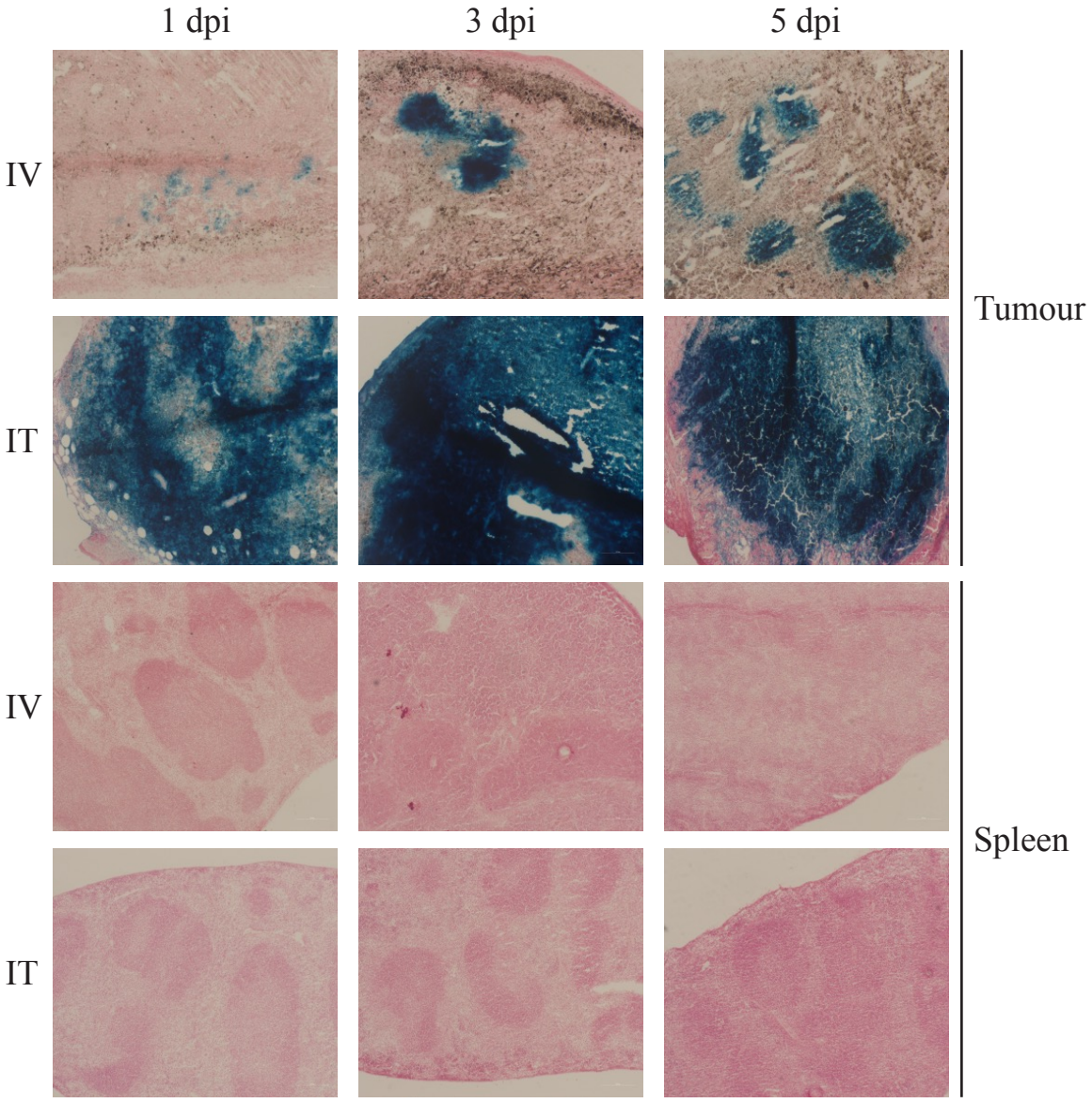

Figure 4.4 | GFP expression and LacZ staining showing tissue distribution of VacV following IT and IV infection

C57BL/6 mice were intradermally implanted with $2x10^5$ B16gp33 cells. 5 days later the mice were treated using 1 x 10^6 P14 T cells using IV injection followed by 1 x 10^8 pfu VacVgp33 using IT or IV routes. At different time points as indicated with each panel, the mice were sacrificed and the respective tissues were collected and frozen in OCT. The tissue slides were then stained with DAPI for GFP analysis (A) or stained for LacZ expression (B). EVOS M5000 microscope was used to capture images of the slides using 5X magnification.

TME following IT injection indicated by both GFP expression and LacZ staining. IV injection resulted in smaller focal regions of replication observed in case of IV delivery. Taken together this data suggests a disconnect between viral infection associated with early gene expression and viral replication and indicates that the viral mediated effects in the TME are more prominent following IT injection.

Chapter 5 — Evaluating the Contribution of Oncolysis in the Efficacy of ACT + OVV

5.1. Introduction

The hallmarks responsible for cancer cell survival, including their ability to proliferate indefinitely, resist apoptosis and evade the immune attack, make them the ideal environment for viral replication[3]. This was the basis of the initial success of Oncolytic Viruses (OVs) as a virotherapy platform. Transient short-lived cancer remission after a natural viral or bacterial infection has been reported during the early and mid-1900s[134,135,277]. In the 1950s, the arrival of transplantable murine models allowed for more controlled testing of the *in vivo* anti-tumour activity of OVs. Moore used the Russian encephalitis virus to inoculate mice bearing the transplantable mouse sarcoma 180[278]. While viral toxicity was a concern and animals eventually succumbed to the infection, tumour regression was observed. Additionally, upon inactivating the virus using either formalin, heat or ultraviolet (UV) rays, no effect on tumour growth was observed. They reported that actively replicating viruses are key requisite to obtain a favorable outcome[278]. The advent of recombinant DNA technology in the following 2-3 decades allowed for engineering viruses to modify their tissue tropism while sustaining their oncolytic capacity. One of the earlier vectors to benefit from genome editing was Herpes Simplex Virus (HSV), where Martuza observed that a thymidine kinase (TK)-negative HSV replicated in dividing cells but not in non-dividing cells. TK-negative HSV was used to treat malignant gliomas by intracerebral inoculation in mice and was shown to eradicate tumours with less incidence of encephalitis[139]. During these times, the immune response against the viral vectors was perceived as being necessary from the safety perspective, but it represented something of a hindrance to the optimal potential of the therapy by prematurely clearing the virus before the tumour is completely destroyed[279]. However, the selective tropism of OVs to the tumours combined with the ability to induce anti-viral immunity implied that they have the potential to, at least transiently, reverse the immune suppression state within the tumour microenvironment (TME). This realization, combined with the advancement in the understanding of the immune system and its role in controlling and/or rejecting tumours, led to the rebranding of OVs as multimodal immunotherapeutic platforms. Moving forward,

pre-clinical testing of different viral backbones in immunocompetent tumour models led to the observation that complete responses after viral therapy were associated with the mounting of anti-tumour immune responses and the capacity to reject re-challenge tumours[279,280]. The placement of OVs among the immunotherapeutics begs the question of whether viral replication is essential for their anti-tumour efficacy.

In the previous chapter, we demonstrated that using IT delivery of OVVs leads to enhancement in the overall survival of mice treated with ACT + OVV. The difference in survival and lack of tumour relapse was statistically significant in case of ACT + VacV treated mice. This points to the importance of having high local concentration of virus within the TME. We postulate that the enhanced therapeutic efficacy observed when using IT injection is due to enhanced oncolysis in the TME. Alternatively, the local presence of higher concentrations of virions in the TME could lead to more prominent effect of virus mediated modulation, including inflammatory changes, within the TME. We hypothesize that the direct effects of VacV replication in the TME complements $CD8^+$ T cell attack of tumours and prevents immune escape. In order to test this hypothesis, we first investigated the methods of virus inactivation with the goal of interfering with the viral replication cycle without completely abolishing viral gene expression, thus allowing VacV to act as a non-oncolytic vaccine. We then compared the therapeutic efficacy of the replicating and inactivated VacV in boosting antigen-specific $CD8^+$ T cells and controlling B16gp33 tumours. Additionally, using microarray, we did a transcriptomic profiling experiment to analyze the effects of both the replicating and inactivated VacV on the TME. We demonstrated that, despite the ability of both the replicating and the inactivated VacV to boost the transferred cells, the replicating virus was indeed therapeutically superior. Moreover, we did not identify differentially expressed genes (DEGs) in the tumours treated with the replicating or the inactivated VacV. Nevertheless, when compared to ACT - treated control the magnitude of the fold change of DEGs was generally higher using the inactivated VacV compared to its replicating counterpart. This work points to the ability of replicating VacV to modulate inflammation levels and cellular functions within the TME, preventing the excessive inflammation that can potentially trigger immune regulatory

pathways and further emphasizes the importance of virus replication or virus-induced oncolysis in preventing immune escape following T cell-based immunotherapy.

5.2. Results

5.2.1. Heat-inactivated VacVgp33 failed to boost P14 transferred cells leading to poor survival of the treated mice

In order to study the role virus replication plays in the therapeutic efficacy of ACT + VacV, we decided to take away the oncolytic capacity of VacV through its inactivation. Viral inactivation however is complicated by the dual role VacV plays as an oncolytic vector and a gene-delivering vaccine. Hence, the method to be used must yield a virus incapable of completing a full replication cycle but has the ability to infect target cells and express - at least to some extent - its transgene. Dai *et al.* showed that using heat inactivated modified vaccinia virus Ankara (heat-iMVA) intratumourally can induce a systemic anti-tumour immune response. Their inactivation protocol involved heating MVA at 55°C for 1 hour, which reduced the infectivity by 1000-fold[281]. We were interested to test whether heat inactivation will affect the ability of VacVgp33 to express its transgene and boost the transferred P14 T cells. To this end, we first tested the infectivity of VacV *in vitro* after being heated at 55°C for 1 hour (denoted as HI-VacV). At high MOIs (10^2 - 1), a few plaques were detected suggesting that a few virions survived the inactivation conditions. However, at MOI of 10^{-1} or less there were no detectable plaques **(Fig. 5.1 A)**. This is a significant reduction in infectivity compared to intact VacV where plaques are still detectable at MOI 10^{-5}. This represents a 10^5-fold reduction in infectivity compared to replicating VacV. In order to assess the effect of heat inactivation on the viral gene expression, we used a GFP-expressing VacV (VacVGFP), where GFP is expressed under an early promoter, p7.5. Thus, detection of GFP expression implies cell infection but not necessarily viral replication. HI-VacVGFP was used to infect CV-1 cells *in vitro*. Fluorescent microscopy was used to visualize GFP 24h following

A

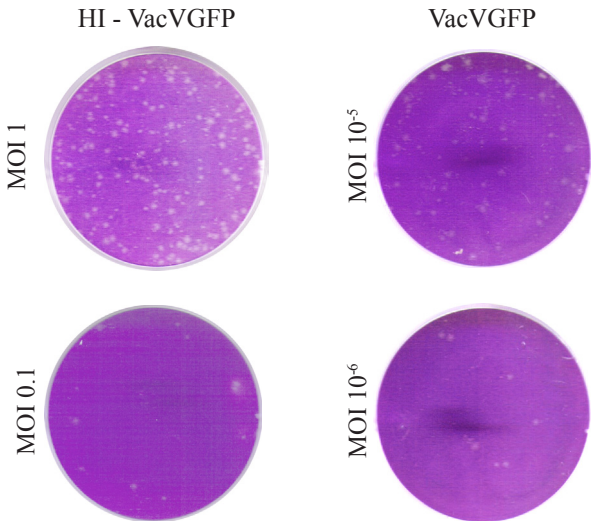
HI - VacVGFP
VacVGFP
MOI 1
MOI 10-5
MOI 0.1
MOI 10-6

B

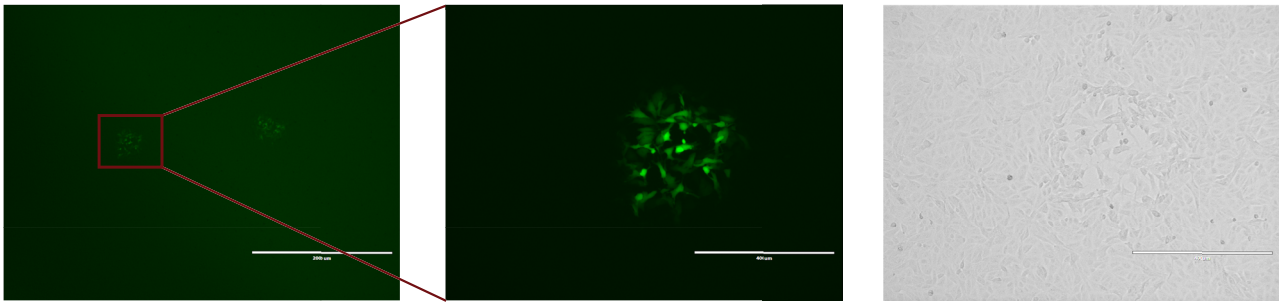

C

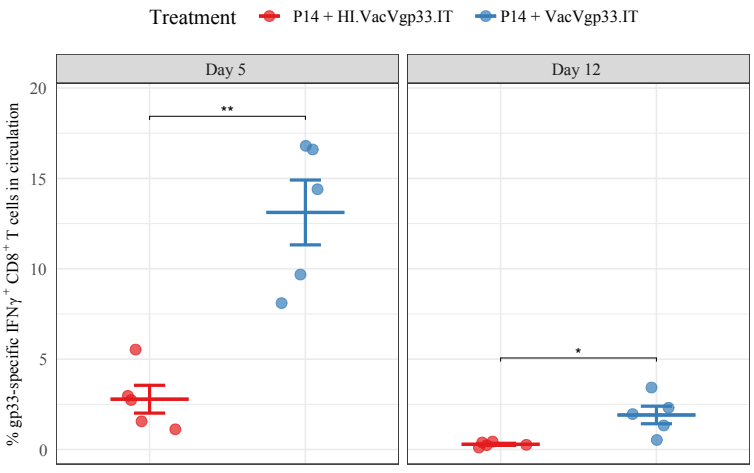
Treatment
P14 + HI.VacVgp33.IT
P14 + VacVgp33.IT
Day 5
Day 12
% gp33-specific IFNγ+ CD8+ T cells in circulation
20
15
10
5
0
**
*

D

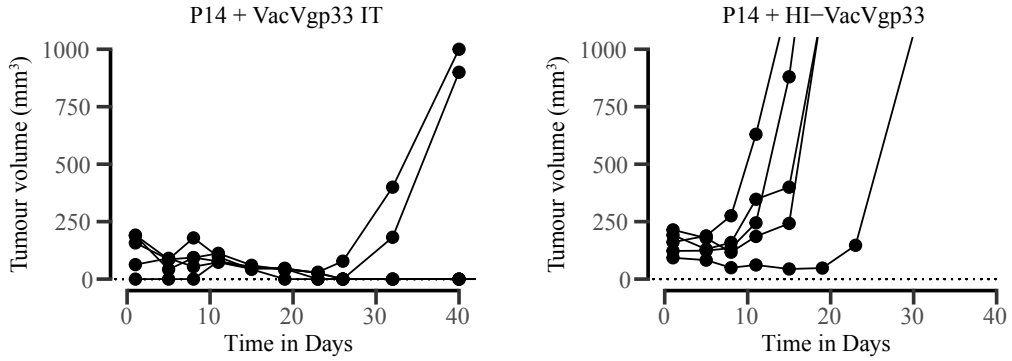
P14 + VacVgp33 IT
P14 + HI−VacVgp33
Tumour volume (mm3)
1000
750
500
250
0
0
10
20
30
40
Time in Days

E

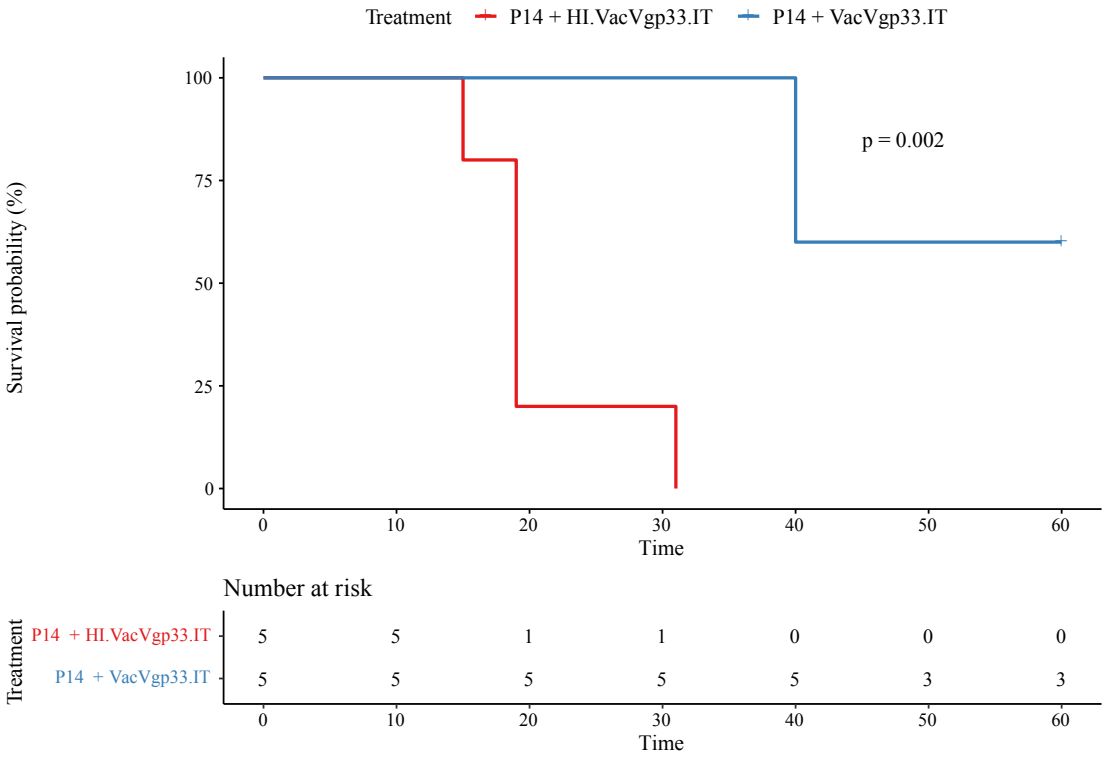
Treatment
P14 + HI.VacVgp33.IT
P14 + VacVgp33.IT
Survival probability (%)
100
75
50
25
0
p = 0.002
0
10
20
30
40
50
60
Time
Number at risk
Treatment
P14 + HI.VacVgp33.IT
P14 + VacVgp33.IT
5 5 1 1 0 0 0
5 5 5 5 5 3 3
0
10
20
30
40
50
60
Time

Figure 5.1 | Heat-inactivated VacVgp33 failed to boost P14 transferred cells leading to poor survival of the treated mice

(A) VacVGFP was heated at 55°C for 1 hour. Plaque assay was used to estimate the viral titer following the inactivation. (B) EVOS M5000 microscope was used to capture images of the infected cells 24h after infection using GFP and transmitted light channels. (C-E) C57BL/6 mice (n=5) were intradermally implanted with $2x10^5$ B16gp33. 5 days later the mice were treated using $1x10^6$ adoptively transferred P14 T cells followed by $1x10^8$ pfu VacVgp33 or HI-VacVgp33 or PBS delivered intratumourally (C) At days 5 and 12 post treatment, blood samples were collected, processed, stained for intracellular IFN-γ and analyzed using flow cytometry. Data is presented as percentage of $IFN\gamma^+$ gp33-specific CD8 T cells in circulation (D) Tumour volumes were continuously measured every third day and are presented as length * width * height (E) Overall survival was monitored for up to 60 days post tumour challenge. The survival statistics were calculated using log-rank test. *$p < 0.05$, **$p < 0.01$, ***$p < 0.001$, ****$p < 0.0001$

infection. After infection with HI-VacVGFP, the GFP expression was only observed where plaques were formed, indicating that viral gene expression was only maintained in the virions that were not inactivated and that inactivated virions failed to express any viral genes despite their presence in high doses **(Fig. 5.1 B)**.

Although the *in vitro* data points to the lack of viral gene expression following heat inactivation, Dai *et al.* reported that heat-iMVA showed better *in vivo* efficacy compared to the replicating MVA in controlling B16F10 tumours[281]. They also demonstrated that the observed efficacy was $CD8^+$ T cell dependent. This intrigued us to assess the ability of the HI-VacVgp33 virus to boost transferred P14 T cells *in vivo* and control B16gp33 tumours. B16gp33 tumour-bearing mice were treated using P14 ACT followed by VacVgp33 or HI-VacVgp33. Blood was collected at days 5 and 12 post virus injection (pvi) and gp33-specific IFNγ-producing $CD8^+$ T cells were quantified using Intracellular cytokine staining (ICS). We observed a significant reduction in the frequency of gp33-specific $CD8^+$ T cell responses in mice treated with P14 + HI-VacVgp33 (*P* value = 0.0007; student t-test), indicating that HI-VacVgp33 failed to drive the expansion of the transferred P14 T cells to the same levels as VacVgp33 **(Fig. 5.1 C)**. The failure to achieve sufficient gp33-specific responses correlated with lack of tumour control in mice treated with either P14 or P14 + HI-VacVgp33 **(Fig. 5.1 D)** and significant reduction in the overall survival of the mice (*P* value = 0.002; log-rank test) (**Fig. 5.1 E**). This experiment points to the inadequacy of heat inactivation as a method to study the contribution of VacV-mediated oncolysis since it not only kills the replicative capacity of VacV, but also its ability to boost the transferred T cells.

5.2.2. Psoralen and Long Wavelength Ultraviolet (PLWUV) kills the replication capacity of VacV while preserving its ability to infect target cells and express its early genes.

Psoralen and Long Wavelength Ultraviolet (PLWUV) was initially developed as a photochemical decontamination method to inactivate pathogenic viruses in plasma and plasma

A

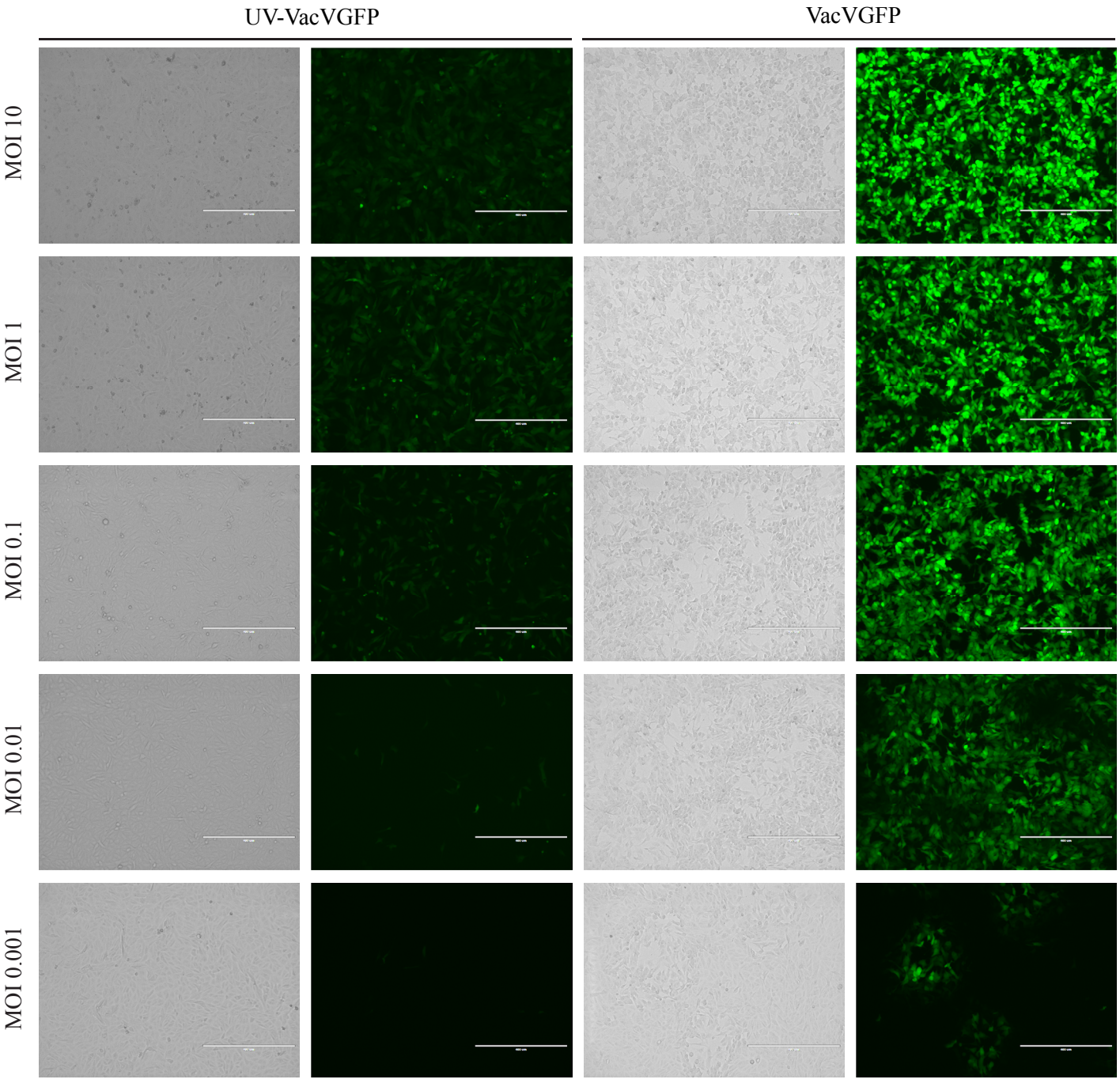

B

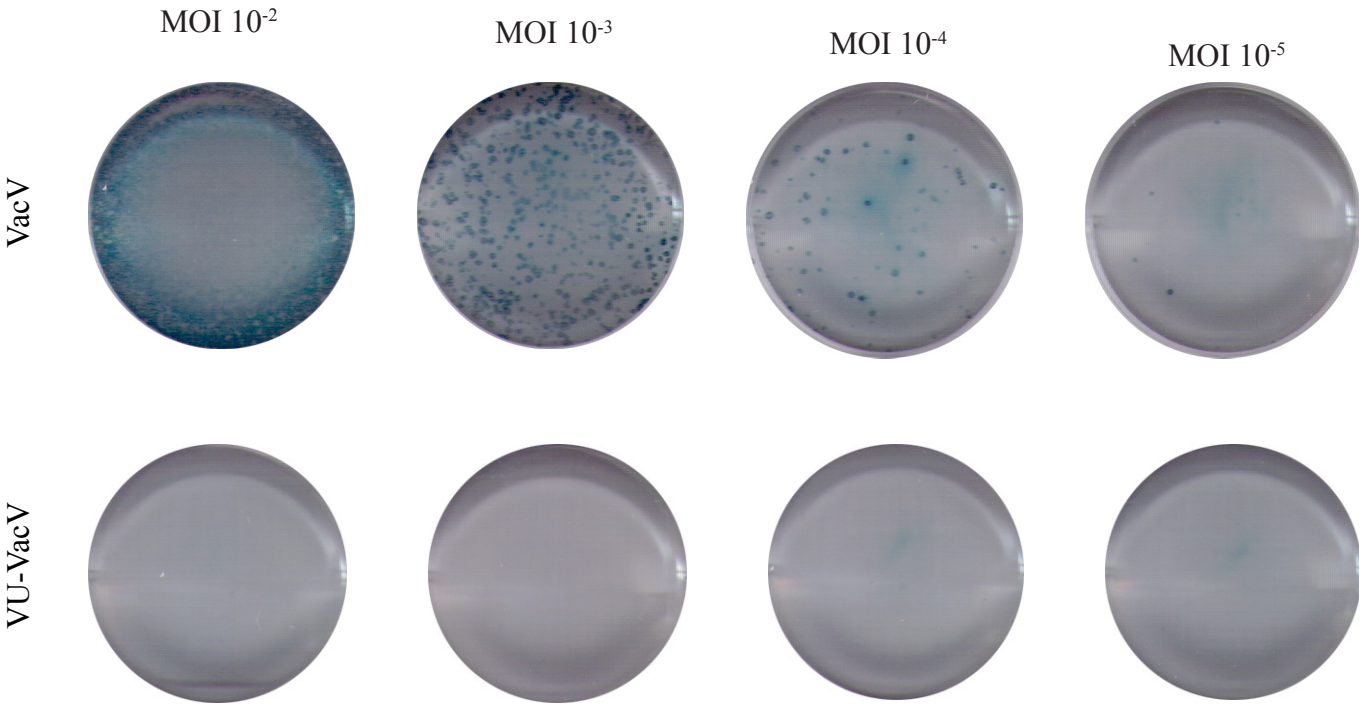
MOI 10^{-2}
MOI 10^{-3}
MOI 10^{-4}
MOI 10^{-5}
VacV
VU-VacV

C

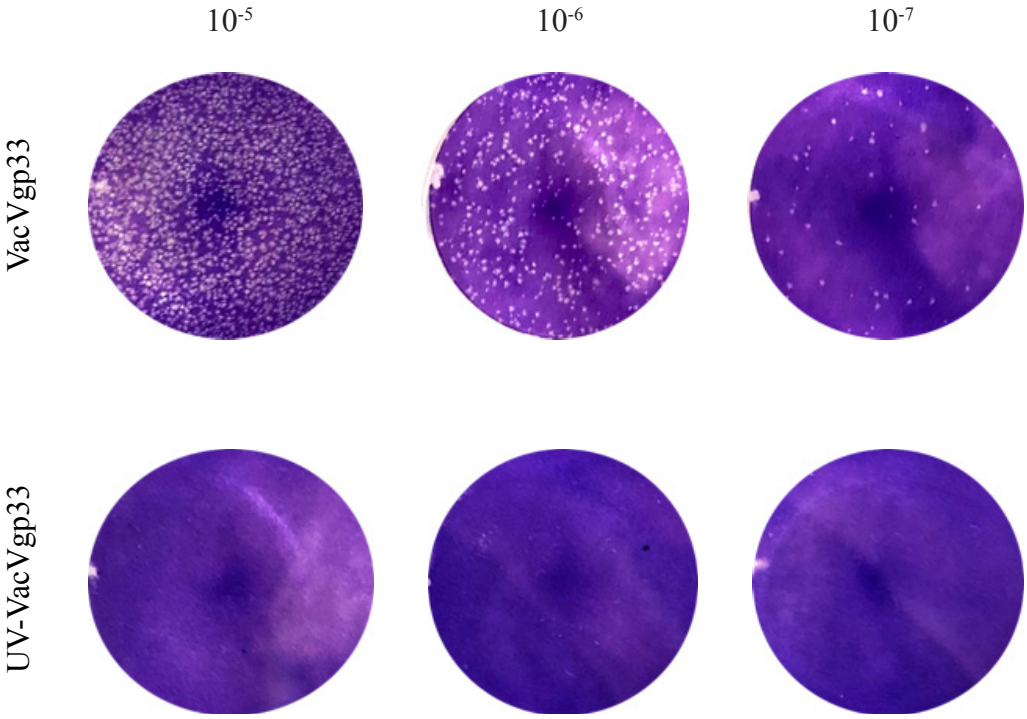
10^{-5}
10^{-6}
10^{-7}
VacVgp33
UV-VacVgp33

Figure 5.2 | Psoralen and Long Wavelength Ultraviolet (PLWUV) kills the replication capacity of VacV while preserving its ability to infect target cells and express its early genes.

VacVGFP was inactivated by incubation with 10 μg/ml psoralen and exposure to 365 nm UV for 10 min (A) VacVGFP or UV-VacVGFP were used to infect CV-1 cells in vitro using MOIs of 10 - 0.001. EVOS M5000 microscope was used to capture images of the infected cells 24h after infection using GFP and transmitted light. (B) X-gal was used to stain CV-1 cells to detect the expression of LacZ reporter gene 24h following infection with VacV or UV-VacV using MOIs of 10 - 0.001. (C) B16gp33 tumour bearing C57BL/6 (n=5) were treated with $1x10^8$ pfu VacVgp33 or UV-VacVgp33 using IT injection. Mice we sacrificed 24h post infection and the tumours were harvested and homogenized. Plaque assay was used to quantify the virus recovered from the tumours.

fractions to minimize the risk of infections associated with blood transfusions[282]. Tsung *et al.* showed that PLWUV could inactivate VacV replication without abolishing its ability to infect cells. They reported that the cells infected with such inactivated virions were able to express reporter genes under early but not late viral promoters without showing any cytopathic effects (CPE)[283]. Additionally, it was shown that the cells infected with PLWUV-inactivated VacV (UV-VacV for short), were not killed and can continue to proliferate[283]. We were intrigued to test whether PLWUV inactivation will eliminate the oncolytic capacity of VacV while maintaining viral gene expression. For the initial characterization of PLWUV inactivation, VacVGFP, in which GFP is expressed under the control of a synthetic early/late promoter, was used. We used psoralen at 10 µg/ml and tested out different LW-UV (365 nm) exposure durations ranging from 2 - 10 mins and found that 10 mins led to complete inactivation indicated by the absence of any viral plaques at all MOIs (data not shown). This inactivation protocol was utilized moving forward in all *in vitro* and *in vivo* experiments. VacVGFP or UV-VacVGFP were used to infect CV-1 cells *in vitro*. Fluorescent microscopy was used to visualize GFP 24h following infection. Consistent with what was reported by Tsung *et al.*, we observed GFP expression following infection with UV-VacVGFP with no signs of CPE **(Fig. 5.2 A)**. The intensity of GFP, however, was less compared to VacVGFP, which is to be expected given that UV-VacVGFP does not replicate. Further, we made use of the LacZ reporter gene, that is expressed under the control of a late promoter (VacV-P11), to confirm the lack of late gene expression following PLWUV inactivation. CV-1 cells were infected with replicating or PLWUV-inactivated VacV. The cells were fixed 24h post infection and stained using X-gal staining. As expected, we did not observe any positive X-gal staining (indicated by a dark blue color) in the cells infected with UV-VacVgp33 **(Fig. 5.2 B)**. Finally, in order to confirm the absence of CPE *in vivo, w*e treated B16gp33 tumour-bearing mice with 1e8 pfu VacVgp33 or UV-VacVgp33 using IT injection. Mice were sacrificed 24h post infection and the tumours were harvested and homogenized. Plaque assay was used to quantify the virus recovered from the tumours. The recovered virus titer from the VacVgp33-treated tumours was estimated to be $2.45x10^9$ pfu/g tumour. On the contrary, we detected no plaques in the UV-VacVgp33-treated

A

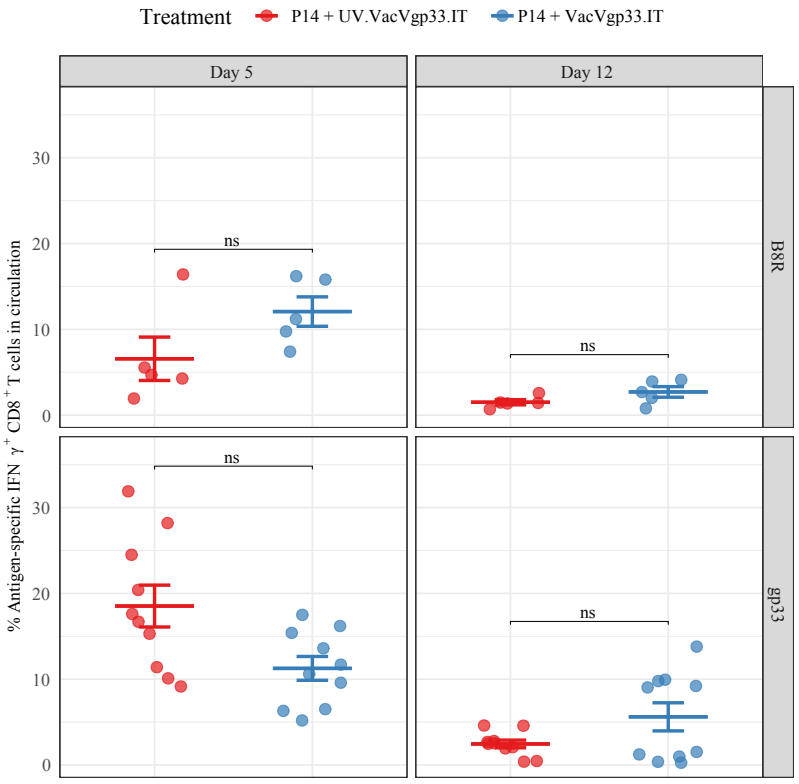
Treatment
P14 + UV.VacVgp33.IT
P14 + VacVgp33.IT
Day 5
Day 12
B8R
gp33
ns
% Antigen-specific IFN γ+ CD8+ T cells in circulation
0
10
20
30

B

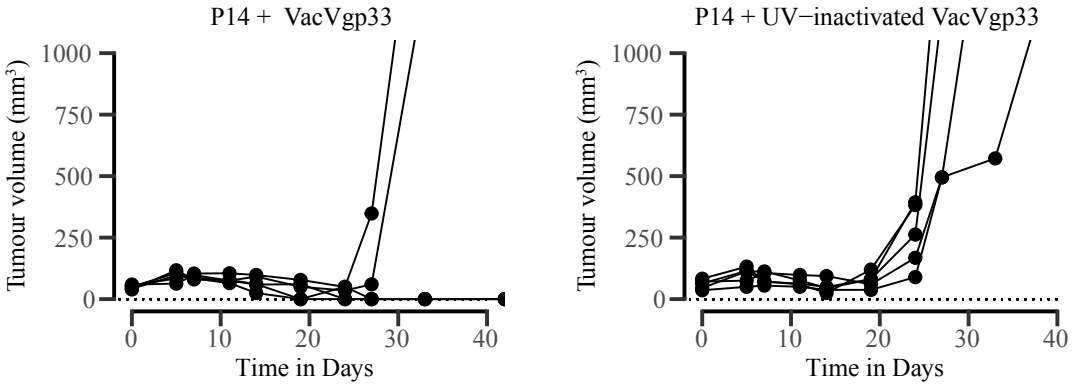
P14 + VacVgp33
P14 + UV−inactivated VacVgp33
Tumour volume (mm3)
Time in Days
0
250
500
750
1000
10
20
30
40

C

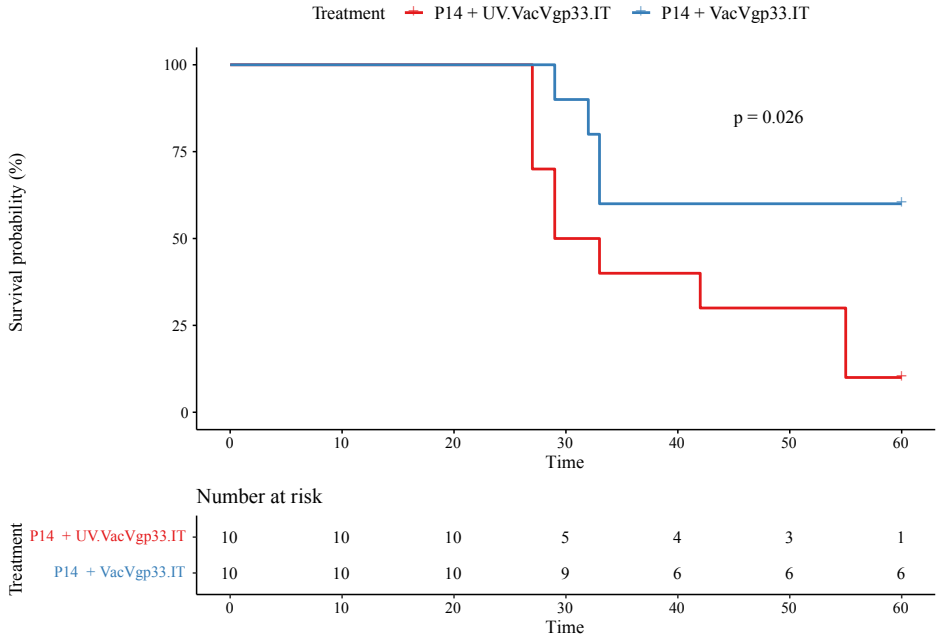

Figure 5.3 | PLWUV-inactivated VacV can boost transferred T cells and cause initial tumour regression but fail to induce durable cure in B16gp33 tumour model

C57BL/6 mice (n=5) were intradermally implanted with 2x105 B16gp33 cells. 5 days later the mice were treated using 1x106 adoptively transferred P14 T cells or PBS followed by 1 x 108 pfu VacVgp33 or UV-VacVgp33 or VacVGFP delivered intratumourally (A) At days 5 and 12 post treatment, blood samples were collected, processed, stained for intracellular IFNγ following in vitro peptide stimulation and analyzed using flow cytometry. (B) Tumour volumes were continuously measured every third day and are presented as length * width * height (C) Overall survival was monitored for up to 60 days post tumour challenge. The survival statistics were calculated using log-rank test. *$p < 0.05$, **$p < 0.01$, ***$p < 0.001$, ****$p < 0.0001$

tumours, confirming the lack of any replicating virions following PLWUV-inactivation which is consistent with the *in vitro* data.

5.2.3. PLWUV-inactivated VacV can boost transferred T cells and cause initial tumour regression but fail to induce durable cure in B16gp33 tumour model

Having proven that PLWUV-inactivated VacV can maintain early gene expression without lysing the target cells, we asked whether UV-VacVgp33 has the ability to boost gp33-specific $CD8^+$ T cells to the same level as VacVgp33. To this end, we treated B16gp33 tumour-bearing mice with P14 T cells + VacVgp33 or UV-VacVgp33 delivered IT. The mice were monitored for tumour growth kinetics and survival. ICS was used to quantify gp33-specific and B8R-specific $CD8^+$ T cell responses at days 5 and 12 pvi, with B8R being an immunodominant VacV antigen and so a marker of antiviral immunity. We did not detect a statistically significant difference in the levels of B8R-specific or gp33-specific $IFN\gamma^+$ $CD8^+$ T cells between mice treated with P14 + VacVgp33 and P14 + UV-VacVgp33, confirming the ability of the inactivated VacVgp33 to express gp33 and other viral early genes and mount an antigen-specific immune response **(Fig. 5.3 A)**. Both treatment groups showed initial tumour control, which was anticipated given the presence of a relatively high frequency of gp33-specific $CD8^+$ T cells in the circulation **(Fig. 5.3 B)**. However, 90% of the mice treated with P14 + UV-VacVgp33 developed relapsing tumours which eventually grew to endpoint. On the other hand, only 40% of the mice treated with P14 + VacVgp33 developed relapsing tumours. This led to a statistically significant difference in the overall survival of mice treated with P14 + VacVgp33 vs. P14 + UV-VacVgp33 (P value = 0.026; log-rank test) **(Fig. 5.3 C)**. This experiment suggests that the replicating virus provides an additional advantage beyond boosting gp33-specific $CD8^+$ T cells to achieve a sustained and durable tumour control.

A

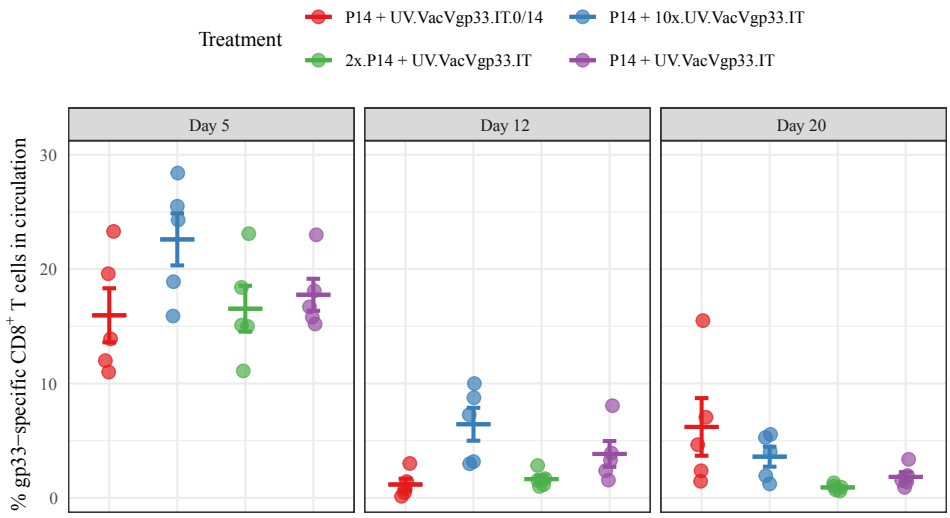
Treatment
P14 + UV.VacVgp33.IT.0/14
P14 + 10x.UV.VacVgp33.IT
2x.P14 + UV.VacVgp33.IT
P14 + UV.VacVgp33.IT
Day 5
Day 12
Day 20
% gp33−specific CD8+ T cells in circulation
30
20
10
0

B

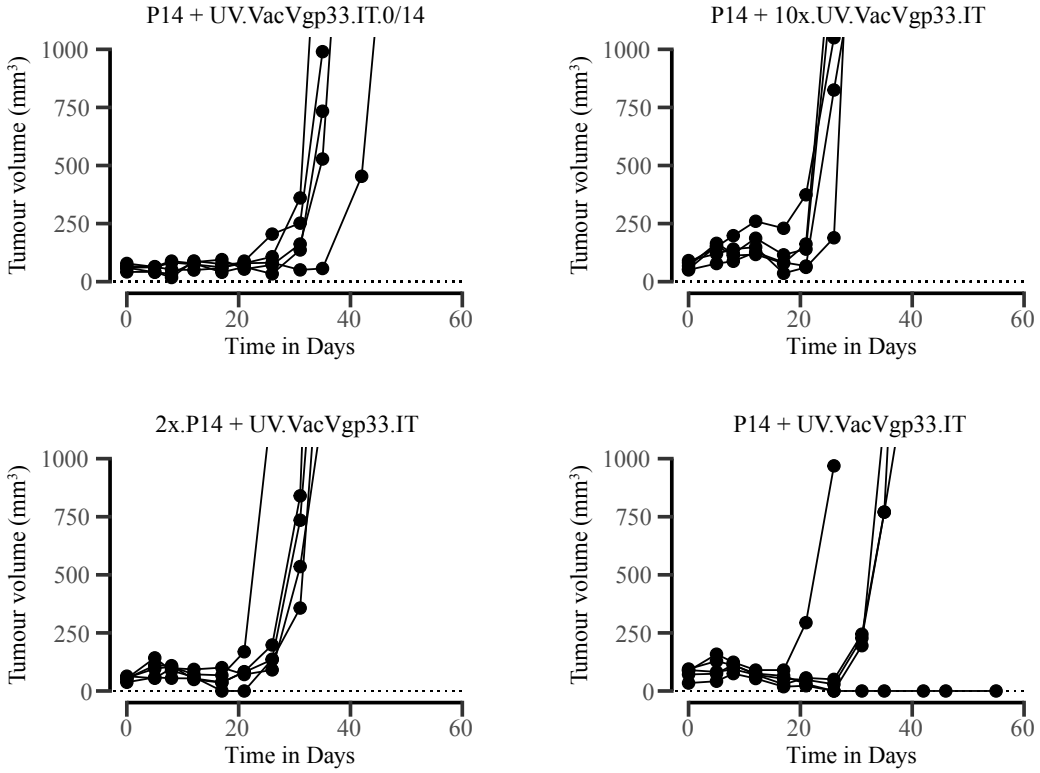
P14 + UV.VacVgp33.IT.0/14
P14 + 10x.UV.VacVgp33.IT
2x.P14 + UV.VacVgp33.IT
P14 + UV.VacVgp33.IT
Tumour volume (mm3)
1000
750
500
250
0
0
20
40
60
Time in Days

C

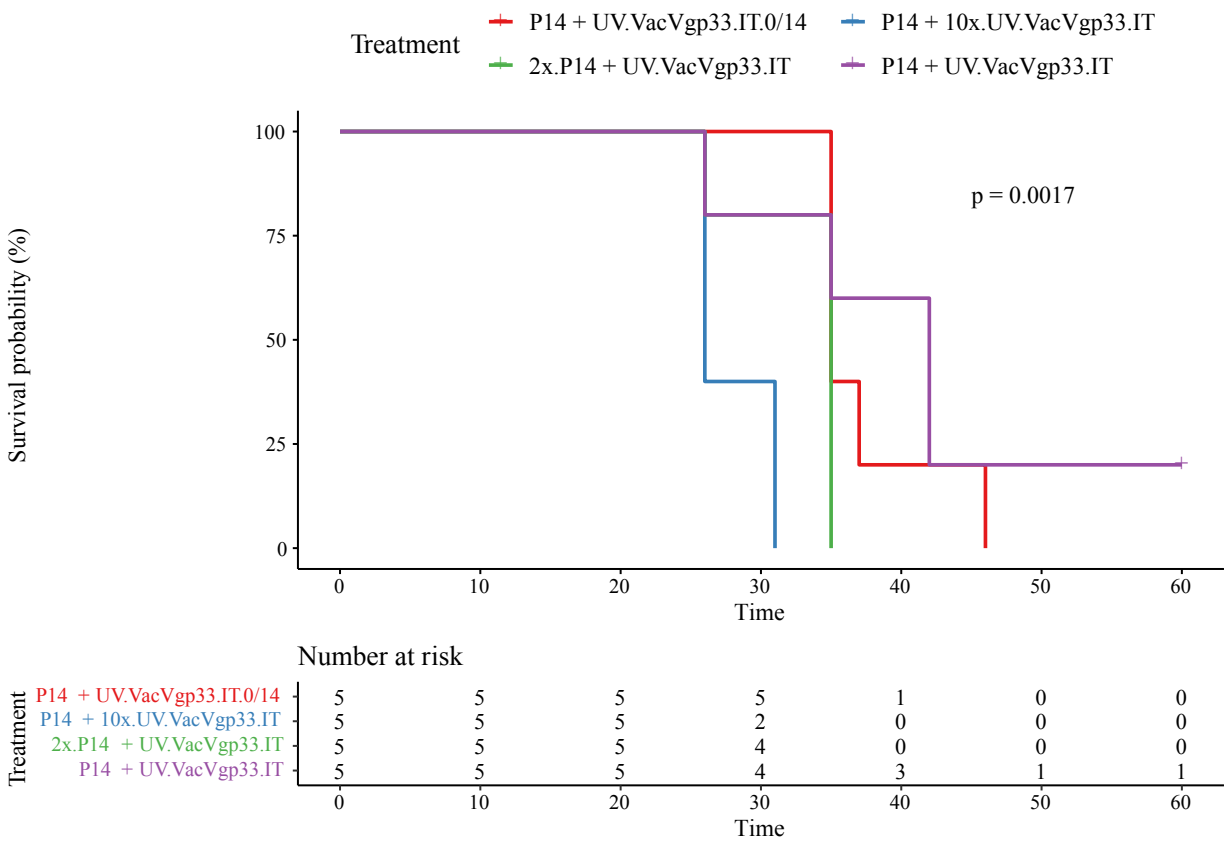

Figure 5.4 | Increasing the dose and/or frequency of PLWUV-inactivated VacV administration or transferred P14 T cells does not improve the efficacy

C57BL/6 mice (n=5) were intradermally implanted with $2x10^5$ B16gp33 cells. 5 days later the mice were treated using $1x10^6$ or $2x10^6$ adoptively transferred P14 T cells followed by 1 x 10^8 pfu UV-VacVgp33 injected once or twice on days 0 or 0 and 14 or 1 x 10^9 delivered intratumourally (A) At days 5, 12 and 20 post treatment, blood samples were collected, processed, stained for intracellular IFNγ and analyzed using flow cytometry. (B) Tumour volumes were continuously measured every third day and are presented as length * width * height (C) Overall survival was monitored for up to 60 days post tumour challenge. The survival statistics were calculated using log-rank test. *$p < 0.05$, **$p < 0.01$, ***$p < 0.001$, ****$p < 0.0001$

5.2.4. Increasing the dose and/or frequency of PLWUV-inactivated VacV administration or transferred P14 T cells does not improve the efficacy

Although the same doses of VacVgp33 and UV-VacVgp33 were used in the previous experiment, the replicating virus can amplify itself leading potentially to an increased viral load and/or prolonged persistence in the TME. In order to account for such variability, we designed an experiment to test whether optimizing the dose or frequency of UV-VacVgp33 injection would lead to an improvement in the efficacy. We treated B16gp33 tumour-bearing mice with standard doses of P14 T cells + UV-VacVgp33 given once or twice at days 0, and 14 pvi (denoted as P14 + UV-VacVgp33 0/14). Alternatively, in other groups, the dosing regimen was kept at one injection / treatment component but a 10x dose of UV-VacVgp33 (denoted as P14 + 10x UV-VacVgp33) or 2x dose of P14 T cells (denoted as 2x P14 + UV-VacVgp33) were used. The mice were monitored for tumour growth kinetics and survival. ICS was used to quantify gp33-specific $CD8^+$ T cell responses at days 5, 12 and 20 pvi. Using 10x UV-VacVgp33 led to boosting of P14 T cells to higher levels compared to other treatment groups at day 5pvi **(Fig. 5.4 A)**. Doubling the injected P14 T cells did not result in any significant increase in the magnitude of gp33-specific responses. At day 12, we observed a dip in gp33-specific responses in all treated groups, which is consistent with the pattern of T cell kinetics that we reported before **(Fig. 5.4 A)**. Injecting UV-VacVgp33 on day 14 led to the expansion of gp33-specific $CD8^+$ T cells when measured at day 20 pvi **(Fig. 5.4 A)**. It is worth noting that the detected gp33-specific $CD8^+$ T cells at day 20 lacked the expression of the congenic marker Thy1.1 that is expressed by P14 T cells, meaning that they were expanded from the repertoire of endogenously derived gp33-specific memory $CD8^+$ T cells. This is contrary to the responses detected on day 5, where 50 - 90 % of $IFN\gamma^+$ gp33-specific cells are $Thy1.1^+$. Despite the increased magnitude (induced by 10x UV-VacVgp33) or prolonged persistence (induced by UV-VacVgp33 injection on day 14 pvi) of gp33-specific responses, we did not notice any significant increase in the efficacy of therapy. As observed in the previous experiment, an initial control of tumour growth was observed in all treatment groups **(Fig. 5.4 B)**. However, all

A

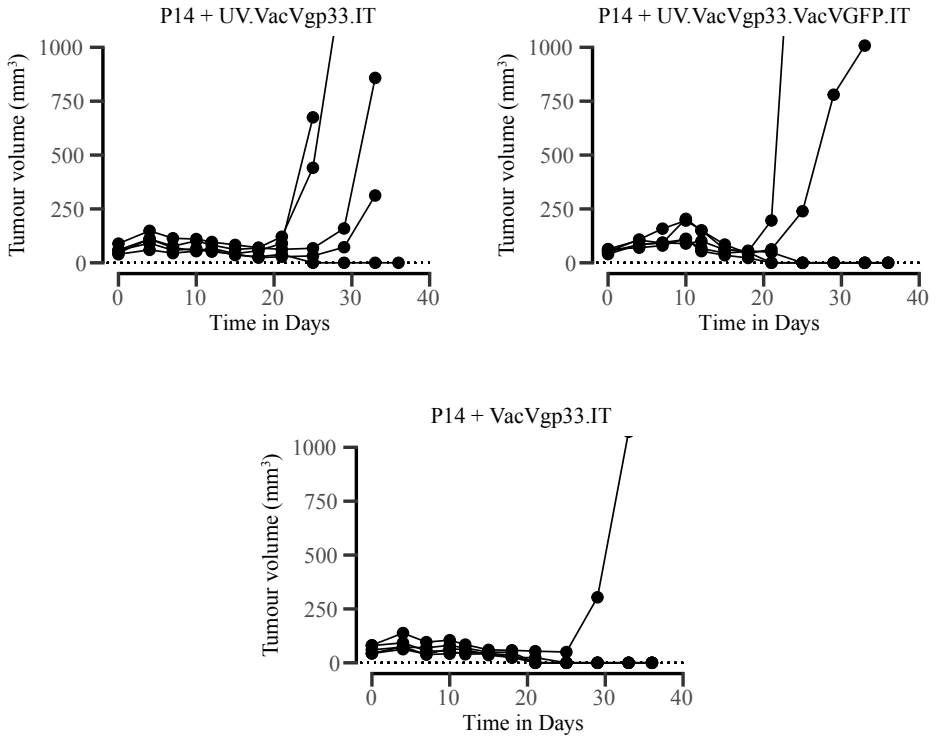
P14 + UV.VacVgp33.IT
P14 + UV.VacVgp33.VacVGFP.IT
P14 + VacVgp33.IT
Tumour volume (mm³)
Time in Days
0
250
500
750
1000
0
10
20
30
40

B

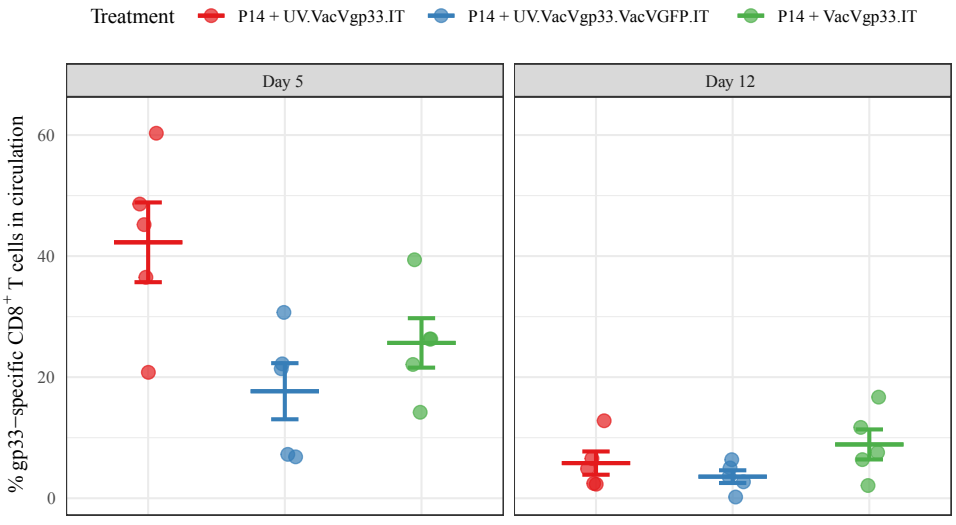
Treatment
P14 + UV.VacVgp33.IT
P14 + UV.VacVgp33.VacVGFP.IT
P14 + VacVgp33.IT
Day 5
Day 12
% gp33−specific CD8⁺ T cells in circulation
0
20
40
60

C

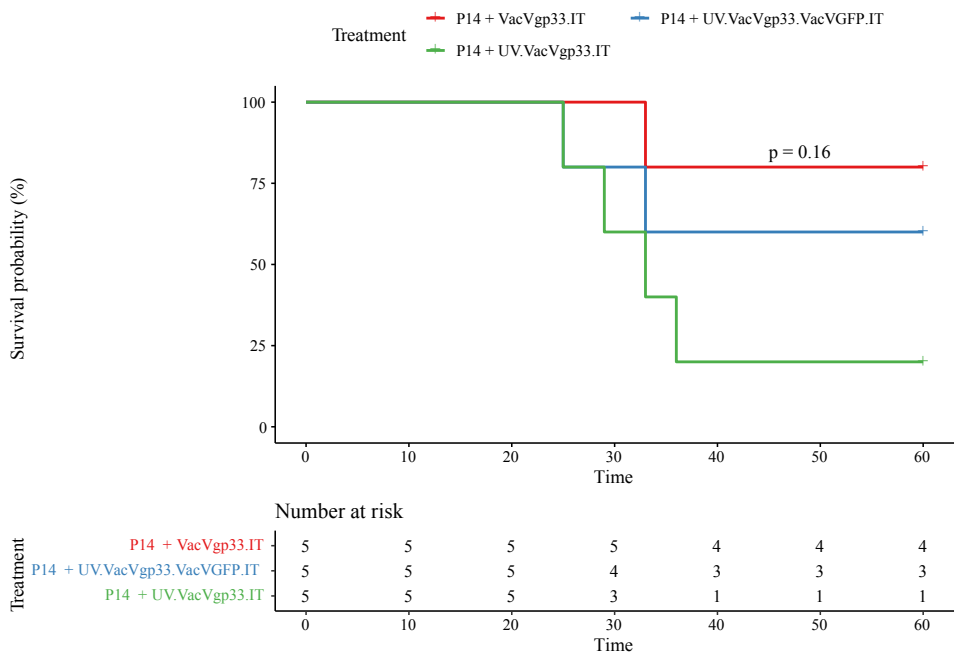

Figure 5.5 | Combining PLWUV-inactivated VacVgp33 with replicating VacV-GFP restores the durable tumour control phenotype

C57BL/6 mice (n=5) were intradermally implanted with $2x10^5$ B16gp33 cells. 5 days later the mice were treated using $1x10^6$ adoptively transferred P14 T cells followed by $1x10^8$ pfu VacVgp33 or UV-VacVgp33 or UV-VacVgp33 + VacVGFP injected intratumourally (A) At days 5 and 12 post treatment, blood samples were collected, processed, stained for intracellular IFNγ and analyzed using flow cytometry. (B) Tumour volumes were continuously measured every third day and are presented as length * width * height (C) Overall survival was monitored for up to 60 days post tumour challenge. The survival statistics were calculated using log-rank test. *p <0.05, **p <0.01, ***p <0.001, ****p <0.0001

the treatment regimens failed to achieve the durable tumour control associated with the replicating VacVgp33. Counterintuitively, the mice treated with P14 + 10x UV-VacVgp33 showed the worst overall survival (median survival = 26 days) compared to P14 + UV-VacVgp33 (median survival = 42 days) (**Fig. 5.4 C**). Performing a log-rank test resulted in a statistically significant difference in survival among the treatments (*P* value = 0.0017). This study suggests that the lack of durable tumour cure observed with UV-VacVgp33 cannot be reversed by optimizing the T cell or the virus dose or by increasing the frequency of virus injections, suggesting a direct mechanistic contribution of virus replication and oncolysis to achieve sustained tumour regression.

5.2.5. Combining PLWUV-inactivated VacVgp33 with replicating VacV-GFP restores the durable tumour control phenotype

Next, we asked whether adding a replicating VacV that doesn't express gp33 to UV-VacVgp33 would restore the phenotype observed with VacVgp33. To this end, we treated B16gp33 tumour-bearing mice with P14 + UV-VacVgp33 + VacVGFP, where both viruses were mixed at equal pfu of 5e7 and delivered in one injection of total pfu equal to that used with VacVgp33 (1e8 pfu). As controls B16gp33 tumour-bearing mice were treated with P14 + VacVgp33 or P14 + UV-VacVgp33. The mice were monitored for tumour growth kinetics and survival. ICS was used to quantify gp33-specific $CD8^+$ T cell responses at 5 and 12 days pvi. The addition of VacVGFP did not affect the ability of UV-VacVgp33 to boost gp33-specific CD8 T cells, and all treatments resulted in comparable levels of $IFN\gamma^+$ gp33-specific $CD8^+$ T cells 5 days pvi **(Fig. 5.5 B)**. Interestingly, 60% of the mice treated with P14 + UV-VacVgp33 + VacVGFP achieved sustained tumour regression, suggesting that the addition of replicating VacVGFP complements UV-VacVgp33 and provides an extra mechanism to prevent tumour relapse **(Fig. 5.5 C)**.

5.2.6. Microarray analysis reveals changes in inflammation, apoptosis and cell cycle/DNA repair pathway signatures despite a scarcity of individual differentially expressed genes in the TME following P14 + VacVgp33 or P14 + UV-VacVgp33

The difference in the outcome observed when treating the tumour with P14 + VacVgp33 or P14 + UV-VacVgp33 prompted us to investigate whether virus inactivation leads to a change in the molecular signature induced by VacV in the TME. To this end, we treated B16gp33 tumour-bearing mice with P14 + VacVgp33 or UV-VacVgp33 or PBS delivered IT. Tumours were then harvested 48 h pvi, homogenized and RNA was extracted for microarray analysis to study the molecular changes within the TME following the respective treatments. We established a workflow for the analysis of the microarray data from raw data into meaningful biological outcomes. First, preprocessing of the data including background correction and expression normalization was done using the oligo package that utilizes multichip average method (RMA) for normalization [246]. The relative log expression of each chip before and after normalization is shown in **fig. 5.6 A-B**. Principal component analysis (PCA) revealed 3 separate clusters, each representing a respective treatment **(Fig. 5.6 C)**. Virus treated groups were separated from the ACT control group along the first principal component axis which accounts for most of the variability among samples (38.8%). On the other hand, the samples treated with the replicating virus were separated from those treated with the inactivated virus along the second principal component which represents only 12.8% of sample variability. It is worth noting that the samples treated with P14 + UV-VacVgp33 showed less tight clustering and two subclusters can be visually identified pointing to less consistency in the molecular signature induced by the P14 + UV-VacVgp33 treatment. We used Pearson correlation to calculate the dissimilarity between the samples and clustered them based on their distances **(Fig. 5.6 D)**. This analysis revealed that samples treated with P14 + VacVgp33 were very similar to those treated with P14 + UV-VacVgp33 as seen from the small distances among the samples and the lack of separation along the first principal component.

A

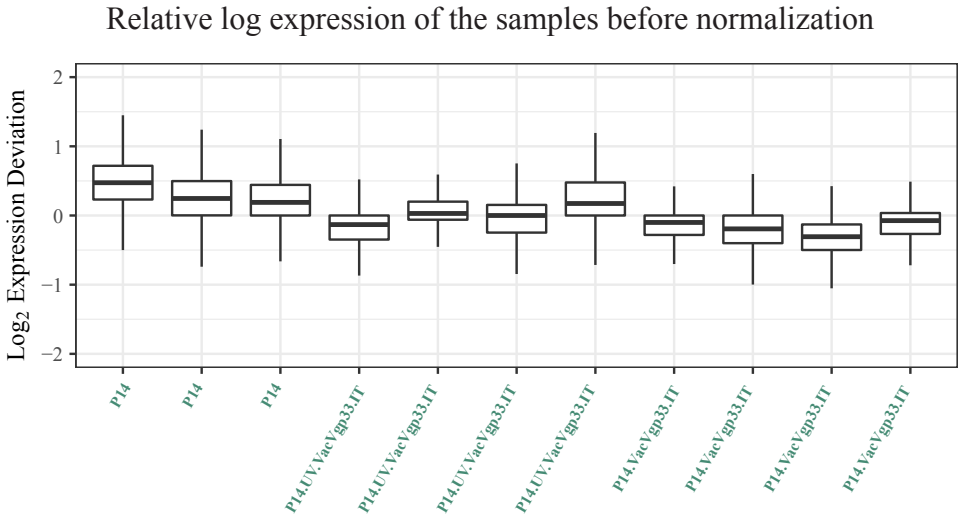
Relative log expression of the samples before normalization
Log2 Expression Deviation
2
1
0
−1
−2
P14
P14
P14
P14.UV.VacVgp33.IT
P14.UV.VacVgp33.IT
P14.UV.VacVgp33.IT
P14.UV.VacVgp33.IT
P14.VacVgp33.IT
P14.VacVgp33.IT
P14.VacVgp33.IT
P14.VacVgp33.IT

B

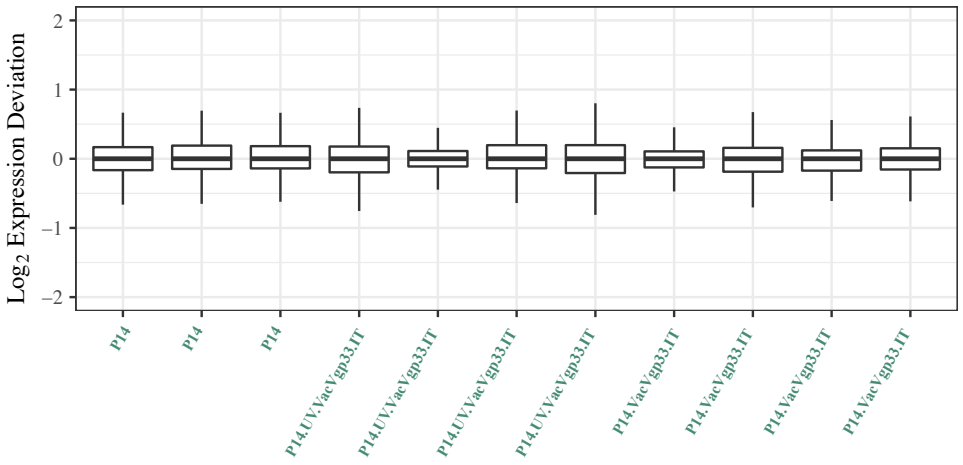
Relative log expression of the samples after normalization
Log2 Expression Deviation
2
1
0
−1
−2
P14
P14
P14
P14.UV.VacVgp33.IT
P14.UV.VacVgp33.IT
P14.UV.VacVgp33.IT
P14.UV.VacVgp33.IT
P14.VacVgp33.IT
P14.VacVgp33.IT
P14.VacVgp33.IT
P14.VacVgp33.IT

C

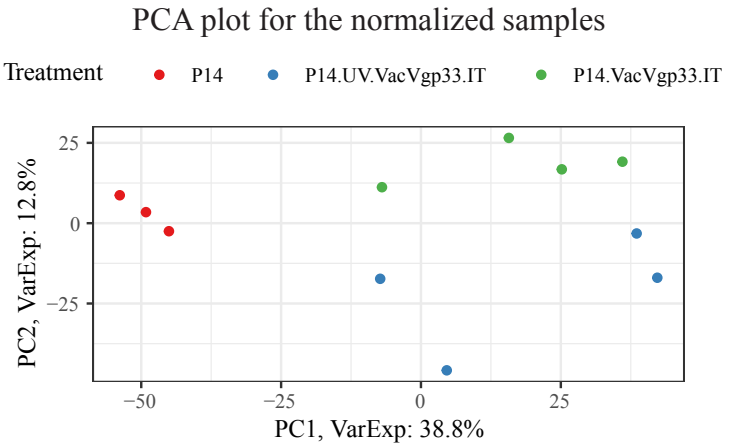
PCA plot for the normalized samples
Treatment
P14
P14.UV.VacVgp33.IT
P14.VacVgp33.IT
PC2, VarExp: 12.8%
25
0
−25
−50
−25
0
25
PC1, VarExp: 38.8%

D

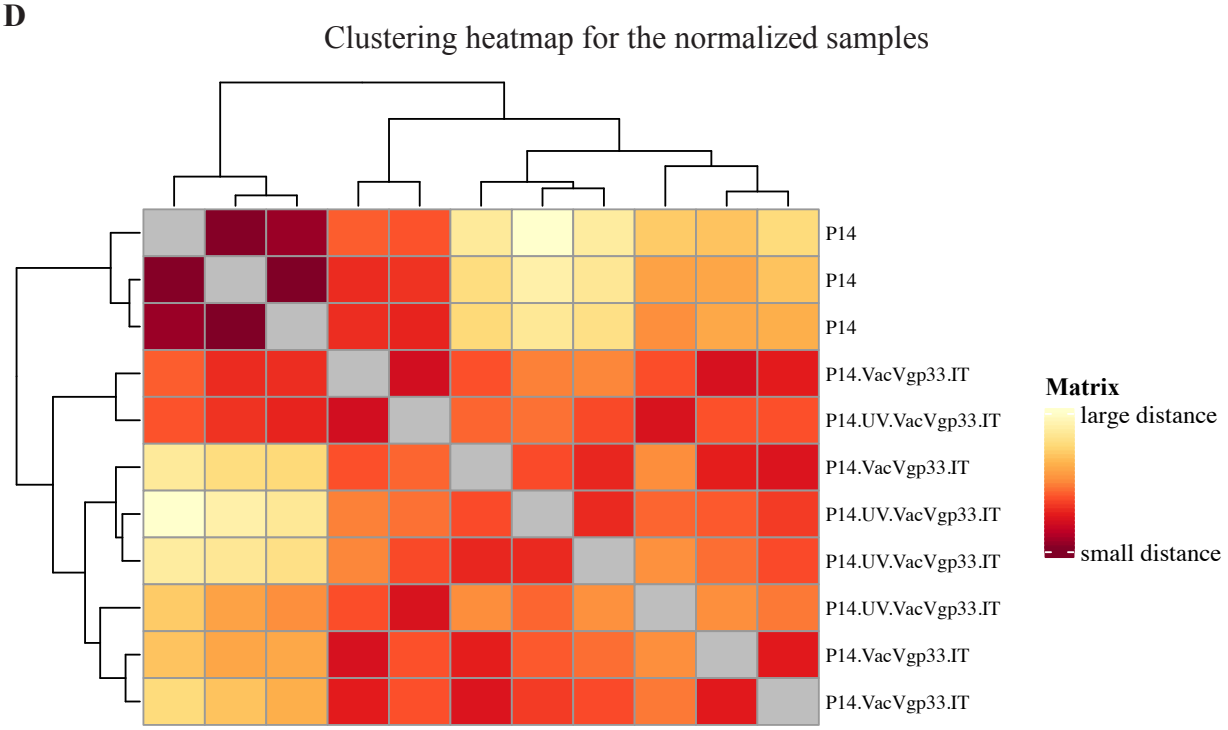

Figure 5.6 | Principal component analysis and clustering of tumour samples yield three different clusters corresponding to different treatment conditions

C57BL/6 mice (n = 3 or 4) were intradermally implanted with $2x10^5$ B16gp33 cells. 5 days later the mice were treated using $1x10^6$ adoptively transferred P14 T cells followed by 1 x 10^8 pfu VacVgp33 or UV-VacVgp33 or PBS (IT). The mice were euthanized 48 h pvi, and the tumours were collected and homogenized for RNA extraction. Total RNA per tumour was used for microarray analysis using the Clariom S mouse chip. (A-B) the oligo package was used for background correction and normalization (C) Principal component analysis was used for dimensionality reduction (D) A distance matrix was calculated using Pearson correlation and was used to perform hierarchical clustering.

A

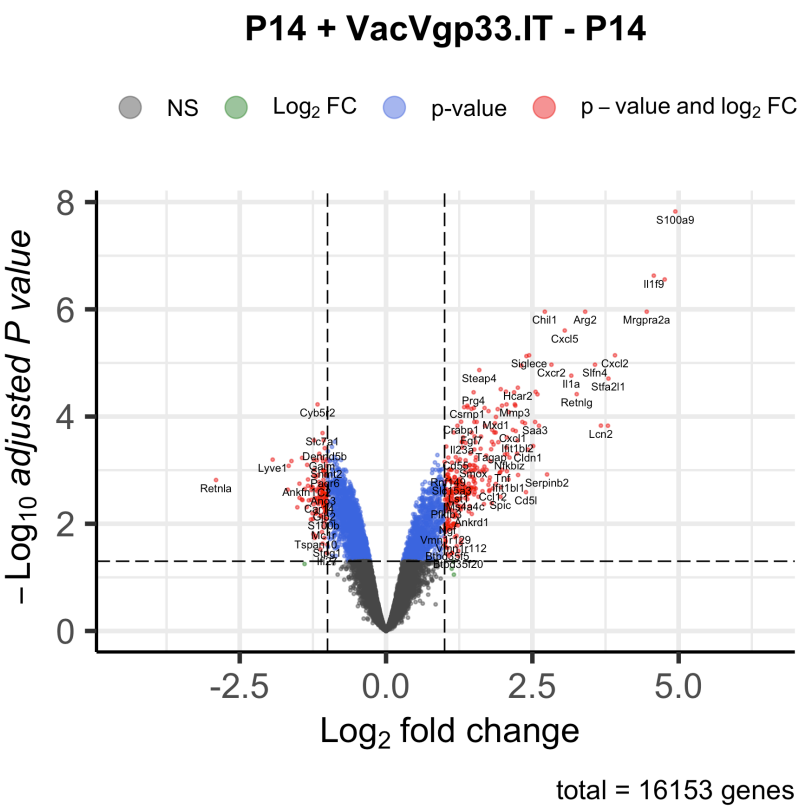
P14 + VacVgp33.IT - P14
NS
Log2 FC
p-value
p – value and log2 FC
– Log10 adjusted P value
Log2 fold change
total = 16153 genes

B

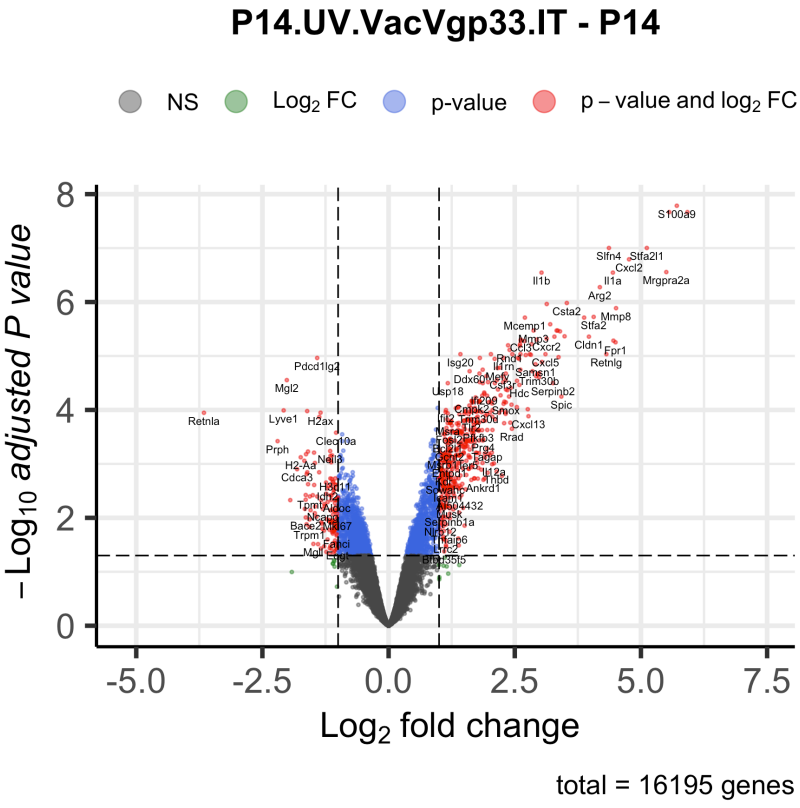
P14.UV.VacVgp33.IT - P14
NS
Log2 FC
p-value
p – value and log2 FC
– Log10 adjusted P value
Log2 fold change
total = 16195 genes

C

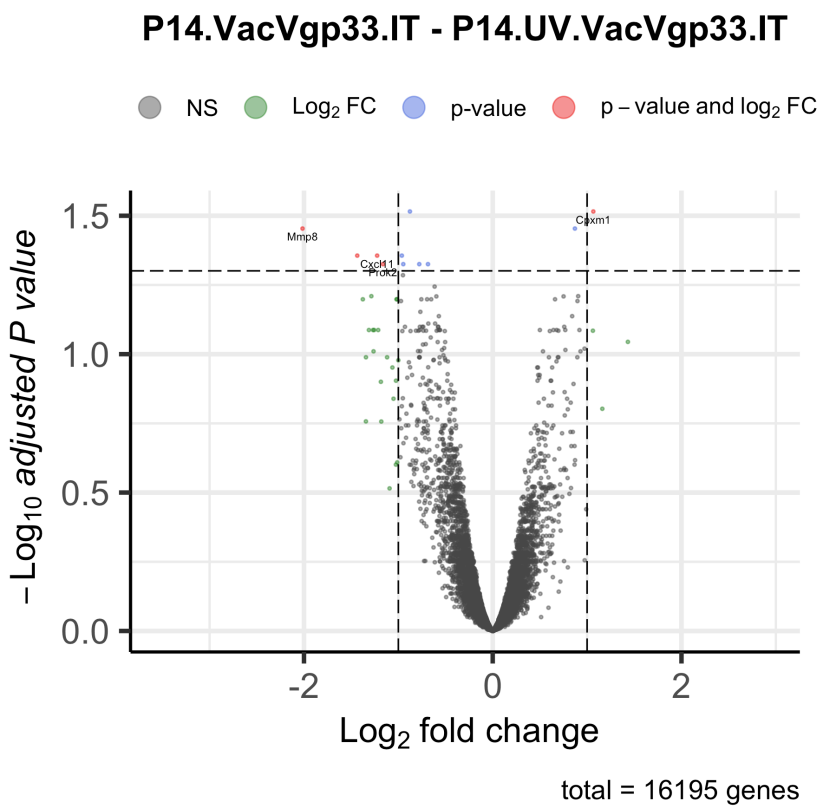
P14.VacVgp33.IT - P14.UV.VacVgp33.IT
NS
Log2 FC
p-value
p – value and log2 FC
Mmp8
Cxcl1
Prok2
Cxcr1
1.5
1.0
0.5
0.0
−Log10 adjusted P value
-2
0
2
Log2 fold change
total = 16195 genes

D

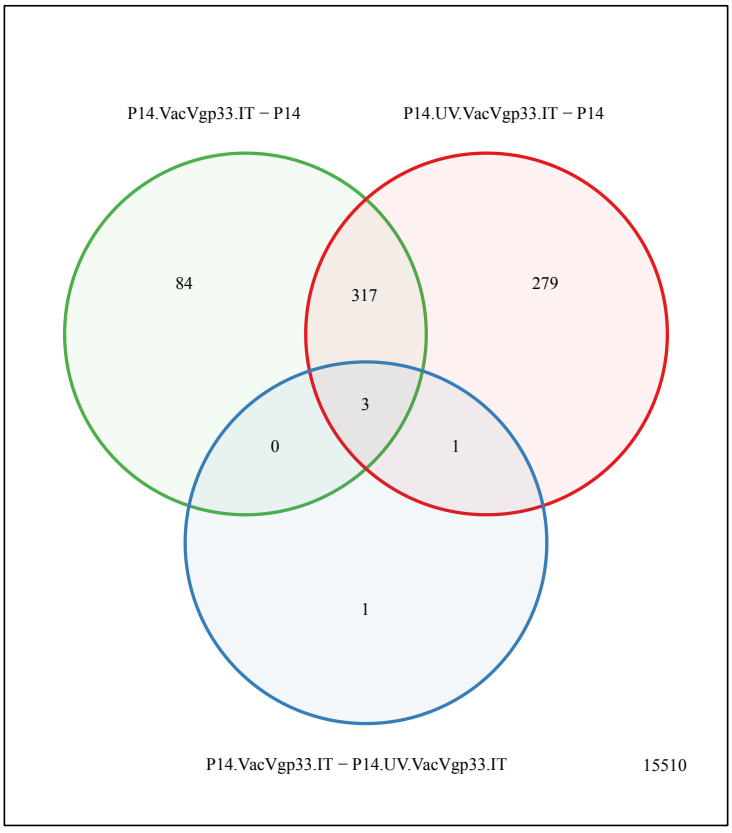
P14.VacVgp33.IT − P14
P14.UV.VacVgp33.IT − P14
84
317
279
3
0
1
1
P14.VacVgp33.IT − P14.UV.VacVgp33.IT
15510

Figure 5.7 | Microarray analysis reveals no DEGs between P14 + VacVgp33 and P14 + UV-VacVgp33 treatments

C57BL/6 mice (n = 3 or 4) were intradermally implanted with $2x10^5$ B16gp33 cells. 5 days later the mice were treated using $1x10^6$ adoptively transferred P14 T cells followed by 1 x 10^8 pfu VacVgp33 or UV-VacVgp33 or PBS (IT). The mice were euthanized 48 h pvi, and the tumours were collected and homogenized for RNA extraction. Total RNA per tumour was used for microarray analysis using the Clariom S mouse chip. (A-C) Limma package in R was used to estimated the DEGs between the different treatments, which are represented in volcano plots. (D) The intersection of DEGs in different comparisons is shown in a venndiagram.

We then sought to calculate the differentially expressed genes (DEGs) among the different treatments using the Limma package[247]. We compared the samples treated with P14 + the replicating or the inactivated VacV against the P14 control and against each other. Genes were called differentially expressed if the expression was altered by at least two-fold with an adjusted P value < 0.05. P14 + UV-VacVgp33 - treated tumours showed more DEGs (596 genes) when compared to P14 relative to P14 + VacVgp33 (404 genes) **(Fig. 5.7 A-B)**. When comparing P14 + VacVgp33 to P14 + UV-VacVgp33 we detected only 5 DEGs **(Fig. 5.7 C)**. We investigated the genes that were differentially expressed by P14 + UV-VacVgp33 but not P14 + VacVgp33 and observed that these genes were altered in the same direction by both the replicating and the inactivated virus. However, the magnitude of change was higher in the samples treated with P14 + UV-VacVgp33 and was sufficient for the genes to cross the significance threshold.

We next sought to compare the replicating and inactivated VacV on the pathway level. To this end, we used Gene Set Enrichment Analysis (GSEA) to evaluate the enrichment of the hallmark pathways[251,253]. Gene Set Enrichment Analysis (GSEA) is a computational method that considers the entire list of genes rather than only analyzing DEGs[251]. The major advantage of GSEA is that small differences in gene expression of individual genes that did not meet the cutoff threshold for fold change and/or statistical significance can still be considered in calculating the enrichment of gene sets. The Molecular Signatures Database (MSigDB) is a collection of curated gene sets developed as a joint project of UC San Diego and the Broad Institute for use with the GSEA software. It is divided into 9 major collections of gene sets, of which the hallmark gene sets, which represent well-defined biological processes condensed from over 4000 overlapping gene sets making them ideal for exploratory studies[253].

Interestingly, when comparing P14 + VacVgp33 to P14 + UV-VacVgp33 treatments, we observed that the inflammatory hallmark pathways were downregulated in case of the replicating VacVgp33 with respect to the UV-VacVgp33 **(Fig. 5.8)**. This points to a stronger magnitude of gene expression changes triggered by the UV-VacVgp33 which is unsurprising given that the immunomodulatory capacity of VacV is tied to viral gene expression during replication. Our

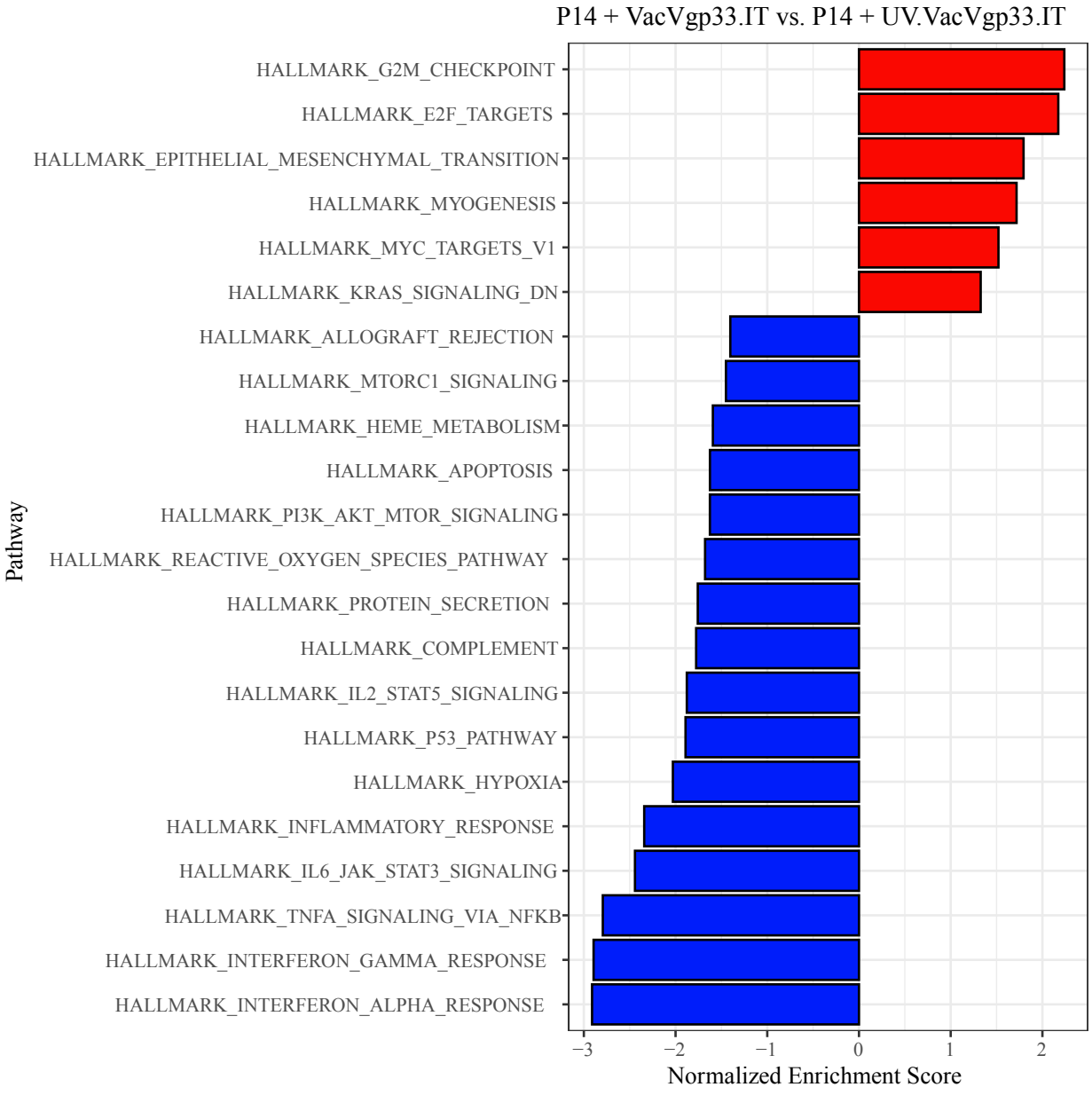
P14 + VacVgp33.IT vs. P14 + UV.VacVgp33.IT
HALLMARK_G2M_CHECKPOINT
HALLMARK_E2F_TARGETS
HALLMARK_EPITHELIAL_MESENCHYMAL_TRANSITION
HALLMARK_MYOGENESIS
HALLMARK_MYC_TARGETS_V1
HALLMARK_KRAS_SIGNALING_DN
HALLMARK_ALLOGRAFT_REJECTION
HALLMARK_MTORC1_SIGNALING
HALLMARK_HEME_METABOLISM
HALLMARK_APOPTOSIS
HALLMARK_PI3K_AKT_MTOR_SIGNALING
HALLMARK_REACTIVE_OXYGEN_SPECIES_PATHWAY
HALLMARK_PROTEIN_SECRETION
HALLMARK_COMPLEMENT
HALLMARK_IL2_STAT5_SIGNALING
HALLMARK_P53_PATHWAY
HALLMARK_HYPOXIA
HALLMARK_INFLAMMATORY_RESPONSE
HALLMARK_IL6_JAK_STAT3_SIGNALING
HALLMARK_TNFA_SIGNALING_VIA_NFKB
HALLMARK_INTERFERON_GAMMA_RESPONSE
HALLMARK_INTERFERON_ALPHA_RESPONSE
Pathway
−3
−2
−1
0
1
2
Normalized Enrichment Score

Figure 5.8 | GSEA reveals a higher magnitude of inflammation associated with P14 + UV-VacVgp33 compared to P14 + VacVgp33

C57BL/6 mice (n = 3 or 4) were intradermally implanted with $2x10^5$ B16gp33 cells. 5 days later the mice were treated using $1x10^6$ adoptively transferred P14 T cells followed by 1 x 10^8 pfu VacVgp33 or UV-VacVgp33 or PBS (IT). The mice were euthanized 48 h pvi, and the tumours were collected and homogenized for RNA extraction. Total RNA per tumour was used for microarray analysis using the Clariom S mouse chip. fGSEA package in R was used to perform GSEA using the Hallmark gene sets from MSigDB. Shown are the normalized enrichment scores (NES) for each gene set. A gene set was called significant if their FDR value is < 0.05.

previous LacZ staining analysis shows tumour wide dissemination of VacV at this time-point and strong gene expression as represented by the intensity of LacZ staining. UV-inactivated VacV is only able to support one round of infection with truncated effect as viral gene expression is constrained to early genes. So, the immunomodulatory effect of UV-inactivated VacV will be absent and the gene expression signature in the tumour will be overwhelmed by infiltrating immunity/tumour attack.

Additionally, metabolic pathways, apoptosis, as well as cell cycle control and genotoxic stress/DNA repair pathways were also differentially regulated by the replicating VacV compared to UV-inactivated VacV. VacV is known to encode genes for blocking cellular apoptosis[284], and disrupting cellular metabolism as these are essential steps in subverting the cellular machinery to support virus replication. Indeed, as outlined earlier, VacV replicates best in cells with a high proliferation rate due to the enhanced availability of biomaterials for its replication. But VacV also needs to maintain the integrity of infected cells until virus replication is complete and so inhibition of apoptosis is an essential component of virus replication. The pathways related to genotoxic stress and cell cycle control are also tied to apoptosis, such as the p53 pathway, as these biological processes have significant overlap. Detection of DNA damage necessitates a pause of the cell cycle so that the damage can be repaired. In the event that the DNA damage cannot be repaired, however, apoptosis of the affected cells is an integral mechanism to prevent propagation of mutations to daughter cells. Furthermore, a recent paper has identified a capacity for VacV to inhibit the DNA repair pathway directly as a means to avoid cellular detection of viral DNA[285]. Thus, it was not surprising that these pathways were manipulated by VacV and that a more extensive effect was observed with replication competent VacV. However, this does not obviate the possibility that these signatures point to an alternative explanation for the lack of gene loss variant mediated relapse in VacV treated mice which will be explored more later.

5.2.7. PLWUV-inactivated VacV is sufficient to induce cure in MC38 tumour model

Next, we sought to test out the efficacy of VacVgp33 and UV-VacVgp33 in a different tumour model. MC38 is an immunogenic murine colorectal cancer cell line that was chemically induced in a female C57BL/6 mouse[243,286]. It has been used as a transplantable tumour model to study several aspects of cancer immunotherapy. To make use of the transgenic P14 mice and gp33-expressing viral vectors, we cloned the gp33 construct into MC38 (done by other lab members). Collective observations from the Wan lab showed that MC38gp33 was able to prime enough CD8 T cell responses making it possible to use an OVV directly without the need for ACT. This is due to its slower growth rate and higher immunogenicity compared to the B16gp33 model. Hence, we treated MC38gp33 tumour-bearing mice with VacVgp33 or UV-VacVgp33. Using ICS, we detected comparable levels of IFNγ-secreting gp33-specific $CD8^+$ T cells in the circulation 5 days post treatment with VacVgp33 or UV-VacVgp33 **(Fig. 5.9 A)**. The responses dropped down by day 12, which is consistent with the T cell kinetics reported earlier in the B16gp33 model. In terms of tumour control, the replicating VacVgp33 was faster to eliminate the tumours, but eventually the mice treated with the replicating or PLWUV-inactivated VacVgp33 showed the same survival proportions of 60% **(Fig 5.9 B-C)**.

A

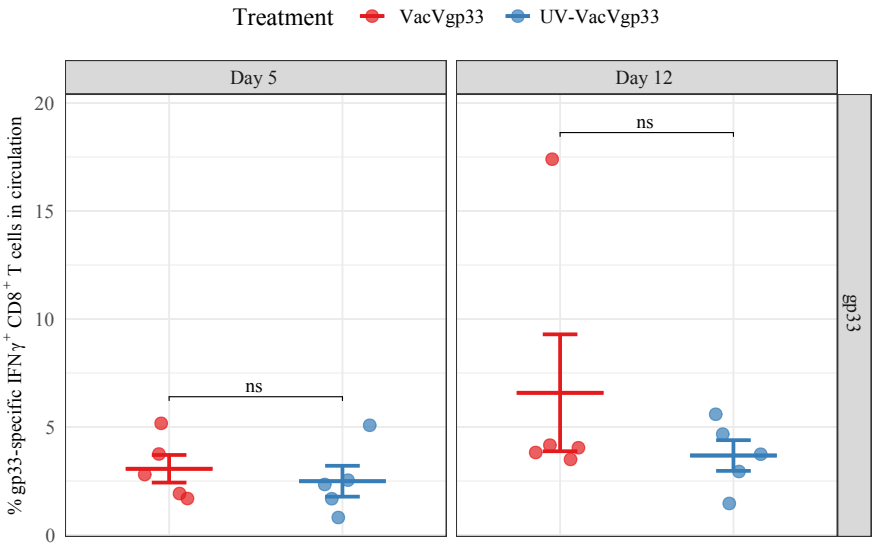
Treatment
VacVgp33
UV-VacVgp33
Day 5
Day 12
gp33
ns
ns
% gp33-specific IFNγ+ CD8+ T cells in circulation
0
5
10
15
20

B

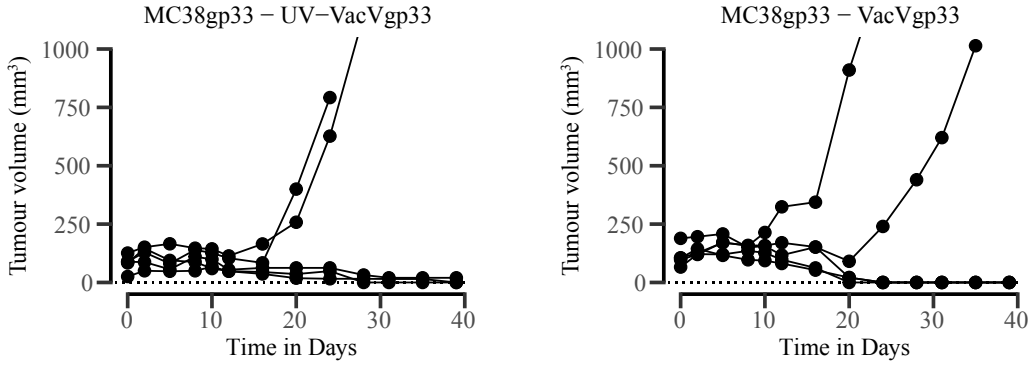
MC38gp33 − UV−VacVgp33
MC38gp33 − VacVgp33
Tumour volume (mm3)
Time in Days
0
250
500
750
1000
0
10
20
30
40

C

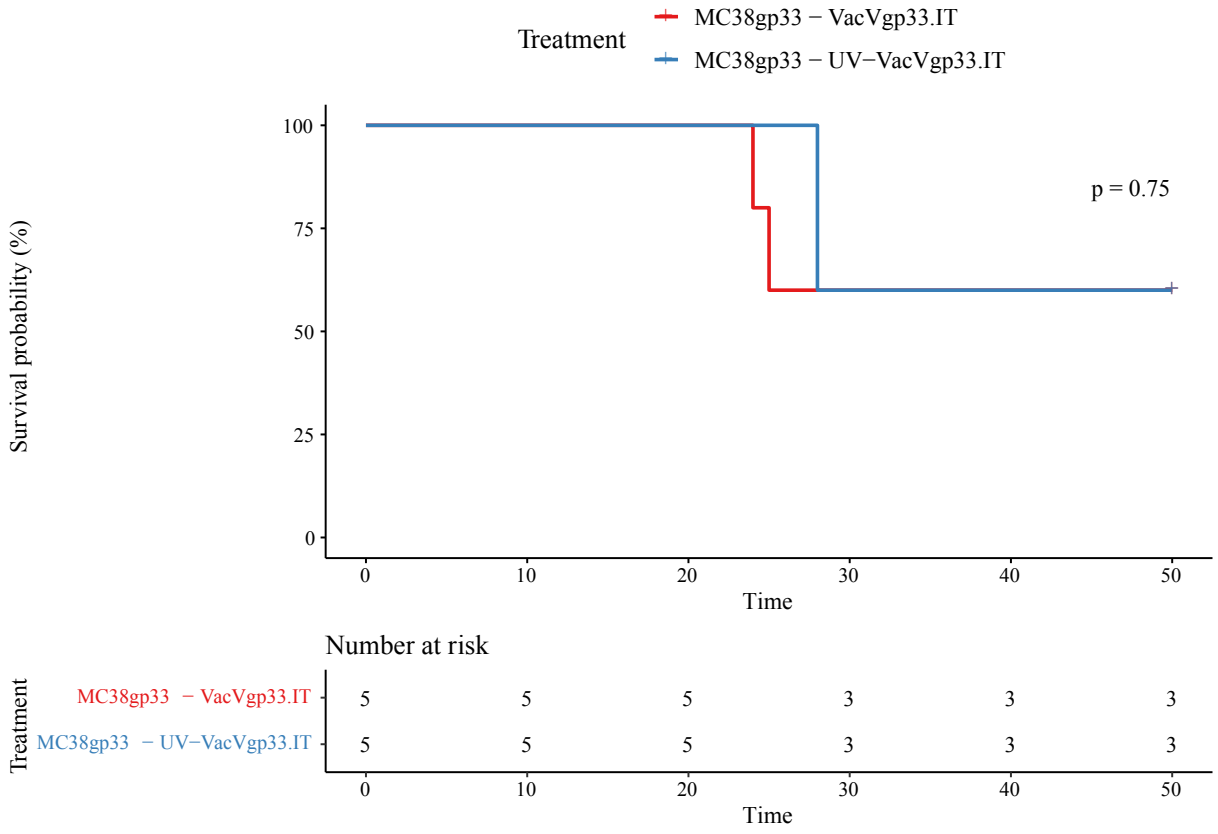

Figure 5.9 | PLWUV-inactivated VacV is sufficient to induce cure in MC38 tumour model

C57BL/6 mice (n=5) were intradermally implanted with $2x10^5$ MC38gp33 cells. 5 days later the mice were treated using 1 x 10^8 pfu VacVgp33 or UV-VacVgp33 IT (A) At days 5 and 12 post treatment, blood samples were collected, processed, stained for intracellular IFNγ following *in vitro* peptide stimulation and analyzed using flow cytometry. (B) Tumour volumes were continuously measured every third day and are presented as length * width * height (C) Overall survival was monitored for up to 60 days post tumour challenge. The survival statistics were calculated using log-rank test. *p < 0.05, **p <0.01, ***p <0.001, ****p <0.0001

Chapter 6 — Investigating the differential effects of VSV and VacV on altering the cellular and transcriptomic landscapes in the TME

6.1. Introduction

In the previous chapter we showed that replicating VacV is required to achieve durable long term tumour control in the B16 melanoma model. We postulated that the benefits associated with the use of the replicating virus are due to direct oncolysis which help eliminate antigen negative variants and prevent immune escape. An alternative hypothesis is that the presence of VacV in the TME leads to transcriptomic changes that mediate the recruitment of innate immune cells complementing the $CD8^+$ T cell attack on the tumour. In this chapter we aim to study the differential effects of VSV and VacV on altering the cellular and molecular profiles in the TME when used in combination with ACT. We conducted a flow cytometry based cellular analysis to study the dynamic changes occurring within the TME at different time-points following ACT + VSV or VacV. Our results revealed no significant differences between VSV and VacV in recruiting different populations to the TME. We then profiled tumours treated with ACT + VSV or VacV using a high throughput microarray and found that VacV causes upregulation of various inflammatory processes and pathways with the exception of type I IFN, which was downregulated compared to VSV. Additionally, VacV caused downregulation of cell metabolism and cell cycle related pathways. Interestingly, such transcriptomic changes were combined with the inhibition of DNA repair pathways which we believe is crucial to prevent therapy-induced antigen loss and drive tumour cells to apoptosis. Collectively, our data uncovers an additional mechanism by which VacV helps eradicate tumour cells. By blocking DNA repair pathways, VacV prevents tumour cells from surviving the DNA damage induced by ROS species and thus stops tumour cells from evolving and losing their target antigen and growing therapy-resistant clones.

6.2. Results

6.2.1. Intratumoural immune analysis over a time course reveals no significant differences in cellular recruitment profile between P14 + VacVgp33 IT and P14 + VSVgp33 IT treatments.

Having observed better outcomes using the IT route for both VacV and VSV treatments correlated with an enhanced direct effect of the virus in the TME, we decided to focus on IT for further characterization. We were interested in studying whether a certain immune population(s) are being recruited specifically by VacV to the TME that would help prevent immune escape. To this end, we sought to thoroughly examine the differences in the cellular landscape of the tumour infiltrating leukocytes (TILs) following P14 + VacVgp33 and P14 + VSVgp33 treatments. B16gp33 tumour bearing mice were treated using P14 T cells and VSVgp33 or VacVgp33 or PBS delivered IT. In order to capture the dynamic changes within the TME we analyzed the TILs over a time course of 3 time-points (day 2,4 and 6 pvi). Table 3.6 summarizes the antibodies and their respective fluorescent channels used in this study. We first calculated the frequencies of different cellular populations relative to the total viable leukocytes recovered from each tumour **(Table 6.1 and Fig. 6.1 A)**. At day 2 pvi, $CD11b^+$ myeloid cells were the predominant population of cells recovered from the tumours ranging from 30-50% across the treatment groups. This was followed by NK cells constituting around 20% of the immune infiltrating cells across the treatment groups. At day 4 pvi, we observed an increase in $CD8^+$ T cells frequency across the treatment groups, albeit with different degrees. P14 + VacVgp33 had the most increase in $CD8^+$ T cells recruitment to the TME at day 4 pvi. Interestingly, P14 + VSVgp33 recruited more NK cells to the TME compared to P14 + VacVgp33 or PBS. The frequency of NK cells was even higher than $CD8^+$ T cells. This was inconsistent with our previous analysis of tumours at day 4 pvi, where NK cells represented a minority across all treatment groups. By day 6 pvi, the frequency of NK cells had plummeted and that of $CD8^+$ T cells had increased up to 60% of the total immune cells in both

A

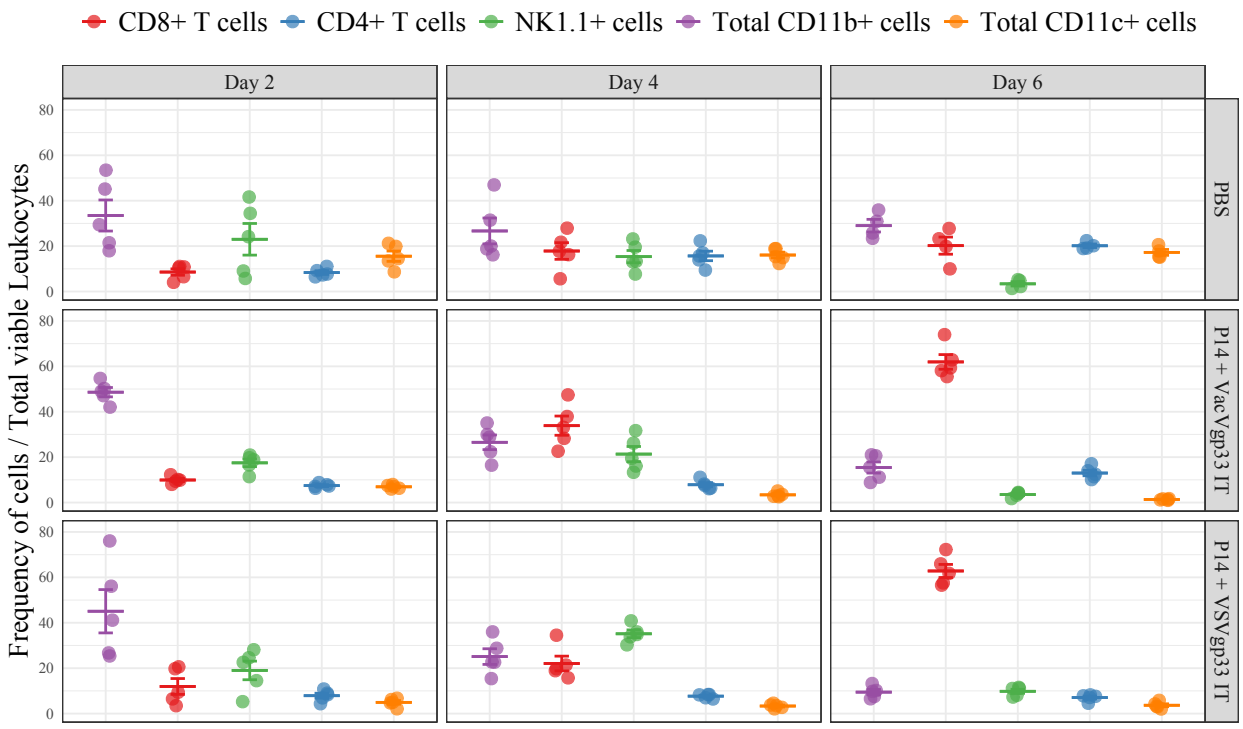
CD8+ T cells
CD4+ T cells
NK1.1+ cells
Total CD11b+ cells
Total CD11c+ cells
Day 2
Day 4
Day 6
PBS
P14 + VacVgp33 IT
P14 + VSVgp33 IT
Frequency of cells / Total viable Leukocytes
0
20
40
60
80

B


Treatment PBS P14 + VacVgp33 IT P14 + VSVgp33 IT
Day 2
Day 4
Day 6
CD8+ T cells
Thy1.1+CD8+ T cells
CD4+ T cells
NK1.1+ cells
Total CD11b+ cells
Ly6G+ CD11b+ cells
log10 (Number of cells / g Tumor)


Treatment
PBS
P14 + VacVgp33 IT
P14 + VSVgp33 IT
Day 2
Day 4
Day 6
Ly6G- Ly6C+ CD11b+ cells
Total CD11c+ cells
CD11b+ CD11c+ cells
CD103+ CD11c+ cells
log10 (Number of cells / g Tumor)

Figure 6.1 | Intratumoural immune analysis over a time course reveals no significant differences between P14 + VacVgp33 IT and P14 + VSVgp33 IT treatments

C57BL/6 mice (n = 5) were intradermally implanted with 2x105 B16gp33 cells. 5 days later the mice were treated using $1x10^6$ adoptively transferred P14 T cells followed by 1 x 10^8 pfu VacVgp33 or VSVgp33 or PBS (IT). At days 2, 4, and 6 pvi, the mice were euthanized and tumours were collected, processed, stained for the shown surface markers and analyzed using flow cytometry. Shown is the frequency of each cell population with respect to the total viable cells recovered for every tumour (A) and $\log_{10}$ transformation of the number of cells normalized to the respective weights of the tumours in g (B). Pairwise t-test with BH correction was performed on each cell population independently. The horizontal bars represent means ± SEM. *P < 0.05, **P<0.01, ***P<0.001, ****P<0.0001.

P14 + VacVgp33 and P14 + VSVgp33 treatment groups. No remarkable changes to $CD4^+$ T cells or $CD11c^+$ cells were observed between the different time-points. PBS treated mice had a higher frequency of $CD11c^+$ DCs compared to P14 + VacVgp33 or P14 + VSVgp33.

We analyzed the different cellular populations individually among the three treatments groups at the three time-points **(Fig. 6.1 B)**. It is worth pointing out that using the normalized number of cells / g tumour for the analysis was not appropriate since most populations experienced heteroscedasticity across the time course. This is due to the drastic changes that occur to different cellular populations at different time-points as a result of our treatments. Log_{10} transformation of the normalized numbers alleviated the problem, and it was thus used for plotting the data and for doing the statistical analysis. Consistent with what we have observed before, both P14 + VacVgp33 and P14 + VSVgp33 treatments led to statistically significant increase in the numbers of total $CD8^+$ T cells as well as $Thy1.1^+$ transferred P14 cells in the TME compared to PBS. $Thy1.1^+$ P14 cells were observed as early as day 2 pvi and their normalized counts remained almost constant throughout the time course. We also saw a gradual decline in the numbers of NK cells present in the TME throughout the time course for PBS and P14 + VacVgp33 treated mice. P14 + VSVgp33 treatment on the other hand maintained a consistent level of NK cells in TME at the three studied time-points and at day 6 pvi, significantly higher numbers of NK cells were observed compared to PBS and P14 + VacVgp33. Additionally, both P14 + VacVgp33 and P14 + VSVgp33 treatments led to significant recruitment of $CD11b^+$ myeloid cells to the TME especially at day 2 pvi. The recruitment of more lymphocytes to the TME at later time-points correlated with a slight drop in the numbers of myeloid cells in all treatment groups. No statistically significant difference in the total number of myeloid cells was observed among the two virus treatments at any time point. Interestingly, the composition of the myeloid populations in the TME appears to be different. At day 6 pvi, P14 + VacVgp33 treated mice had slightly more $Ly6G^+ Ly6C^{int}$ cells, albeit not to a significant level. P14 + VSVgp33 treated tumours, on the other hand, had statistically significant increase in $Ly6G^- Ly6C^{int/hi}$ cells compared to both P14 and P14 + VacVgp33 treated mice. Moreover, P14 + VacVgp33 treated tumours displayed a gradual

decline in the total CD11c$^+$ DCs in the TME. This was contrary to P14 + VSVgp33 treatment that led to statistically significant increase in the total CD11c$^+$ DCs as well as in the two analyzed DC subpopulations: CD103$^+$DCs (cDC1) and CD11b$^+$DCs (cDC2) at day 6 pvi. Altogether, while some differences were observed between the immune infiltrating populations in the tumours treated with ACT + VSV or VacV, no striking differences among the analyzed populations were observed that might explain the different clinical outcomes.

6.2.2. *In vivo* depletion of NK1.1$^+$ cells or Ly6G$^+$ cells does not affect the efficacy of P14 + VacVgp33 treatment

Next, we used *in vivo* depletion antibodies to selectively remove certain immune populations to identify whether they play a role in the overall efficacy of P14 + VacVgp33 treatment and/or help prevent tumour relapse. B16gp33 tumour-bearing mice were treated using P14 T cells and VacVgp33 delivered IT. We used *in vivo* depletion antibodies that target CD8$^+$, NK1.1$^+$, and Ly6G$^+$ cells. The detailed depletion protocols are described in the materials and methods section (Chapter 2). We focused on NK cells and neutrophils in addition to CD8$^+$ T cells for this depletion experiment because NK cells have known function to kill tumour cells in an antigen independent fashion and neutrophils are supportive to NK and CD8$^+$ T cell killing function. NK cell killing is mediated by stress signals/ligands on the tumour and so VacV treated tumours may be more susceptible to NK cell killing, especially with the increased viral load of IT injection. Thus, these innate immune killer cells could be responsible for eliminating antigen negative variant cells during P14 + VacVgp33 treatment, despite recruiting lower numbers. In all treatment groups, we monitored tumour regression, and the overall survival of mice to demonstrate the roles these different cellular population play in our therapeutic model. As anticipated, CD8$^+$ T cells depletion led to loss of tumour control. This supports our understanding that CD8$^+$ T cells are indeed indispensable for tumour control in our therapeutic model **(Fig. 6.2 A)**. Depletion of NK1.1$^+$ or Ly6G$^+$ cells had no statistically significant effect on tumour control nor on the overall

A

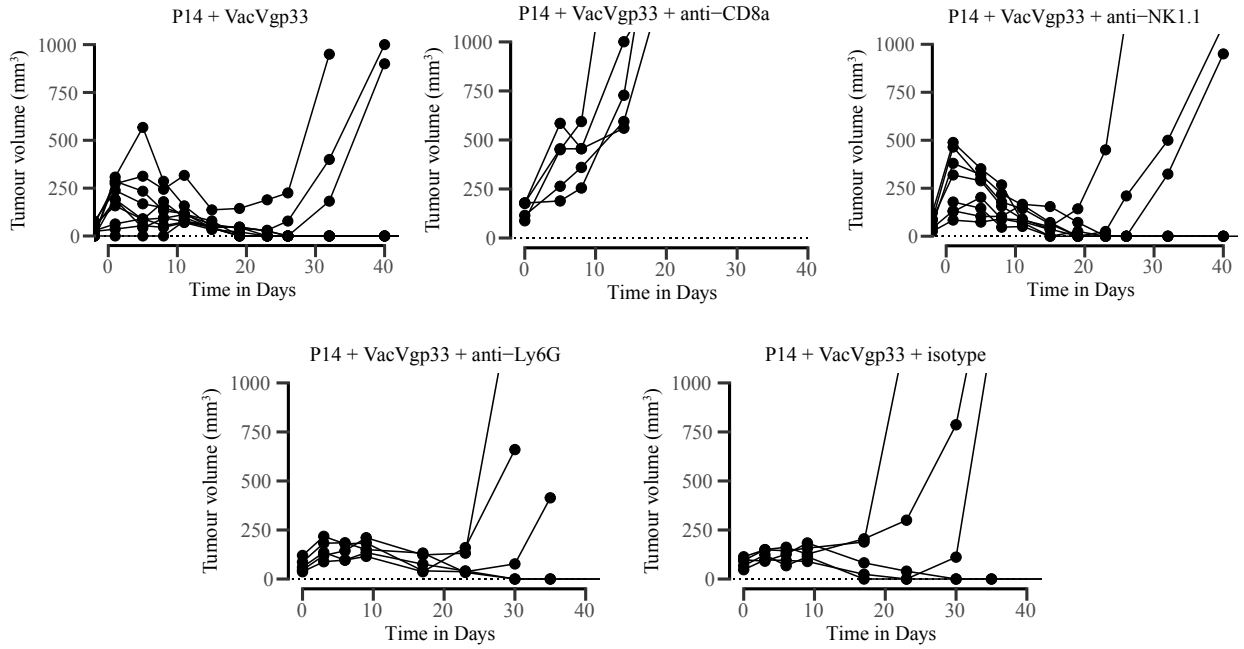
P14 + VacVgp33
P14 + VacVgp33 + anti−CD8a
P14 + VacVgp33 + anti−NK1.1
P14 + VacVgp33 + anti−Ly6G
P14 + VacVgp33 + isotype
Tumour volume (mm3)
Time in Days
0
250
500
750
1000
0
10
20
30
40

B

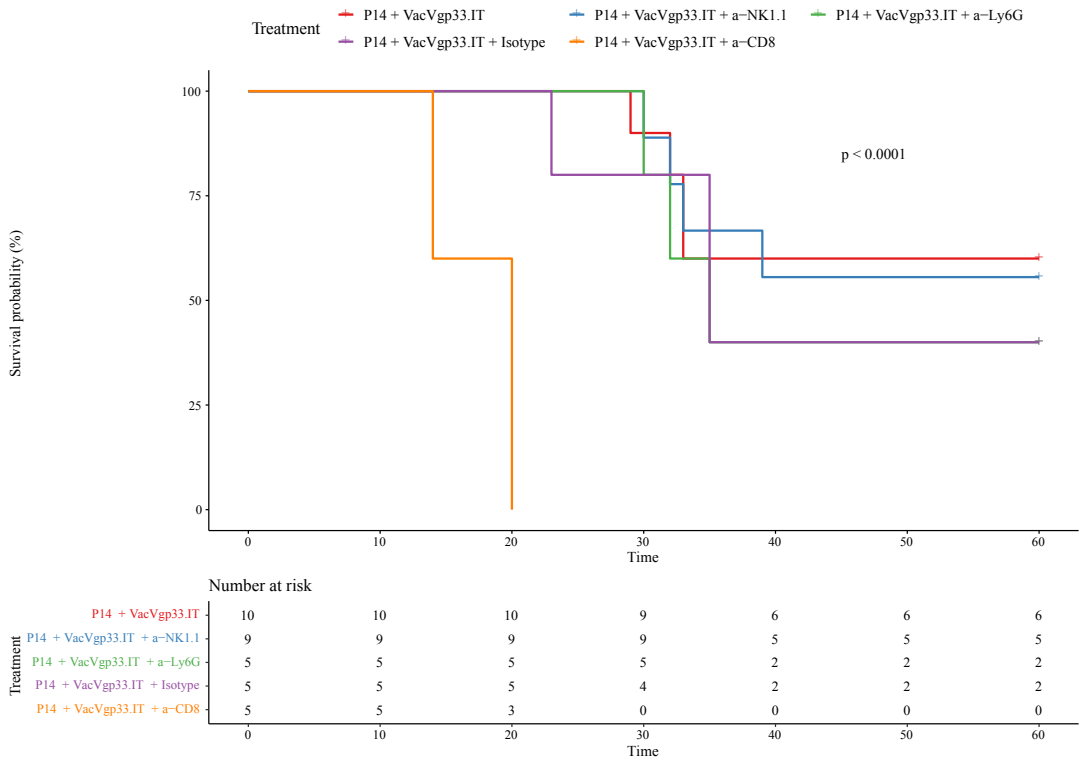
Treatment
P14 + VacVgp33.IT
P14 + VacVgp33.IT + a−NK1.1
P14 + VacVgp33.IT + a−Ly6G
P14 + VacVgp33.IT + Isotype
P14 + VacVgp33.IT + a−CD8
Survival probability (%)
p < 0.0001
Time
Number at risk
P14 + VacVgp33.IT 10 10 10 9 6 6 6
P14 + VacVgp33.IT + a−NK1.1 9 9 9 9 5 5 5
P14 + VacVgp33.IT + a−Ly6G 5 5 5 5 2 2 2
P14 + VacVgp33.IT + Isotype 5 5 5 4 2 2 2
P14 + VacVgp33.IT + a−CD8 5 5 3 0 0 0 0

Figure 6.2 | In vivo depletion of NK1.1+ cells or Ly6G+ cells does not affect the efficacy of P14 + VacVgp33 treatment

C57BL/6 mice (n=5) were intradermally implanted with $2x10^5$ B16gp33 cells. 5 days later the mice were treated using $1x10^6$ adoptively transferred P14 T cells followed by 1 x 10^8 pfu VacVgp33 (IT). 250µg of each of the antibodies were delivered IP one day before virus injection and again one day after injection. Weekly injections of antibodies were used to maintain the depletion with the exception of Ly6G that was injected every 4th day. (A) Tumour volumes were continuously measured every 2-4 days. The volumes were calculated as length x width x height. (B) Overall survival was monitored for up to 60 days post tumour challenge and log-rank test was used to calculate the survival statistics.

survival of mice **(fig 6.2 A-B)**. Hence, we concluded that unlike $CD8^+$ T cells which are necessary for the success of the therapy, NK cells and neutrophils appear to be dispensable.

6.2.3. Microarray analysis reveals distinct inflammatory profiles in the TME following VacV or VSV treatment

The lack of significant differences in the immune populations infiltrating the TME following P14 + VacVgp33 and P14 + VSVgp33 treatments prompted us to investigate whether molecular processes can explain the different outcomes observed using both viruses. To this end, we treated B16gp33 tumour-bearing mice with P14 + VacVgp33 or VSVgp33 or PBS delivered IT. Tumours were then harvested 48 h pvi, homogenized and RNA was extracted for microarray analysis to study the molecular changes within the TME following the respective treatments. We used the same analysis workflow described in the chapter 5. **Fig. 6.3 A-B** show the relative log expression of each chip before and after normalization. We then performed principal component analysis (PCA) to assess whether samples receiving the same treatments would cluster together **(Fig. 6.3 C)**. Samples of the same treatment group were nicely clustered along the first two principal components where the first component accounted for 38.9% of the variation between samples while the second component accounted for 12.9% of the variation. Pearson correlation was used to calculate the dissimilarity between samples and generate a matrix of distances that was used to perform unsupervised hierarchical clustering **(Fig. 6.3 D)**. We observed that P14 + VacVgp33 treated tumours displayed the greatest dissimilarity distance compared to both P14 control and P14 + VSVgp33 treated tumours.

In order to estimate the differentially expressed genes (DEGs) between the different treatment conditions we used the Limma package[247]. We were interested in examining how each virus alters the transcriptomic profile within the TME relative to the ACT control. Additionally, we were curious to analyze the DEGs between VacV and VSV treated tumours. Genes were considered differentially expressed if at least 2-fold change is returned with an adjusted *P* value

A

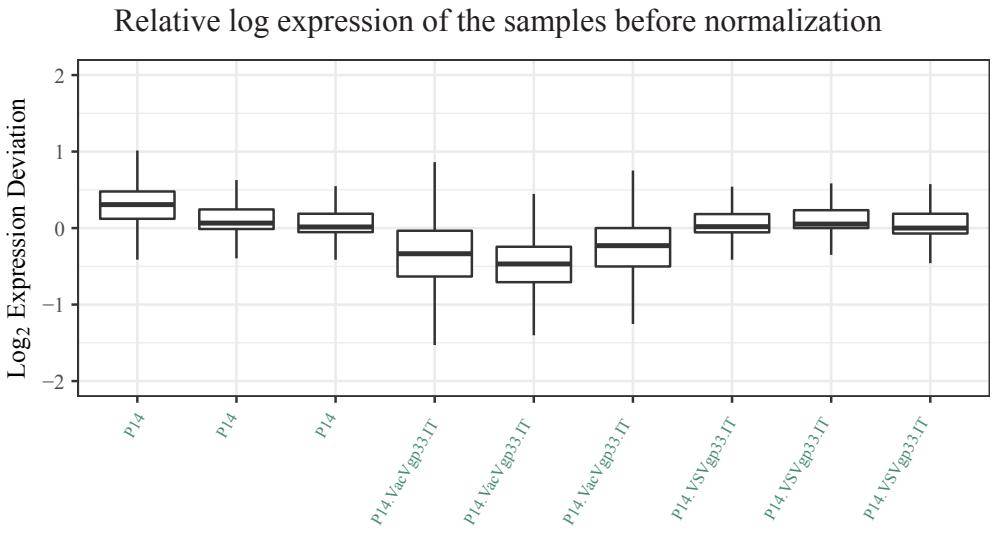
Relative log expression of the samples before normalization
Log2 Expression Deviation
2
1
0
−1
−2
P14
P14
P14
P14.VacVgp33.IT
P14.VacVgp33.IT
P14.VacVgp33.IT
P14.VSVgp33.IT
P14.VSVgp33.IT
P14.VSVgp33.IT

B

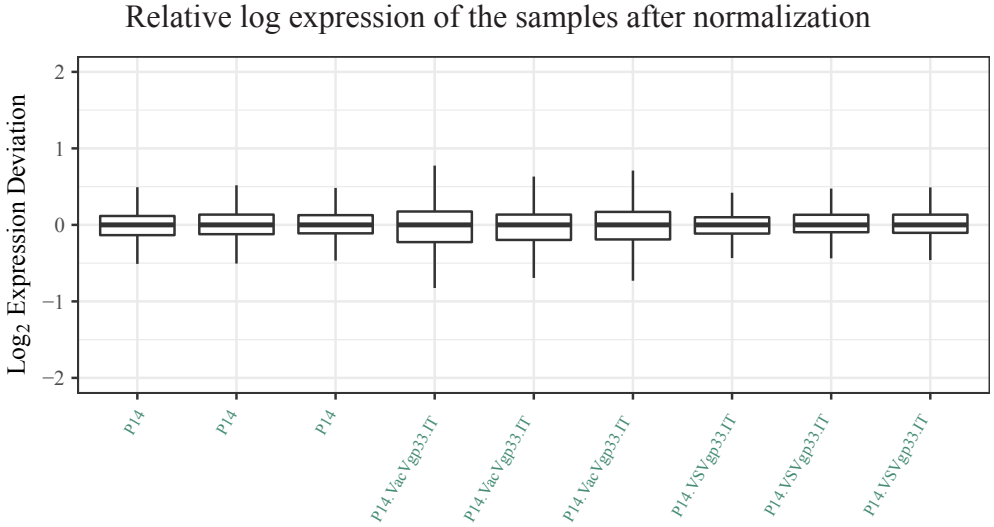
Relative log expression of the samples after normalization
Log2 Expression Deviation
2
1
0
−1
−2
P14
P14
P14
P14.VacVgp33.IT
P14.VacVgp33.IT
P14.VacVgp33.IT
P14.VSVgp33.IT
P14.VSVgp33.IT
P14.VSVgp33.IT

C

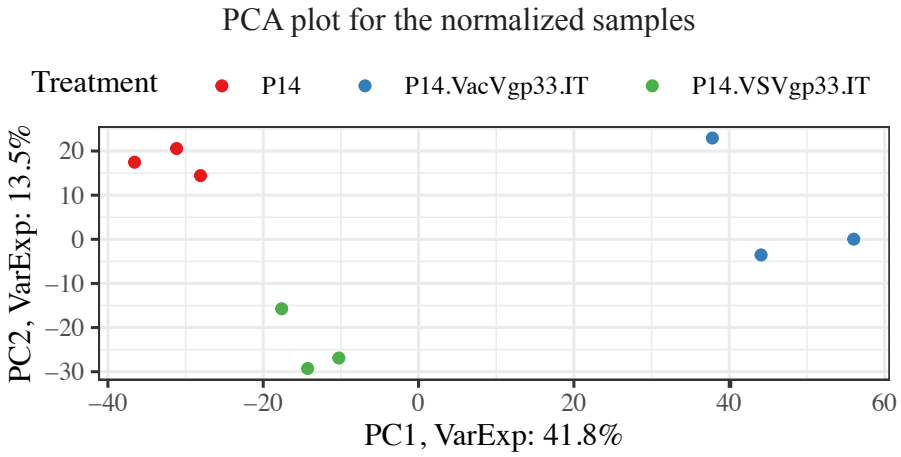
PCA plot for the normalized samples
Treatment
P14
P14.VacVgp33.IT
P14.VSVgp33.IT
PC2, VarExp: 13.5%
20
10
0
−10
−20
−30
−40
−20
0
20
40
60
PC1, VarExp: 41.8%

D

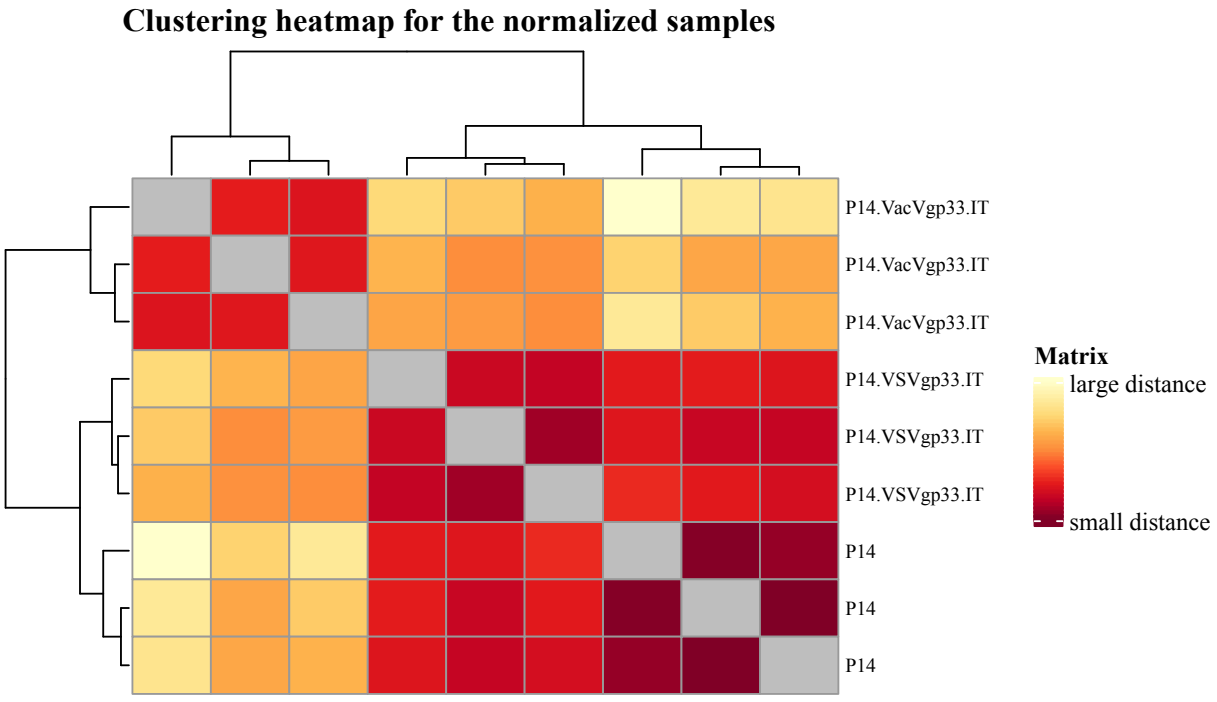

Figure 6.3 | Principal component analysis and clustering of tumour samples yield three different clusters corresponding to different treatment conditions

C57BL/6 mice (n = 3 or 4) were intradermally implanted with $2x10^5$ B16gp33 cells. 5 days later the mice were treated using $1x10^6$ adoptively transferred P14 T cells followed by 1 x 10^8 pfu VSVgp33 or VacVgp33 or PBS (IT). The mice were euthanized 48 h pvi, and the tumours were collected and homogenized for RNA extraction. Total RNA per tumour was used for microarray analysis using the Clariom S mouse chip. (A-B) the oligo package was used for background correction and normalization (C) Principal component analysis was used for dimensionality reduction (D) A distance matrix was calculated using Pearson correlation and was used to perform hierarchical clustering.

< 0.05. Comparing P14 + VacVgp33 treated tumours to P14 treated tumours revealed a total of 422 DEGs **(Fig. 6.4 A)**. On the other hand, P14 + VSVgp33 treatment resulted in 158 DEGs when compared to P14 treatment **(Fig. 6.4 B)**. We also identified 223 DEGs when comparing P14 + VacVgp33 to P14 + VSVgp33 treatments **(Fig. 6.4 C)**. A Venn diagram representing the intersection of DEGs is shown in **figure 6.4 D**. The full lists of DEGs in each comparison are presented in **Supplementary Tables 1, 2 and 3.**

While the identification of differentially expressed genes (DEGs) indeed provides valuable information regarding the molecular changes across treatments, it remains challenging to manually spot complex mechanistic changes by observing changes in the expression of individual genes. For better interpretability of the data, we performed enrichment analysis to identify the biological processes and/or pathways that are significantly impacted following a given treatment. We first did an overrepresentation analysis (ORA) on the lists of DEGs using the Biological Process (BP) domain of the Gene Ontology (GO) annotations to identify the overrepresented biological processes[248]. Because of the acyclic parent-child relationship of the GO terms, redundancy in terms is commonly observed. We used an algorithm (GOSemSim) that calculates the semantic similarity between terms and simplifies the output of the enrichment analysis[287]. The top 50 enriched terms of each comparison are shown in **Figure 6.5 A-C**. When comparing each virus to the control, almost all the enriched terms reflected immune related processes. Chemotaxis, cell migration, cytokine secretion, IL-1 and IL-6 production were common themes observed with both VacV and VSV treatments. Additionally, both viruses stimulated Interferon type I and type II responses and Tumour Necrosis Factor (TNF) - mediated responses. When comparing P14 + VacVgp33 against P14 + VSVgp33 treated tumours, the terms enriched included leukocyte adhesion, T cell activation, phagocytosis, cell migration and differentiation, active inflammatory response among others. To highlight the relationships between the enriched terms, an enrichment map was plotted for each enrichment analysis **(Fig. 6.5 D-F)**. In conclusion, both VacV and VSV induce strong inflammatory responses within the TME. Although different GO terms were enriched, the biological themes were generally consistent and did not point to distinct processes induced by

A

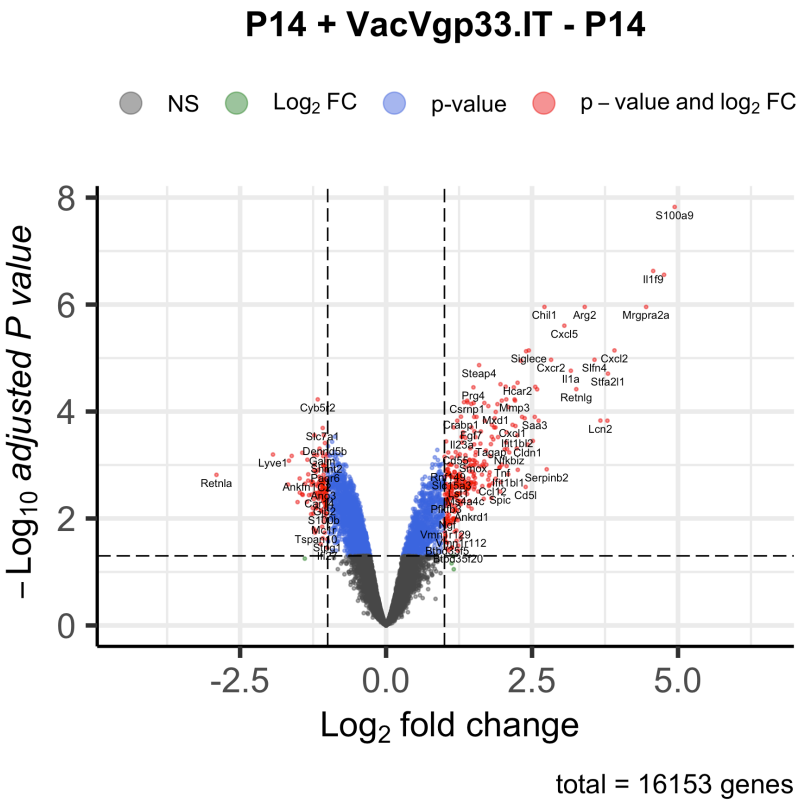
P14 + VacVgp33.IT - P14
NS
Log2 FC
p-value
p – value and log2 FC
– Log10 adjusted P value
Log2 fold change
total = 16153 genes

B

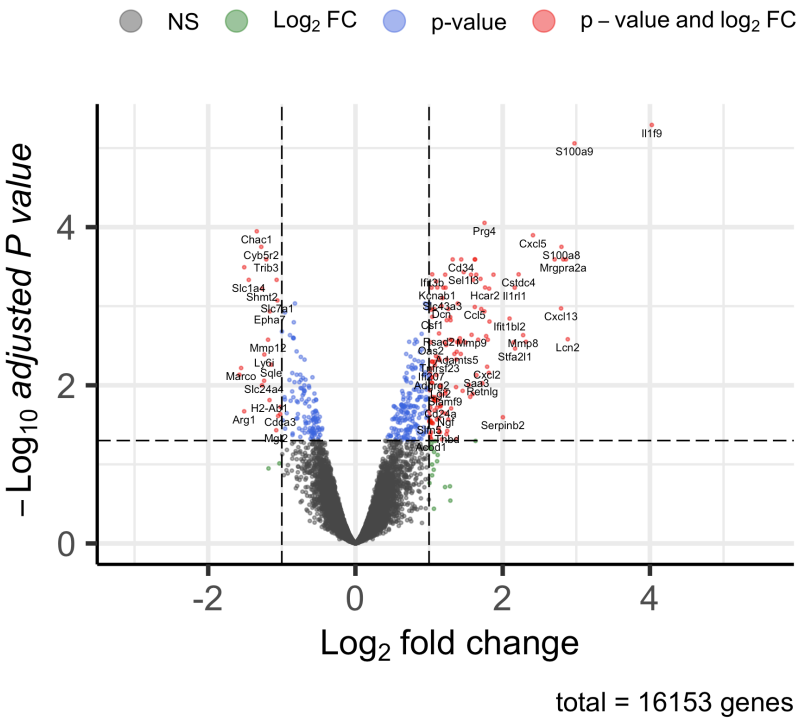
P14 + VSVgp33.IT - P14
NS
Log2 FC
p-value
p – value and log2 FC
– Log10 adjusted P value
Log2 fold change
total = 16153 genes

C

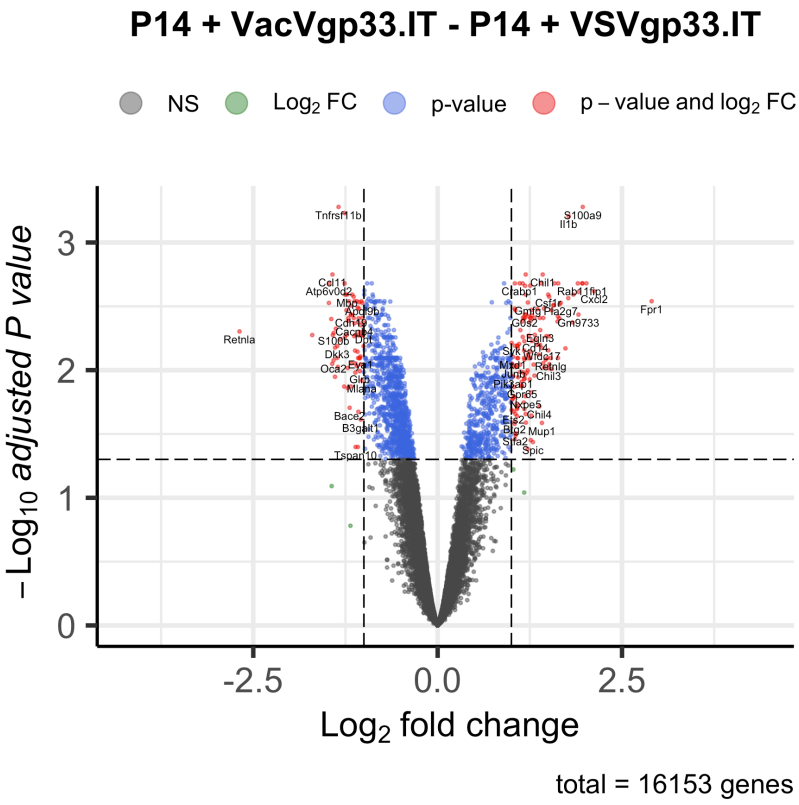
P14 + VacVgp33.IT - P14 + VSVgp33.IT
NS
Log2 FC
p-value
p – value and log2 FC
– Log10 adjusted P value
Log2 fold change
-2.5
0.0
2.5
0
1
2
3
Tnfrsf11b
S100a9
Il1b
Retnla
Fpr1
Cxcl2
Gm9733
Chil1
Chil3
Mup1
Spic
total = 16153 genes

D

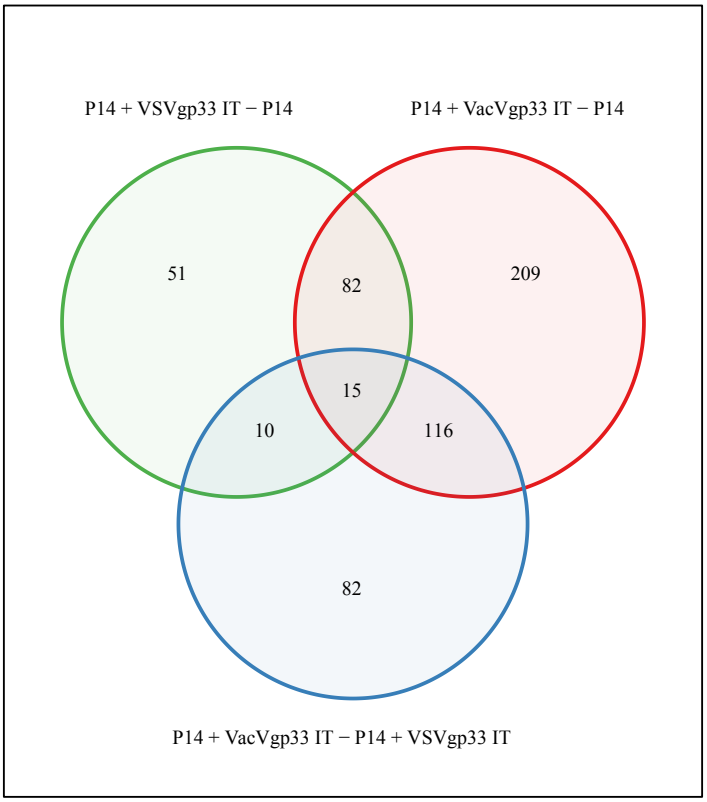
P14 + VSVgp33 IT − P14
P14 + VacVgp33 IT − P14
51
82
209
15
10
116
82
P14 + VacVgp33 IT − P14 + VSVgp33 IT

Figure 6.4 | Microarray analysis reveals transcriptomic differences among P14 + VacVgp33, P14 + VSVgp33 and P14 treatments

C57BL/6 mice (n = 3 or 4) were intradermally implanted with $2x10^5$ B16gp33 cells. 5 days later the mice were treated using $1x10^6$ adoptively transferred P14 T cells followed by 1 x 10^8 pfu VacVgp33 or VSVgp33 or PBS (IT). The mice were euthanized 48 h pvi, and the tumours were collected and homogenized for RNA extraction. Total RNA per tumour was used for microarray analysis using the Clariom S mouse chip. (A-C) Limma package in R was used to estimated the DEGs between the different treatments, which are represented in volcano plots. (D) The intersection of DEGs in different comparisons is shown in a venndiagram.

A

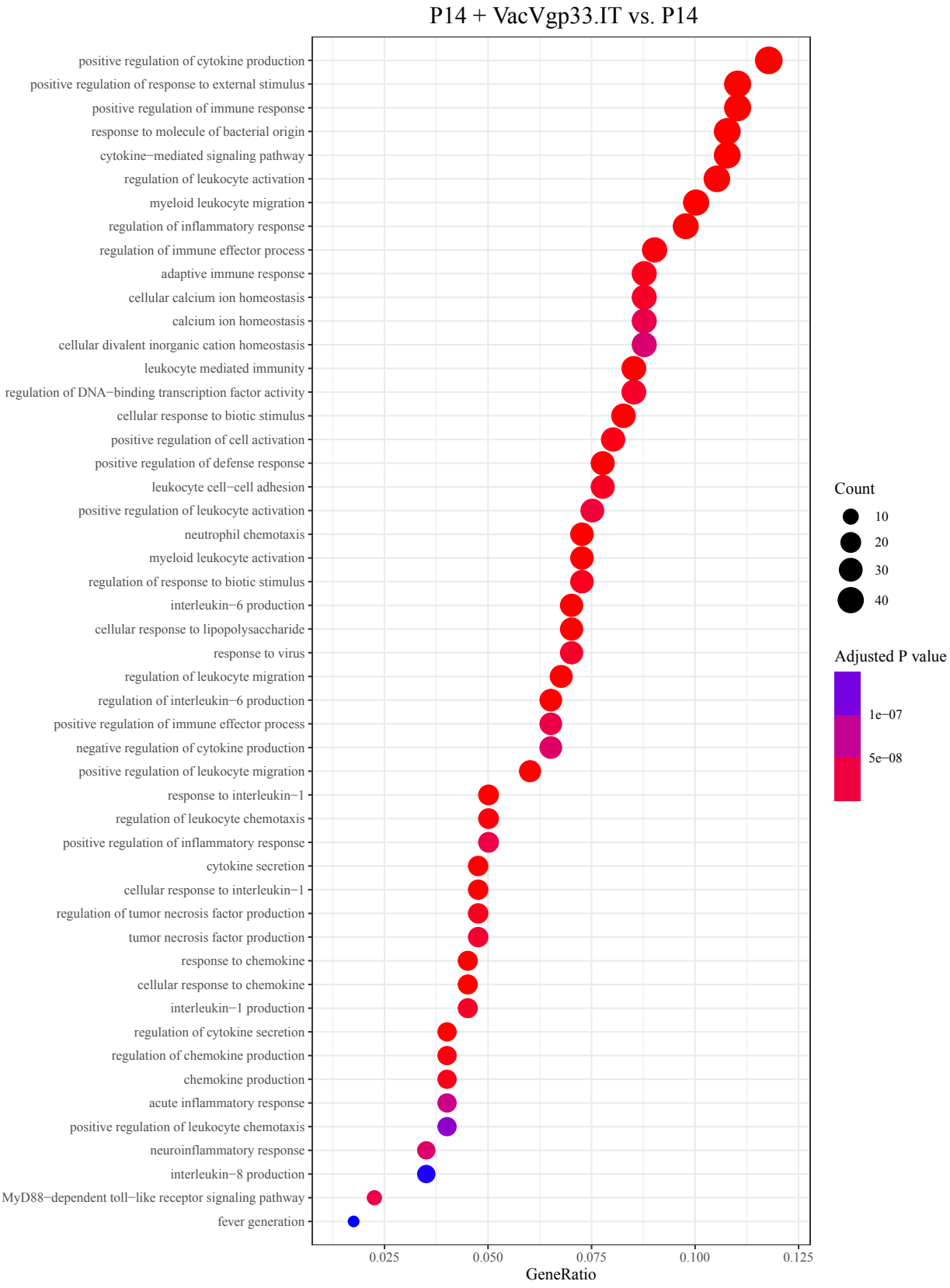
P14 + VacVgp33.IT vs. P14
positive regulation of cytokine production
positive regulation of response to external stimulus
positive regulation of immune response
response to molecule of bacterial origin
cytokine−mediated signaling pathway
regulation of leukocyte activation
myeloid leukocyte migration
regulation of inflammatory response
regulation of immune effector process
adaptive immune response
cellular calcium ion homeostasis
calcium ion homeostasis
cellular divalent inorganic cation homeostasis
leukocyte mediated immunity
regulation of DNA−binding transcription factor activity
cellular response to biotic stimulus
positive regulation of cell activation
positive regulation of defense response
leukocyte cell−cell adhesion
positive regulation of leukocyte activation
neutrophil chemotaxis
myeloid leukocyte activation
regulation of response to biotic stimulus
interleukin−6 production
cellular response to lipopolysaccharide
response to virus
regulation of leukocyte migration
regulation of interleukin−6 production
positive regulation of immune effector process
negative regulation of cytokine production
positive regulation of leukocyte migration
response to interleukin−1
regulation of leukocyte chemotaxis
positive regulation of inflammatory response
cytokine secretion
cellular response to interleukin−1
regulation of tumor necrosis factor production
tumor necrosis factor production
response to chemokine
cellular response to chemokine
interleukin−1 production
regulation of cytokine secretion
regulation of chemokine production
chemokine production
acute inflammatory response
positive regulation of leukocyte chemotaxis
neuroinflammatory response
interleukin−8 production
MyD88−dependent toll−like receptor signaling pathway
fever generation
0.025
0.050
0.075
0.100
0.125
GeneRatio
Count
10
20
30
40
Adjusted P value
1e−07
5e−08

B

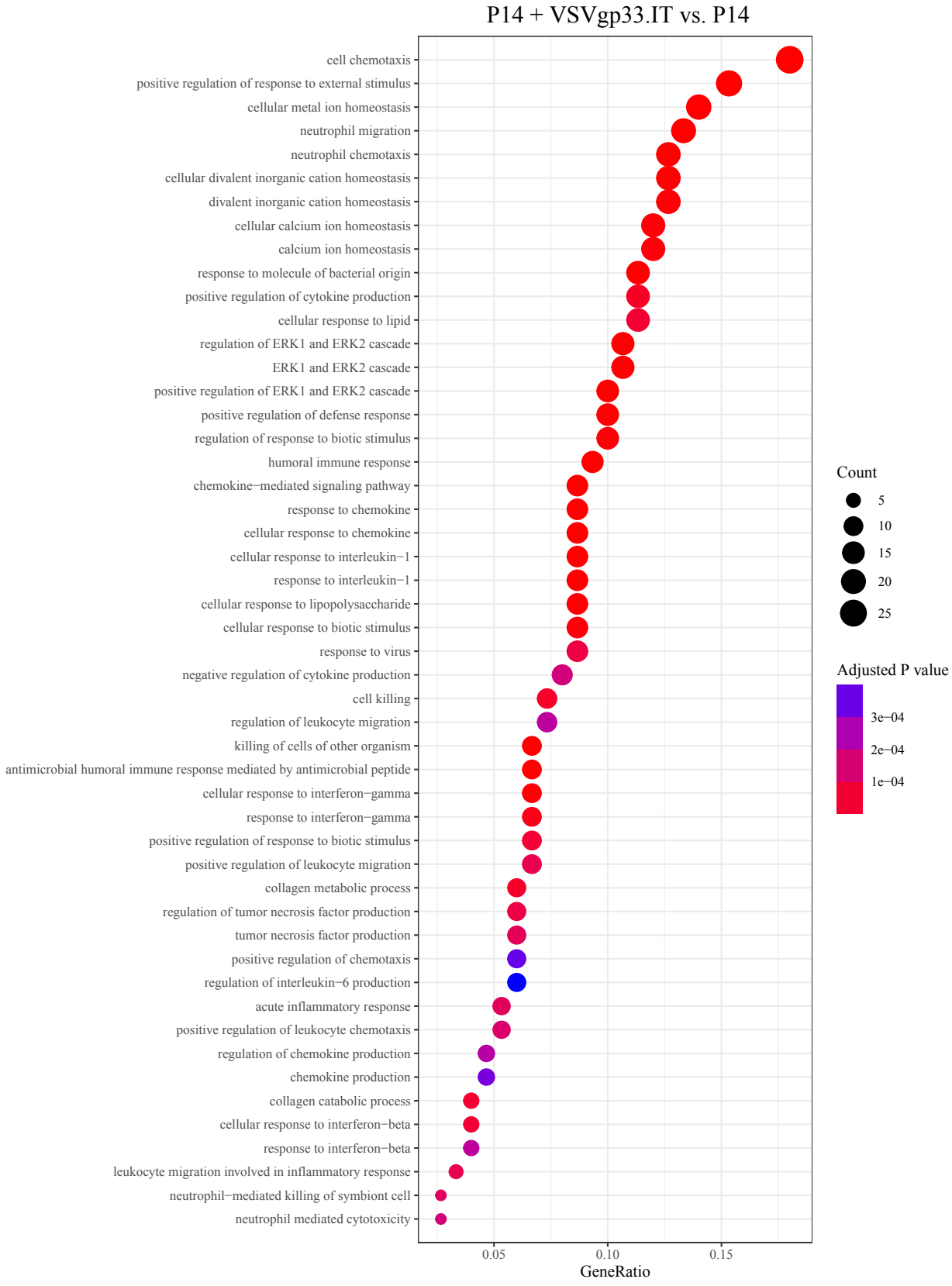
P14 + VSVgp33.IT vs. P14
cell chemotaxis
positive regulation of response to external stimulus
cellular metal ion homeostasis
neutrophil migration
neutrophil chemotaxis
cellular divalent inorganic cation homeostasis
divalent inorganic cation homeostasis
cellular calcium ion homeostasis
calcium ion homeostasis
response to molecule of bacterial origin
positive regulation of cytokine production
cellular response to lipid
regulation of ERK1 and ERK2 cascade
ERK1 and ERK2 cascade
positive regulation of ERK1 and ERK2 cascade
positive regulation of defense response
regulation of response to biotic stimulus
humoral immune response
chemokine−mediated signaling pathway
response to chemokine
cellular response to chemokine
cellular response to interleukin−1
response to interleukin−1
cellular response to lipopolysaccharide
cellular response to biotic stimulus
response to virus
negative regulation of cytokine production
cell killing
regulation of leukocyte migration
killing of cells of other organism
antimicrobial humoral immune response mediated by antimicrobial peptide
cellular response to interferon−gamma
response to interferon−gamma
positive regulation of response to biotic stimulus
positive regulation of leukocyte migration
collagen metabolic process
regulation of tumor necrosis factor production
tumor necrosis factor production
positive regulation of chemotaxis
regulation of interleukin−6 production
acute inflammatory response
positive regulation of leukocyte chemotaxis
regulation of chemokine production
chemokine production
collagen catabolic process
cellular response to interferon−beta
response to interferon−beta
leukocyte migration involved in inflammatory response
neutrophil−mediated killing of symbiont cell
neutrophil mediated cytotoxicity
0.05
0.10
0.15
GeneRatio
Count
5
10
15
20
25
Adjusted P value
3e−04
2e−04
1e−04

C

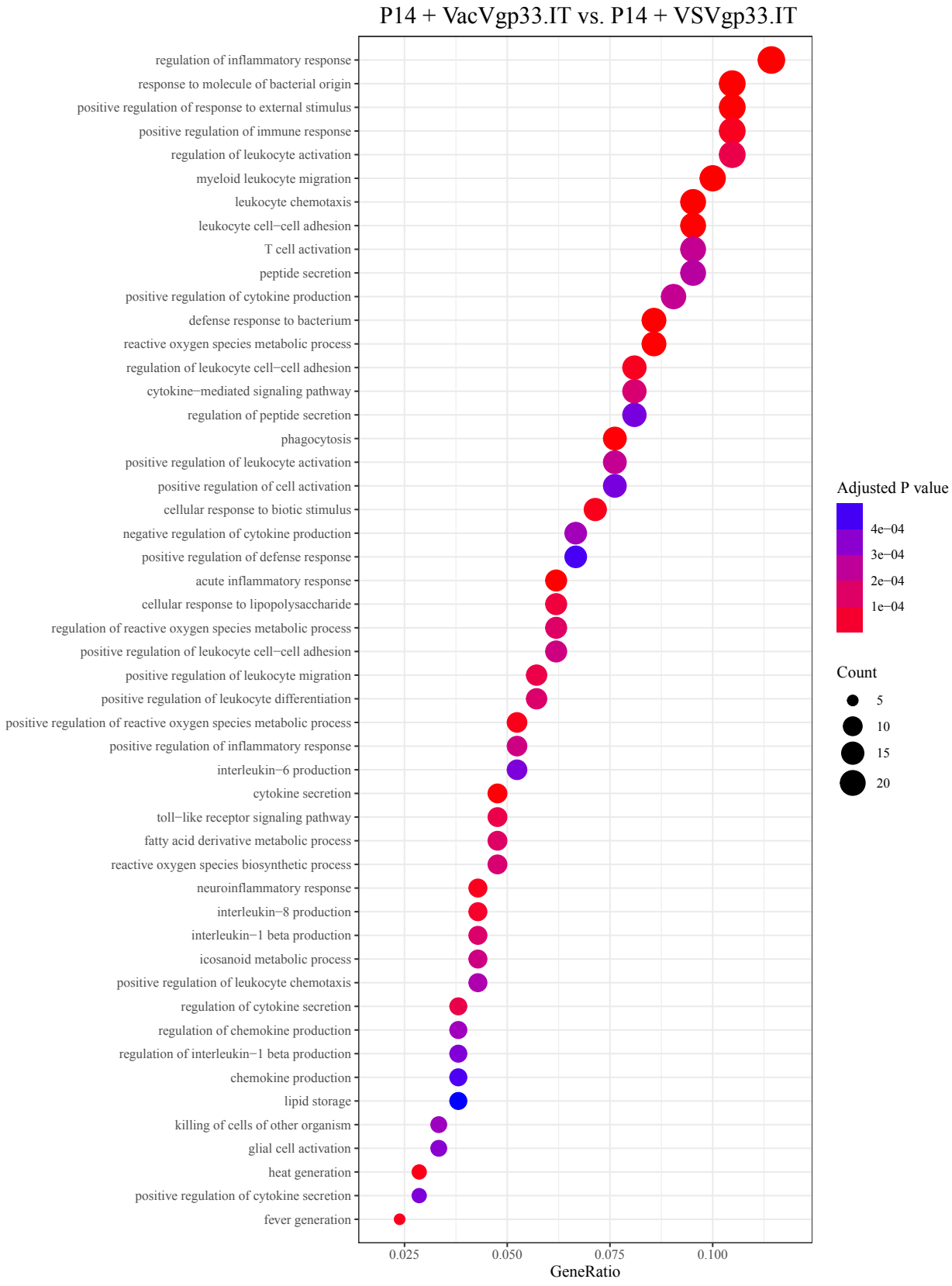
P14 + VacVgp33.IT vs. P14 + VSVgp33.IT
regulation of inflammatory response
response to molecule of bacterial origin
positive regulation of response to external stimulus
positive regulation of immune response
regulation of leukocyte activation
myeloid leukocyte migration
leukocyte chemotaxis
leukocyte cell−cell adhesion
T cell activation
peptide secretion
positive regulation of cytokine production
defense response to bacterium
reactive oxygen species metabolic process
regulation of leukocyte cell−cell adhesion
cytokine−mediated signaling pathway
regulation of peptide secretion
phagocytosis
positive regulation of leukocyte activation
positive regulation of cell activation
cellular response to biotic stimulus
negative regulation of cytokine production
positive regulation of defense response
acute inflammatory response
cellular response to lipopolysaccharide
regulation of reactive oxygen species metabolic process
positive regulation of leukocyte cell−cell adhesion
positive regulation of leukocyte migration
positive regulation of leukocyte differentiation
positive regulation of reactive oxygen species metabolic process
positive regulation of inflammatory response
interleukin−6 production
cytokine secretion
toll−like receptor signaling pathway
fatty acid derivative metabolic process
reactive oxygen species biosynthetic process
neuroinflammatory response
interleukin−8 production
interleukin−1 beta production
icosanoid metabolic process
positive regulation of leukocyte chemotaxis
regulation of cytokine secretion
regulation of chemokine production
regulation of interleukin−1 beta production
chemokine production
lipid storage
killing of cells of other organism
glial cell activation
heat generation
positive regulation of cytokine secretion
fever generation
0.025
0.050
0.075
0.100
GeneRatio
Adjusted P value
4e−04
3e−04
2e−04
1e−04
Count
5
10
15
20

D

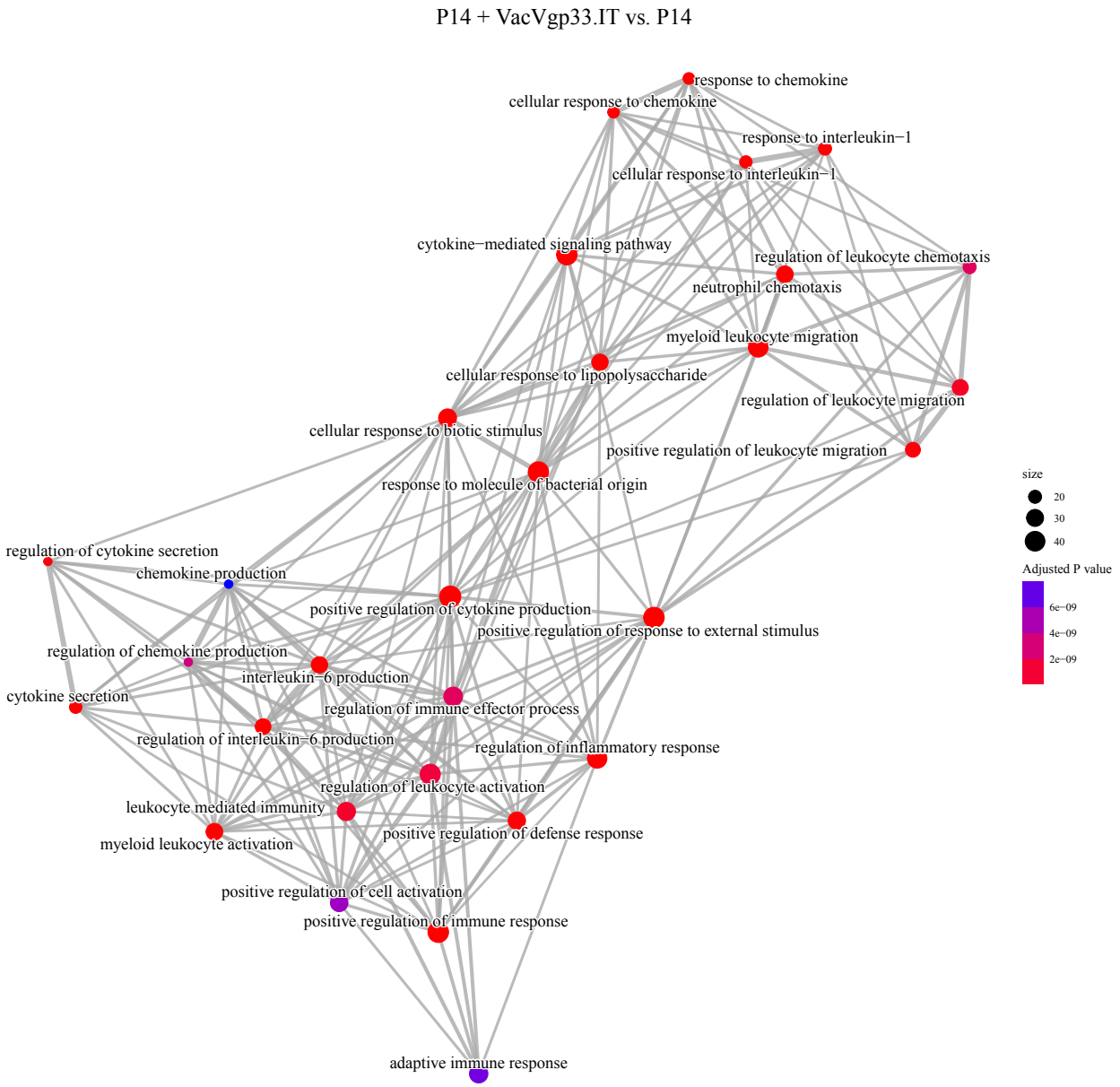
P14 + VacVgp33.IT vs. P14
response to chemokine
cellular response to chemokine
response to interleukin−1
cellular response to interleukin−1
cytokine−mediated signaling pathway
regulation of leukocyte chemotaxis
neutrophil chemotaxis
myeloid leukocyte migration
cellular response to lipopolysaccharide
regulation of leukocyte migration
cellular response to biotic stimulus
positive regulation of leukocyte migration
response to molecule of bacterial origin
regulation of cytokine secretion
chemokine production
positive regulation of cytokine production
positive regulation of response to external stimulus
regulation of chemokine production
interleukin−6 production
cytokine secretion
regulation of immune effector process
regulation of interleukin−6 production
regulation of inflammatory response
regulation of leukocyte activation
leukocyte mediated immunity
positive regulation of defense response
myeloid leukocyte activation
positive regulation of cell activation
positive regulation of immune response
adaptive immune response
size
20
30
40
Adjusted P value
6e−09
4e−09
2e−09

E

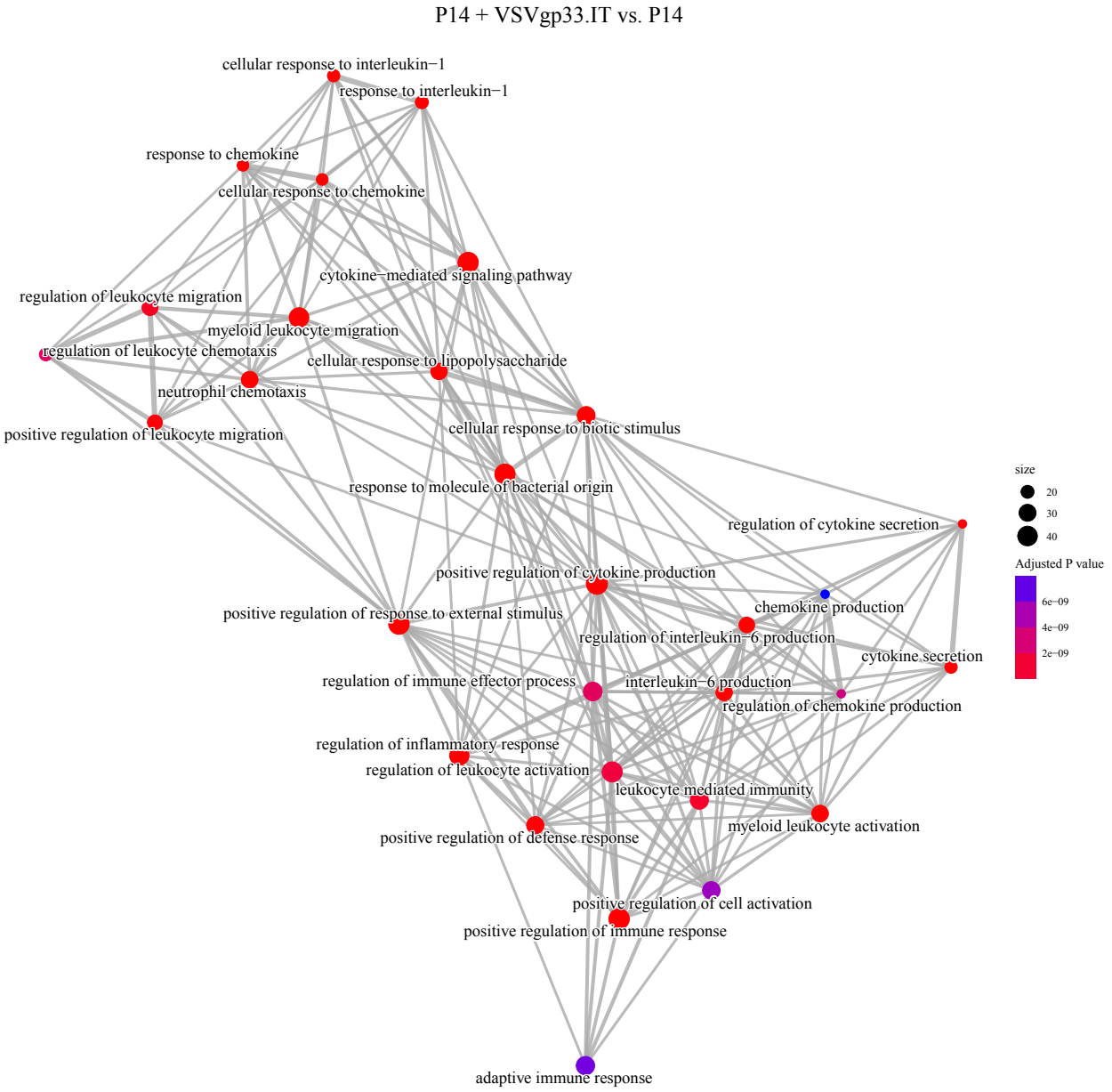
P14 + VSVgp33.IT vs. P14
cellular response to interleukin−1
response to interleukin−1
response to chemokine
cellular response to chemokine
cytokine−mediated signaling pathway
regulation of leukocyte migration
myeloid leukocyte migration
regulation of leukocyte chemotaxis
cellular response to lipopolysaccharide
neutrophil chemotaxis
positive regulation of leukocyte migration
cellular response to biotic stimulus
response to molecule of bacterial origin
regulation of cytokine secretion
positive regulation of cytokine production
chemokine production
positive regulation of response to external stimulus
regulation of interleukin−6 production
cytokine secretion
regulation of immune effector process
interleukin−6 production
regulation of chemokine production
regulation of inflammatory response
regulation of leukocyte activation
leukocyte mediated immunity
myeloid leukocyte activation
positive regulation of defense response
positive regulation of cell activation
positive regulation of immune response
adaptive immune response
size
20
30
40
Adjusted P value
6e−09
4e−09
2e−09

F

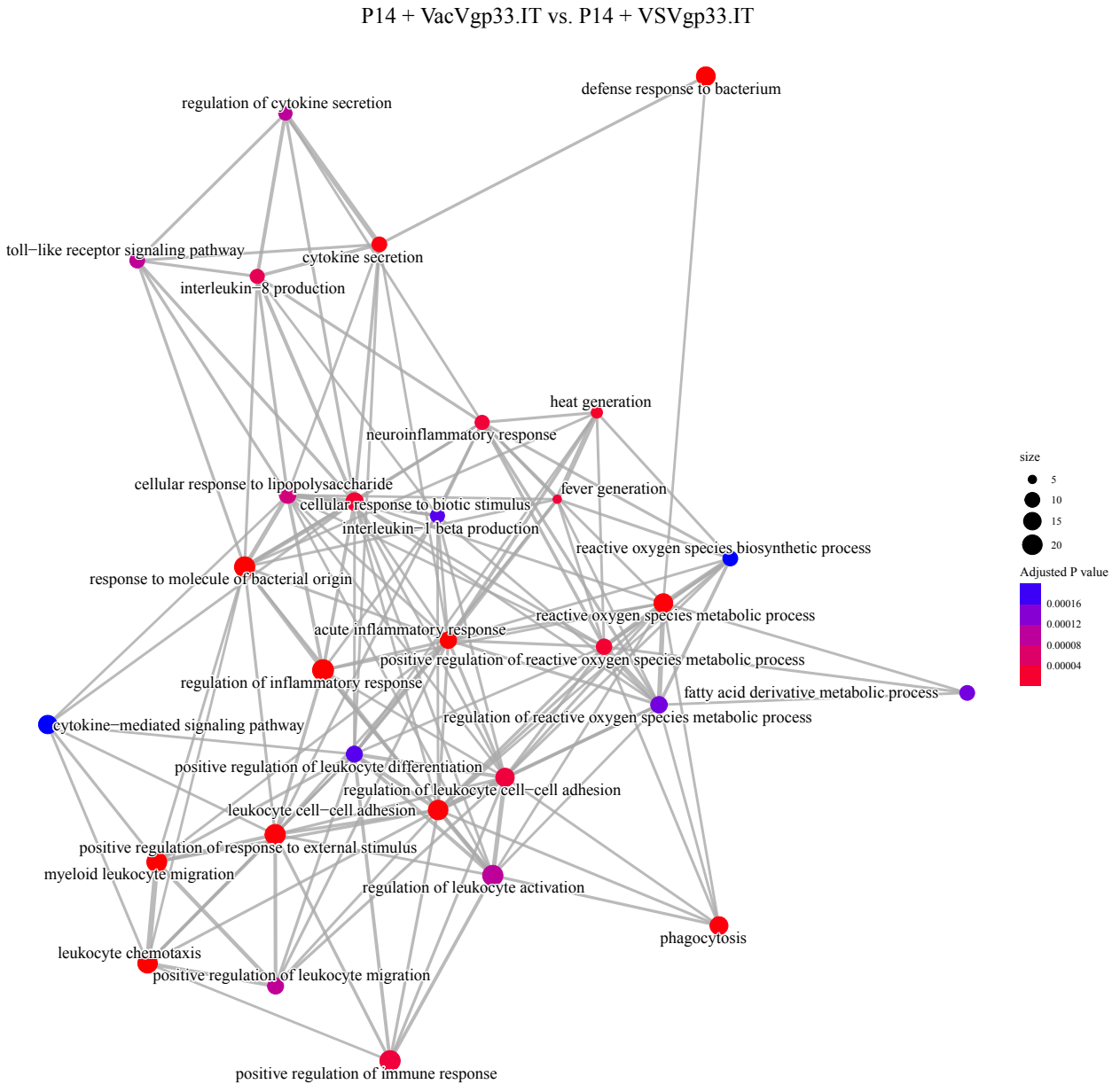
P14 + VacVgp33.IT vs. P14 + VSVgp33.IT
defense response to bacterium
regulation of cytokine secretion
toll−like receptor signaling pathway
cytokine secretion
interleukin−8 production
heat generation
neuroinflammatory response
cellular response to lipopolysaccharide
cellular response to biotic stimulus
fever generation
interleukin−1 beta production
reactive oxygen species biosynthetic process
response to molecule of bacterial origin
reactive oxygen species metabolic process
acute inflammatory response
positive regulation of reactive oxygen species metabolic process
regulation of inflammatory response
fatty acid derivative metabolic process
regulation of reactive oxygen species metabolic process
cytokine−mediated signaling pathway
positive regulation of leukocyte differentiation
regulation of leukocyte cell−cell adhesion
leukocyte cell−cell adhesion
positive regulation of response to external stimulus
myeloid leukocyte migration
regulation of leukocyte activation
phagocytosis
leukocyte chemotaxis
positive regulation of leukocyte migration
positive regulation of immune response
size
5
10
15
20
Adjusted P value
0.00016
0.00012
0.00008
0.00004

Figure 6.5 | GO enrichment analysis reveals over-representation of similar BP terms between P14 + VacVgp33 and P14 + VSVgp33 treatments

C57BL/6 mice (n = 3 or 4) were intradermally implanted with $2x10^5$ B16gp33 cells. 5 days later the mice were treated using $1x10^6$ adoptively transferred P14 T cells followed by 1 x 10^8 pfu VacVgp33 (IT). The mice were euthanized 48 h pvi, and the tumours were collected and homogenized for RNA extraction. Total RNA per tumour was used for microarray analysis using the Clariom S mouse chip. (A-C) Over-representation analysis using ClusterProfiler package in R was done to analyze the enrichment of BP terms of GO. Shown are the top 50 enriched terms in each comparison. (D-F) Enrichment maps were created to highlight the interconnectivity of the top 30 terms in each comparison.

either virus to explain the observed difference in tumour control.

6.2.4. VacV causes the enrichment of immune processes and the downregulation of cell proliferation and metabolic processes within the TME

One of the weaknesses of using ORA is that it only focuses on the DEGs that meet the cutoff threshold of fold change and statistical significance. This might bias the results since the biological effects of transcription changes do not correlate linearly with a defined magnitude of change. Thus, we elected to perform GSEA using the different gene sets from MSigDB. We decided to focus the analysis on the tumours treated with P14 + VacVgp33 vs P14 + VSVgp33. We first investigated the enrichment of the hallmark gene sets and found that tumours treated with P14 + VacVgp33 had a signature enriched for inflammatory gene sets (**Fig. 6.6 A**). Alternatively, gene sets representing metabolic pathways, cell replication or DNA repair were downregulated relative to P14 + VSVgp33 treated tumours. The hallmark gene sets are broad in nature and serve the purpose of identifying trends in the data for further investigation, thus we decided to query additional pathway databases to assess the enrichment of gene sets under 4 biological themes: immune pathways, metabolic pathways, cell cycle-related pathways, and DNA repair pathways. The canonical branch of the C2 module of MSigDB represents a collection of gene sets derived from different databases including Reactome, Wikipathways, and KEGG. Additionally, the C5 module comprises gene sets derived from the GO and represent the GO annotations. We focused on the sub-collection representing the GO-BP. To avoid statistical bias, we curated the previously mentioned gene sets into one list and performed GSEA on the full list. We then filtered the statistically significant pathways and grouped them into the 4 biological themes previously mentioned.

Consistent with the results of the hallmark GSEA, our analysis demonstrated the enrichment of a plethora of immune related pathways in P14 + VacVgp33 treated tumours relative

A

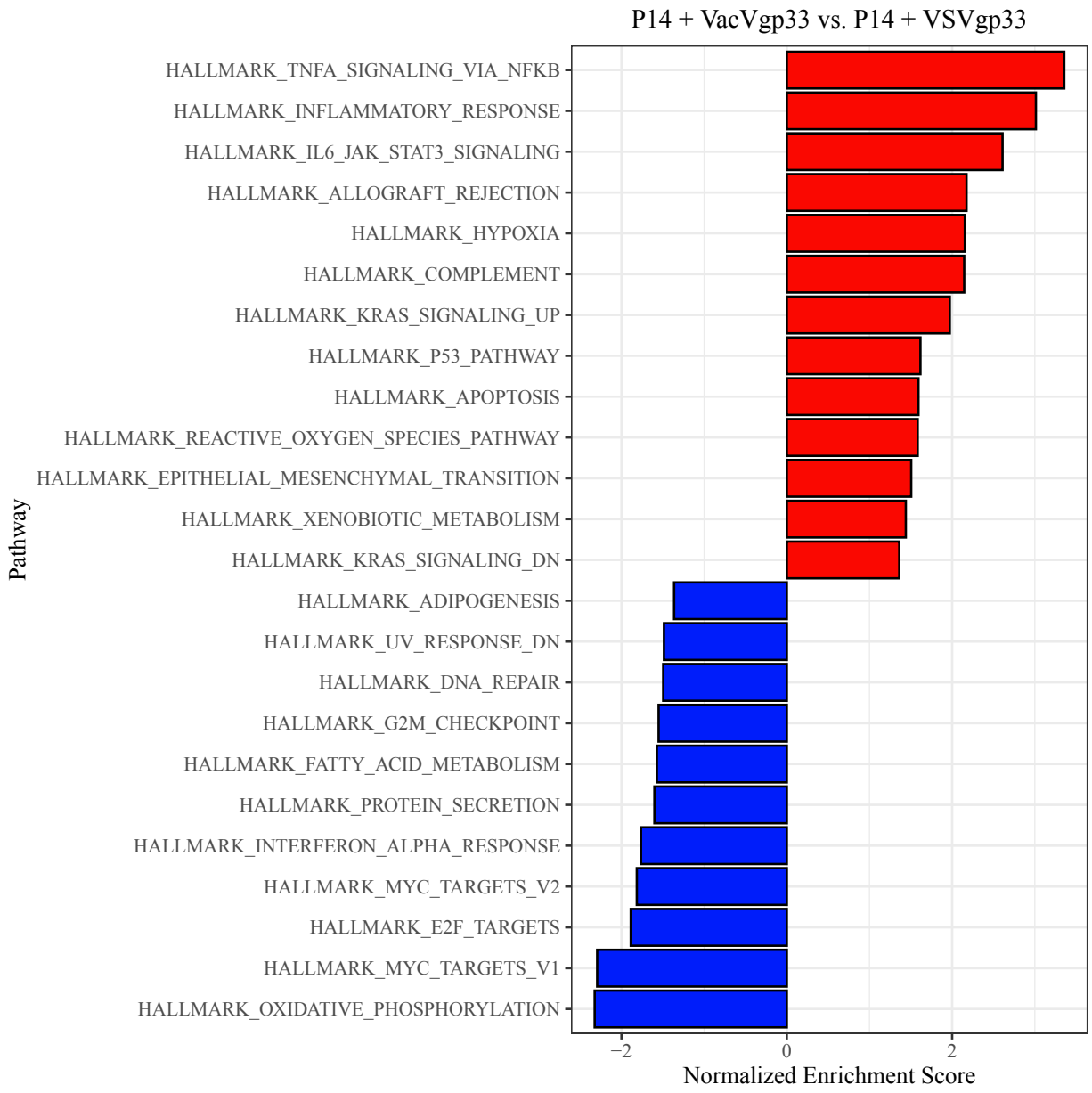
P14 + VacVgp33 vs. P14 + VSVgp33
HALLMARK_TNFA_SIGNALING_VIA_NFKB
HALLMARK_INFLAMMATORY_RESPONSE
HALLMARK_IL6_JAK_STAT3_SIGNALING
HALLMARK_ALLOGRAFT_REJECTION
HALLMARK_HYPOXIA
HALLMARK_COMPLEMENT
HALLMARK_KRAS_SIGNALING_UP
HALLMARK_P53_PATHWAY
HALLMARK_APOPTOSIS
HALLMARK_REACTIVE_OXYGEN_SPECIES_PATHWAY
HALLMARK_EPITHELIAL_MESENCHYMAL_TRANSITION
HALLMARK_XENOBIOTIC_METABOLISM
HALLMARK_KRAS_SIGNALING_DN
HALLMARK_ADIPOGENESIS
HALLMARK_UV_RESPONSE_DN
HALLMARK_DNA_REPAIR
HALLMARK_G2M_CHECKPOINT
HALLMARK_FATTY_ACID_METABOLISM
HALLMARK_PROTEIN_SECRETION
HALLMARK_INTERFERON_ALPHA_RESPONSE
HALLMARK_MYC_TARGETS_V2
HALLMARK_E2F_TARGETS
HALLMARK_MYC_TARGETS_V1
HALLMARK_OXIDATIVE_PHOSPHORYLATION
Pathway
−2
0
2
Normalized Enrichment Score

B

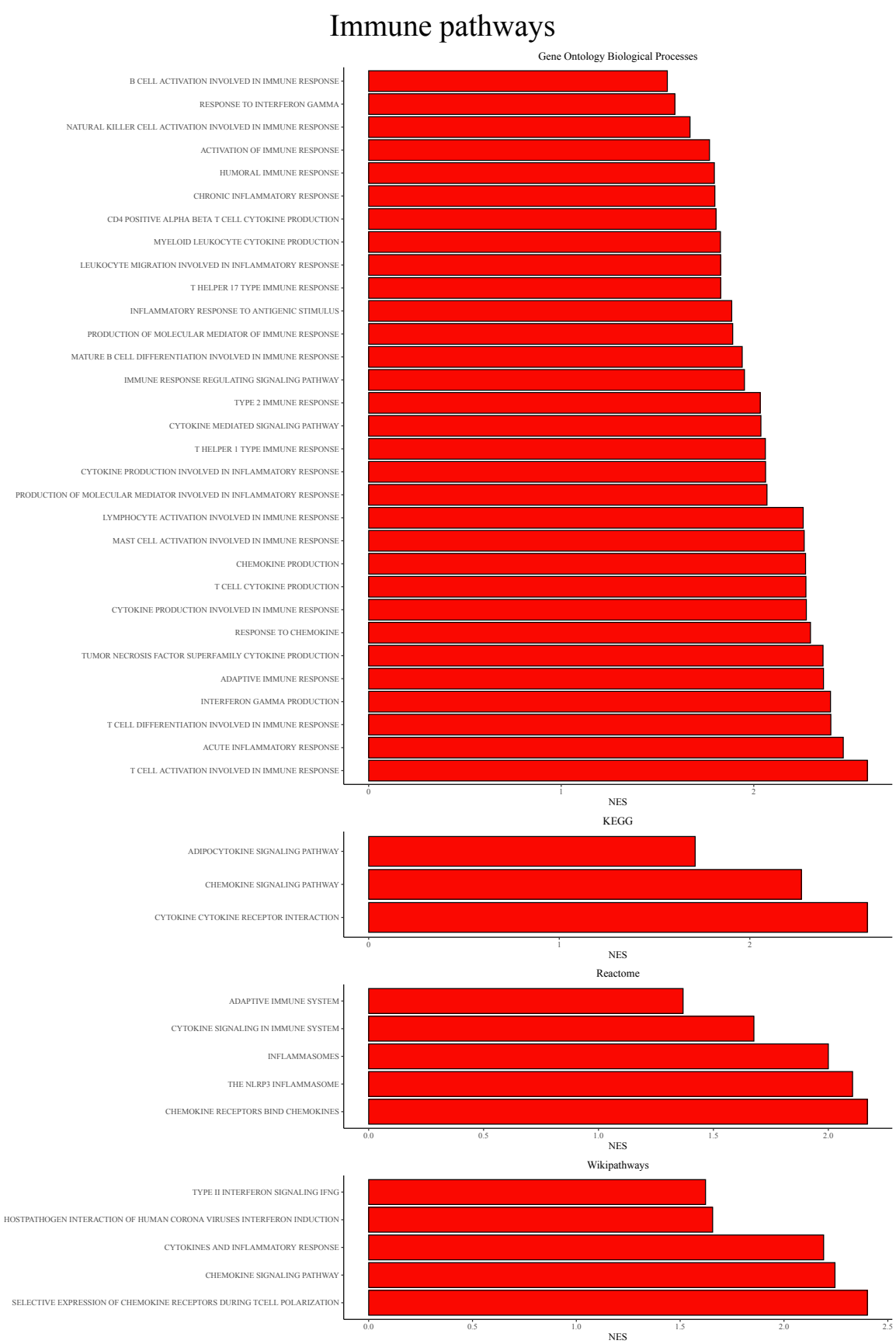
Immune pathways
Gene Ontology Biological Processes
B CELL ACTIVATION INVOLVED IN IMMUNE RESPONSE
RESPONSE TO INTERFERON GAMMA
NATURAL KILLER CELL ACTIVATION INVOLVED IN IMMUNE RESPONSE
ACTIVATION OF IMMUNE RESPONSE
HUMORAL IMMUNE RESPONSE
CHRONIC INFLAMMATORY RESPONSE
CD4 POSITIVE ALPHA BETA T CELL CYTOKINE PRODUCTION
MYELOID LEUKOCYTE CYTOKINE PRODUCTION
LEUKOCYTE MIGRATION INVOLVED IN INFLAMMATORY RESPONSE
T HELPER 17 TYPE IMMUNE RESPONSE
INFLAMMATORY RESPONSE TO ANTIGENIC STIMULUS
PRODUCTION OF MOLECULAR MEDIATOR OF IMMUNE RESPONSE
MATURE B CELL DIFFERENTIATION INVOLVED IN IMMUNE RESPONSE
IMMUNE RESPONSE REGULATING SIGNALING PATHWAY
TYPE 2 IMMUNE RESPONSE
CYTOKINE MEDIATED SIGNALING PATHWAY
T HELPER 1 TYPE IMMUNE RESPONSE
CYTOKINE PRODUCTION INVOLVED IN INFLAMMATORY RESPONSE
PRODUCTION OF MOLECULAR MEDIATOR INVOLVED IN INFLAMMATORY RESPONSE
LYMPHOCYTE ACTIVATION INVOLVED IN IMMUNE RESPONSE
MAST CELL ACTIVATION INVOLVED IN IMMUNE RESPONSE
CHEMOKINE PRODUCTION
T CELL CYTOKINE PRODUCTION
CYTOKINE PRODUCTION INVOLVED IN IMMUNE RESPONSE
RESPONSE TO CHEMOKINE
TUMOR NECROSIS FACTOR SUPERFAMILY CYTOKINE PRODUCTION
ADAPTIVE IMMUNE RESPONSE
INTERFERON GAMMA PRODUCTION
T CELL DIFFERENTIATION INVOLVED IN IMMUNE RESPONSE
ACUTE INFLAMMATORY RESPONSE
T CELL ACTIVATION INVOLVED IN IMMUNE RESPONSE
0
1
2
NES
KEGG
ADIPOCYTOKINE SIGNALING PATHWAY
CHEMOKINE SIGNALING PATHWAY
CYTOKINE CYTOKINE RECEPTOR INTERACTION
0
1
2
NES
Reactome
ADAPTIVE IMMUNE SYSTEM
CYTOKINE SIGNALING IN IMMUNE SYSTEM
INFLAMMASOMES
THE NLRP3 INFLAMMASOME
CHEMOKINE RECEPTORS BIND CHEMOKINES
0.0
0.5
1.0
1.5
2.0
NES
Wikipathways
TYPE II INTERFERON SIGNALING IFNG
HOSTPATHOGEN INTERACTION OF HUMAN CORONA VIRUSES INTERFERON INDUCTION
CYTOKINES AND INFLAMMATORY RESPONSE
CHEMOKINE SIGNALING PATHWAY
SELECTIVE EXPRESSION OF CHEMOKINE RECEPTORS DURING TCELL POLARIZATION
0.0
0.5
1.0
1.5
2.0
2.5
NES

C

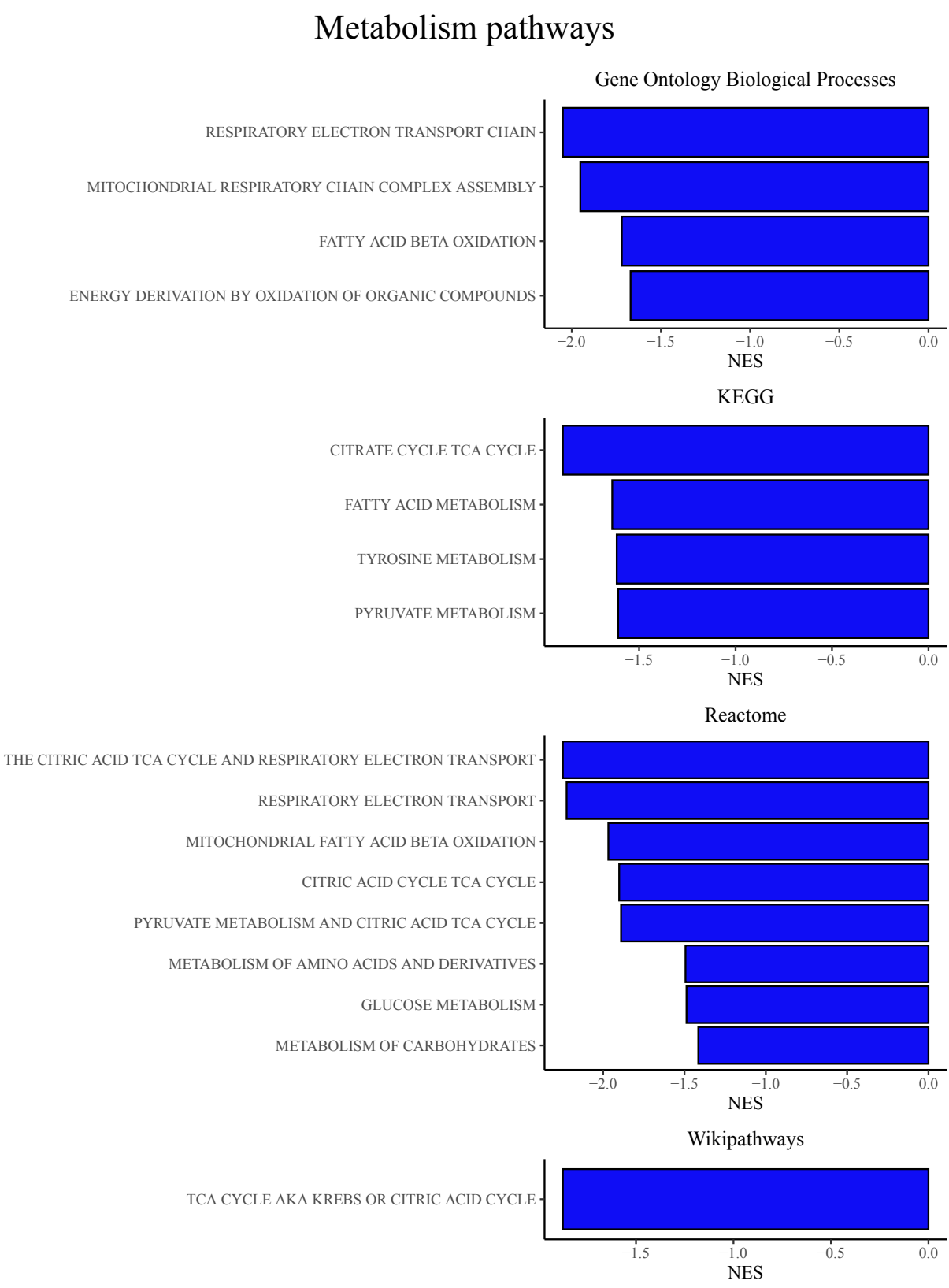
Metabolism pathways
Gene Ontology Biological Processes
RESPIRATORY ELECTRON TRANSPORT CHAIN
MITOCHONDRIAL RESPIRATORY CHAIN COMPLEX ASSEMBLY
FATTY ACID BETA OXIDATION
ENERGY DERIVATION BY OXIDATION OF ORGANIC COMPOUNDS
−2.0
−1.5
−1.0
−0.5
0.0
NES
KEGG
CITRATE CYCLE TCA CYCLE
FATTY ACID METABOLISM
TYROSINE METABOLISM
PYRUVATE METABOLISM
−1.5
−1.0
−0.5
0.0
NES
Reactome
THE CITRIC ACID TCA CYCLE AND RESPIRATORY ELECTRON TRANSPORT
RESPIRATORY ELECTRON TRANSPORT
MITOCHONDRIAL FATTY ACID BETA OXIDATION
CITRIC ACID CYCLE TCA CYCLE
PYRUVATE METABOLISM AND CITRIC ACID TCA CYCLE
METABOLISM OF AMINO ACIDS AND DERIVATIVES
GLUCOSE METABOLISM
METABOLISM OF CARBOHYDRATES
−2.0
−1.5
−1.0
−0.5
0.0
NES
Wikipathways
TCA CYCLE AKA KREBS OR CITRIC ACID CYCLE
−1.5
−1.0
−0.5
0.0
NES

D

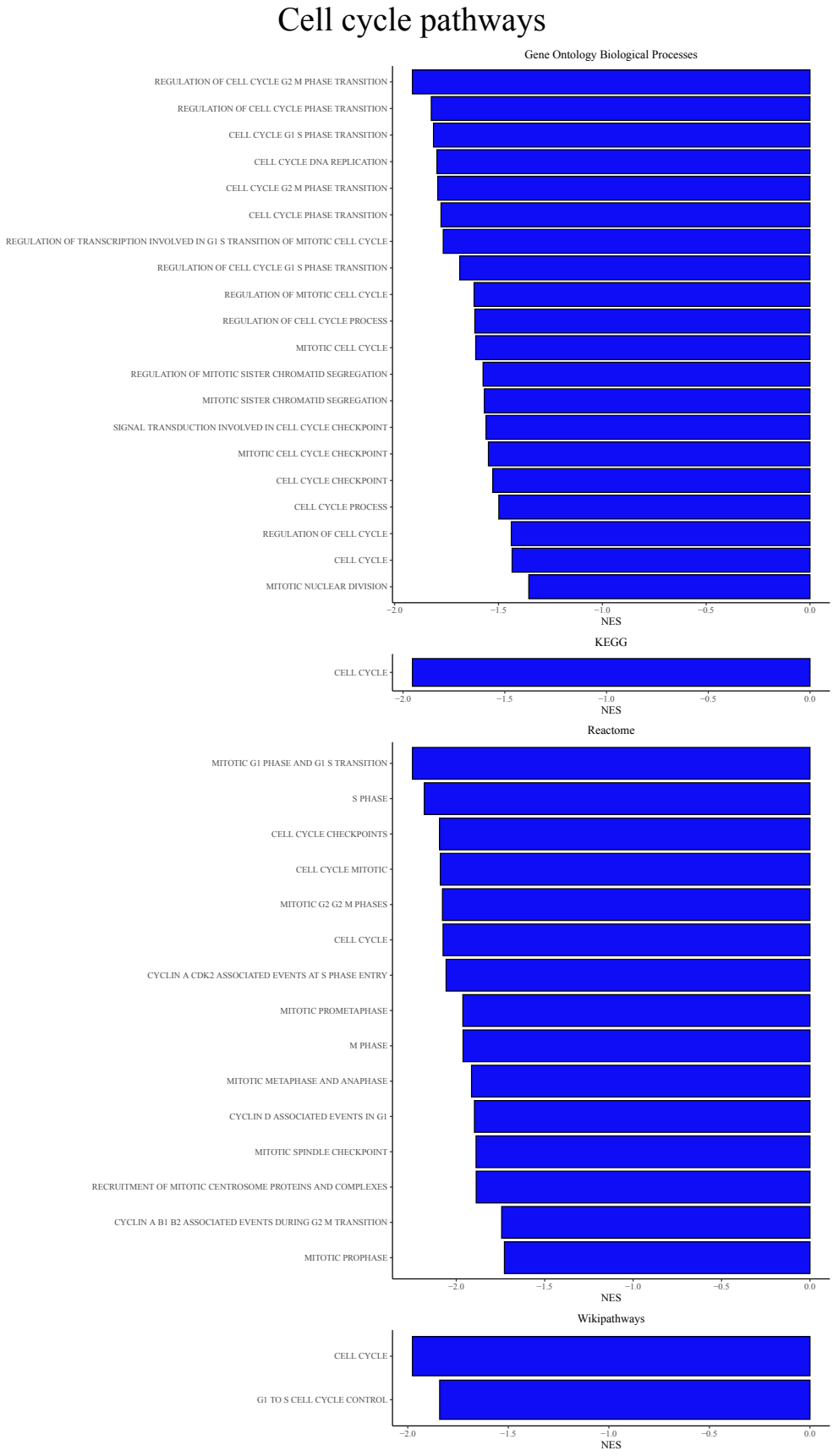
Cell cycle pathways
Gene Ontology Biological Processes
REGULATION OF CELL CYCLE G2 M PHASE TRANSITION
REGULATION OF CELL CYCLE PHASE TRANSITION
CELL CYCLE G1 S PHASE TRANSITION
CELL CYCLE DNA REPLICATION
CELL CYCLE G2 M PHASE TRANSITION
CELL CYCLE PHASE TRANSITION
REGULATION OF TRANSCRIPTION INVOLVED IN G1 S TRANSITION OF MITOTIC CELL CYCLE
REGULATION OF CELL CYCLE G1 S PHASE TRANSITION
REGULATION OF MITOTIC CELL CYCLE
REGULATION OF CELL CYCLE PROCESS
MITOTIC CELL CYCLE
REGULATION OF MITOTIC SISTER CHROMATID SEGREGATION
MITOTIC SISTER CHROMATID SEGREGATION
SIGNAL TRANSDUCTION INVOLVED IN CELL CYCLE CHECKPOINT
MITOTIC CELL CYCLE CHECKPOINT
CELL CYCLE CHECKPOINT
CELL CYCLE PROCESS
REGULATION OF CELL CYCLE
CELL CYCLE
MITOTIC NUCLEAR DIVISION
−2.0
−1.5
−1.0
−0.5
0.0
NES
KEGG
CELL CYCLE
−2.0
−1.5
−1.0
−0.5
0.0
NES
Reactome
MITOTIC G1 PHASE AND G1 S TRANSITION
S PHASE
CELL CYCLE CHECKPOINTS
CELL CYCLE MITOTIC
MITOTIC G2 G2 M PHASES
CELL CYCLE
CYCLIN A CDK2 ASSOCIATED EVENTS AT S PHASE ENTRY
MITOTIC PROMETAPHASE
M PHASE
MITOTIC METAPHASE AND ANAPHASE
CYCLIN D ASSOCIATED EVENTS IN G1
MITOTIC SPINDLE CHECKPOINT
RECRUITMENT OF MITOTIC CENTROSOME PROTEINS AND COMPLEXES
CYCLIN A B1 B2 ASSOCIATED EVENTS DURING G2 M TRANSITION
MITOTIC PROPHASE
−2.0
−1.5
−1.0
−0.5
0.0
NES
Wikipathways
CELL CYCLE
G1 TO S CELL CYCLE CONTROL
−2.0
−1.5
−1.0
−0.5
0.0
NES

E

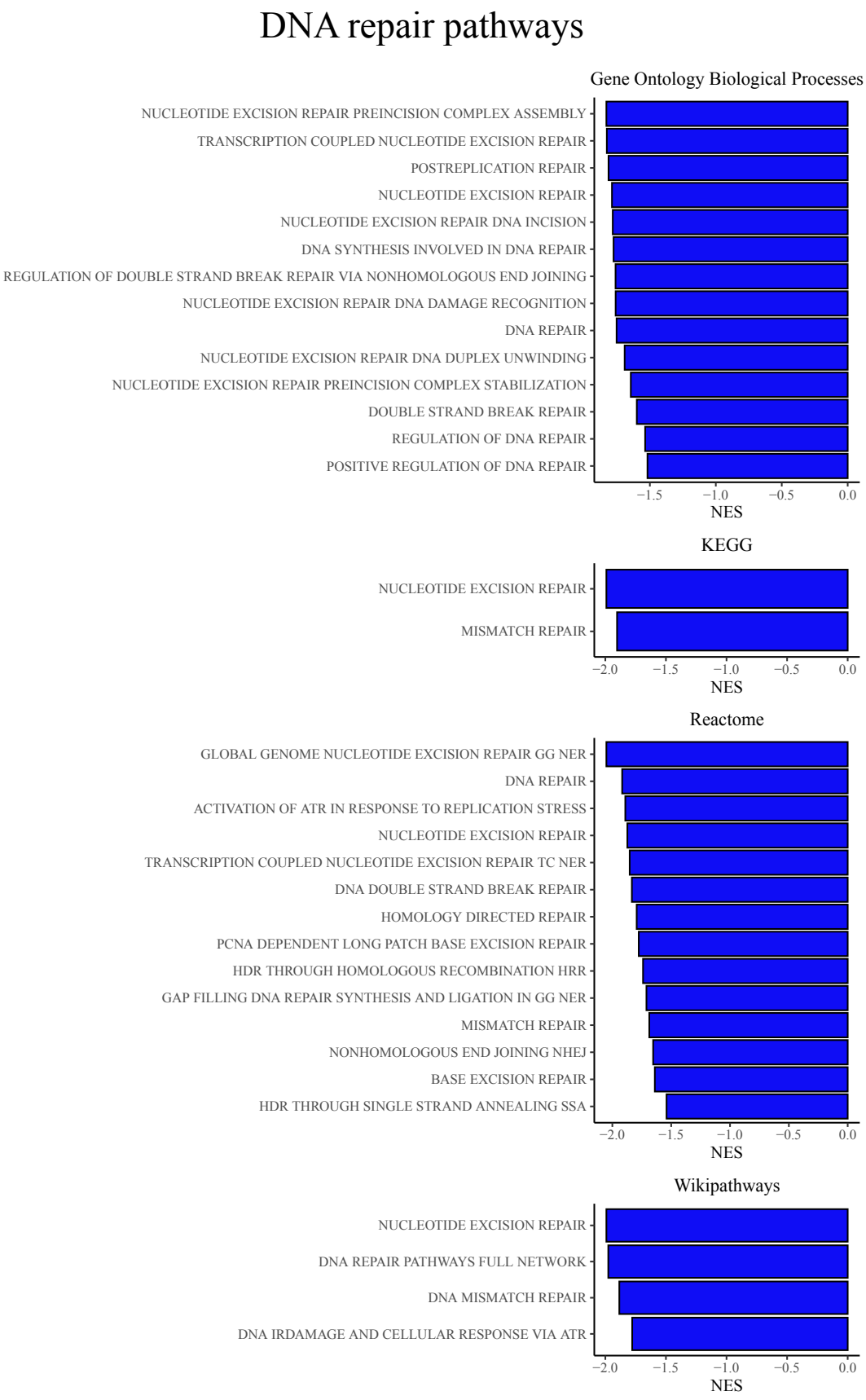
DNA repair pathways
Gene Ontology Biological Processes
NUCLEOTIDE EXCISION REPAIR PREINCISION COMPLEX ASSEMBLY
TRANSCRIPTION COUPLED NUCLEOTIDE EXCISION REPAIR
POSTREPLICATION REPAIR
NUCLEOTIDE EXCISION REPAIR
NUCLEOTIDE EXCISION REPAIR DNA INCISION
DNA SYNTHESIS INVOLVED IN DNA REPAIR
REGULATION OF DOUBLE STRAND BREAK REPAIR VIA NONHOMOLOGOUS END JOINING
NUCLEOTIDE EXCISION REPAIR DNA DAMAGE RECOGNITION
DNA REPAIR
NUCLEOTIDE EXCISION REPAIR DNA DUPLEX UNWINDING
NUCLEOTIDE EXCISION REPAIR PREINCISION COMPLEX STABILIZATION
DOUBLE STRAND BREAK REPAIR
REGULATION OF DNA REPAIR
POSITIVE REGULATION OF DNA REPAIR
−1.5 −1.0 −0.5 0.0
NES
KEGG
NUCLEOTIDE EXCISION REPAIR
MISMATCH REPAIR
−2.0 −1.5 −1.0 −0.5 0.0
NES
Reactome
GLOBAL GENOME NUCLEOTIDE EXCISION REPAIR GG NER
DNA REPAIR
ACTIVATION OF ATR IN RESPONSE TO REPLICATION STRESS
NUCLEOTIDE EXCISION REPAIR
TRANSCRIPTION COUPLED NUCLEOTIDE EXCISION REPAIR TC NER
DNA DOUBLE STRAND BREAK REPAIR
HOMOLOGY DIRECTED REPAIR
PCNA DEPENDENT LONG PATCH BASE EXCISION REPAIR
HDR THROUGH HOMOLOGOUS RECOMBINATION HRR
GAP FILLING DNA REPAIR SYNTHESIS AND LIGATION IN GG NER
MISMATCH REPAIR
NONHOMOLOGOUS END JOINING NHEJ
BASE EXCISION REPAIR
HDR THROUGH SINGLE STRAND ANNEALING SSA
−2.0 −1.5 −1.0 −0.5 0.0
NES
Wikipathways
NUCLEOTIDE EXCISION REPAIR
DNA REPAIR PATHWAYS FULL NETWORK
DNA MISMATCH REPAIR
DNA IRDAMAGE AND CELLULAR RESPONSE VIA ATR
−2.0 −1.5 −1.0 −0.5 0.0
NES

Figure 6.6 | GSEA reveals differential pathway regulation between P14 + VacVgp33 and P14 + VSVgp33 treatments

C57BL/6 mice (n = 3 or 4) were intradermally implanted with $2x10^5$ B16gp33 cells. 5 days later the mice were treated using $1x10^6$ adoptively transferred P14 T cells followed by 1 x 10^8 pfu VacVgp33 or VSVgp33 or PBS (IT). The mice were euthanized 48 h pvi, and the tumours were collected and homogenized for RNA extraction. Total RNA per tumour was used for microarray analysis using the Clariom S mouse chip. (A-E) fGSEA package in R was used to perform GSEA using the Hallmark gene sets or subsets from C2 and C5 modules of MSigDB. Shown are the normalized enrichment scores (NES) for each gene set P14 + VacVgp33 vs P14 + VSVgp33 treatments. A gene set was called significant if their FDR value is < 0.05.

to P14 + VSVgp33 (**Fig. 6.6 B**). Enrichment of Th1, Th17, Interferon gamma responses, TNF superfamily response, cytokine and chemokine production were observed. Interestingly, type I Interferon responses were downregulated by VacV compared to VSV, which is consistent with what we had reported before. These results point to the more inflammatory nature of VacV leading to more robust immune processes in the TME and reversal of the immune suppression.

We then looked at the alteration of the metabolic processes within the TME as a result of P14 + VacVgp33 vs P14 + VSVgp33. Contrary to the immune pathways, we observed significant downregulation of major metabolic pathways including the citric acid cycle (TCA cycle), fatty acid metabolism, mitochondrial electron transport chain, glucose metabolism and amino acid metabolism (**Fig. 6.6 C**). This indicates a general metabolic shutdown within the TME which halts tumour progression and pushes the tumour cells towards apoptosis. These findings were further supported when analyzing cell cycle related pathways, where we saw a general downregulation of pathways representing mitotic S and M phases, or those representing the transition from G1/G2 to S phase (**Fig. 6.6 D**). Additionally, cell cycle checkpoint and cell cycle regulatory pathways were downregulated pointing to the interruption of cell proliferation.

6.2.5. VacV causes the shutdown of DNA repair pathways eliminating the chance of antigen loss and immune escape

The combined effect of immune attack and viral replication in the TME leads to the DNA damage in the tumour cells. Multiple DNA repair pathways can be activated in response to DNA damage in an attempt to rescue the cell and restore its genomic integrity[288]. However, such repair processes open the door for gene loss and can potentially lead to the emergence of new antigen-negative clones of cells that can escape the immune attack. Earlier analysis of the relapsed B16gp33 tumours by Nguyen *et al.* showed that relapsing tumour cells indeed lose the target antigen[241]. Upon analysis of the DNA repair pathways, we observed a shutdown in all DNA repair pathways in tumours treated with P14 + VacVgp33 compared to P14 + VSVgp33 (**Fig. 6.6**

E). These findings led to further investigations of the effect of DNA repair pathways on mediating antigen loss and immune escape in collaboration with Sreedevi Kesavan and Scott Walsh.

The work done by Kesavan and Walsh showed that infection of tumour cells by VSV or VacV causes comparable DNA double stranded breaks. As a result, upregulation of Nibrin (NBS1), a member of double strand DNA break repair complex, was observed following viral infection of B16gp33 cells using VSV or VacV (**Fig 6.7 A**). Interestingly however, in case of VSV infection, NBS1 was localized to the nucleus, whereas in case of VacV infection, NBS1 could be detected in the nucleus and the cytoplasm. The nature of VacV replication being in the cytoplasm could explain the reason for NBS1 presence in the cytoplasm, where the DNA repair machinery could be hijacked by the virus to ensure the genomic integrity of the newly synthesized viral genome. As a result, double stranded DNA breaks in the host cell genome are not repaired. In order to assess the antigen loss following viral infection, Kesavan and Walsh engineered B16 cells so that the gp33 coding sequence is linked to GFP through P2A sequences (B16gp33GFP), such that the loss of gp33 is accompanied by reduced fluorescence or complete loss of GFP signal. Using these cells, they were able to show that cells infected with VSV led to more GFP-negative (and hence gp33-negative) cells compared to VacV infected cells (**Fig. 6.7 B**). Additionally, infection of B16 cells with VSV in the presence of DNA repair inhibitor molecules, either Mirin and AZD7648, led to statistically significant increase in the proportion of dying cells. Cell death was not observed in cells treated with the inhibitor molecules alone so these results indicate that inhibiting DNA repair can synergize with viral oncolysis and increase cell death (**Fig. 6.7 C**). In this context, the synergy appears to be due to a bystander effect, as no direct effect on virus replication was observed. Rather, enhanced tumour death may be a result of cells accruing DNA damage during treatment being pushed towards apoptosis when DNA repair mechanisms are inhibited. In order to mimic the *in vivo* therapeutic protocol, they infected B16gp33GFP cells with VSV followed by co-culturing the surviving cells with P14 T cells. Interestingly, B16gp33GFP cells that were infected in the presence Mirin or AZD7648 showed reduced incidence of GFP (and antigen) loss (**Fig. 6.7 D**). Taken together, this data suggests that the downregulation of DNA repair machinery

A

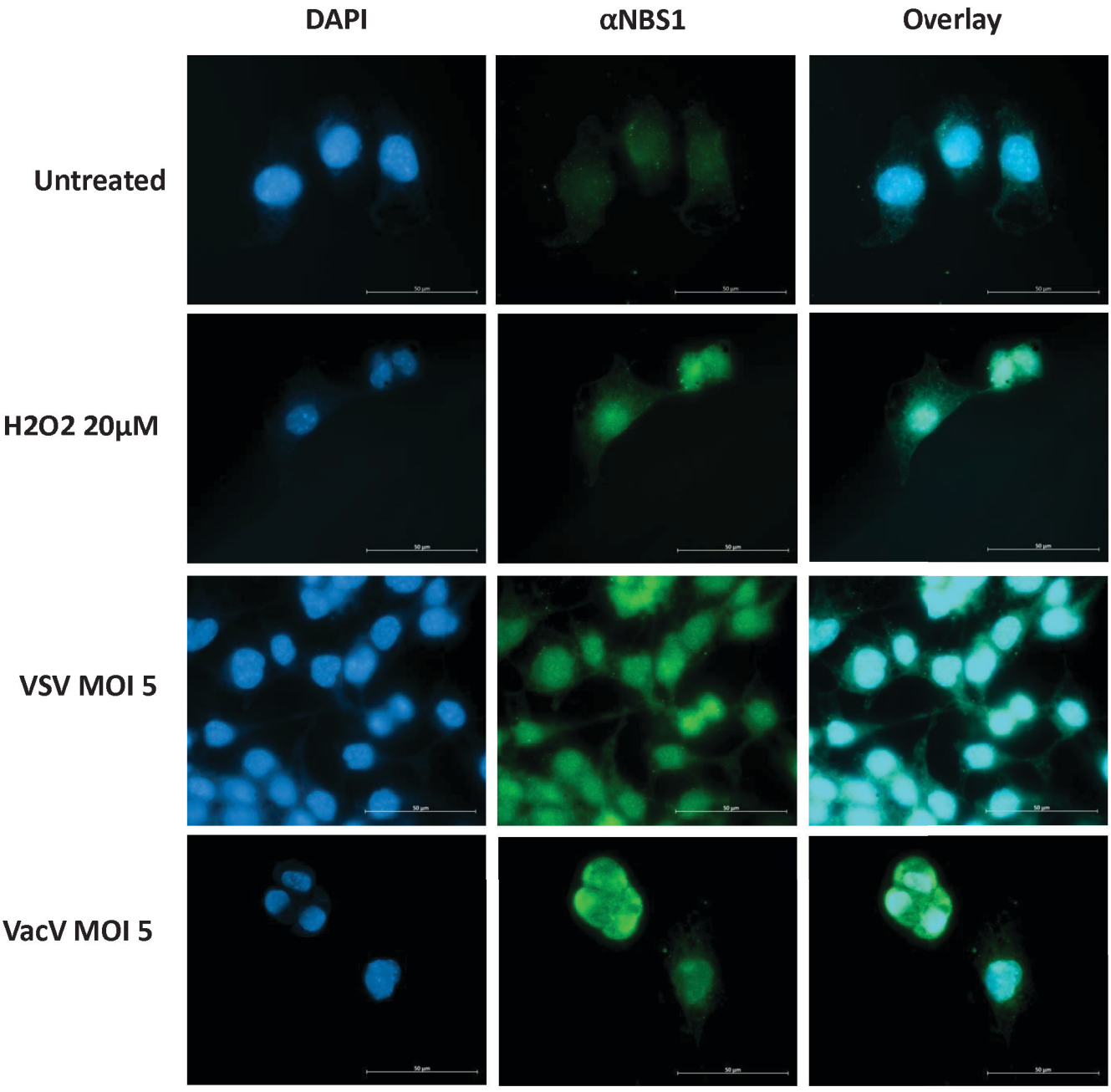

B

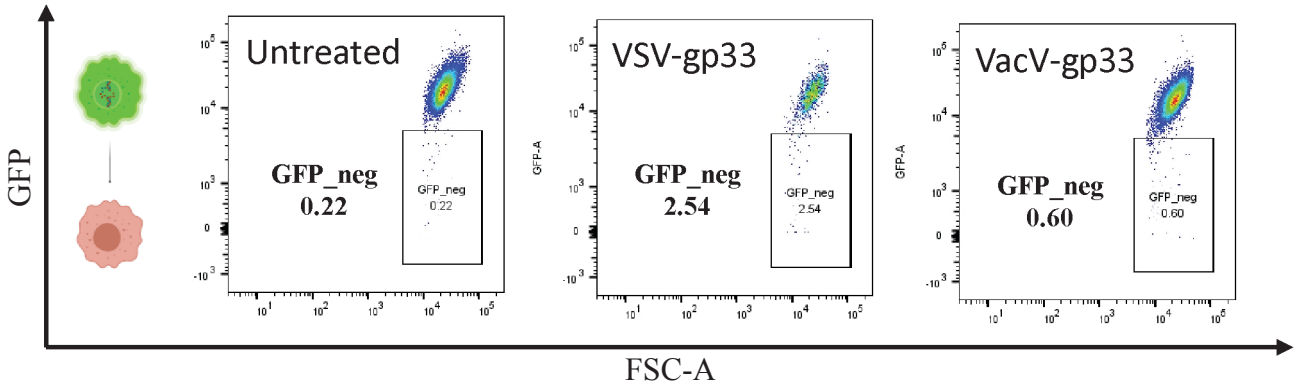
GFP
FSC-A
Untreated
GFP_neg
0.22
VSV-gp33
GFP_neg
2.54
VacV-gp33
GFP_neg
0.60
GFP-A

C

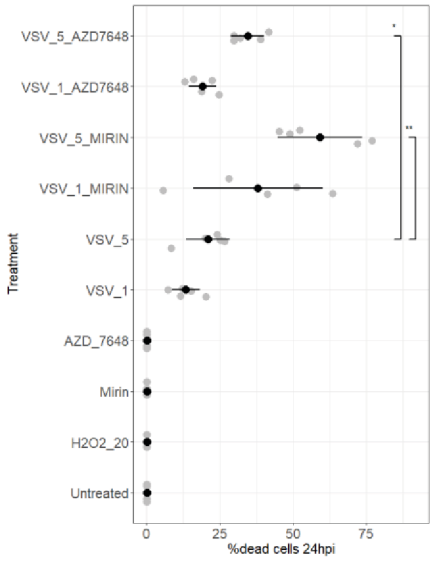
VSV_5_AZD7648
VSV_1_AZD7648
VSV_5_MIRIN
VSV_1_MIRIN
VSV_5
VSV_1
AZD_7648
Mirin
H2O2_20
Untreated
Treatment
0
25
50
75
%dead cells 24hpi

D

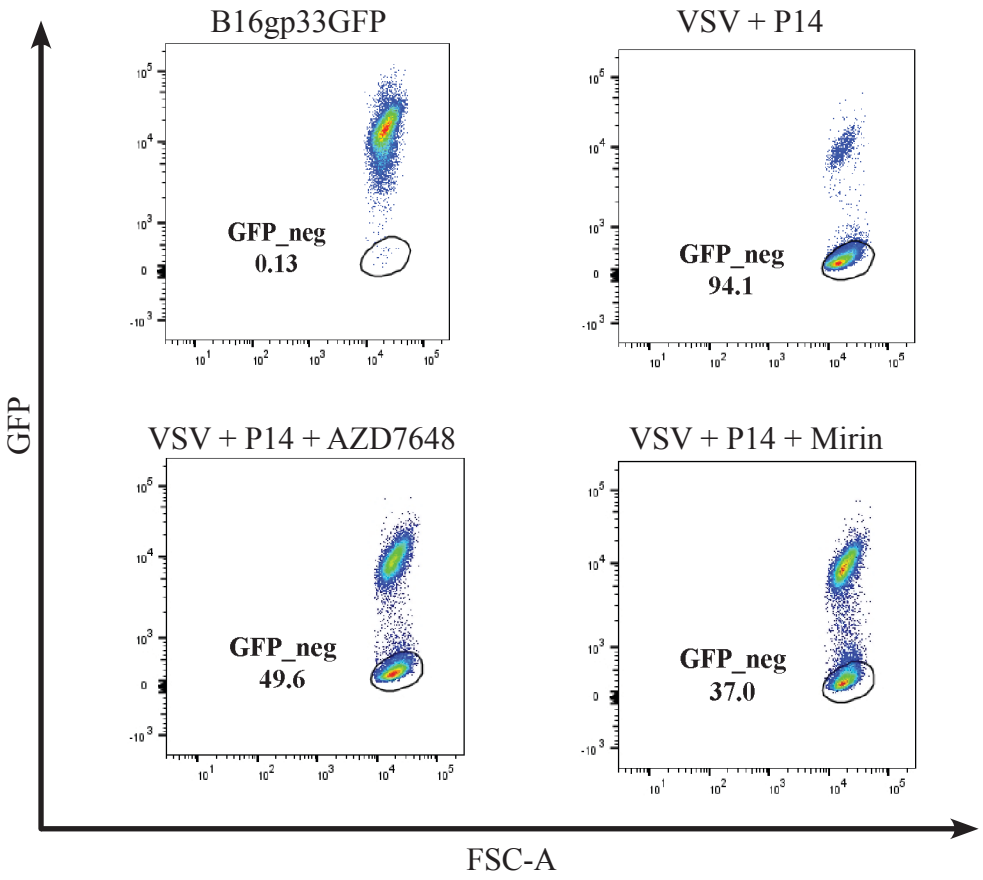

Figure 6.7 | VacV causes the shutdown of DNA repair pathways eliminating the chance of antigen loss and immune escape (Data courtesy of Sreedevi Kesavan)

(A) 5e4 CV1 cells were grown on glass coverslips and treated with either VSV or Vaccinia (MOI = 5) for 6 h, 20 μM of H_2O_2 for 1 hour or left untreated. Samples were then fixed, permeabilized and incubated with anti-NBS1 antibody for 24 h followed by a Rabbit anti-mouse-A488 for 2 h. Cells were then counterstained with Hoechst and the images were taken the next day at 63X magnification under an oil emersion lens. (B-C) 7.5e4 B16gp33GFP cells were infected with VSV or VacV (MOI =5) for 18-24 hours or H_2O_2 at 20 μM for 1-3 hour in the presence of absence of Mirin or AZD7648. Cells were fixed and analyzed for loss of GFP via flow cytometry or analyzed for % of dead cells. (D) 5e4 B16gp33GFP cells were infected with VSV or VSV + Mirin or VSV + AZD7648 for 24h and then media was changed. Cells were left to re-populate for a week and were then cocultured with P14 T-effector cells for 24 hours. The cells were analyzed for GFP expression via flow cytometry.

by VacV could be one of the mechanisms underlying its ability to cause durable tumour control and prevent tumour relapse and immune escape.

Chapter 7 — Investigating the effects of cellular and molecular signatures observed in ACT + VacV treated tumours on the disease progression/outcome in human patients.

7.1. Introduction

Immunotherapy in its different flavors has ushered in a new era of anti-tumour therapies, with long-term responses and significant survival advantages observed in multiple tumours. Most patients, however, do not benefit from these therapies. Therefore, the identification of predictive biomarkers for the response of immunotherapeutics, especially the ICBs, has been an active area of research. Inherent properties of certain tumours (e.g. high tumour mutational burden) has been correlated with better responses to ICBs and more favorable outcomes. While it is not feasible to alter the inherent properties of tumour cells, therapies aimed at reprogramming the tumour microenvironment help make therapy-resistant tumours susceptible to immunotherapies. In the previous chapter, we described the cellular and transcriptomic changes induced by ACT + OVV in the TME. We highlighted the differences between VSV and VacV on different cellular processes related to inflammation and immunity, cell cycle progression, cell metabolism and DNA repair pathways. In this chapter, we aim to investigate whether the transcriptomic changes induced by ACT + VacV correlate with disease progression in human melanoma patients. We hypothesize that a balanced inflammatory signature similar to what was observed as a result of ACT + VacV treatment correlates with positive prognosis and better overall survival in cancer patients. Our results showed that melanomas with high infiltration of $CD8^+$ T cells or M1 macrophages share common pathway-expression profiles with each other as well as with mouse tumours treated with ACT + VacV. Additionally, the transcriptomic signatures induced by ACT + VacV, beyond those related to immune cell infiltration, indeed correlated with favorable responses and a statistically significant increase in the survival of patients suggesting that ACT + VacV treatment reprograms the TME towards a favorable responsive phenotype.

7.2. Results

7.2.1. Infiltration of CD8$^+$ T cells and M1 Macrophages in Skin Cutaneous Melanoma (SKCM) correlates with better overall survival

The intratumoural analysis of the immune populations following ACT + OVV demonstrated the ability of the therapy to activate and recruit lymphoid and myeloid populations to the TME with the CD8$^+$ T cells being the predominant population 6 days pvi. We were interested in examining whether the presence of such populations correlates with better outcomes in melanoma patients. To this end, we analyzed the cohort of Skin Cutaneous Melanoma (SKCM) data generated by The Cancer Genome Atlas (TCGA). Clinical data of the patients was obtained from the cBio Cancer Genomics Portal (http://cbioportal.org)[254,255]. In order to estimate the relative presence of different immune populations we used CIBERSORTx, an *in silico* flow cytometry method developed by Newman *et al.*[289]. It uses a deconvolution algorithm to estimate the abundance of different cell types from bulk tissue RNA sequencing (RNAseq) data. We used the output of CIBERSORTx to stratify the patients into groups of high, intermediate and low infiltration of each cellular population. We focused on the high and low groups which account for the top and bottom quartiles of the data. First, we performed PCA to reduce the dimensionality of the data and assessed how the infiltration of each population correlate with the variance of the data along the first two PCs. We observed that patients with high or low infiltration of either CD8$^+$ T cells or M1 macrophages were separated along the first principal component, while other populations did not have a noticeable clustering pattern along PC1 and PC2 (**Fig. 7.1 A**). We then asked whether there is a direct correlation between CD8$^+$ T cells and M1 macrophages infiltration. Using Pearson correlation, we observed a weak positive correlation between the infiltration levels of both populations with a correlation coefficient of 0.39 (**Fig. 7.1 B**). To get a better understanding of the relationship between the infiltration of CD8$^+$ T cells and M1 macrophages, we created an upset plot that quantifies the number of patients in each possible combination of infiltrations (**Fig.**

7.1 C). Next, we performed differential gene expression analysis between patients with high and low infiltration of $CD8^+$ T cells and M1 macrophages using DESeq2 package[290]. Patients with high infiltration of $CD8^+$ T cells had statistically significant upregulation of T cell specific genes including *CD8A, NKG7, IFNG, CCL5, GZMB, GZMH, TBX21, IL2RB* (**Fig. 7.1 D**). On the other hand, tumours with high M1 macrophages infiltration showed a statistically significant upregulation of M1 macrophages specific genes including *STAT1, IFNG, IFIT3, CXCL9, CXCL10, IL12RB1, IRF1* (**Fig. 7.1 E**). These results indeed validate the *in silico* sorting done using CIBERSORTx. The high expression of CXCL9 and CXCL10 in tumours with high M1 macrophages infiltration explains the correlation between $CD8^+$ T cells and M1 macrophages, since $CXCR3^+$ T cells migrate along the CXCL9 and CXCL10 gradients. It is worth noting that M1 enriched tumours showed a statistically significant upregulation of the *MS4A1* gene, which encodes for CD20, indicating enrichment of B cells in such tumours as well. We were interested in analyzing the enriched pathways associated with either $CD8^+$ T cells or M1 macrophages. To this end, we performed GSEA using the hallmark pathways on the ranked gene lists from tumours with high vs. low infiltration of either $CD8^+$ T cells or M1 macrophages (**Fig. 7.1 F-G**). Interestingly, tumours enriched for either $CD8^+$ T cells or M1 macrophages were positively enriched for all the immune-specific hallmark pathways while being negatively enriched for cell cycle and replication pathways. Additionally, tumours with high M1 macrophages infiltration showed a statistically significant downregulation in DNA repair pathways. $CD8^+$ T cell enriched tumours also showed a downregulation in DNA repair pathways but not to the level of statistical significance. Last but not least, we performed a univariate survival analysis to assess the effect of infiltration of each individual cellular population on the overall survival of patients. Patients with high levels of infiltrations of $CD8^+$ T cells or M1 Macrophages had a statistically significant improvement in the overall survival **(Fig. 7.1 H)**. The median survival of patients with high $CD8^+$ T cells infiltration was 103.2 months compared to 62.8 months in case of low $CD8^+$ T cell infiltration (*P* value = 0.005; log-rank test). Patients with high infiltration of M1 macrophages had a median survival of 138.8 months compared to a median survival of 50.1 months for patients with low infiltration (*P*

A

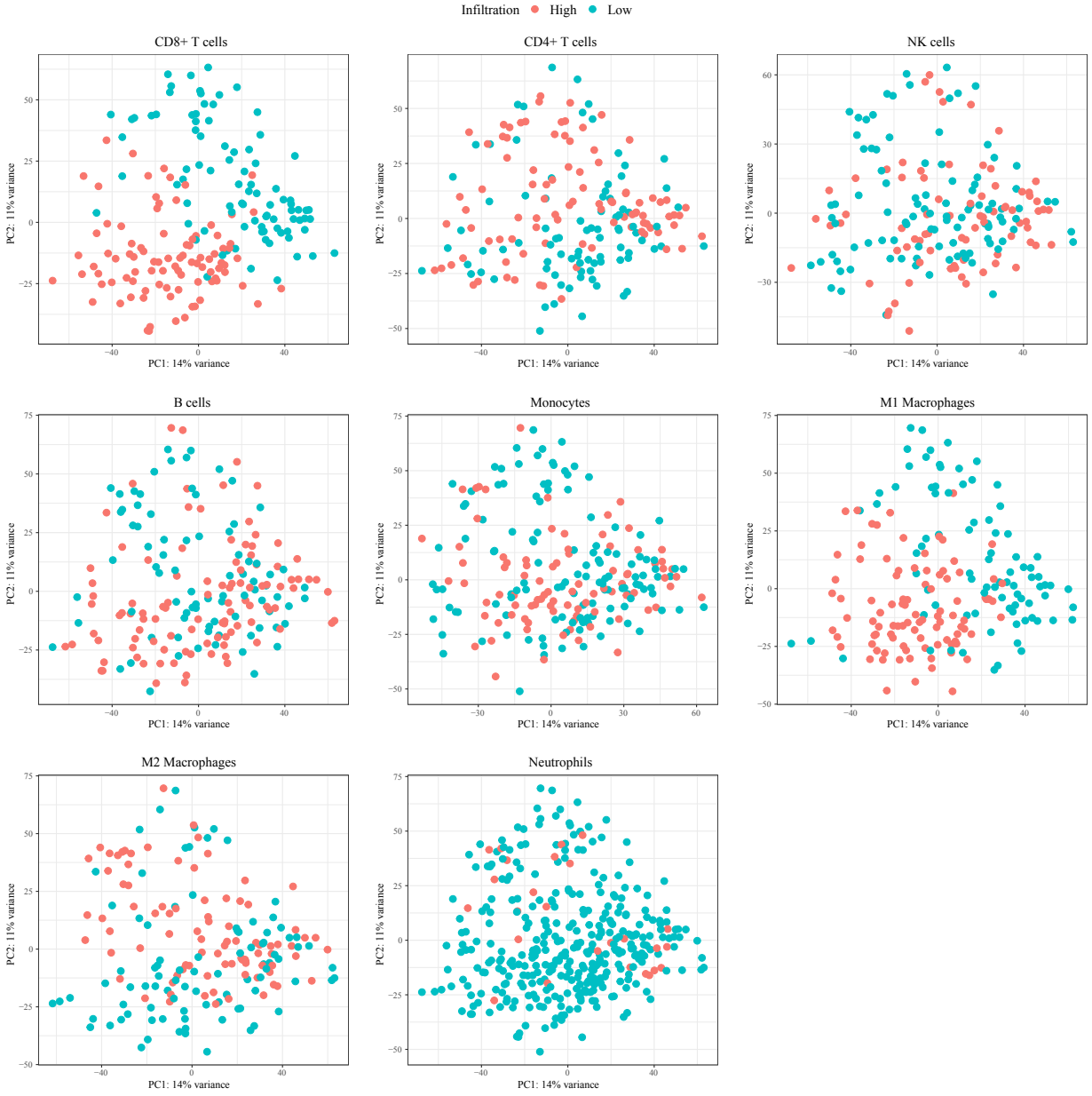
Infiltration High Low
CD8+ T cells
CD4+ T cells
NK cells
B cells
Monocytes
M1 Macrophages
M2 Macrophages
Neutrophils
PC1: 14% variance
PC2: 11% variance

B

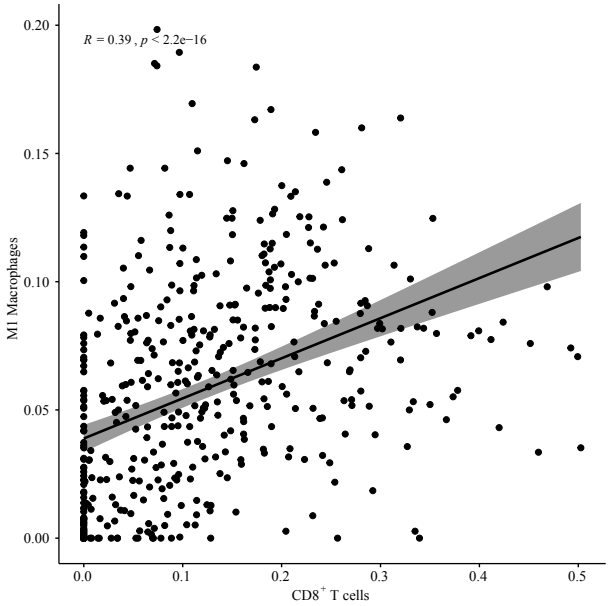
R = 0.39 , p < 2.2e−16
M1 Macrophages
CD8+ T cells
0.00
0.05
0.10
0.15
0.20
0.0
0.1
0.2
0.3
0.4
0.5

C

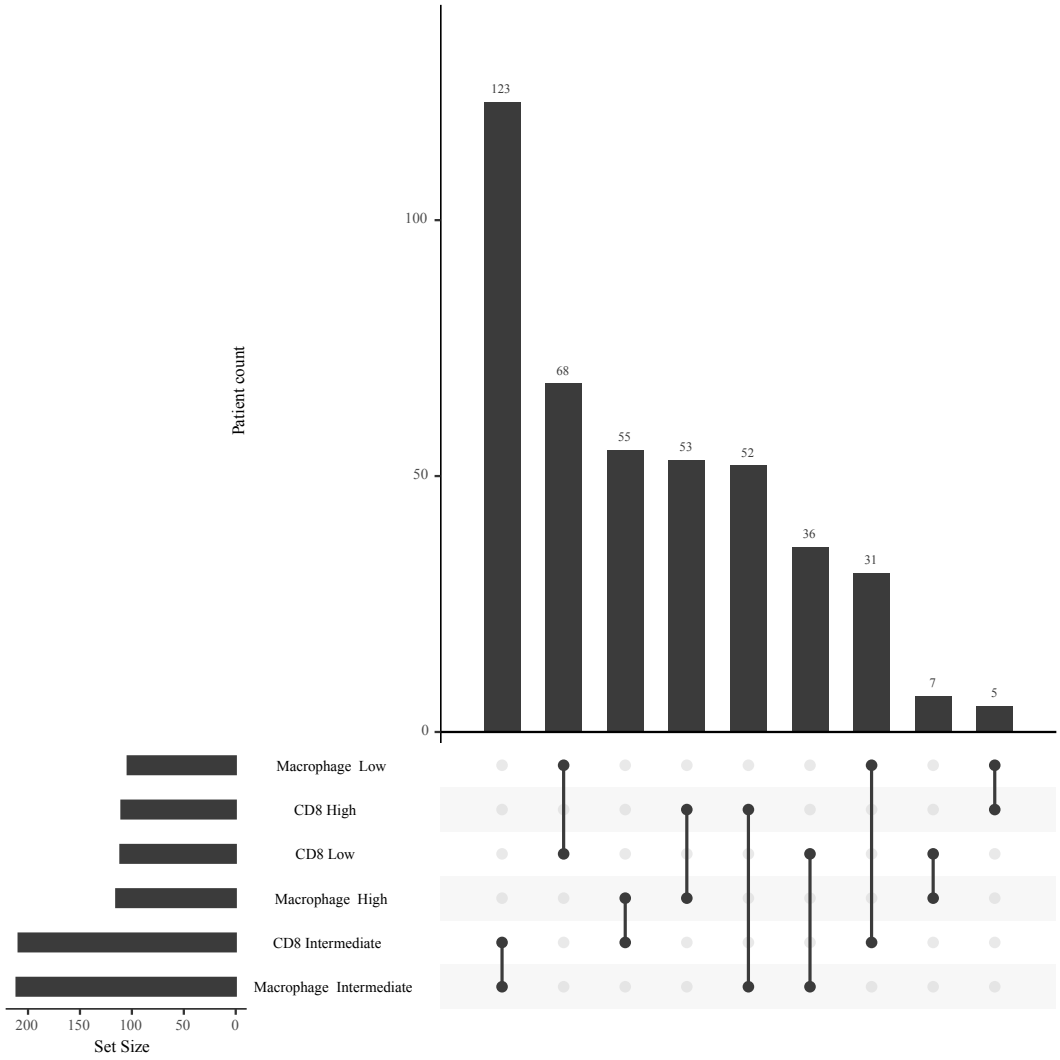
Patient count
123
68
55
53
52
36
31
7
5
Macrophage Low
CD8 High
CD8 Low
Macrophage High
CD8 Intermediate
Macrophage Intermediate
Set Size
200
150
100
50
0

D

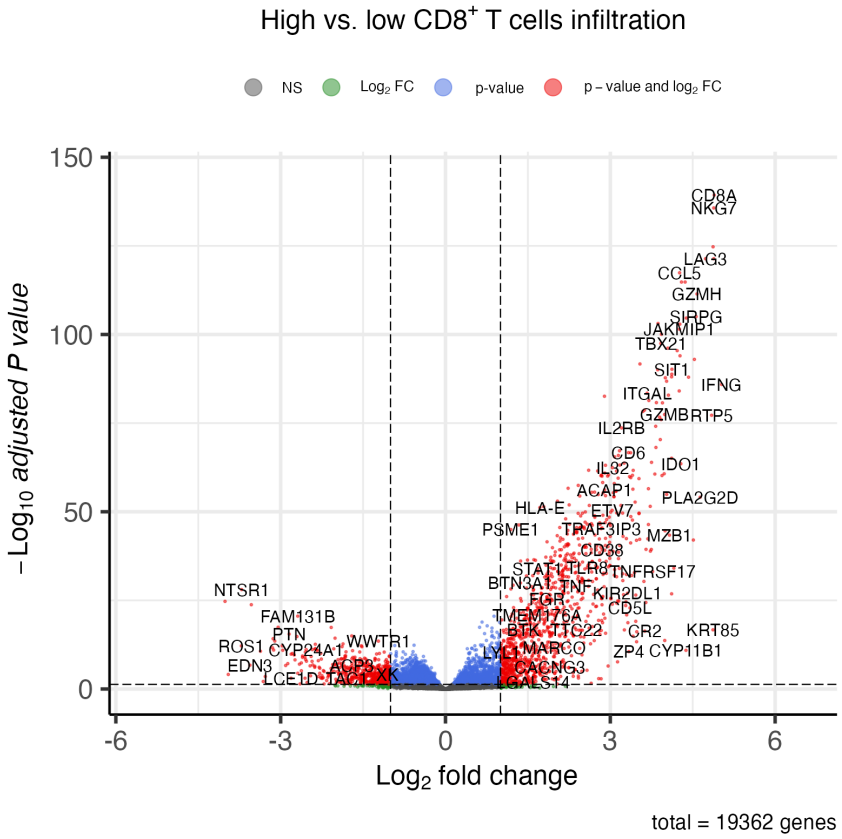
High vs. low CD8+ T cells infiltration
NS
Log2 FC
p-value
p – value and log2 FC
– Log10 adjusted P value
Log2 fold change
total = 19362 genes

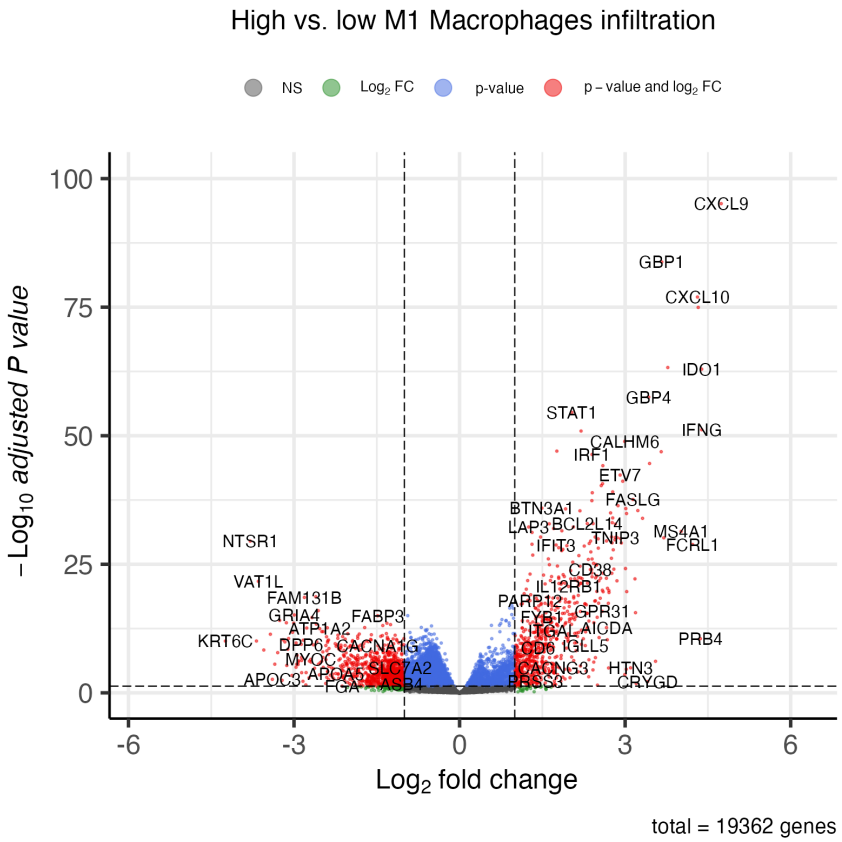
High vs. low M1 Macrophages infiltration
NS
Log2 FC
p-value
p – value and log2 FC
– Log10 adjusted P value
Log2 fold change
total = 19362 genes

E

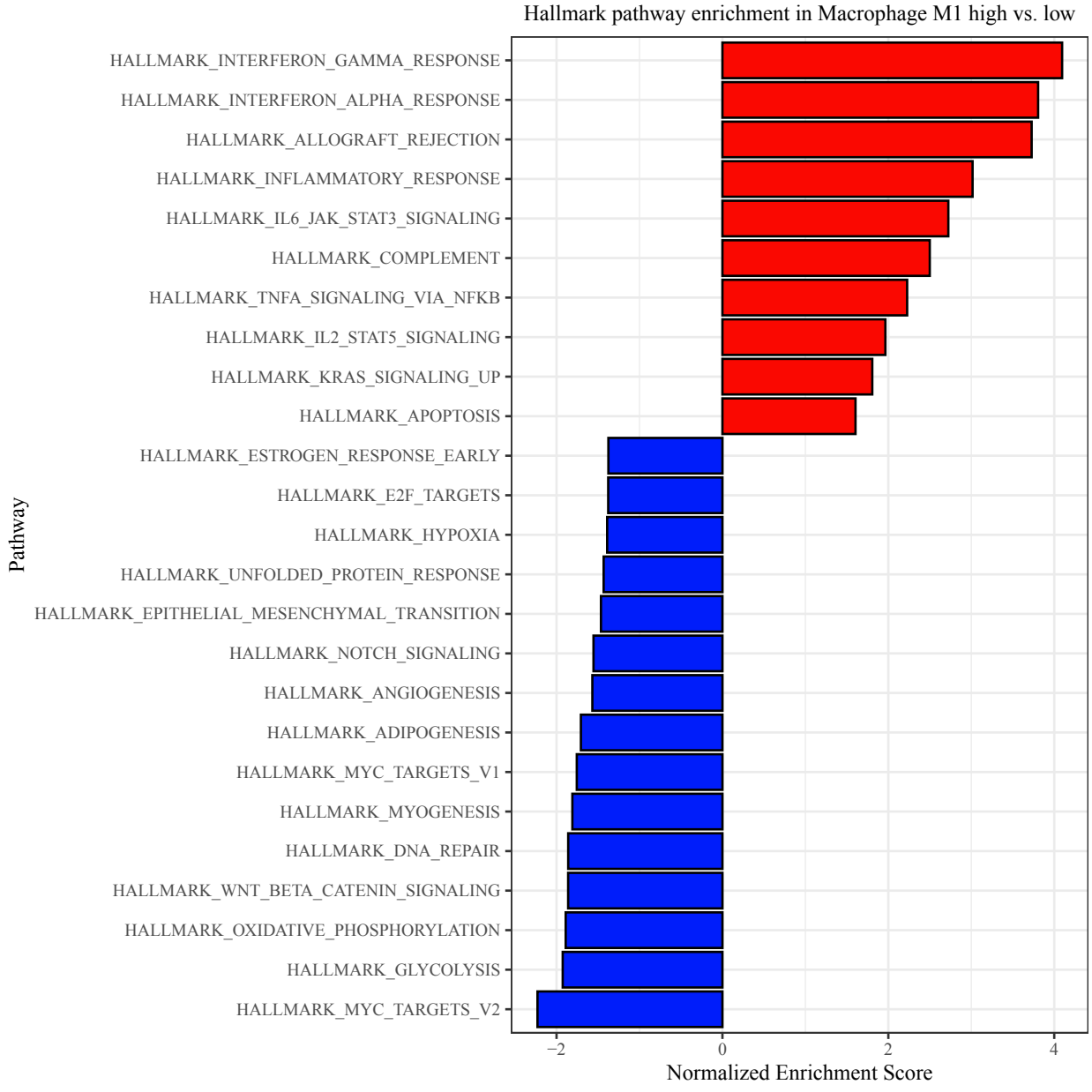
Hallmark pathway enrichment in Macrophage M1 high vs. low
HALLMARK_INTERFERON_GAMMA_RESPONSE
HALLMARK_INTERFERON_ALPHA_RESPONSE
HALLMARK_ALLOGRAFT_REJECTION
HALLMARK_INFLAMMATORY_RESPONSE
HALLMARK_IL6_JAK_STAT3_SIGNALING
HALLMARK_COMPLEMENT
HALLMARK_TNFA_SIGNALING_VIA_NFKB
HALLMARK_IL2_STAT5_SIGNALING
HALLMARK_KRAS_SIGNALING_UP
HALLMARK_APOPTOSIS
HALLMARK_ESTROGEN_RESPONSE_EARLY
HALLMARK_E2F_TARGETS
HALLMARK_HYPOXIA
HALLMARK_UNFOLDED_PROTEIN_RESPONSE
HALLMARK_EPITHELIAL_MESENCHYMAL_TRANSITION
HALLMARK_NOTCH_SIGNALING
HALLMARK_ANGIOGENESIS
HALLMARK_ADIPOGENESIS
HALLMARK_MYC_TARGETS_V1
HALLMARK_MYOGENESIS
HALLMARK_DNA_REPAIR
HALLMARK_WNT_BETA_CATENIN_SIGNALING
HALLMARK_OXIDATIVE_PHOSPHORYLATION
HALLMARK_GLYCOLYSIS
HALLMARK_MYC_TARGETS_V2
Pathway
−2
0
2
4
Normalized Enrichment Score

F

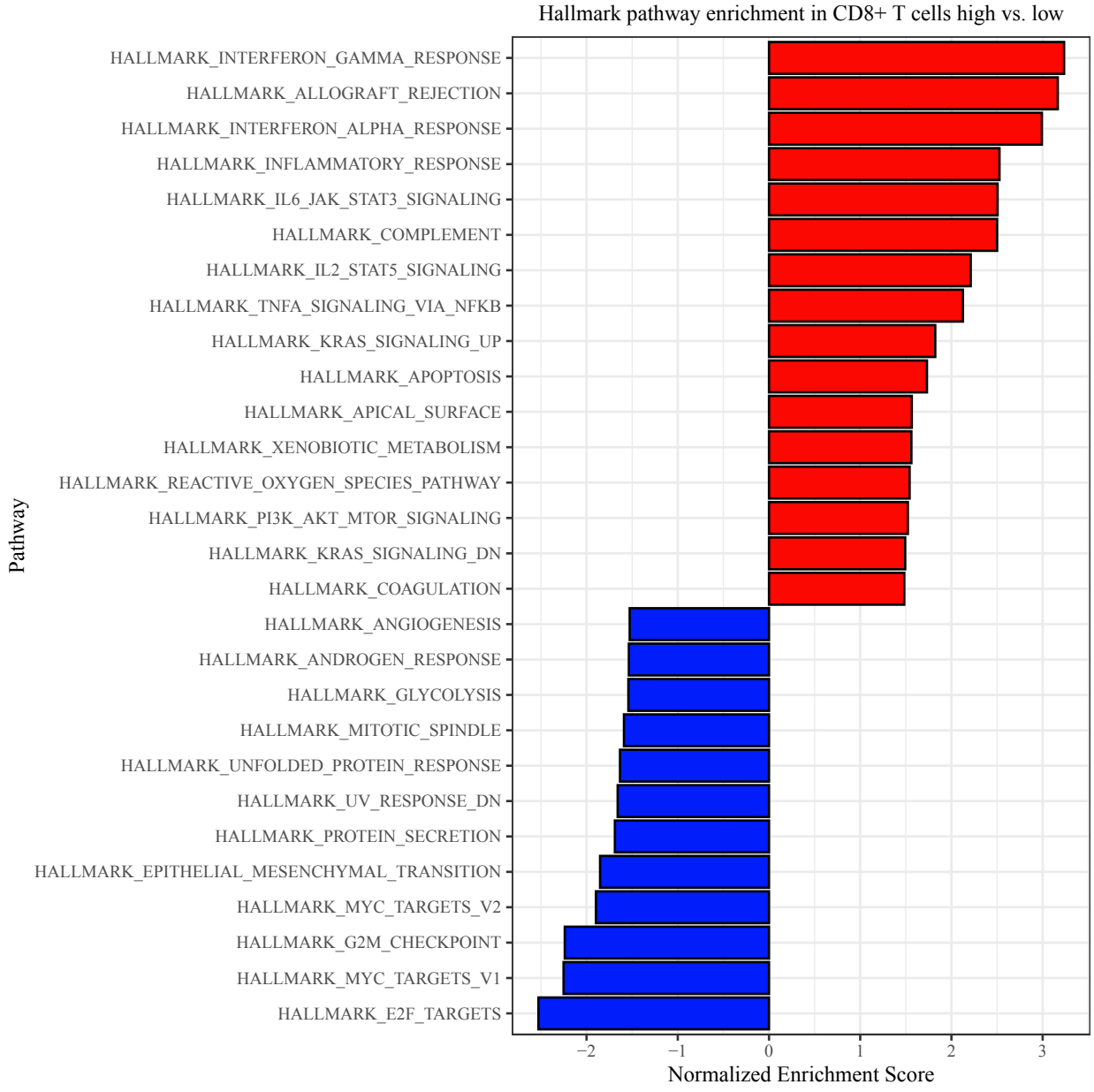
Hallmark pathway enrichment in CD8+ T cells high vs. low
HALLMARK_INTERFERON_GAMMA_RESPONSE
HALLMARK_ALLOGRAFT_REJECTION
HALLMARK_INTERFERON_ALPHA_RESPONSE
HALLMARK_INFLAMMATORY_RESPONSE
HALLMARK_IL6_JAK_STAT3_SIGNALING
HALLMARK_COMPLEMENT
HALLMARK_IL2_STAT5_SIGNALING
HALLMARK_TNFA_SIGNALING_VIA_NFKB
HALLMARK_KRAS_SIGNALING_UP
HALLMARK_APOPTOSIS
HALLMARK_APICAL_SURFACE
HALLMARK_XENOBIOTIC_METABOLISM
HALLMARK_REACTIVE_OXYGEN_SPECIES_PATHWAY
HALLMARK_PI3K_AKT_MTOR_SIGNALING
HALLMARK_KRAS_SIGNALING_DN
HALLMARK_COAGULATION
HALLMARK_ANGIOGENESIS
HALLMARK_ANDROGEN_RESPONSE
HALLMARK_GLYCOLYSIS
HALLMARK_MITOTIC_SPINDLE
HALLMARK_UNFOLDED_PROTEIN_RESPONSE
HALLMARK_UV_RESPONSE_DN
HALLMARK_PROTEIN_SECRETION
HALLMARK_EPITHELIAL_MESENCHYMAL_TRANSITION
HALLMARK_MYC_TARGETS_V2
HALLMARK_G2M_CHECKPOINT
HALLMARK_MYC_TARGETS_V1
HALLMARK_E2F_TARGETS
Pathway
−2
−1
0
1
2
3
Normalized Enrichment Score

G

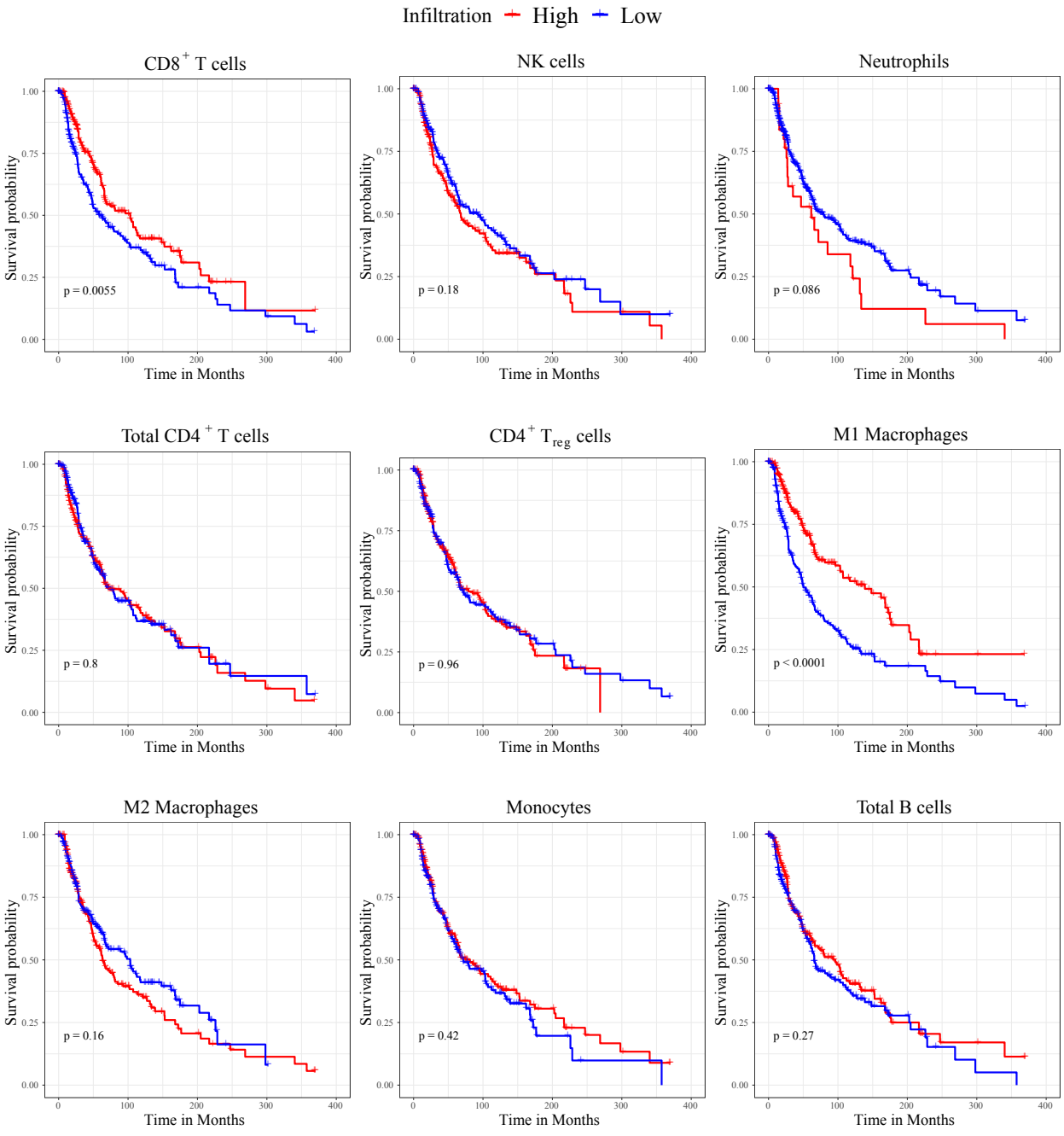
Infiltration High Low
CD8+ T cells
NK cells
Neutrophils
Total CD4+ T cells
CD4+ Treg cells
M1 Macrophages
M2 Macrophages
Monocytes
Total B cells
Survival probability
Time in Months
p = 0.0055
p = 0.18
p = 0.086
p = 0.8
p = 0.96
p < 0.0001
p = 0.16
p = 0.42
p = 0.27

Figure 7.1 | Infiltration of $CD8^+$ T cells and M1 Macrophages in Skin Cutaneous Melanoma (SKCM) correlates with the upregulation of inflammatory pathways and better overall survival of patients

Bulk RNAseq data from a cohort of 473 Skin Cutaneous Melanoma (SKCM) patients from The Cancer Genome Atlas (TCGA) was submitted to CIBERSORTx for estimation of immune populations. The clinical data of patients was obtained from the cBio Cancer Genomics Portal (cbioportal). (A) Scatter plot showing the relationship between high and low infiltration of each population to the first two principal components. (B - C) Scatter plot / upset plot showing the relationship between CD8+ T cells and M1 macrophages infiltration in SKCM tumours. (D) Volcano plots showing the DEGs between tumours with high and low infiltration of CD8+ T cells or M1 macrophages. (E-F) GSEA showing hallmark pathway enrichment of tumours with high and low infiltration of CD8+ T cells or M1 macrophages. (G) Kaplan-Meier plots showing the effect of the relative presence of immune populations on the overall survival of patients.

value < 0.0001; log-rank test). The infiltration of other cellular populations including total $CD4^+$ T cells, T_{reg} cells, NK cells, total B cell, M2 macrophages, monocytes and neutrophils did not show a statistically significant difference in survival of patients. In conclusion, the infiltration of tumours with $CD8^+$ T cells or M1 macrophages is correlated with an inflammatory pathway signature and an increase in the overall survival of patients.

7.2.2. Hallmark pathways differentially regulated by ACT + VacV are predictive of positive prognosis in SKCM patients

Next, we sought to investigate the effects of up- or downregulation of the hallmark pathways on the survival of SKCM patients irrespective of the level immune cell infiltration. To this end, we used gene set variation analysis (GSVA) to estimate sample-wise gene set enrichment score[256]. This allowed us to convert the matrix of gene expression obtained from RNAseq into a matrix of pathway scores. We performed hierarchical clustering analysis using Pearson correlation to calculate the similarity in expression of different pathways **(Fig. 7.2 A)**. We observed that pathways clustered into 6 clusters that are summarized in **table 7.1**. Some clusters included pathways that represent a common biological theme e.g., cluster 1 included pathways associated with the activation of inflammatory responses, while cluster 4 had pathways associated with metabolic events. Additionally, we observed a negative correlation between inflammatory pathways and metabolic pathways as well as pathways related to cell replication, which suggests that the activation of immune responses within the TME limits the metabolic processes and the replication capacity of tumour cells. DNA repair pathways also negatively correlated with the activation of the inflammatory pathways. In order to examine the effect of each individual pathway on the disease prognosis, we used a univariate cox proportional hazard model to assess the hazard ratio associated with each pathway independently **(Fig. 7.2 B)**[291]. Interestingly, all hallmark pathways associated with inflammatory responses (cluster 1) had a hazard ratio (HR) < 1 pointing to a favorable prognosis in patients expressing any of the aforementioned pathways.

A

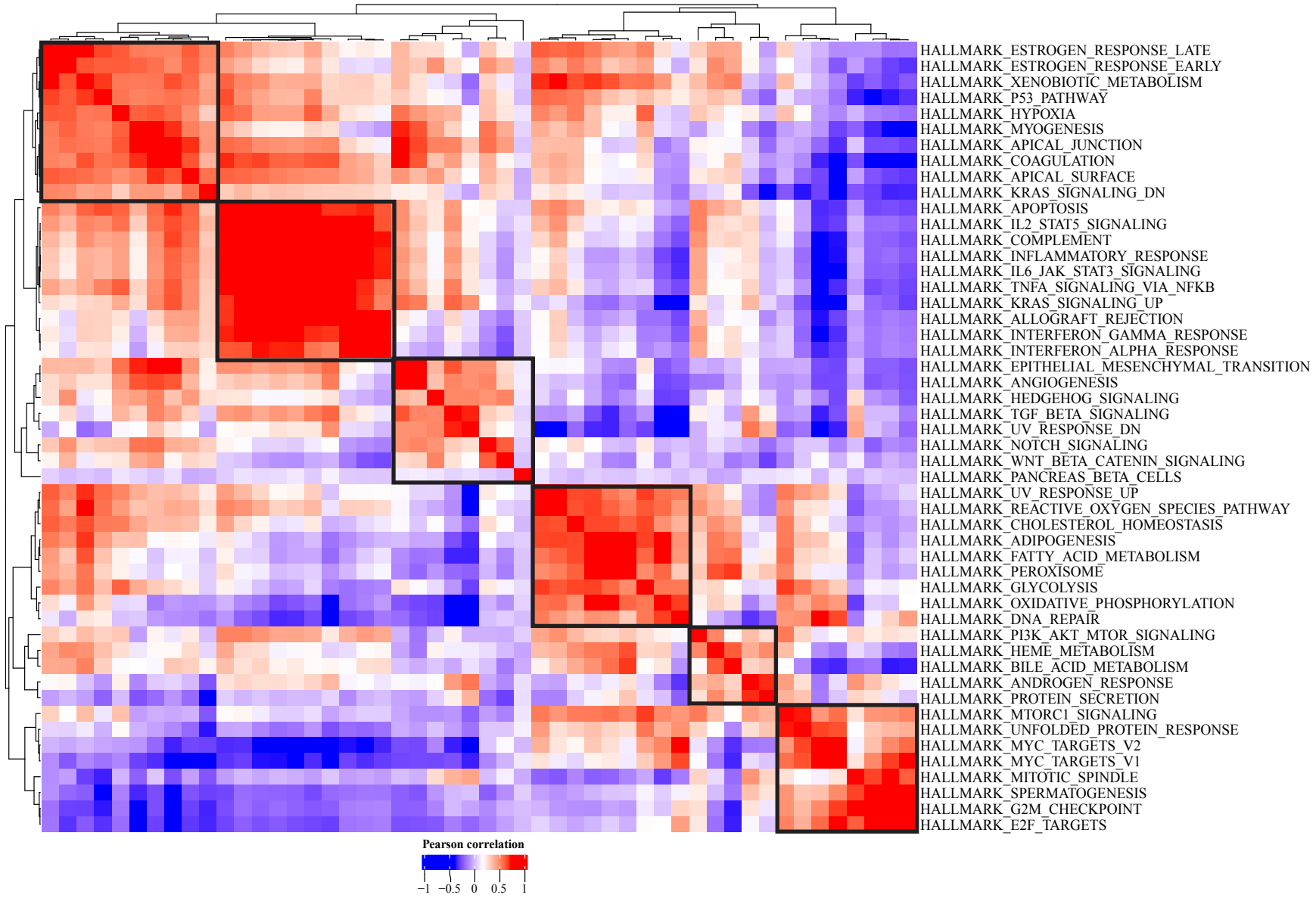
HALLMARK_ESTROGEN_RESPONSE_LATE
HALLMARK_ESTROGEN_RESPONSE_EARLY
HALLMARK_XENOBIOTIC_METABOLISM
HALLMARK_P53_PATHWAY
HALLMARK_HYPOXIA
HALLMARK_MYOGENESIS
HALLMARK_APICAL_JUNCTION
HALLMARK_COAGULATION
HALLMARK_APICAL_SURFACE
HALLMARK_KRAS_SIGNALING_DN
HALLMARK_APOPTOSIS
HALLMARK_IL2_STAT5_SIGNALING
HALLMARK_COMPLEMENT
HALLMARK_INFLAMMATORY_RESPONSE
HALLMARK_IL6_JAK_STAT3_SIGNALING
HALLMARK_TNFA_SIGNALING_VIA_NFKB
HALLMARK_KRAS_SIGNALING_UP
HALLMARK_ALLOGRAFT_REJECTION
HALLMARK_INTERFERON_GAMMA_RESPONSE
HALLMARK_INTERFERON_ALPHA_RESPONSE
HALLMARK_EPITHELIAL_MESENCHYMAL_TRANSITION
HALLMARK_ANGIOGENESIS
HALLMARK_HEDGEHOG_SIGNALING
HALLMARK_TGF_BETA_SIGNALING
HALLMARK_UV_RESPONSE_DN
HALLMARK_NOTCH_SIGNALING
HALLMARK_WNT_BETA_CATENIN_SIGNALING
HALLMARK_PANCREAS_BETA_CELLS
HALLMARK_UV_RESPONSE_UP
HALLMARK_REACTIVE_OXYGEN_SPECIES_PATHWAY
HALLMARK_CHOLESTEROL_HOMEOSTASIS
HALLMARK_ADIPOGENESIS
HALLMARK_FATTY_ACID_METABOLISM
HALLMARK_PEROXISOME
HALLMARK_GLYCOLYSIS
HALLMARK_OXIDATIVE_PHOSPHORYLATION
HALLMARK_DNA_REPAIR
HALLMARK_PI3K_AKT_MTOR_SIGNALING
HALLMARK_HEME_METABOLISM
HALLMARK_BILE_ACID_METABOLISM
HALLMARK_ANDROGEN_RESPONSE
HALLMARK_PROTEIN_SECRETION
HALLMARK_MTORC1_SIGNALING
HALLMARK_UNFOLDED_PROTEIN_RESPONSE
HALLMARK_MYC_TARGETS_V2
HALLMARK_MYC_TARGETS_V1
HALLMARK_MITOTIC_SPINDLE
HALLMARK_SPERMATOGENESIS
HALLMARK_G2M_CHECKPOINT
HALLMARK_E2F_TARGETS
Pearson correlation
−1 −0.5 0 0.5 1

B

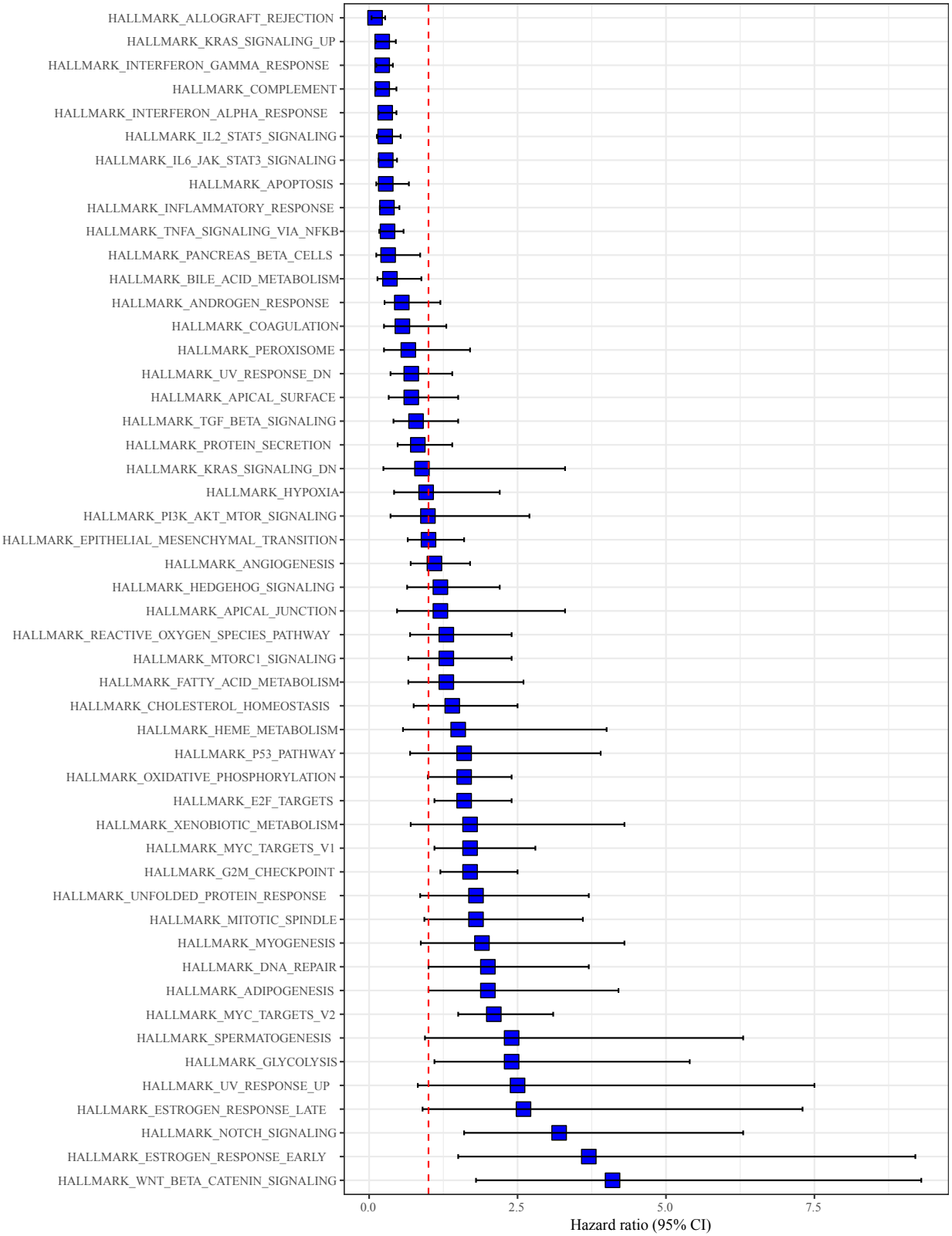
HALLMARK_ALLOGRAFT_REJECTION
HALLMARK_KRAS_SIGNALING_UP
HALLMARK_INTERFERON_GAMMA_RESPONSE
HALLMARK_COMPLEMENT
HALLMARK_INTERFERON_ALPHA_RESPONSE
HALLMARK_IL2_STAT5_SIGNALING
HALLMARK_IL6_JAK_STAT3_SIGNALING
HALLMARK_APOPTOSIS
HALLMARK_INFLAMMATORY_RESPONSE
HALLMARK_TNFA_SIGNALING_VIA_NFKB
HALLMARK_PANCREAS_BETA_CELLS
HALLMARK_BILE_ACID_METABOLISM
HALLMARK_ANDROGEN_RESPONSE
HALLMARK_COAGULATION
HALLMARK_PEROXISOME
HALLMARK_UV_RESPONSE_DN
HALLMARK_APICAL_SURFACE
HALLMARK_TGF_BETA_SIGNALING
HALLMARK_PROTEIN_SECRETION
HALLMARK_KRAS_SIGNALING_DN
HALLMARK_HYPOXIA
HALLMARK_PI3K_AKT_MTOR_SIGNALING
HALLMARK_EPITHELIAL_MESENCHYMAL_TRANSITION
HALLMARK_ANGIOGENESIS
HALLMARK_HEDGEHOG_SIGNALING
HALLMARK_APICAL_JUNCTION
HALLMARK_REACTIVE_OXYGEN_SPECIES_PATHWAY
HALLMARK_MTORC1_SIGNALING
HALLMARK_FATTY_ACID_METABOLISM
HALLMARK_CHOLESTEROL_HOMEOSTASIS
HALLMARK_HEME_METABOLISM
HALLMARK_P53_PATHWAY
HALLMARK_OXIDATIVE_PHOSPHORYLATION
HALLMARK_E2F_TARGETS
HALLMARK_XENOBIOTIC_METABOLISM
HALLMARK_MYC_TARGETS_V1
HALLMARK_G2M_CHECKPOINT
HALLMARK_UNFOLDED_PROTEIN_RESPONSE
HALLMARK_MITOTIC_SPINDLE
HALLMARK_MYOGENESIS
HALLMARK_DNA_REPAIR
HALLMARK_ADIPOGENESIS
HALLMARK_MYC_TARGETS_V2
HALLMARK_SPERMATOGENESIS
HALLMARK_GLYCOLYSIS
HALLMARK_UV_RESPONSE_UP
HALLMARK_ESTROGEN_RESPONSE_LATE
HALLMARK_NOTCH_SIGNALING
HALLMARK_ESTROGEN_RESPONSE_EARLY
HALLMARK_WNT_BETA_CATENIN_SIGNALING
0.0
2.5
5.0
7.5
Hazard ratio (95% CI)

C

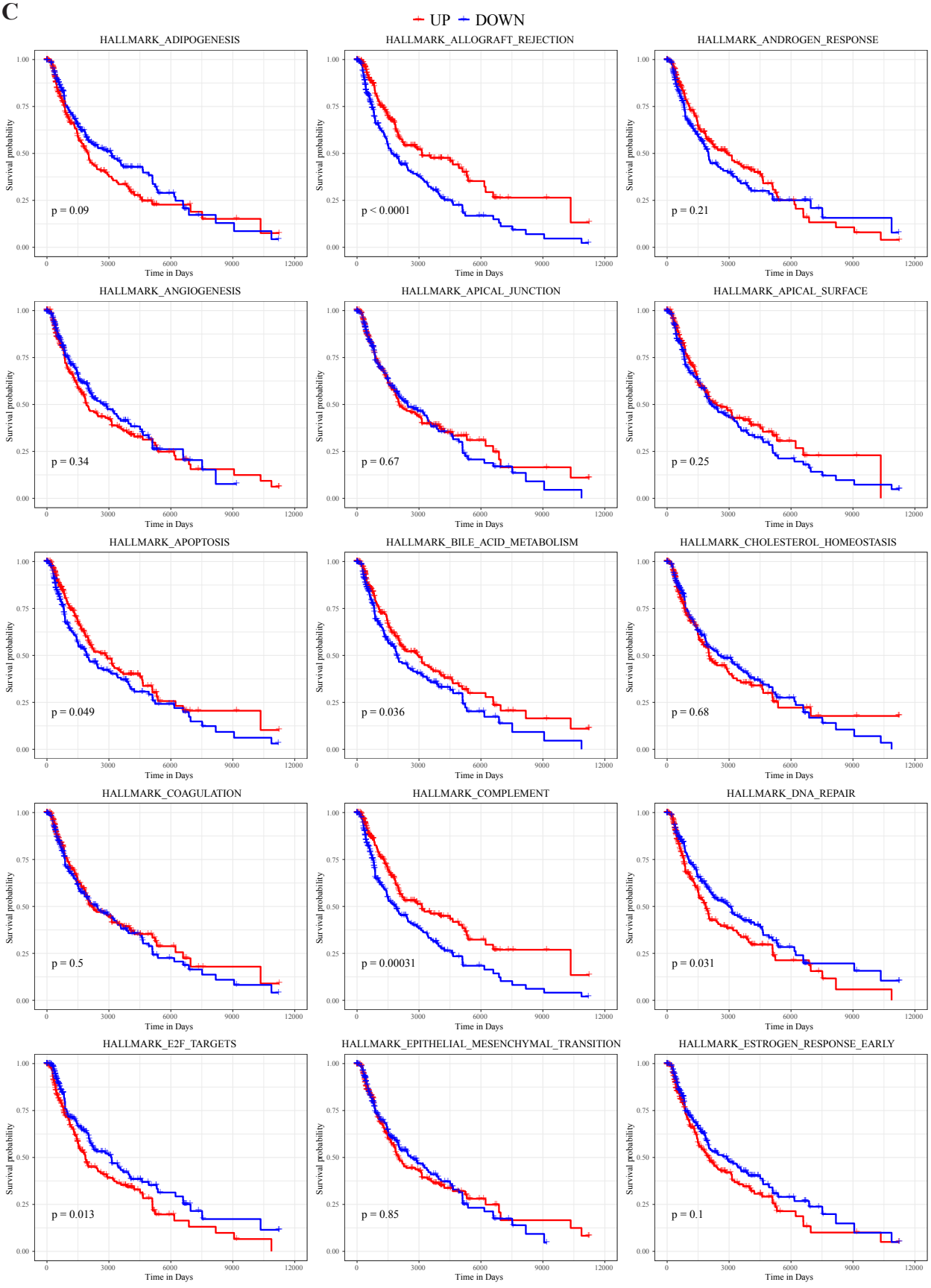
UP
DOWN
HALLMARK_ADIPOGENESIS
p = 0.09
HALLMARK_ALLOGRAFT_REJECTION
p < 0.0001
HALLMARK_ANDROGEN_RESPONSE
p = 0.21
HALLMARK_ANGIOGENESIS
p = 0.34
HALLMARK_APICAL_JUNCTION
p = 0.67
HALLMARK_APICAL_SURFACE
p = 0.25
HALLMARK_APOPTOSIS
p = 0.049
HALLMARK_BILE_ACID_METABOLISM
p = 0.036
HALLMARK_CHOLESTEROL_HOMEOSTASIS
p = 0.68
HALLMARK_COAGULATION
p = 0.5
HALLMARK_COMPLEMENT
p = 0.00031
HALLMARK_DNA_REPAIR
p = 0.031
HALLMARK_E2F_TARGETS
p = 0.013
HALLMARK_EPITHELIAL_MESENCHYMAL_TRANSITION
p = 0.85
HALLMARK_ESTROGEN_RESPONSE_EARLY
p = 0.1
Survival probability
Time in Days

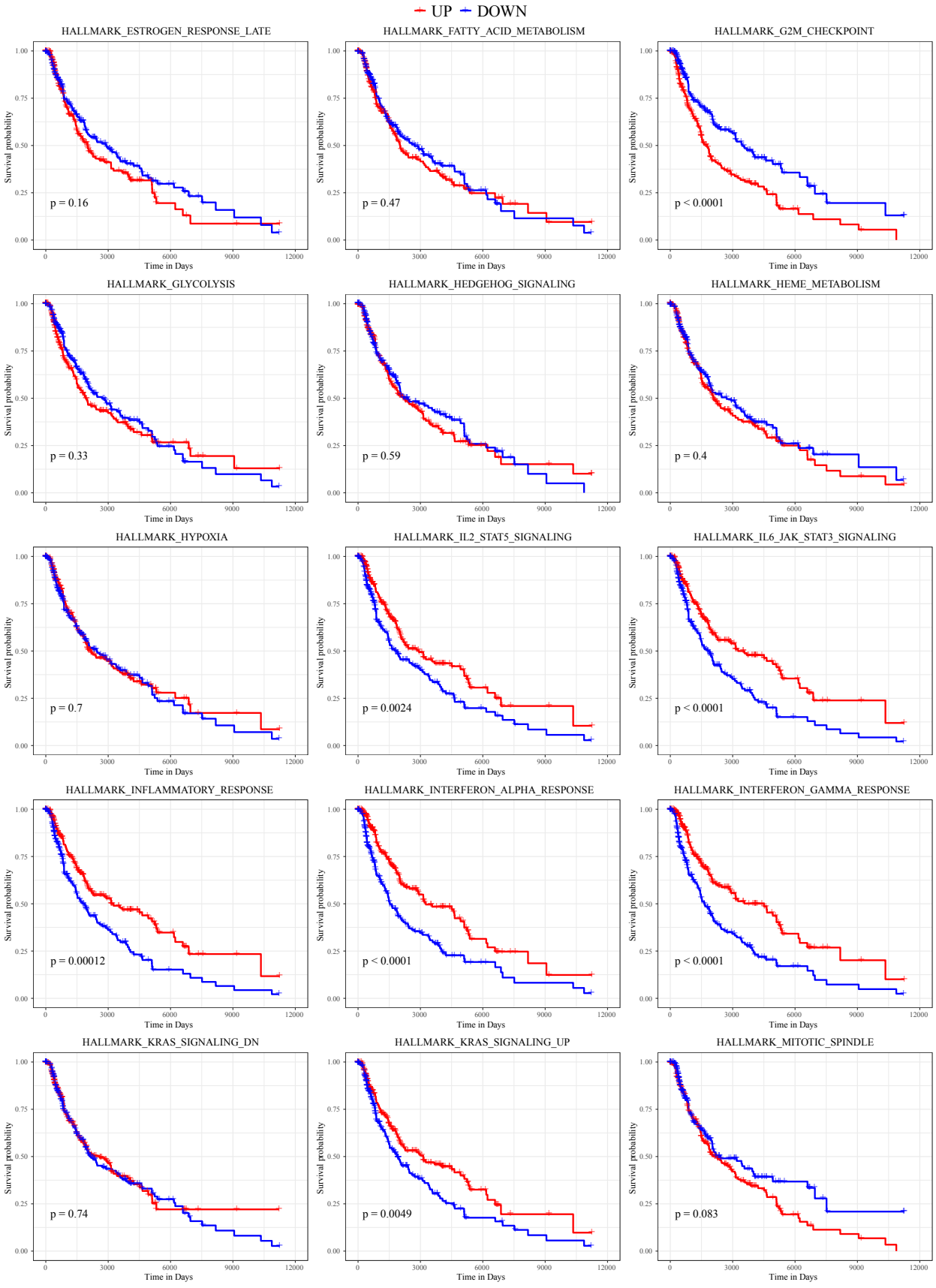
UP
DOWN
HALLMARK_ESTROGEN_RESPONSE_LATE
p = 0.16
HALLMARK_FATTY_ACID_METABOLISM
p = 0.47
HALLMARK_G2M_CHECKPOINT
p < 0.0001
HALLMARK_GLYCOLYSIS
p = 0.33
HALLMARK_HEDGEHOG_SIGNALING
p = 0.59
HALLMARK_HEME_METABOLISM
p = 0.4
HALLMARK_HYPOXIA
p = 0.7
HALLMARK_IL2_STAT5_SIGNALING
p = 0.0024
HALLMARK_IL6_JAK_STAT3_SIGNALING
p < 0.0001
HALLMARK_INFLAMMATORY_RESPONSE
p = 0.00012
HALLMARK_INTERFERON_ALPHA_RESPONSE
p < 0.0001
HALLMARK_INTERFERON_GAMMA_RESPONSE
p < 0.0001
HALLMARK_KRAS_SIGNALING_DN
p = 0.74
HALLMARK_KRAS_SIGNALING_UP
p = 0.0049
HALLMARK_MITOTIC_SPINDLE
p = 0.083
Survival probability
Time in Days

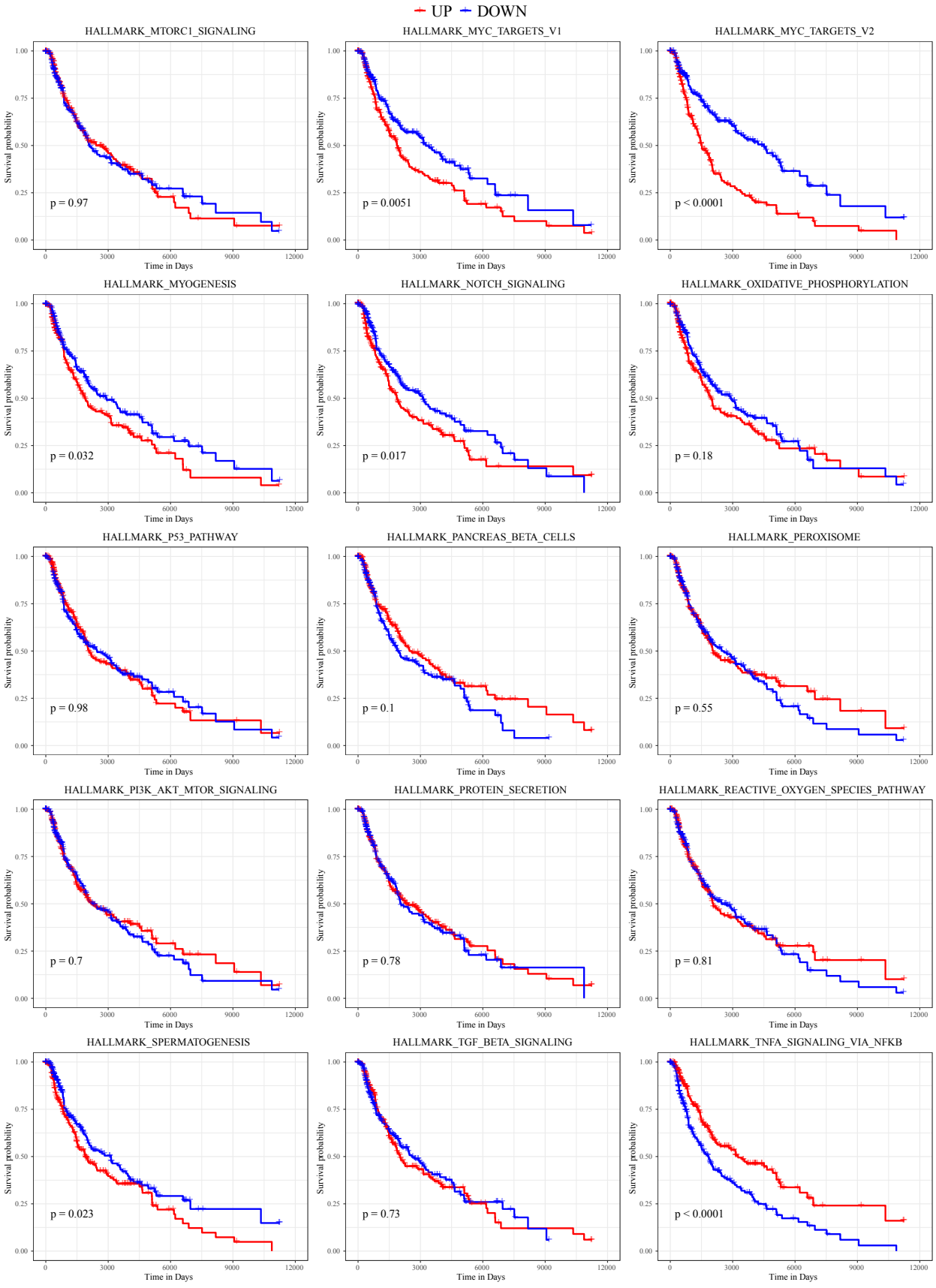
UP
DOWN
HALLMARK_MTORC1_SIGNALING
p = 0.97
HALLMARK_MYC_TARGETS_V1
p = 0.0051
HALLMARK_MYC_TARGETS_V2
p < 0.0001
HALLMARK_MYOGENESIS
p = 0.032
HALLMARK_NOTCH_SIGNALING
p = 0.017
HALLMARK_OXIDATIVE_PHOSPHORYLATION
p = 0.18
HALLMARK_P53_PATHWAY
p = 0.98
HALLMARK_PANCREAS_BETA_CELLS
p = 0.1
HALLMARK_PEROXISOME
p = 0.55
HALLMARK_PI3K_AKT_MTOR_SIGNALING
p = 0.7
HALLMARK_PROTEIN_SECRETION
p = 0.78
HALLMARK_REACTIVE_OXYGEN_SPECIES_PATHWAY
p = 0.81
HALLMARK_SPERMATOGENESIS
p = 0.023
HALLMARK_TGF_BETA_SIGNALING
p = 0.73
HALLMARK_TNFA_SIGNALING_VIA_NFKB
p < 0.0001
Survival probability
Time in Days

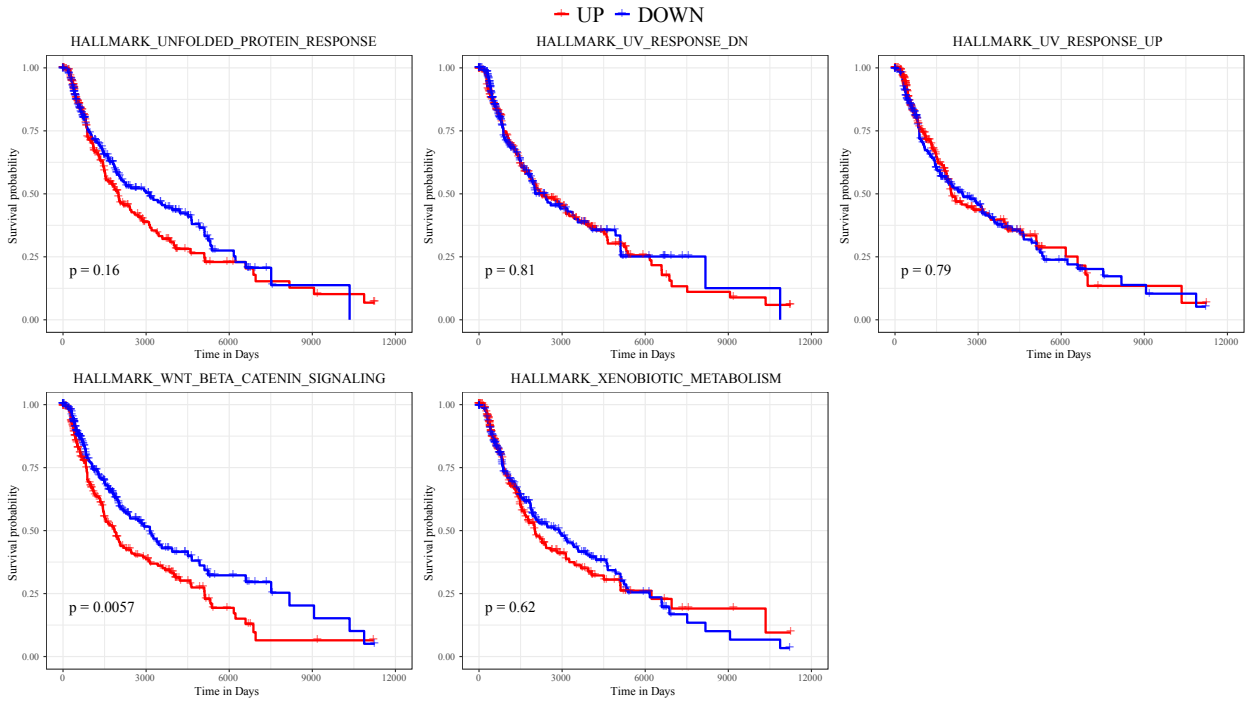

Figure 7.2 | Hallmark pathways activated by ACT + VacV correlate with better survival in SKCM patients

Bulk RNAseq data SKCM patients (n = 473) from TCGA was used to run GSVA to estimate patient gene enrichment scores for the Hallmark pathways from MSigDB. (A) Hierarchical clustering using pearson correlation for distance calculation was used to estimate the similarity in pathway expression among patients. (B) Univariate cox proportional hazard model was used to analyze the effect of each individual pathway on disease prognosis. (C) Patients were stratified based on the median scores for each pathway into High and low groups, and univariate overall survival analysis was performed and the resulting Kaplan-Meier plots are shown. Log-rank test was used for *P* value calculation.

Table 7.1 | Clusters of hallmark pathways resulting from hierarchical clustering analysis using pearson correlation to estimate the distances between individual hallmark pathways

Cluster 1	Cluster 2	Cluster 3	Cluster 4	Cluster 5	Cluster 6
HALLMARK_APOPTOSIS	HALLMARK_HYPOXIA	HALLMARK_ANGIOGENESIS	HALLMARK_ADIPOGENESIS	HALLMARK_PI3K_AKT_MTOR_SIGNALING	HALLMARK_UNFOLDED_PROTEIN_RESPONSE
HALLMARK_IL2_STAT5_SIGNALING	HALLMARK_ESTROGEN_RESPONSE_EARLY	HALLMARK_HEDGEHOG_SIGNALING	HALLMARK_FATTY_ACID_METABOLISM	HALLMARK_XENOBIOTIC_METABOLISM	HALLMARK_MYC_TARGETS_V2
HALLMARK_COMPLEMENT	HALLMARK_MYOGENESIS	HALLMARK_TGF_BETA_SIGNALING	HALLMARK_PEROXISOME	HALLMARK_ESTROGEN_RESPONSE_LATE	HALLMARK_MYC_TARGETS_V1
HALLMARK_INFLAMMATORY_RESPONSE	HALLMARK_P53_PATHWAY	HALLMARK_UV_RESPONSE_DN	HALLMARK_MTORC1_SIGNALING	HALLMARK_UV_RESPONSE_UP	HALLMARK_PROTEIN_SECRETION
HALLMARK_IL6_JAK_STAT3_SIGNALING	HALLMARK_COAGULATION	HALLMARK_NOTCH_SIGNALING	HALLMARK_GLYCOLYSIS	HALLMARK_REACTIVE_OXYGEN_SPECIES_PATHWAY	HALLMARK_MITOTIC_SPINDLE
HALLMARK_TNFA_SIGNALING_VIA_NFKB	HALLMARK_APICAL_SURFACE	HALLMARK_WNT_BETA_CATENIN_SIGNALING	HALLMARK_OXIDATIVE_PHOSPHORYLATION	HALLMARK_CHOLESTEROL_HOMEOSTASIS	HALLMARK_SPERMATOGENESIS
HALLMARK_KRAS_SIGNALING_UP	HALLMARK_KRAS_SIGNALING_DN	HALLMARK_ANDROGEN_RESPONSE	HALLMARK_DNA_REPAIR	HALLMARK_HEME_METABOLISM	HALLMARK_G2M_CHECKPOINT
HALLMARK_ALLOGRAFT_REJECTION	HALLMARK_APICAL_JUNCTION	HALLMARK_PANCREAS_BETA_CELLS		HALLMARK_BILE_ACID_METABOLISM	HALLMARK_E2F_TARGETS
HALLMARK_INTERFERON_GAMMA_RESPONSE	HALLMARK_EPITHELIAL_MESENCHYMAL_TRANSITION				
HALLMARK_INTERFERON_ALPHA_RESPONSE					

Table 7.2 | Hazard ratio (HR) associated with each hallmark pathway calculated using univariate cox proportional hazard model

Pathway	HR	*P* value
HALLMARK_ALLOGRAFT_REJECTION	0.1	2.3e-06
HALLMARK_COMPLEMENT	0.22	5.5e-05
HALLMARK_INTERFERON_GAMMA_RESPONSE	0.22	7e-07
HALLMARK_KRAS_SIGNALING_UP	0.22	3e-05
HALLMARK_IL2_STAT5_SIGNALING	0.27	0.00018
HALLMARK_INTERFERON_ALPHA_RESPONSE	0.27	1.8e-06
HALLMARK_APOPTOSIS	0.28	0.0041
HALLMARK_IL6_JAK_STAT3_SIGNALING	0.28	1.4e-06
HALLMARK_INFLAMMATORY_RESPONSE	0.3	4.2e-06
HALLMARK_TNFA_SIGNALING_VIA_NFKB	0.31	2e-04
HALLMARK_PANCREAS_BETA_CELLS	0.32	0.024
HALLMARK_BILE_ACID_METABOLISM	0.35	0.025
HALLMARK_ANDROGEN_RESPONSE	0.55	0.13
HALLMARK_COAGULATION	0.56	0.17
HALLMARK_PEROXISOME	0.66	0.4
HALLMARK_APICAL_SURFACE	0.71	0.39
HALLMARK_UV_RESPONSE_DN	0.71	0.33
HALLMARK_TGF_BETA_SIGNALING	0.79	0.49
HALLMARK_PROTEIN_SECRETION	0.82	0.48
HALLMARK_KRAS_SIGNALING_DN	0.89	0.86
HALLMARK_HYPOXIA	0.96	0.92
HALLMARK_PI3K_AKT_MTOR_SIGNALING	0.99	0.98
HALLMARK_EPITHELIAL_MESENCHYMAL_TRANSITION	1	0.95
HALLMARK_ANGIOGENESIS	1.1	0.72
HALLMARK_APICAL_JUNCTION	1.2	0.66
HALLMARK_HEDGEHOG_SIGNALING	1.2	0.57
HALLMARK_FATTY_ACID_METABOLISM	1.3	0.43
HALLMARK_MTORC1_SIGNALING	1.3	0.49
HALLMARK_REACTIVE_OXYGEN_SPECIES_PATHWAY	1.3	0.42
HALLMARK_CHOLESTEROL_HOMEOSTASIS	1.4	0.31
HALLMARK_HEME_METABOLISM	1.5	0.4

Table 7.2 | Hazard ratio (HR) associated with each hallmark pathway calculated using univariate cox proportional hazard model

Pathway	HR	*P* value
HALLMARK_E2F_TARGETS	1.6	0.014
HALLMARK_OXIDATIVE_PHOSPHORYLATION	1.6	0.054
HALLMARK_P53_PATHWAY	1.6	0.26
HALLMARK_G2M_CHECKPOINT	1.7	0.0075
HALLMARK_MYC_TARGETS_V1	1.7	0.029
HALLMARK_XENOBIOTIC_METABOLISM	1.7	0.24
HALLMARK_MITOTIC_SPINDLE	1.8	0.08
HALLMARK_UNFOLDED_PROTEIN_RESPONSE	1.8	0.12
HALLMARK_MYOGENESIS	1.9	0.1
HALLMARK_ADIPOGENESIS	2	0.05
HALLMARK_DNA_REPAIR	2	0.036
HALLMARK_MYC_TARGETS_V2	2.1	4.5e-05
HALLMARK_GLYCOLYSIS	2.4	0.027
HALLMARK_SPERMATOGENESIS	2.4	0.067
HALLMARK_UV_RESPONSE_UP	2.5	0.11
HALLMARK_ESTROGEN_RESPONSE_LATE	2.6	0.079
HALLMARK_NOTCH_SIGNALING	3.2	0.0011
HALLMARK_ESTROGEN_RESPONSE_EARLY	3.7	0.0051
HALLMARK_WNT_BETA_CATENIN_SIGNALING	4.1	0.00098

Alternatively, pathways associated with cell proliferation e.g. G2M checkpoint or cell metabolism e.g. Glycolysis had a HR > 1, suggesting a worse prognosis. Notably, the activation of DNA repair pathways was predictive of bad prognosis in SKCM patients. The HR ratios for each pathway are summarized in **table 7.2**. Lastly, we stratified the patients based on the median GSVA score for each pathway and performed a univariate survival analysis to analyze the effect of each pathway on the overall survival of patients **(Fig. 7.2 C)**. Kaplan-Meier survival curves were consistent with the results from the cox proportional hazard analysis, where pathways with HR < 1 were associated with a statistically significant improvement in the overall survival in patients with upregulation of such pathways. On the other hand, downregulation of pathways with a suggested bad prognosis (HR > 1) correlated with a statistically significant improvement of overall survival of patients. In conclusion, the molecular signature instilled in the TME by the ACT + VacV that is represented in the upregulation of inflammatory pathways and the downregulation of DNA repair pathways, cell metabolism, and cell replication is predictive of better survival in SKCM patients. This data makes a strong case for the impact that ACT + VacV treatment has on altering the TME on both cellular and molecular levels and shows that such changes are predictive of favorable responses in SKCMs and correlate with better overall survival of the patients.

Chapter 8 — Discussion

8.1. Studying the effect of the viral backbone on the Efficacy of ACT + OVV

Harnessing the power of immune system has revolutionized the way cancer patients are treated. The realization that immune evasion is amongst the hallmarks of cancer has led to considerable efforts to reverse the tumour-mediated immunosuppressive state and reinvigorate tumour immunity[3]. Here, we report a unique therapeutic platform that combines two of the most powerful tools in cancer immunotherapy. Our data illustrates the synergy and complementarity between ACT and OVV, where a small starting number of $CD8^+$ T cells can be expanded *in vivo* by the action of OVV leading to robust tumour control. The OVV-mediated *in vivo* expansion of the adoptively transferred $CD8^+$ T cells reduces the initial required number of $CD8^+$ T cells without compromising the therapeutic efficacy, which reduces both the cost and the duration of the *in vitro* culture of $CD8^+$ T cells. Additionally, OVVs induces the recruitment of tumour specific $CD8^+$ T cells to the TME leading to the "push and pull" effect. Moreover, unlike the standard practice in T cell-based therapies[292], our protocol does not require any preparative lymphodepletion. This helps further simplify the therapeutic protocol and protects the patients from any opportunistic infections that might arise as a result of the lymphopenic state. Furthermore, lymphodepletion preparative regimens and the subsequent IL-2 treatment following ACT infusion were reported to underlie the most common toxicities associated with ACT using tumour infiltrating lymphocytes (TILs)[293].

The pursuit to identify the viral backbone best suited for use as an OVV vector is a devious one. The Wan lab has previously shown the superiority of VSV as a booster OVV in the context of prime-boost regimens[187,188,236]. Recent work by Nguyen and Walsh to use VSV-based OVV in combination with ACT has uncovered two issues to be addressed. The first being that, in the B16gp33 model, despite the impressive complete tumour regression achieved following ACT + VSVgp33, tumour relapse occurs shortly after remission[241]. The second is that the strong induction of type I IFN caused by VSV contributes to autoimmune pathology as highlighted by Walsh in his studies using the RIP-gp model[239]. This has prompted us to continue our pursuit in

finding a viral backbone that capitalizes on the outcomes achieved by VSV and improves upon the issues previously described. Walsh *et al.* showed that the inherent ability of VacV to block type I IFN through the expression of various viral proteins e.g. B18, uncouples anti-tumour immunity and autoimmune toxicity. It then became apparent to us that the contrast in genomic composition between VSV, being a simple RNA virus with 5 genes, and VacV, being a complex DNA virus with more than 200 genes, is worthy of investigation. In this thesis I initially focused on studying how VSV and VacV compare in terms of their anti-tumour efficacy. By using the B16gp33 model, I observed that there was indeed an improvement in the overall survival of mice treated with ACT + VacVgp33 compared to those treated with ACT + VSVgp33 (**Fig. 3.3**). Nevertheless, tumour relapse following remission was still observed in most mice treated with either virus. This promoted us to investigate the effect of the OVV route of administration.

8.2. Evaluating the effect of OVV route of administration on the efficacy of ACT + OVV

The selection of the optimum route of delivering OVs is crucial to prevent treatment failure. Intratumoural delivery is the most commonly used route for OV delivery. It allows for the precise control of the viral concentration at the tumour site, bypasses the systemic virus neutralization and prevents its premature clearance[294,295]. IT delivery is better suited for surface tumours e.g., melanoma, but it can be challenging for deeper tumours e.g., glioblastoma. Additionally, tumours that have metastasized to multiple locations could be difficult to locally target. Intravenous delivery on the other hand, relies on the tropism of OVs to arrive at the tumour site and start replicating. It allows for viral distribution at any site and precludes the need for special interventional procedures associated with IT delivery[294]. Nevertheless, it is difficult to control the concentration of the virus arriving at the tumour site as many factors can systemically neutralize and/or clear the virus before arriving at the tumour site, introducing inconsistency in the therapeutic outcomes.

Here, we compared the use of IT and IV routes for delivering two OVVs of different families. Our results show that IT was the superior route of delivery for both viruses in terms of tumour control and overall survival of mice **(Fig. 3.5)**. Interestingly, despite the poor systemic expansion of $CD8^+$ T cells by VSVgp33 when delivered IT, it resulted in a trend of better overall survival compared to IV. When comparing VSVgp33 IT directly against VacVgp33 IT, we detected significantly less gp33 specific $CD8^+$ T cells in the circulation in case of the former. However, both viruses recruited equal numbers of P14 T cells to the TME **(Fig. 3.9)**. This could explain why VSVgp33 IT performed well in our model. It is worth mentioning that in case of IT delivery of VacVgp33, we were able to detect systemic expansion of gp33 specific $CD8^+$ T cells, which indicates the potential of P14 + VacVgp33 IT therapy to attack distant tumours and achieve abscopal effects. Further experimentation to fully study the extent of treating distant tumours using IT VacVgp33 is still required. Additionally, despite the faster kinetics of $CD8^+$ T cell proliferation in case of IV delivery of VacV **(Fig. 3.8)**, we did not detect a statistically significant difference in the numbers of $CD8^+$ T cells recruited to the TME between IT and IV delivered VacVgp33 **(Fig. 3.7)**.

We made use of the unique replication properties of VacV by utilizing two reporter systems, GFP which is expressed under the control of an early promoter, and LacZ which is expressed under the control a late promoter. This allowed us to resolve productive and non-productive viral infection at different sites following IT or IV injection. Our data show that IT injection indeed maximizes viral infection and replication in the tumour tissue. IV injection on the other hand results in less viral infection and replication in the TME. Additionally, despite detecting early viral gene expression in the spleens of mice treated with IV VacV, no viral replication was detected; indicating that the infection of secondary lymphoid organs is non-productive. Thus, we conclude that IT delivery of VacV enhances the viral mediated effects within the TME. Meanwhile, IV injection appears to have a more pronounced effect systemically and only limited infection of the tumour, which may blunt VacV interaction with tumour cells and its modulation of the TME. Altogether, our data point to an advantage of the IT route over the IV one in our model. In addition,

we demonstrate the flexibility of VacV, where it can achieve systemic $CD8^+$ T cell responses after being delivered IT. The significantly lower incidence of relapse associated with P14 + VacVgp33 in B16gp33 model intrigued us to dive more into studying the broader effects VacV has on the TME.

8.3. Evaluating the Contribution of Oncolysis in the Efficacy of ACT + OVV

The rebranding of oncolytic viral therapy (OVT) as a form of immunotherapy has indeed added an extra dimension to the functionality of OVs. As a result, the necessity of productive viral replication in the context of OVT has been recently questioned[296]. Our lab has always been interested in the immune stimulating properties of viruses. By engineering OVs to express tumour-associated antigens (TAAs), we pushed the OVs far into the immunotherapy territory early on. We have previously demonstrated that without the induction of tumour specific $CD8^+$ T cell responses, tumour control using OVT is minimal at best[187]. However, in the presence of sufficient anti-tumour immune responses, the question of how important viral oncolysis is remains open to answers. Immunotherapy is a double-edged sword, it can not only attack and eliminate tumour cells, but also, sculpt the tumour immunogenicity and give rise to immune escape variants. The solution to this problem is to deploy a multimodal therapeutic platform that works through non-redundant mechanisms, not allowing enough time or room for the tumour to evolve and suppress the immune attack. The work described here showcases the importance of viral replication in complementing immunotherapy and preventing cancer immune escape especially when dealing with aggressive and immunosuppressive tumours, such as B16 melanomas.

VacV is the prototype of the Poxviruses family that is highly noted for its role in eliminating smallpox[297]. Poxviruses are large, enveloped DNA viruses that replicate in the cytoplasm by forming cytoplasmic foci known as DNA factories[221]. VacV gene expression happens in three temporally consecutive stages: early, intermediate, and late[298]. The viral genome together with factors and enzymes required for the transcription of early genes are packaged in the core of

the infectious viral particles. DNA replication proteins, on the other hand, are not packaged in the virions but are translated from viral early mRNAs[297,299]. Upon viral entry into the host cell, the genome is released from the virion core and DNA replication machinery starts to replicate the viral genome within two hours of viral entry. The progeny DNA serves as the template for the expression of intermediate and late-stage genes that require the successive synthesis of intermediate and late transcription factors respectively[195,299,300]. This unique mechanism of regulation allows for the use of VacV for gene delivery without causing CPE in the infected cells. Tsung *et al.* showed that using psoralen to cross-link the VacV genome combined with long wavelength ultraviolet radiation (365 nm) exposure can cause double stranded breaks that renders viral infection abortive[283]. Since the expression of early genes is mediated by factors that are packaged in the virions, the unsuccessful genome replication does not affect the expression of such genes. However, the expression of intermediate and late genes would be affected by the lack of viral genome replication. It is worth mentioning that the PLWUV inactivation process is a random process and virions do not necessarily have the same degree of genome damage even when being exposed to the same inactivation conditions. The double-strand breaks will occur depending on the location of DNA cross-linking caused by psoralen. This implies that longer genes have higher chances of being affected than shorter ones. Thus, despite the independence of early genes on genome replication, individual genes might still be affected depending on the concentration of psoralen used and the duration of UV exposure. Using PLWUV-inactivation, we were able to transform VacV into a non-oncolytic vaccine, since the inactivation interferes with the ability of the virus to undergo successful replication while preserving its capacity to infect target cells and express early viral genes **(Fig. 4.2)**. We demonstrated that, despite the ability of the inactivated VacV to boost TAA-specific $CD8^+$ T cell responses to the same levels as the replicating virus, it was not able to prevent the immune escape and achieve sustained tumour regression **(Fig. 4.3)**. We also showed that increasing the potency of the treatment does not change the outcome **(Fig. 4.4)**. However, re-introducing an oncolytic component to the therapy, delivered through a separate viral vector, restored the capacity of the therapy to achieve durable

cure and prevent immune escape **(Fig. 4.5)**. While this work provides evidence that supports the importance of virus replication in achieving durable tumour control, more experimentation is required to arrive at the exact mechanism by which oncolysis prevents immune escape. Direct lysis of tumour cells is indeed one of the ways by which OVs can attack tumour cells in a non-antigen specific manner. Alternatively, oncolysis-mediated antigen spreading is another potential mechanism by which virus replication can indirectly lead to more sustained tumour control. Efforts by other lab members using different tumour models revealed that using ACT + OVV in the absence of endogenous lymphocytes - achieved by either using *in vivo* depletion antibodies or using genetically deficient NRG mice[301] leads to the development of immune escape variants[240]. It appears that recruiting and activating $CD8^+$ T cells specific for tumour antigens other than those initially targeted is imperative for completely eradicating the tumour and preventing immune escape. Interestingly, the dependence of therapy success on viral replication was model-specific. When treating MC38gp33 tumours, the of PLWUV inactivated VacV resulted in the same therapeutic outcome compared to the replicating VacV **(Fig. 4.10)**. It is well accepted in literature that MC38 is a highly immunogenic tumour model in which numerous neo-epitopes have been characterized[286]. The lack of discrepancy in the therapeutic outcome between the replicating and the inactivated virus in controlling MC38gp33 tumours can be interpreted in two different ways. On the one hand, MC38, being highly immunogenic, could be less sensitive to immunoediting. On the other hand, the $CD8^+$ T cell-mediated immune attack on the tumour might be enough to induce antigen spreading.

Our microarray data shows that the inactivation of VacV resulted in more DEGs relative to the replicating VacV when compared against the ACT control **(Fig. 4.8)**. However, we failed to detect a biologically significant number of DEGs when comparing the tumours treated with the replicating versus the inactivated VacV. On a pathway level, both the replicating and the inactivated VacV resulted in identical molecular signatures in the TME when compared to P14 controls. Instead, the magnitude of gene expression fold change or pathway enrichment score rather than the gene or pathway identity was the differentiating factor between VacV and UV-VacV

(Fig. 4.9). VacV is known to cause "host shutoff", which is a phenomenon describing the ability of viruses to profoundly suppress host protein synthesis while driving viral protein synthesis[302]. Shutoff by targeting host cell DNA synthesis, RNA production and processing, mRNA translation, and protein degradation have all been reported in the context of VacV infection [302]. The prevention of host mRNA synthesis protects the virus from the cellular anti-viral proteins and at the same time frees up the cellular translation machinery for viral mRNAs and allows for more viral protein synthesis. Moreover, VacV infection was shown to induce a global degradation of host and viral mRNA[303]. The shutoff of tumour cells resulting from replicating VacV treatment could explain the difference seen in the level of gene expression observed between the replicating and the inactivated virus. Additionally, since UV-VacV is only able to support one round of infection, viral gene expression is constrained to early gene expression and thus the immune modulatory effect associated with replicating VacV are absent and the gene expression signature in the tumour is overwhelmed by the immune attack of the tumour. Interestingly, the more inflammatory profile resulting from the inactivated virus did not help prevent tumour relapse. Nevertheless, we would like to point out that the microarray was based on RNA harvested from tumours at 48 h pvi. The persistence of inflammation within the TME at later time-points is yet to be evaluated. While Dai *et al.* had success with the heat-iMVA in treating B16F10 tumours, their treatment protocol involved repeated administration of the virus on weekly basis throughout the study[281]. Consistent with what we have observed, they reported that heat-iMVA was more inflammatory and resulted in the production of type I interferon, and proinflammatory cytokines and chemokines. Additionally, in the absence of $CD8^+$ T cells, the heat-iMVA had little to no effect on tumour growth, indicating that $CD8^+$ T cell attack on the tumour is indispensable for tumour control[281]. In conclusion, the work we presented here points to the importance of viral replication in complementing the immune attack on the tumour to achieve durable responses in our treatment model. This is especially true in immunosuppressive tumours that require non-redundant mechanisms to tackle the evolving nature of tumour cells. The PLWUV inactivation is an effective method to inactivate poxviruses while maintaining their early gene expression, $CD8^+$ T cell expansion capacity as well

as their inflammatory properties. Despite falling short compared to its replicating counterpart, we think PLWUV-inactivated VacV provides a very attractive platform that is worthy of further investigation since it provides a much safer alternative without many compromises that would be very desirable for clinical use.

8.4. Investigating the differential effects of VSV and VacV on altering the cellular and transcriptomic landscapes in the TME

We demonstrated that using IT delivery of OVVs leads to enhancement in the overall survival of mice treated with ACT + OVV. This points to the importance of having high local concentration of virus within the TME. Additionally, we established the importance of viral replication in the TME. Besides the enhanced oncolysis, we postulated that the local presence of higher concentrations of virions in the TME could lead to more prominent effect of virus mediated modulation, including inflammatory changes, within the TME. We first investigated the differential recruitment of different immune populations to the TME following ACT + VSV or VacV. NK cells were shown to play a role in the immune response against VacV[304]. Earlier studies pointed to the activation, proliferation, and accumulation of NK cells at the site of VacV infection[305,306]. Another innate immune population that was shown to play a role in the context of VacV infection is neutrophils[307]. Duffy *et al.* reported that neutrophils are able to transport viral antigens from the dermis to the bone marrow and generate virus specific $CD8^+$ T cell responses[308]. In another study, nuclear factor kappa B (NFκB) mediated release of proinflammatory cytokines and chemokines following VacV infection caused the recruitment of neutrophils to the infection site. Modified VacV vectors that lack viral proteins with NFκB inhibitor activity e.g., A52, K7 and B15, were shown to induce better recruitment of neutrophils to the infection site, where neutrophils acquire APC features and migrate to secondary lymphoid organs, engaging and activating antigen specific $CD8^+$ T cells[307]. These studies and others highlighting the roles of NK cells and neutrophils in responding to VacV infection prompted us to test whether the recruitment

of such cells to the TME would complement the function of $CD8^+$ T cells and prevent antigen-negative tumour relapse. Our data indeed showed the recruitment of both NK cells and neutrophils to the TME following P14 + VacVgp33 treatment. The difference in the normalized numbers was statistically significant compared to controls (**Fig. 3.9**). However, we did not detect a statistically significant difference between P14 + VacVgp33 and P14 + VSVgp33 treatments in the number of neutrophils recruited to the TME. Interestingly, P14 + VSVgp33 treatment recruited more NK cells to the TME compared to P14 + VacVgp33. Additionally, *in vivo* depletion of $NK1.1^+$ cells or $Ly6G^+$ myeloid cells had no effect on the efficacy of P14 + VacVgp33 treatment **(Fig. 3.10)**. These findings collectively demonstrate that neither NK cells nor neutrophils underlie the ability of VacVgp33 to achieve superior outcomes and prevent tumour relapse. $CD8^+$ T cells, on the other hand, are indispensable for the efficacy of the therapy as *in vivo* depletion of $CD8^+$ T cells abrogates tumour control.

The inability to identify distinct cellular populations that explain the underlying difference in the outcome between P14 + VSVgp33 and P14 + VacVgp33 pushed us to explore the molecular signature induced by each virus in the TME. We were interested to explore whether virus induced transcriptomic profiles might have an influence on the functionality of the tumour infiltrating leukocytes as well as the genomic stability of the tumour cells. Our microarray results indeed showed some similarities in the inflammatory profile of both viruses as 97 genes were found to be differentially expressed by both viruses when compared to the P14 control. Nevertheless, we observed significant differences in the molecular signature each virus elicits within the TME. We identified 223 DEGs between P14 + VacVgp33 and P14 + VSVgp33 treated tumours. For easier biological interpretability we examined the differences on pathway level using ORA and GSEA. We used the hallmark pathway database to get an understanding of the general trends in the data, and then we classified our analysis into four main themes comprising: immune pathways, metabolic pathways, cell cycle pathways and DNA repair pathways. In terms of immune pathways, it was evident that VacV was more inflammatory compared to VSV since the majority of inflammatory pathways analyzed were enriched in VacV treated tumour compared to the VSV treated ones.

One exception to this observation was the type I IFN, where the VSV treated tumours were found to be significantly enriched for type I IFN responses compared to the VacV treated ones (**Fig. 3.13**). These findings are in agreement with our previous work that demonstrated potent type I IFN induction 5 hours following VSV infection[239]. VacV on the other hand is reported to encode multiple factors that inhibit type I IFN production and function. For example, E3 is a multi-domain protein that interferes with the production of type I IFN. The C-terminal dsRNA-binding domain binds dsRNA and prevents the activation of dsRNA-binding pathogen recognition receptors (PRRs)[309]. E3 was also reported to bind poly (dA-dT) preventing its transcription into poly (A-U) RNA by RNA polymerase III, which in turn prevents the activation of retinoic acid-inducible gene I (RIG-I) and IFN type I production[310]. Another protein encoded by the VacV is the B18 protein which acts as a type I IFN-binding protein. It binds more specifically to IFNα both in solution and when associated with cell surface preventing IFN from binding to its receptor and inducing IFN-mediated antiviral state in the uninfected cells[311]. It is worth mentioning that VacV does indeed induce some components of type I IFN signaling, which was evident when compared to the controls. However, the effect was significantly tuned down relative to that seen in VSV treated tumours. Alternatively, our analysis revealed that P14 + VacVgp33 treatment caused a statistically significant enrichment of the TNFα signaling via NFκB pathway compared to P14 + VSVgp33 **(Fig 3.13)**. TNF signaling can have both proinflammatory and anti-inflammatory properties depending on where it is secreted from, the receptor it binds to, and the presence of other stimuli in the local environment[312]. It was shown to enhance TCR-dependent activation of $CD4^+$ and $CD8^+$ T cells by lowering the threshold level required for TCR activation[313], enhancing T cell proliferation, and increasing cytokine production[314]. These effects were shown to be mediated mainly by TNF receptor 2 (TNFR2). Moreover, TNF signaling through TNFR2 was reported to increase the expression of anti-apoptotic molecules such as Bcl-2, Bcl-xL, and survivin during the early phase of T cell activation[315]. Alternatively, TNF receptor 1 (TNFR1) was shown to mediate apoptotic death during clonal contraction[312,316]. In the context of regulatory T cells (T_{regs}), TNF was reported to downregulate their suppressive capacity[317,318] or to promote their proliferation and

accumulation in other instances[319]. These data suggest that, depending on the inflammatory factors present within the local milieu, TNF has the potential to tip the balance between effector T cells and T_{regs} in either direction. In the current work, we demonstrated that P14 + VacVgp33 treatment significantly downregulates the T_{regs} population in the spleens of treated mice **(Fig. 3.4)**. We did not analyze the levels of T_{regs} in the TME of B16gp33 tumours following P14 + VacVgp33 or P14 + VSVgp33 treatments. However, other members of the Wan lab have previously shown that depletion of T_{regs} in the context of P14 + VSVgp33 can lead to better outcomes and less incidence of tumour relapse (data not shown). It would be interesting to investigate whether VacV treatment leads to less T_{regs} in the TME and whether the reduced number and/or functionality of T_{regs} is mediated by the strong TNF signaling elicited by the VacV.

The shutdown of DNA repair pathways observed in case of P14 + VacVgp33 treatment is indeed an interesting finding. The viral oncolysis combined with the immune attack on the tumour leads to DNA damage, which in turn activates the DNA repair machinery. Kesavan and Walsh conducted a series of experiments to test whether DNA damage and subsequent repair mediates antigen gene loss causing the emergence of therapy resistant clones. They first showed that cells infected with either VSV or VacV experienced similar levels of double stranded breaks. They also showed that the NBS1 protein localizes in the cytoplasm rather than the nucleus in VacV-infected cells (**Fig. 3.14**). This could be attributed to the replication of VacV in the cytoplasm, where the virus hijacks the DNA repair machinery to secure the integrity of the viral genome in the new progeny. This entails the absence of functional DNA repair machinery from the nucleus which ultimately leads to less incidence of antigen loss and also drives the host cells towards apoptosis due to failure to repair the DNA damage. Next, they engineered a B16gp33 cell line where gp33 is linked to GFP, such that cells experiencing antigen loss can be detected as GFP^{-ve} cells. They observed that infecting such cells with VSV resulted in significantly higher numbers of GFP^{-ve} cells compared to those infected with VacV. Upon the addition of DNA repair inhibitors (Mirin and AZD7648) to VSV-infected cells, they observed a decrease in the number of antigen negative cells and an increase in the number of dead cells. Together, these results suggest that

the downregulation of DNA repair pathways represents another mechanism deployed by VacV to prevent antigen-loss-mediated tumour relapse.

8.5. Investigating the effects of cellular and molecular signatures observed in ACT + VacV treated tumours on the disease progression/outcome in human patients.

Having identified a series of pathways differentially regulated by P14 + VacVgp33 treatment compared to P14 + VSVgp33, we used computational approaches to extrapolate these findings on patient data to investigate the potential significance of such pathways on the prognosis of disease in patients with SKCM. Our analysis revealed that the upregulation of the inflammatory hallmark pathways is correlated with a statistically significant reduction in the hazard ratio, indicating a favorable disease prognosis. This was confirmed through analyzing the survival of patients with high or low expression of such pathways **(Fig. 3.16)**. Additionally, using *in silico* cytometry, we identified $CD8^+$ T cells and M1 macrophages to be key populations associated with better survival in SKCM patients **(Fig. 3.15)**. We indeed demonstrated that an influx of tumour specific $CD8^+$ T cells into the TME can be achieved within days after ACT + OVV treatment, regardless of the viral backbone used. We did not analyze the frequency or functionality of M1 macrophages in the TME. However, earlier work from our lab demonstrated that the addition of a histone deacetylase (HDAC) inhibitor, MS275, to ACT + VSVgp33 treatment resulted in the polarization of the macrophage population within the TME towards M1 phenotype which eliminated tumour escape variants and led to durable tumour control[241]. Interestingly, patients with high M1 macrophage infiltration in the TME had negative enrichment for DNA repair pathways compared to those with low M1 macrophage infiltration. DNA repair inhibitors have been used as monotherapies or in combination with chemotherapy to treat different malignancies[320]. Many chemotherapeutics were shown to cause DNA damage of tumour cells. Cells that are able to repair the damage survive such therapies and evolve to develop therapy resistance. Thus, adding

DNA repair inhibitors to the therapeutic protocol drives tumour cells towards apoptosis and prevents therapy resistance. In the context of immunotherapy, double strand breaks in the genome occurring in proximity of an antigen gene may result in the loss of a neoantigen as the non-mutated allele on the sister chromatid is used as a template for repair. In the absence of repair, the cell suffering the double strand break will be eliminated via apoptosis. This implies that an intrinsic synergy exists between DNA repair inhibition and T cell centric therapy as the cells will either die by T cell killing or genotoxic-stress induced apoptosis. Thus, DNA repair inhibition provides a global benefit in tumour immunotherapy. Our data suggests that therapeutic modalities that incorporate a functional blockade/inhibition of DNA repair would extend this benefit to a broader range of tumours. Allowing tumours that have retained DNA repair function to experience the same benefit as those that have lost it. Taken together, these findings demonstrate that the transcriptomic reprogramming of the TME elicited by ACT + VacV treatment can potentially lead to better treatment outcomes and can sensitize tumours for other platforms of immunotherapies like immune checkpoint blockade (ICB).

In conclusion, we extensively investigated the use of VSV- and VacV-based OVVs in combination with ACT and learned that VacV is superior in achieving durable tumour control. We were not able to identify differences in the immune cells infiltrating the TME following P14 + VSVgp33 or P14 + VacVgp33 treatment. However, on a molecular level, we found that VacV causes more drastic changes, activating more inflammatory pathways while shutting down cellular metabolism and cell cycle pathways. In addition, the inhibition of DNA repair pathways is crucial to prevent antigen loss and drive the cells towards apoptosis making VacV a dynamic multimodal OVV backbone. Importantly, the pathway signature induced by P14 + VacVgp33 correlates with positive prognosis and better overall survival in SKCM patients. Moreover, in this work, we provided a framework for analysis of microarray data, and patient RNAseq data which could be very easily extended to other in-house generated data or public datasets of relevance to fellow scientists. We acknowledge that the microarray technology used in this thesis, while powerful in identifying patterns in the data, lacks the granularity provided by the single

cell technologies. For instance, while we detected the enrichment and downregulation of several pathways, such findings are based on the average signal coming from the entire tumour RNA. It's not technically possible to resolve such signals or identify which cells are responsible for them in the TME in our current data set. Additionally, our cellular studies aimed to identify and quantify the different cellular populations in the TME. Nevertheless, the fitness and functionality of such cells were not assessed. More recent technologies like single cell RNA sequencing (scRNAseq) have allowed an unprecedented level of detail when performing transcriptomic analyses. A natural progression to the work done in this thesis is to make use of such technologies and dive deeper in the TME and study the heterogeneity in cell states of the relevant populations. For example, we demonstrated that $CD8^+$ T cells were indispensable for the success of ACT + OVV therapy and showed that both VSV and VacV recruit similar levels of antigen specific $CD8^+$ T cells to the TME. However, we did not investigate the $CD8^+$ T cell states, functional capacity, or the transcriptomic signatures of the T cells in both conditions. Additionally, TCR sequencing can shed light on the diversity of $CD8^+$ T cell clones present within the TME beside gp33-specific cells. Going a step further, using technologies that provide spatial information alongside the gene expression e.g. MERfish, will be of extreme relevance when studying the composition of TME. We indeed tried using immunohistochemistry to stain B16gp33 tumours following ACT + OVV treatment. Unfortunately, we ran into issues of background noise and unspecific antibody binding. This is due to the presence of pigment produced by tumour and cell debris as a result of oncolysis especially when using the IT route to deliver OVVs.

8.6. Concluding Remarks

This thesis focused on characterizing the ACT + OVV therapeutic protocol. I extended upon the previous efforts from members of the Wan lab and investigated the use of a VacV based OVV in combination with ACT to treat B16 tumours. In the work presented throughout chapters 3 - 7, we can appreciate that ACT + OVV represents a unique immunotherapeutic platform with

multimodal mechanisms of action. In our protocol, ACT is performed in the absence of preparative lymphodepletion and without the need for subsequent IL-2 injections. OVVs expand and recruit the transferred T cells and other immune cells to the TME by reprogramming the TME. Additionally, mechanisms such as vascular shutdown have been also reported in the context of OVs but haven't been addressed here. Our efforts in comparing the use of VacV vs. VSV in combination with ACT shed light on additional changes induced by VacV in the TME. Besides a more diverse inflammatory profile, metabolic shutdown, cell cycle arrest and the inhibition of DNA repair processes were observed in VacV treated tumours. In collaboration with Kesavan and Walsh, we unveiled the importance of inhibiting DNA repair in preventing antigen loss and immune escape. Additionally, we demonstrated the importance of viral replication in complementing the immune attack on the tumours following ACT + VacV therapy. While this was model specific and not every tumour would benefit from oncolysis, it remains available in the diverse arsenal of tools that VacV encompasses. We think that VacV is a great all-around platform that excels as an oncolytic virus, a gene delivery system, and a vaccine that stimulates and engages the host immune system.

Bibliography

1 Brenner, D. R. *et al.* Projected estimates of cancer in Canada in 2020. CMAJ 192, E199-E205, doi:10.1503/cmaj.191292 (2020).

2 Hanahan, D. & Weinberg, R. A. The hallmarks of cancer. Cell 100, 57-70, doi:10.1016/s0092-8674(00)81683-9 (2000).

3 Hanahan, D. & Weinberg, R. A. Hallmarks of cancer: the next generation. Cell 144, 646-674, doi:10.1016/j.cell.2011.02.013 (2011).

4 Denton, A. E., Roberts, E. W. & Fearon, D. T. Stromal Cells in the Tumour Microenvironment. Adv Exp Med Biol 1060, 99-114, doi:10.1007/978-3-319-78127-3_6 (2018).

5 Li, T. *et al.* Hepatocellular carcinoma-associated fibroblasts trigger NK cell dysfunction via PGE2 and IDO. Cancer Lett 318, 154-161, doi:10.1016/j.canlet.2011.12.020 (2012).

6 Uyttenhove, C. *et al.* Evidence for a tumoural immune resistance mechanism based on tryptophan degradation by indoleamine 2,3-dioxygenase. Nat Med 9, 1269-1274, doi:10.1038/nm934 (2003).

7 Naito, Y. *et al.* CD8+ T cells infiltrated within cancer cell nests as a prognostic factor in human colorectal cancer. Cancer Res 58, 3491-3494 (1998).

8 Zhang, L. *et al.* Intratumoural T cells, recurrence, and survival in epithelial ovarian cancer. N Engl J Med 348, 203-213, doi:10.1056/NEJMoa020177 (2003).

9 Waldman, A. D., Fritz, J. M. & Lenardo, M. J. A guide to cancer immunotherapy: from T cell basic science to clinical practice. Nat Rev Immunol 20, 651-668, doi:10.1038/s41577-020-0306-5 (2020).

10 Decker, W. K. & Safdar, A. Bioimmunoadjuvants for the treatment of neoplastic and infectious disease: Coley's legacy revisited. Cytokine Growth Factor Rev 20, 271-281, doi:10.1016/j.cytogfr.2009.07.004 (2009).

11 Starnes, C. O. Coley's toxins in perspective. Nature 357, 11-12, doi:10.1038/357011a0 (1992).

12 Burnet, F. M. The concept of immunological surveillance. Prog Exp Tumour Res 13, 1-27, doi:10.1159/000386035 (1970).

13 Shankaran, V. *et al.* IFNgamma and lymphocytes prevent primary tumour development

and shape tumour immunogenicity. Nature 410, 1107-1111, doi:10.1038/35074122 (2001).

14 Schreiber, R. D., Old, L. J. & Smyth, M. J. Cancer immunoediting: integrating immunity's roles in cancer suppression and promotion. Science 331, 1565-1570, doi:10.1126/science.1203486 (2011).

15 Vesely, M. D., Kershaw, M. H., Schreiber, R. D. & Smyth, M. J. Natural innate and adaptive immunity to cancer. Annu Rev Immunol 29, 235-271, doi:10.1146/annurev-immunol-031210-101324 (2011).

16 Mittal, D., Gubin, M. M., Schreiber, R. D. & Smyth, M. J. New insights into cancer immunoediting and its three component phases--elimination, equilibrium and escape. Curr Opin Immunol 27, 16-25, doi:10.1016/j.coi.2014.01.004 (2014).

17 Efremova, M. *et al.* Targeting immune checkpoints potentiates immunoediting and changes the dynamics of tumour evolution. Nat Commun 9, 32, doi:10.1038/s41467-017-02424-0 (2018).

18 O'Donnell, J. S., Teng, M. W. L. & Smyth, M. J. Cancer immunoediting and resistance to T cell-based immunotherapy. Nat Rev Clin Oncol 16, 151-167, doi:10.1038/s41571-018-0142-8 (2019).

19 Sigal, L. J. in Encyclopedia of Immunobiology (ed Michael J. H. Ratcliffe) 286-290 (Academic Press, 2016).

20 Chaplin, D. D. Overview of the immune response. J Allergy Clin Immunol 125, S3-S23, doi:10.1016/j.jaci.2009.12.980 (2010).

21 Acuto, O. & Michel, F. CD28-mediated co-stimulation: a quantitative support for TCR signalling. Nature Reviews Immunology 3, 939-951 (2003).

22 Curtsinger, J. M., Johnson, C. M. & Mescher, M. F. CD8 T cell clonal expansion and development of effector function require prolonged exposure to antigen, costimulation, and signal 3 cytokine. The Journal of Immunology 171, 5165-5171 (2003).

23 Curtsinger, J. M., Valenzuela, J. O., Agarwal, P., Lins, D. & Mescher, M. F. Cutting edge: type I IFNs provide a third signal to CD8 T cells to stimulate clonal expansion and differentiation. The Journal of Immunology 174, 4465-4469 (2005).

24 Fife, B. T. & Bluestone, J. A. Control of peripheral T-cell tolerance and autoimmunity

via the CTLA-4 and PD-1 pathways. Immunol Rev 224, 166-182, doi:10.1111/j.1600-065X.2008.00662.x (2008).

25 Brunet, J.-F. *et al.* A new member of the immunoglobulin superfamily—CTLA-4. Nature 328, 267-270 (1987).

26 Dariavach, P., Mattéi, M. G., Golstein, P. & Lefranc, M. P. Human Ig superfamily CTLA□4 gene: chromosomal localization and identity of protein sequence between murine and human CTLA□4 cytoplasmic domains. European journal of immunology 18, 1901-1905 (1988).

27 Linsley, P. S. *et al.* Human B7-1 (CD80) and B7-2 (CD86) bind with similar avidities but distinct kinetics to CD28 and CTLA-4 receptors. Immunity 1, 793-801 (1994).

28 Linsley, P. S. *et al.* CTLA-4 is a second receptor for the B cell activation antigen B7. The Journal of experimental medicine 174, 561-569 (1991).

29 Walunas, T. L. *et al.* CTLA-4 can function as a negative regulator of T cell activation. Immunity 1, 405-413 (1994).

30 Intlekofer, A. M. & Thompson, C. B. At the bench: preclinical rationale for CTLA□4 and PD□1 blockade as cancer immunotherapy. Journal of leukocyte biology 94, 25-39 (2013).

31 Schneider, H. *et al.* Reversal of the TCR stop signal by CTLA-4. science 313, 1972-1975 (2006).

32 Krummel, M. F. & Allison, J. P. CD28 and CTLA-4 have opposing effects on the response of T cells to stimulation. The Journal of experimental medicine 182, 459-465 (1995).

33 Qureshi, O. S. *et al.* Trans-endocytosis of CD80 and CD86: a molecular basis for the cell-extrinsic function of CTLA-4. Science 332, 600-603 (2011).

34 Takahashi, T. *et al.* Immunologic self-tolerance maintained by CD25+ CD4+ regulatory T cells constitutively expressing cytotoxic T lymphocyte–associated antigen 4. The Journal of experimental medicine 192, 303-310 (2000).

35 Leach, D. R., Krummel, M. F. & Allison, J. P. Enhancement of antitumour immunity by CTLA-4 blockade. Science 271, 1734-1736 (1996).

36 Fecci, P. E. *et al.* Systemic CTLA-4 blockade ameliorates glioma-induced changes to the CD4+ T cell compartment without affecting regulatory T-cell function. Clinical cancer research 13, 2158-2167 (2007).

37 Mangsbo, S. M. *et al.* Enhanced tumour eradication by combining CTLA-4 or PD-1 blockade with CpG therapy. Journal of immunotherapy 33, 225-235 (2010).

38 Yang, Y.-F. *et al.* Enhanced induction of antitumour T-cell responses by cytotoxic T lymphocyte-associated molecule-4 blockade: the effect is manifested only at the restricted tumour-bearing stages. Cancer research 57, 4036-4041 (1997).

39 Van Elsas, A., Hurwitz, A. A. & Allison, J. P. Combination immunotherapy of B16 melanoma using anti–cytotoxic T lymphocyte–associated antigen 4 (CTLA-4) and granulocyte/macrophage colony-stimulating factor (GM-CSF)-producing vaccines induces rejection of subcutaneous and metastatic tumours accompanied by autoimmune depigmentation. The Journal of experimental medicine 190, 355-366 (1999).

40 Hodi, F. S. *et al.* Improved survival with ipilimumab in patients with metastatic melanoma. New England Journal of Medicine 363, 711-723 (2010).

41 Schadendorf, D. *et al.* Pooled analysis of long-term survival data from phase II and phase III trials of ipilimumab in unresectable or metastatic melanoma. Journal of clinical oncology 33, 1889 (2015).

42 Kwon, E. D. *et al.* Ipilimumab versus placebo after radiotherapy in patients with metastatic castration-resistant prostate cancer that had progressed after docetaxel chemotherapy (CA184-043): a multicentre, randomised, double-blind, phase 3 trial. The lancet oncology 15, 700-712 (2014).

43 Reck, M. *et al.* Ipilimumab in combination with paclitaxel and carboplatin as first-line therapy in extensive-disease-small-cell lung cancer: results from a randomized, double-blind, multicenter phase 2 trial. Annals of Oncology 24, 75-83 (2013).

44 Lynch, T. J. *et al.* Ipilimumab in combination with paclitaxel and carboplatin as first-line treatment in stage IIIB/IV non–small-cell lung cancer: results from a randomized, double-blind, multicenter phase II study. Journal of clinical oncology 30, 2046-2054 (2012).

45 Yang, J. C. *et al.* Ipilimumab (anti-CTLA4 antibody) causes regression of metastatic renal cell cancer associated with enteritis and hypophysitis. Journal of immunotherapy (Hagerstown, Md.: 1997) 30, 825 (2007).

46 van Rooij, N. *et al.* Tumour exome analysis reveals neoantigen-specific T-cell reactivity

in an ipilimumab-responsive melanoma. Journal of clinical oncology: official journal of the American Society of Clinical Oncology 31 (2013).

47 Snyder, A. *et al.* Genetic basis for clinical response to CTLA-4 blockade in melanoma. New England Journal of Medicine 371, 2189-2199 (2014).

48 Peggs, K. S., Quezada, S. A., Chambers, C. A., Korman, A. J. & Allison, J. P. Blockade of CTLA-4 on both effector and regulatory T cell compartments contributes to the antitumour activity of anti–CTLA-4 antibodies. Journal of Experimental Medicine 206, 1717-1725 (2009).

49 Sharma, N., Vacher, J. & Allison, J. P. TLR1/2 ligand enhances antitumour efficacy of CTLA-4 blockade by increasing intratumoural Treg depletion. Proceedings of the National Academy of Sciences 116, 10453-10462 (2019).

50 Baksh, K. & Weber, J. in Seminars in oncology. 363-377 (Elsevier).

51 Nishimura, H., Minato, N., Nakano, T. & Honjo, T. Immunological studies on PD-1 deficient mice: implication of PD-1 as a negative regulator for B cell responses. International immunology 10, 1563-1572 (1998).

52 Keir, M. E., Butte, M. J., Freeman, G. J. & Sharpe, A. H. PD-1 and its ligands in tolerance and immunity. Annu. Rev. Immunol. 26, 677-704 (2008).

53 Freeman, G. J. *et al.* Engagement of the PD-1 immunoinhibitory receptor by a novel B7 family member leads to negative regulation of lymphocyte activation. The Journal of experimental medicine 192, 1027-1034 (2000).

54 Barber, D. L. *et al.* Restoring function in exhausted CD8 T cells during chronic viral infection. Nature 439, 682-687 (2006).

55 Wei, S. C. *et al.* Distinct cellular mechanisms underlie anti-CTLA-4 and anti-PD-1 checkpoint blockade. Cell 170, 1120-1133. e1117 (2017).

56 Hirano, F. *et al.* Blockade of B7-H1 and PD-1 by monoclonal antibodies potentiates cancer therapeutic immunity. Cancer research 65, 1089-1096 (2005).

57 Iwai, Y. *et al.* Involvement of PD-L1 on tumour cells in the escape from host immune system and tumour immunotherapy by PD-L1 blockade. Proceedings of the National Academy of Sciences 99, 12293-12297 (2002).

58 Strome, S. E. *et al.* B7-H1 blockade augments adoptive T-cell immunotherapy for

squamous cell carcinoma. Cancer research 63, 6501-6505 (2003).

59 Hamanishi, J. *et al.* Programmed cell death 1 ligand 1 and tumour-infiltrating CD8+ T lymphocytes are prognostic factors of human ovarian cancer. Proceedings of the National Academy of Sciences 104, 3360-3365 (2007).

60 Thompson, R. H. *et al.* Tumour B7-H1 is associated with poor prognosis in renal cell carcinoma patients with long-term follow-up. Cancer research 66, 3381-3385 (2006).

61 Thompson, R. H. *et al.* PD-1 is expressed by tumour-infiltrating immune cells and is associated with poor outcome for patients with renal cell carcinoma. Clinical cancer research 13, 1757-1761 (2007).

62 Hargadon, K. M., Johnson, C. E. & Williams, C. J. Immune checkpoint blockade therapy for cancer: an overview of FDA-approved immune checkpoint inhibitors. International immunopharmacology 62, 29-39 (2018).

63 Brahmer, J. R. *et al.* Phase I study of single-agent anti–programmed death-1 (MDX-1106) in refractory solid tumours: safety, clinical activity, pharmacodynamics, and immunologic correlates. Journal of clinical oncology 28, 3167 (2010).

64 Gong, J., Chehrazi-Raffle, A., Reddi, S. & Salgia, R. Development of PD-1 and PD-L1 inhibitors as a form of cancer immunotherapy: a comprehensive review of registration trials and future considerations. Journal for immunotherapy of cancer 6, 1-18 (2018).

65 Robert, C. *et al.* Anti-programmed-death-receptor-1 treatment with pembrolizumab in ipilimumab-refractory advanced melanoma: a randomised dose-comparison cohort of a phase 1 trial. The Lancet 384, 1109-1117 (2014).

66 Weber, J. S. *et al.* Nivolumab versus chemotherapy in patients with advanced melanoma who progressed after anti-CTLA-4 treatment (CheckMate 037): a randomised, controlled, open-label, phase 3 trial. The lancet oncology 16, 375-384 (2015).

67 Herbst, R. S. *et al.* Pembrolizumab versus docetaxel for previously treated, PD-L1-positive, advanced non-small-cell lung cancer (KEYNOTE-010): a randomised controlled trial. The Lancet 387, 1540-1550 (2016).

68 Reck, M. *et al.* Pembrolizumab versus chemotherapy for PD-L1–positive non–small-cell lung cancer. N engl J med 375, 1823-1833 (2016).

69 Ferris, R. L. *et al.* Nivolumab for recurrent squamous-cell carcinoma of the head and neck. N Engl J Med 375, 1856-1867 (2016).

70 Cohen, E. E. *et al.* Pembrolizumab versus methotrexate, docetaxel, or cetuximab for recurrent or metastatic head-and-neck squamous cell carcinoma (KEYNOTE-040): a randomised, open-label, phase 3 study. The Lancet 393, 156-167 (2019).

71 Bellmunt, J. *et al.* Pembrolizumab as second-line therapy for advanced urothelial carcinoma. New England Journal of Medicine 376, 1015-1026 (2017).

72 Sharma, P. *et al.* Nivolumab in metastatic urothelial carcinoma after platinum therapy (CheckMate 275): a multicentre, single-arm, phase 2 trial. The lancet oncology 18, 312-322 (2017).

73 Moskowitz, C. H. *et al.* Pembrolizumab in relapsed/refractory classical Hodgkin lymphoma: primary end point analysis of the phase 2 Keynote-087 study. Blood 128, 1107 (2016).

74 Ansell, S. M. *et al.* PD-1 blockade with nivolumab in relapsed or refractory Hodgkin's lymphoma. New England Journal of Medicine 372, 311-319 (2015).

75 Rosenberg, J. E. *et al.* Atezolizumab in patients with locally advanced and metastatic urothelial carcinoma who have progressed following treatment with platinum-based chemotherapy: a single-arm, multicentre, phase 2 trial. The Lancet 387, 1909-1920 (2016).

76 Powles, T. *et al.* Atezolizumab versus chemotherapy in patients with platinum-treated locally advanced or metastatic urothelial carcinoma (IMvigor211): a multicentre, open-label, phase 3 randomised controlled trial. The Lancet 391, 748-757 (2018).

77 Rittmeyer, A. *et al.* Atezolizumab versus docetaxel in patients with previously treated non-small-cell lung cancer (OAK): a phase 3, open-label, multicentre randomised controlled trial. The Lancet 389, 255-265 (2017).

78 Schmid, P. *et al.* Atezolizumab and nab-paclitaxel in advanced triple-negative breast cancer. New England Journal of Medicine 379, 2108-2121 (2018).

79 Horn, L. *et al.* First-line atezolizumab plus chemotherapy in extensive-stage small-cell lung cancer. New England Journal of Medicine 379, 2220-2229 (2018).

80 Kaufman, H. L. *et al.* Avelumab in patients with chemotherapy-refractory metastatic Merkel cell carcinoma: a multicentre, single-group, open-label, phase 2 trial. The lancet oncology

17, 1374-1385 (2016).

81 Patel, M. R. *et al.* Avelumab in metastatic urothelial carcinoma after platinum failure (JAVELIN Solid Tumour): pooled results from two expansion cohorts of an open-label, phase 1 trial. The Lancet Oncology 19, 51-64 (2018).

82 Powles, T. *et al.* Efficacy and safety of durvalumab in locally advanced or metastatic urothelial carcinoma: updated results from a phase 1/2 open-label study. JAMA oncology 3, e172411-e172411 (2017).

83 Motzer, R. J. *et al.* Avelumab plus axitinib versus sunitinib for advanced renal-cell carcinoma. New England Journal of Medicine 380, 1103-1115 (2019).

84 Antonia, S. J. *et al.* Durvalumab after chemoradiotherapy in stage III non–small-cell lung cancer. New England Journal of Medicine 377, 1919-1929 (2017).

85 Kumar, V. *et al.* Current diagnosis and management of immune related adverse events (irAEs) induced by immune checkpoint inhibitor therapy. Frontiers in pharmacology 8, 49 (2017).

86 Postow, M. A., Sidlow, R. & Hellmann, M. D. Immune-related adverse events associated with immune checkpoint blockade. New England Journal of Medicine 378, 158-168 (2018).

87 Nishijima, T. F., Shachar, S. S., Nyrop, K. A. & Muss, H. B. Safety and tolerability of PD□1/PD□L1 inhibitors compared with chemotherapy in patients with advanced cancer: a meta□analysis. The oncologist 22, 470-479 (2017).

88 Jacquelot, N. *et al.* Predictors of responses to immune checkpoint blockade in advanced melanoma. Nature Communications 8, 592, doi:10.1038/s41467-017-00608-2 (2017).

89 Loo, K., Smithy, J. W., Postow, M. A. & Betof Warner, A. Factors Determining Long-Term Antitumour Responses to Immune Checkpoint Blockade Therapy in Melanoma. Frontiers in Immunology 12, doi:10.3389/fimmu.2021.810388 (2022).

90 Roelofsen, L. M., Kaptein, P. & Thommen, D. S. Multimodal predictors for precision immunotherapy. Immuno-Oncology and Technology 14, 100071, doi:https://doi.org/10.1016/j.iotech.2022.100071 (2022).

91 Southam, C. M., Brunschwig, A., Levin, A. G. & Dizon, Q. S. Effect of leukocytes on transplantability of human cancer. Cancer 19, 1743-1753, doi:10.1002/1097-0142(196611)19:11<1743::aid-cncr2820191143>3.0.co;2-u (1966).

92 Weiden, P. L. *et al.* Antileukemic effect of graft-versus-host disease in human recipients of allogeneic-marrow grafts. N Engl J Med 300, 1068-1073, doi:10.1056/NEJM197905103001902 (1979).

93 Rosenberg, S. A. *et al.* Use of tumour-infiltrating lymphocytes and interleukin-2 in the immunotherapy of patients with metastatic melanoma. A preliminary report. N Engl J Med 319, 1676-1680, doi:10.1056/NEJM198812223192527 (1988).

94 Rosenberg, S. A. *et al.* Treatment of patients with metastatic melanoma with autologous tumour-infiltrating lymphocytes and interleukin 2. J Natl Cancer Inst 86, 1159-1166, doi:10.1093/jnci/86.15.1159 (1994).

95 Rosenberg, S. A. *et al.* Durable complete responses in heavily pretreated patients with metastatic melanoma using T-cell transfer immunotherapy. Clin Cancer Res 17, 4550-4557, doi:10.1158/1078-0432.CCR-11-0116 (2011).

96 Restifo, N. P., Dudley, M. E. & Rosenberg, S. A. Adoptive immunotherapy for cancer: harnessing the T cell response. Nat Rev Immunol 12, 269-281, doi:10.1038/nri3191 (2012).

97 Bronte, V. *et al.* Identification of a CD11b(+)/Gr-1(+)/CD31(+) myeloid progenitor capable of activating or suppressing CD8(+) T cells. Blood 96, 3838-3846 (2000).

98 Seung, L. P., Rowley, D. A., Dubey, P. & Schreiber, H. Synergy between T-cell immunity and inhibition of paracrine stimulation causes tumour rejection. Proc Natl Acad Sci U S A 92, 6254-6258 (1995).

99 Gattinoni, L. *et al.* Removal of homeostatic cytokine sinks by lymphodepletion enhances the efficacy of adoptively transferred tumour-specific CD8+ T cells. J Exp Med 202, 907-912, doi:10.1084/jem.20050732 (2005).

100 Paulos, C. M. *et al.* Microbial translocation augments the function of adoptively transferred self/tumour-specific CD8+ T cells via TLR4 signaling. J Clin Invest 117, 2197-2204, doi:10.1172/JCI32205 (2007).

101 Cameron, R. B., Spiess, P. J. & Rosenberg, S. A. Synergistic antitumour activity of tumour-infiltrating lymphocytes, interleukin 2, and local tumour irradiation. Studies on the mechanism of action. J Exp Med 171, 249-263 (1990).

102 Cheever, M. A., Greenberg, P. D., Fefer, A. & Gillis, S. Augmentation of the anti-tumour

therapeutic efficacy of long-term cultured T lymphocytes by in vivo administration of purified interleukin 2. J Exp Med 155, 968-980 (1982).

103 Rosenberg, S. A. Cell transfer immunotherapy for metastatic solid cancer--what clinicians need to know. Nat Rev Clin Oncol 8, 577-585, doi:10.1038/nrclinonc.2011.116 (2011).

104 Morgan, R. A., Dudley, M. E. & Rosenberg, S. A. Adoptive cell therapy: genetic modification to redirect effector cell specificity. Cancer J 16, 336-341, doi:10.1097/PPO.0b013e3181eb3879 (2010).

105 Chinnasamy, N. *et al.* A TCR targeting the HLA-A*0201-restricted epitope of MAGE-A3 recognizes multiple epitopes of the MAGE-A antigen superfamily in several types of cancer. J Immunol 186, 685-696, doi:10.4049/jimmunol.1001775 (2011).

106 Morgan, R. A. *et al.* Cancer regression in patients after transfer of genetically engineered lymphocytes. Science 314, 126-129, doi:10.1126/science.1129003 (2006).

107 Liu, K. & Rosenberg, S. A. Transduction of an IL-2 gene into human melanoma-reactive lymphocytes results in their continued growth in the absence of exogenous IL-2 and maintenance of specific antitumour activity. J Immunol 167, 6356-6365, doi:10.4049/jimmunol.167.11.6356 (2001).

108 Hsu, C. *et al.* Cytokine-independent growth and clonal expansion of a primary human CD8+ T-cell clone following retroviral transduction with the IL-15 gene. Blood 109, 5168-5177, doi:10.1182/blood-2006-06-029173 (2007).

109 Bendle, G. M. *et al.* Lethal graft-versus-host disease in mouse models of T cell receptor gene therapy. Nat Med 16, 565-570, 561p following 570, doi:10.1038/nm.2128 (2010).

110 Shao, H. *et al.* TCR mispairing in genetically modified T cells was detected by fluorescence resonance energy transfer. Mol Biol Rep 37, 3951-3956, doi:10.1007/s11033-010-0053-y (2010).

111 Gross, G., Waks, T. & Eshhar, Z. Expression of immunoglobulin-T-cell receptor chimeric molecules as functional receptors with antibody-type specificity. Proc Natl Acad Sci U S A 86, 10024-10028, doi:10.1073/pnas.86.24.10024 (1989).

112 Irving, B. A. & Weiss, A. The cytoplasmic domain of the T cell receptor zeta chain is sufficient to couple to receptor-associated signal transduction pathways. Cell 64, 891-901, doi:10.1016/0092-8674(91)90314-o (1991).

113 Maher, J., Brentjens, R. J., Gunset, G., Riviere, I. & Sadelain, M. Human T-lymphocyte cytotoxicity and proliferation directed by a single chimeric TCRzeta /CD28 receptor. Nat Biotechnol 20, 70-75, doi:10.1038/nbt0102-70 (2002).

114 Hombach, A. *et al.* Tumour-specific T cell activation by recombinant immunoreceptors: CD3 zeta signaling and CD28 costimulation are simultaneously required for efficient IL-2 secretion and can be integrated into one combined CD28/CD3 zeta signaling receptor molecule. J Immunol 167, 6123-6131, doi:10.4049/jimmunol.167.11.6123 (2001).

115 Pule, M. A. *et al.* A chimeric T cell antigen receptor that augments cytokine release and supports clonal expansion of primary human T cells. Mol Ther 12, 933-941, doi:10.1016/j.ymthe.2005.04.016 (2005).

116 Eyquem, J. *et al.* Targeting a CAR to the TRAC locus with CRISPR/Cas9 enhances tumour rejection. Nature 543, 113-117, doi:10.1038/nature21405 (2017).

117 Kochenderfer, J. N. *et al.* Eradication of B-lineage cells and regression of lymphoma in a patient treated with autologous T cells genetically engineered to recognize CD19. Blood 116, 4099-4102, doi:10.1182/blood-2010-04-281931 (2010).

118 Miller, B. C. & Maus, M. V. CD19-Targeted CAR T Cells: A New Tool in the Fight against B Cell Malignancies. Oncol Res Treat 38, 683-690, doi:10.1159/000442170 (2015).

119 Brentjens, R. J. *et al.* Eradication of systemic B-cell tumours by genetically targeted human T lymphocytes co-stimulated by CD80 and interleukin-15. Nat Med 9, 279-286, doi:10.1038/nm827 (2003).

120 Pule, M. A. *et al.* Virus-specific T cells engineered to coexpress tumour-specific receptors: persistence and antitumour activity in individuals with neuroblastoma. Nat Med 14, 1264-1270, doi:10.1038/nm.1882 (2008).

121 Chinnasamy, D. *et al.* Gene therapy using genetically modified lymphocytes targeting VEGFR-2 inhibits the growth of vascularized syngenic tumours in mice. J Clin Invest 120, 3953-3968, doi:10.1172/JCI43490 (2010).

122 Neelapu, S. S. *et al.* Chimeric antigen receptor T-cell therapy - assessment and management of toxicities. Nat Rev Clin Oncol 15, 47-62, doi:10.1038/nrclinonc.2017.148 (2018).

123 Saxena, M., van der Burg, S. H., Melief, C. J. M. & Bhardwaj, N. Therapeutic cancer

vaccines. Nat Rev Cancer 21, 360-378, doi:10.1038/s41568-021-00346-0 (2021).

124 Vansteenkiste, J. F. *et al.* Efficacy of the MAGE-A3 cancer immunotherapeutic as adjuvant therapy in patients with resected MAGE-A3-positive non-small-cell lung cancer (MAGRIT): a randomised, double-blind, placebo-controlled, phase 3 trial. Lancet Oncol 17, 822-835, doi:10.1016/S1470-2045(16)00099-1 (2016).

125 Giaccone, G. *et al.* A phase III study of belagenpumatucel-L, an allogeneic tumour cell vaccine, as maintenance therapy for non-small cell lung cancer. Eur J Cancer 51, 2321-2329, doi:10.1016/j.ejca.2015.07.035 (2015).

126 Butts, C. *et al.* Tecemotide (L-BLP25) versus placebo after chemoradiotherapy for stage III non-small-cell lung cancer (START): a randomised, double-blind, phase 3 trial. Lancet Oncol 15, 59-68, doi:10.1016/S1470-2045(13)70510-2 (2014).

127 Rini, B. I. *et al.* IMA901, a multipeptide cancer vaccine, plus sunitinib versus sunitinib alone, as first-line therapy for advanced or metastatic renal cell carcinoma (IMPRINT): a multicentre, open-label, randomised, controlled, phase 3 trial. Lancet Oncol 17, 1599-1611, doi:10.1016/S1470-2045(16)30408-9 (2016).

128 Middleton, G. *et al.* Gemcitabine and capecitabine with or without telomerase peptide vaccine GV1001 in patients with locally advanced or metastatic pancreatic cancer (TeloVac): an open-label, randomised, phase 3 trial. Lancet Oncol 15, 829-840, doi:10.1016/S1470-2045(14)70236-0 (2014).

129 Lawson, D. H. *et al.* Randomized, Placebo-Controlled, Phase III Trial of Yeast-Derived Granulocyte-Macrophage Colony-Stimulating Factor (GM-CSF) Versus Peptide Vaccination Versus GM-CSF Plus Peptide Vaccination Versus Placebo in Patients With No Evidence of Disease After Complete Surgical Resection of Locally Advanced and/or Stage IV Melanoma: A Trial of the Eastern Cooperative Oncology Group-American College of Radiology Imaging Network Cancer Research Group (E4697). J Clin Oncol 33, 4066-4076, doi:10.1200/JCO.2015.62.0500 (2015).

130 Kantoff, P. W. *et al.* Sipuleucel-T immunotherapy for castration-resistant prostate cancer. N Engl J Med 363, 411-422, doi:10.1056/NEJMoa1001294 (2010).

131 Chen, D. S. & Mellman, I. Elements of cancer immunity and the cancer-immune set point.

Nature 541, 321-330, doi:10.1038/nature21349 (2017).

132 Xia, T., Konno, H., Ahn, J. & Barber, G. N. Deregulation of STING Signaling in Colorectal Carcinoma Constrains DNA Damage Responses and Correlates With Tumourigenesis. Cell Rep 14, 282-297, doi:10.1016/j.celrep.2015.12.029 (2016).

133 Galluzzi, L., Buque, A., Kepp, O., Zitvogel, L. & Kroemer, G. Immunogenic cell death in cancer and infectious disease. Nat Rev Immunol 17, 97-111, doi:10.1038/nri.2016.107 (2017).

134 Dock, G. The influence of complicating diseases upon leukemia. Am J Med Sci 127, 563–592 (1904).

135 Pelner, L., Fowler, G. A. & Nauts, H. C. Effects of concurrent infections and their toxins on the course of leukemia. Acta Med Scand Suppl 338, 1-47 (1958).

136 Southam, C. M. Present status of oncolytic virus studies. Trans N Y Acad Sci 22, 657-673, doi:10.1111/j.2164-0947.1960.tb00739.x (1960).

137 Russell, S. J., Peng, K. W. & Bell, J. C. Oncolytic virotherapy. Nat Biotechnol 30, 658-670, doi:10.1038/nbt.2287 (2012).

138 Asada, T. Treatment of human cancer with mumps virus. Cancer 34, 1907-1928, doi:10.1002/1097-0142(197412)34:6<1907::aid-cncr2820340609>3.0.co;2-4 (1974).

139 Martuza, R. L., Malick, A., Markert, J. M., Ruffner, K. L. & Coen, D. M. Experimental therapy of human glioma by means of a genetically engineered virus mutant. Science 252, 854, doi:10.1126/science.1851332 (1991).

140 Liu, T. C., Galanis, E. & Kirn, D. Clinical trial results with oncolytic virotherapy: a century of promise, a decade of progress. Nat Clin Pract Oncol 4, 101-117, doi:10.1038/ncponc0736 (2007).

141 Senzer, N. N. *et al.* Phase II clinical trial of a granulocyte-macrophage colony-stimulating factor-encoding, second-generation oncolytic herpesvirus in patients with unresectable metastatic melanoma. J Clin Oncol 27, 5763-5771, doi:10.1200/JCO.2009.24.3675 (2009).

142 Andtbacka, R. H. I. *et al.* Final analyses of OPTiM: a randomized phase III trial of talimogene laherparepvec versus granulocyte-macrophage colony-stimulating factor in unresectable stage III-IV melanoma. J Immunother Cancer 7, 145, doi:10.1186/s40425-019-0623-z (2019).

143 Lichty, B. D., Breitbach, C. J., Stojdl, D. F. & Bell, J. C. Going viral with cancer immunotherapy. Nat Rev Cancer 14, 559-567, doi:10.1038/nrc3770 (2014).

144 Diaz, R. M. *et al.* Oncolytic immunovirotherapy for melanoma using vesicular stomatitis virus. Cancer Res 67, 2840-2848, doi:10.1158/0008-5472.can-06-3974 (2007).

145 Liu, B. L. *et al.* ICP34.5 deleted herpes simplex virus with enhanced oncolytic, immune stimulating, and anti-tumour properties. Gene Ther 10, 292-303, doi:10.1038/sj.gt.3301885 (2003).

146 Moehler, M. H. *et al.* Parvovirus H-1-induced tumour cell death enhances human immune response in vitro via increased phagocytosis, maturation, and cross-presentation by dendritic cells. Hum Gene Ther 16, 996-1005, doi:10.1089/hum.2005.16.996 (2005).

147 Breitbach, C. J. *et al.* Targeted inflammation during oncolytic virus therapy severely compromises tumour blood flow. Mol Ther 15, 1686-1693, doi:10.1038/sj.mt.6300215 (2007).

148 Boagni, D. A., Ravirala, D. & Zhang, S. X. Current strategies in engaging oncolytic viruses with antitumour immunity. Mol Ther Oncolytics 22, 98-113, doi:10.1016/j.omto.2021.05.002 (2021).

149 Edukulla, R. *et al.* Antitumoural immune response by recruitment and expansion of dendritic cells in tumours infected with telomerase-dependent oncolytic viruses. Cancer Res 69, 1448-1458, doi:10.1158/0008-5472.CAN-08-1160 (2009).

150 Bernt, K. M., Ni, S., Tieu, A. T. & Lieber, A. Assessment of a combined, adenovirus-mediated oncolytic and immunostimulatory tumour therapy. Cancer Res 65, 4343-4352, doi:10.1158/0008-5472.CAN-04-3527 (2005).

151 Li, J. *et al.* Chemokine expression from oncolytic vaccinia virus enhances vaccine therapies of cancer. Mol Ther 19, 650-657, doi:10.1038/mt.2010.312 (2011).

152 Kaufman, H. L. *et al.* Local and distant immunity induced by intralesional vaccination with an oncolytic herpes virus encoding GM-CSF in patients with stage IIIc and IV melanoma. Ann Surg Oncol 17, 718-730, doi:10.1245/s10434-009-0809-6 (2010).

153 Kim, J. H. *et al.* Systemic armed oncolytic and immunologic therapy for cancer with JX-594, a targeted poxvirus expressing GM-CSF. Mol Ther 14, 361-370, doi:10.1016/j.ymthe.2006.05.008 (2006).

154 Choi, I. K. *et al.* Oncolytic adenovirus co-expressing IL-12 and IL-18 improves tumour-specific immunity via differentiation of T cells expressing IL-12Rbeta2 or IL-18Ralpha. Gene Ther 18, 898-909, doi:10.1038/gt.2011.37 (2011).

155 Gaston, D. C. *et al.* Production of bioactive soluble interleukin-15 in complex with interleukin-15 receptor alpha from a conditionally-replicating oncolytic HSV-1. PLoS One 8, e81768, doi:10.1371/journal.pone.0081768 (2013).

156 Stephenson, K. B., Barra, N. G., Davies, E., Ashkar, A. A. & Lichty, B. D. Expressing human interleukin-15 from oncolytic vesicular stomatitis virus improves survival in a murine metastatic colon adenocarcinoma model through the enhancement of anti-tumour immunity. Cancer Gene Ther 19, 238-246, doi:10.1038/cgt.2011.81 (2012).

157 Ino, Y., Saeki, Y., Fukuhara, H. & Todo, T. Triple combination of oncolytic herpes simplex virus-1 vectors armed with interleukin-12, interleukin-18, or soluble B7-1 results in enhanced antitumour efficacy. Clin Cancer Res 12, 643-652, doi:10.1158/1078-0432.CCR-05-1494 (2006).

158 Lee, Y. S. *et al.* Enhanced antitumour effect of oncolytic adenovirus expressing interleukin-12 and B7-1 in an immunocompetent murine model. Clin Cancer Res 12, 5859-5868, doi:10.1158/1078-0432.CCR-06-0935 (2006).

159 Passaro, C. *et al.* Arming an Oncolytic Herpes Simplex Virus Type 1 with a Single-chain Fragment Variable Antibody against PD-1 for Experimental Glioblastoma Therapy. Clin Cancer Res 25, 290-299, doi:10.1158/1078-0432.CCR-18-2311 (2019).

160 Rosewell Shaw, A. *et al.* Adenovirotherapy Delivering Cytokine and Checkpoint Inhibitor Augments CAR T Cells against Metastatic Head and Neck Cancer. Mol Ther 25, 2440-2451, doi:10.1016/j.ymthe.2017.09.010 (2017).

161 Yu, F. *et al.* T-cell engager-armed oncolytic vaccinia virus significantly enhances antitumour therapy. Mol Ther 22, 102-111, doi:10.1038/mt.2013.240 (2014).

162 Breitbach, C. J. *et al.* Targeting tumour vasculature with an oncolytic virus. Mol Ther 19, 886-894, doi:10.1038/mt.2011.26 (2011).

163 Hastie, E. & Grdzelishvili, V. Z. Vesicular stomatitis virus as a flexible platform for oncolytic virotherapy against cancer. J Gen Virol 93, 2529-2545, doi:10.1099/vir.0.046672-0 (2012).

164 Ge, P. *et al.* Cryo-EM model of the bullet-shaped vesicular stomatitis virus. Science 327, 689-693, doi:10.1126/science.1181766 (2010).

165 Melzer, M. K., Lopez-Martinez, A. & Altomonte, J. Oncolytic Vesicular Stomatitis Virus as a Viro-Immunotherapy: Defeating Cancer with a “Hammer” and “Anvil”. Biomedicines 5, doi:10.3390/biomedicines5010008 (2017).

166 Stanifer, M. L., Cureton, D. K. & Whelan, S. P. A recombinant vesicular stomatitis virus bearing a lethal mutation in the glycoprotein gene uncovers a second site suppressor that restores fusion. J Virol 85, 8105-8115, doi:10.1128/JVI.00735-11 (2011).

167 Stojdl, D. F. *et al.* The murine double-stranded RNA-dependent protein kinase PKR is required for resistance to vesicular stomatitis virus. J Virol 74, 9580-9585, doi:10.1128/jvi.74.20.9580-9585.2000 (2000).

168 Lyles, D. S. Cytopathogenesis and inhibition of host gene expression by RNA viruses. Microbiol Mol Biol Rev 64, 709-724, doi:10.1128/MMBR.64.4.709-724.2000 (2000).

169 Ahmed, M. *et al.* Ability of the matrix protein of vesicular stomatitis virus to suppress beta interferon gene expression is genetically correlated with the inhibition of host RNA and protein synthesis. J Virol 77, 4646-4657, doi:10.1128/jvi.77.8.4646-4657.2003 (2003).

170 Stojdl, D. F. *et al.* VSV strains with defects in their ability to shutdown innate immunity are potent systemic anti-cancer agents. Cancer Cell 4, 263-275, doi:10.1016/s1535-6108(03)00241-1 (2003).

171 Altomonte, J. *et al.* Exponential enhancement of oncolytic vesicular stomatitis virus potency by vector-mediated suppression of inflammatory responses in vivo. Mol Ther 16, 146-153, doi:10.1038/sj.mt.6300343 (2008).

172 Wu, L. *et al.* rVSV(M Delta 51)-M3 is an effective and safe oncolytic virus for cancer therapy. Hum Gene Ther 19, 635-647, doi:10.1089/hum.2007.163 (2008).

173 Wongthida, P. *et al.* Type III IFN interleukin-28 mediates the antitumour efficacy of oncolytic virus VSV in immune-competent mouse models of cancer. Cancer Res 70, 4539-4549, doi:10.1158/0008-5472.CAN-09-4658 (2010).

174 Swiecki, M. & Colonna, M. Unraveling the functions of plasmacytoid dendritic cells during viral infections, autoimmunity, and tolerance. Immunol Rev 234, 142-162, doi:10.1111/

j.0105-2896.2009.00881.x (2010).

175 Lund, J. M. *et al.* Recognition of single-stranded RNA viruses by Toll-like receptor 7. Proc Natl Acad Sci U S A 101, 5598-5603, doi:10.1073/pnas.0400937101 (2004).

176 Akira, S., Uematsu, S. & Takeuchi, O. Pathogen recognition and innate immunity. Cell 124, 783-801, doi:10.1016/j.cell.2006.02.015 (2006).

177 Swiecki, M., Gilfillan, S., Vermi, W., Wang, Y. & Colonna, M. Plasmacytoid dendritic cell ablation impacts early interferon responses and antiviral NK and CD8(+) T cell accrual. Immunity 33, 955-966, doi:10.1016/j.immuni.2010.11.020 (2010).

178 Fernandez, M., Porosnicu, M., Markovic, D. & Barber, G. N. Genetically engineered vesicular stomatitis virus in gene therapy: application for treatment of malignant disease. J Virol 76, 895-904, doi:10.1128/jvi.76.2.895-904.2002 (2002).

179 Shin, E. J. *et al.* Interleukin-12 expression enhances vesicular stomatitis virus oncolytic therapy in murine squamous cell carcinoma. Laryngoscope 117, 210-214, doi:10.1097/01.mlg.0000246194.66295.d8 (2007).

180 Miller, J. M., Bidula, S. M., Jensen, T. M. & Reiss, C. S. Vesicular stomatitis virus modified with single chain IL-23 exhibits oncolytic activity against tumour cells in vitro and in vivo. Int J Interferon Cytokine Mediat Res 2010, 63-72, doi:10.2147/ijicmr.s9528 (2010).

181 Leveille, S., Goulet, M. L., Lichty, B. D. & Hiscott, J. Vesicular stomatitis virus oncolytic treatment interferes with tumour-associated dendritic cell functions and abrogates tumour antigen presentation. J Virol 85, 12160-12169, doi:10.1128/JVI.05703-11 (2011).

182 Galivo, F. *et al.* Interference of CD40L-mediated tumour immunotherapy by oncolytic vesicular stomatitis virus. Hum Gene Ther 21, 439-450, doi:10.1089/hum.2009.143 (2010).

183 Obuchi, M., Fernandez, M. & Barber, G. N. Development of recombinant vesicular stomatitis viruses that exploit defects in host defense to augment specific oncolytic activity. J Virol 77, 8843-8856, doi:10.1128/jvi.77.16.8843-8856.2003 (2003).

184 Willmon, C. L. *et al.* Expression of IFN-beta enhances both efficacy and safety of oncolytic vesicular stomatitis virus for therapy of mesothelioma. Cancer Res 69, 7713-7720, doi:10.1158/0008-5472.CAN-09-1013 (2009).

185 Patel, M. R. *et al.* Vesicular stomatitis virus expressing interferon-beta is oncolytic and

promotes antitumour immune responses in a syngeneic murine model of non-small cell lung cancer. Oncotarget 6, 33165-33177, doi:10.18632/oncotarget.5320 (2015).

186 Zinkernagel, R. M., Adler, B. & Holland, J. J. Cell-mediated immunity to vesicular stomatitis virus infections in mice. Exp Cell Biol 46, 53-70, doi:10.1159/000162882 (1978).

187 Bridle, B. W. *et al.* Potentiating cancer immunotherapy using an oncolytic virus. Mol Ther 18, 1430-1439, doi:10.1038/mt.2010.98 (2010).

188 Bridle, B. W. *et al.* Privileged Antigen Presentation in Splenic B Cell Follicles Maximizes T Cell Responses in Prime-Boost Vaccination. J Immunol 196, 4587-4595, doi:10.4049/jimmunol.1600106 (2016).

189 Goebel, S. J. *et al.* The complete DNA sequence of vaccinia virus. Virology 179, 247-266, 517-263, doi:10.1016/0042-6822(90)90294-2 (1990).

190 Behbehani, A. M. The smallpox story: life and death of an old disease. Microbiological reviews 47, 455-509 (1983).

191 Minnigan, H. & Moyer, R. Intracellular location of rabbit poxvirus nucleic acid within infected cells as determined by in situ hybridization. Journal of virology 55, 634-643 (1985).

192 McFadden, G. Poxvirus tropism. Nature Reviews Microbiology 3, 201-213 (2005).

193 Mercer, J. & Helenius, A. Vaccinia virus uses macropinocytosis and apoptotic mimicry to enter host cells. Science 320, 531-535 (2008).

194 Moss, B. in Seminars in cell & developmental biology. 89-96 (Elsevier).

195 Broyles, S. S. Vaccinia virus transcription. J Gen Virol 84, 2293-2303, doi:10.1099/vir.0.18942-0 (2003).

196 Smith, G. L. & Moss, B. Infectious poxvirus vectors have capacity for at least 25 000 base pairs of foreign DNA. Gene 25, 21-28 (1983).

197 Miller, J. D. *et al.* Human effector and memory CD8+ T cell responses to smallpox and yellow fever vaccines. Immunity 28, 710-722 (2008).

198 Smith, G. L. *et al.* Vaccinia virus immune evasion: mechanisms, virulence and immunogenicity. Journal of General Virology 94, 2367-2392, doi:doi:10.1099/vir.0.055921-0 (2013).

199 Foloppe, J. *et al.* Targeted delivery of a suicide gene to human colorectal tumours by a

conditionally replicating vaccinia virus. Gene therapy 15, 1361-1371 (2008).

200 Kirn, D. H. & Thorne, S. H. Targeted and armed oncolytic poxviruses: a novel multi-mechanistic therapeutic class for cancer. Nat Rev Cancer 9, 64-71, doi:10.1038/nrc2545 (2009).

201 Thorne, S. H. *et al.* Rational strain selection and engineering creates a broad-spectrum, systemically effective oncolytic poxvirus, JX-963. J Clin Invest 117, 3350-3358, doi:10.1172/jci32727 (2007).

202 Gnant, M. F. *et al.* Tumour-specific gene delivery using recombinant vaccinia virus in a rabbit model of liver metastases. Journal of the National Cancer Institute 91, 1744-1750 (1999).

203 Buller, R. M. L., Smith, G. L., Cremer, K., Notkins, A. & Moss, B. Decreased virulence of recombinant vaccinia virus expression vectors is associated with a thymidine kinase-negative phenotype. Nature 317, 813-815 (1985).

204 Hengstschläger, M. *et al.* Different regulation of thymidine kinase during the cell cycle of normal versus DNA tumour virus-transformed cells. Journal of Biological Chemistry 269, 13836-13842 (1994).

205 Buller, R. M. L., Chakrabarti, S., Moss, B. & Fredricksont, T. Cell proliferative response to vaccinia virus is mediated by VGF. Virology 164, 182-192 (1988).

206 Buller, R., Chakrabarti, S., Cooper, J., Twardzik, D. & Moss, B. Deletion of the vaccinia virus growth factor gene reduces virus virulence. Journal of virology 62, 866-874 (1988).

207 McCart, J. A. *et al.* Systemic cancer therapy with a tumour-selective vaccinia virus mutant lacking thymidine kinase and vaccinia growth factor genes. Cancer Res 61, 8751-8757 (2001).

208 Kirn, D. H., Wang, Y., Le Boeuf, F., Bell, J. & Thorne, S. H. Targeting of interferon-beta to produce a specific, multi-mechanistic oncolytic vaccinia virus. PLoS Med 4, e353, doi:10.1371/journal.pmed.0040353 (2007).

209 Yang, S. *et al.* A new recombinant vaccinia with targeted deletion of three viral genes: its safety and efficacy as an oncolytic virus. Gene Therapy 14, 638-647 (2007).

210 Jones, E. V. & Moss, B. Mapping of the vaccinia virus DNA polymerase gene by marker rescue and cell-free translation of selected RNA. Journal of virology 49, 72-77 (1984).

211 Lee-Chen, G.-J. & Niles, E. G. Transcription and translation mapping of the 13 genes in the vaccinia virus Hindlll D fragment. Virology 163, 52-63 (1988).

212 Smith, G. L., Chan, Y. S. & Kerr, S. M. Transcriptional mapping and nucleotide sequence of a vaccinia virus gene encoding a polypeptide with extensive homology to DNA ligases. Nucleic acids research 17, 9051-9062 (1989).

213 Smith, G. L., Carlos, A. d. & Chan, Y. S. Vaccinia virus encodes a thymidylate kinase gene: sequence and transcriptional mapping. Nucleic acids research 17, 7581-7590 (1989).

214 Kotwal, G. J., Hügin, A. W. & Moss, B. Mapping and insertional mutagenesis of a vaccinia virus gene encoding a 13,800-Da secreted protein. Virology 171, 579-587 (1989).

215 Moore, J. B. & Smith, G. L. Steroid hormone synthesis by a vaccinia enzyme: a new type of virus virulence factor. The EMBO journal 11, 1973-1980 (1992).

216 Ng, A., Tscharke, D. C., Reading, P. C. & Smith, G. L. The vaccinia virus A41L protein is a soluble 30 kDa glycoprotein that affects virus virulence. Journal of General Virology 82, 2095-2105 (2001).

217 Guo, Z. S. *et al.* Vaccinia virus-mediated cancer immunotherapy: cancer vaccines and oncolytics. Journal for ImmunoTherapy of Cancer 7, 6, doi:10.1186/s40425-018-0495-7 (2019).

218 Tolonen, N., Doglio, L., Schleich, S. & Locker, J. K. Vaccinia virus DNA replication occurs in endoplasmic reticulum-enclosed cytoplasmic mini-nuclei. Molecular biology of the cell 12, 2031-2046 (2001).

219 Rosel, J. & Moss, B. Transcriptional and translational mapping and nucleotide sequence analysis of a vaccinia virus gene encoding the precursor of the major core polypeptide 4b. Journal of virology 56, 830-838 (1985).

220 Vos, J. C. & Stunnenberg, H. G. Derepression of a novel class of vaccinia virus genes upon DNA replication. The EMBO journal 7, 3487-3492 (1988).

221 Katsafanas, G. C. & Moss, B. Colocalization of transcription and translation within cytoplasmic poxvirus factories coordinates viral expression and subjugates host functions. Cell Host Microbe 2, 221-228, doi:10.1016/j.chom.2007.08.005 (2007).

222 Smith, G. L., Vanderplasschen, A. & Law, M. The formation and function of extracellular enveloped vaccinia virus. J Gen Virol 83, 2915-2931, doi:10.1099/0022-1317-83-12-2915 (2002).

223 Rodriguez, J. F. & Smith, G. L. IPTG-dependent vaccinia virus: identification of a virus protein enabling virion envelopment by Golgi membrane and egress. Nucleic Acids Research 18,

5347-5351, doi:10.1093/nar/18.18.5347 (1990).

224 Smith, G. L., Vanderplasschen, A. & Law, M. The formation and function of extracellular enveloped vaccinia virus. Journal of General Virology 83, 2915-2931, doi:https://doi.org/10.1099/0022-1317-83-12-2915 (2002).

225 Hiller, G., Weber, K., Schneider, L., Parajsz, C. & Jungwirth, C. Interaction of assembled progeny pox viruses with the cellular cytoskeleton. Virology 98, 142-153 (1979).

226 Law, M. & Smith, G. L. Antibody neutralization of the extracellular enveloped form of vaccinia virus. Virology 280, 132-142 (2001).

227 Macedo, N., Miller, D. M., Haq, R. & Kaufman, H. L. Clinical landscape of oncolytic virus research in 2020. Journal for ImmunoTherapy of Cancer 8, e001486, doi:10.1136/jitc-2020-001486 (2020).

228 Breitbach, C. J. *et al.* Intravenous delivery of a multi-mechanistic cancer-targeted oncolytic poxvirus in humans. Nature 477, 99-102, doi:10.1038/nature10358 (2011).

229 Underhill, D. M. & Ozinsky, A. Phagocytosis of microbes: complexity in action. Annu Rev Immunol 20, 825-852, doi:10.1146/annurev.immunol.20.103001.114744 (2002).

230 Fisher, K. D. & Seymour, L. W. HPMA copolymers for masking and retargeting of therapeutic viruses. Adv Drug Deliv Rev 62, 240-245, doi:10.1016/j.addr.2009.12.003 (2010).

231 Eto, Y., Yoshioka, Y., Mukai, Y., Okada, N. & Nakagawa, S. Development of PEGylated adenovirus vector with targeting ligand. Int J Pharm 354, 3-8, doi:10.1016/j.ijpharm.2007.08.025 (2008).

232 Alemany, R., Suzuki, K. & Curiel, D. T. Blood clearance rates of adenovirus type 5 in mice. J Gen Virol 81, 2605-2609, doi:10.1099/0022-1317-81-11-2605 (2000).

233 Green, N. K. *et al.* Extended plasma circulation time and decreased toxicity of polymer-coated adenovirus. Gene Ther 11, 1256-1263, doi:10.1038/sj.gt.3302295 (2004).

234 Power, A. T. & Bell, J. C. Taming the Trojan horse: optimizing dynamic carrier cell/oncolytic virus systems for cancer biotherapy. Gene Ther 15, 772-779, doi:10.1038/gt.2008.40 (2008).

235 Ilett, E. J. *et al.* Dendritic cells and T cells deliver oncolytic reovirus for tumour killing despite pre-existing anti-viral immunity. Gene Ther 16, 689-699, doi:10.1038/gt.2009.29 (2009).

236 Bridle, B. W. *et al.* Oncolytic vesicular stomatitis virus quantitatively and qualitatively improves primary CD8(+) T-cell responses to anticancer vaccines. Oncoimmunology 2, e26013, doi:10.4161/onci.26013 (2013).

237 Fousek, K. & Ahmed, N. The evolution of T-cell therapies for solid malignancies. Clinical Cancer Research 21, 3384-3392 (2015).

238 Klebanoff, C. A., Gattinoni, L. & Restifo, N. P. Sorting through subsets: which T-cell populations mediate highly effective adoptive immunotherapy? Journal of immunotherapy (Hagerstown, Md. : 1997) 35, 651-660, doi:10.1097/CJI.0b013e31827806e6 (2012).

239 Walsh, S. R. *et al.* Type I IFN blockade uncouples immunotherapy-induced antitumour immunity and autoimmune toxicity. J Clin Invest 129, 518-530, doi:10.1172/JCI121004 (2019).

240 Walsh, S. R. *et al.* Endogenous T cells prevent tumour immune escape following adoptive T cell therapy. J Clin Invest 129, 5400-5410, doi:10.1172/JCI126199 (2019).

241 Nguyen, A. *et al.* HDACi Delivery Reprograms Tumour-Infiltrating Myeloid Cells to Eliminate Antigen-Loss Variants. Cell Rep 24, 642-654, doi:10.1016/j.celrep.2018.06.040 (2018).

242 Prevost-Blondel, A. *et al.* Tumour-infiltrating lymphocytes exhibiting high ex vivo cytolytic activity fail to prevent murine melanoma tumour growth in vivo. J Immunol 161, 2187-2194 (1998).

243 Rosenberg, S. A., Spiess, P. & Lafreniere, R. A new approach to the adoptive immunotherapy of cancer with tumour-infiltrating lymphocytes. Science 233, 1318-1321, doi:10.1126/science.3489291 (1986).

244 Oldstone, M. B. *et al.* Vaccination to prevent persistent viral infection. J Virol 67, 4372-4378, doi:10.1128/JVI.67.7.4372-4378.1993 (1993).

245 Zhang, L. *et al.* Delivery of viral-vectored vaccines by B cells represents a novel strategy to accelerate CD8(+) T-cell recall responses. Blood 121, 2432-2439, doi:10.1182/blood-2012-06-438481 (2013).

246 Carvalho, B. S. & Irizarry, R. A. A framework for oligonucleotide microarray preprocessing. Bioinformatics 26, 2363-2367, doi:10.1093/bioinformatics/btq431 (2010).

247 Ritchie, M. E. *et al.* limma powers differential expression analyses for RNA-sequencing and microarray studies. Nucleic Acids Res 43, e47, doi:10.1093/nar/gkv007 (2015).

248 Boyle, E. I. *et al.* GO::TermFinder—open source software for accessing Gene Ontology information and finding significantly enriched Gene Ontology terms associated with a list of genes. Bioinformatics 20, 3710-3715, doi:10.1093/bioinformatics/bth456 (2004).

249 Yu, G., Wang, L. G., Han, Y. & He, Q. Y. clusterProfiler: an R package for comparing biological themes among gene clusters. OMICS 16, 284-287, doi:10.1089/omi.2011.0118 (2012).

250 Wu, T. *et al.* clusterProfiler 4.0: A universal enrichment tool for interpreting omics data. Innovation (N Y) 2, 100141, doi:10.1016/j.xinn.2021.100141 (2021).

251 Subramanian, A. *et al.* Gene set enrichment analysis: A knowledge-based approach for interpreting genome-wide expression profiles. Proceedings of the National Academy of Sciences 102, 15545, doi:10.1073/pnas.0506580102 (2005).

252 Sergushichev, A. A. An algorithm for fast preranked gene set enrichment analysis using cumulative statistic calculation. bioRxiv, 060012, doi:10.1101/060012 (2016).

253 Liberzon, A. *et al.* The Molecular Signatures Database (MSigDB) hallmark gene set collection. Cell Syst 1, 417-425, doi:10.1016/j.cels.2015.12.004 (2015).

254 Cerami, E. *et al.* The cBio cancer genomics portal: an open platform for exploring multidimensional cancer genomics data. Cancer Discov 2, 401-404, doi:10.1158/2159-8290.CD-12-0095 (2012).

255 Gao, J. *et al.* Integrative analysis of complex cancer genomics and clinical profiles using the cBioPortal. Sci Signal 6, pl1, doi:10.1126/scisignal.2004088 (2013).

256 Hanzelmann, S., Castelo, R. & Guinney, J. GSVA: gene set variation analysis for microarray and RNA-seq data. BMC Bioinformatics 14, 7, doi:10.1186/1471-2105-14-7 (2013).

257 Therneau, T. M. A Package for Survival Analysis in R. (2021).

258 Newman, A. M. *et al.* Robust enumeration of cell subsets from tissue expression profiles. Nat Methods 12, 453-457, doi:10.1038/nmeth.3337 (2015).

259 Team, R. (2020).

260 Wickham, H. *et al.* Welcome to the Tidyverse. Journal of Open Source Software 4, 1686-1686 (2019).

261 Wickham, H. (2021).

262 Wickham, H. ggplot2: Elegant Graphics for Data Analysis. (Springer-Verlag New York,

2016).

263 Gu, Z., Eils, R. & Schlesner, M. Complex heatmaps reveal patterns and correlations in multidimensional genomic data. Bioinformatics 32, 2847-2849, doi:10.1093/bioinformatics/btw313 (2016).

264 Kassambara, A., Kosinski, M. & Biecek, P. (2021).

265 Kassambara, A. (2021).

266 Pol, J. G. *et al.* Maraba virus as a potent oncolytic vaccine vector. Mol Ther 22, 420-429, doi:10.1038/mt.2013.249 (2014).

267 Klebanoff, C. A. *et al.* Central memory self/tumour-reactive CD8+ T cells confer superior antitumour immunity compared with effector memory T cells. Proc Natl Acad Sci U S A 102, 9571-9576, doi:10.1073/pnas.0503726102 (2005).

268 Zeng, R. *et al.* Synergy of IL-21 and IL-15 in regulating CD8+ T cell expansion and function. J Exp Med 201, 139-148, doi:10.1084/jem.20041057 (2005).

269 He, S. *et al.* Characterization of the metabolic phenotype of rapamycin-treated CD8+ T cells with augmented ability to generate long-lasting memory cells. PLoS One 6, e20107, doi:10.1371/journal.pone.0020107 (2011).

270 Gattinoni, L. *et al.* Acquisition of full effector function in vitro paradoxically impairs the in vivo antitumour efficacy of adoptively transferred CD8+ T cells. J Clin Invest 115, 1616-1626, doi:10.1172/JCI24480 (2005).

271 Gattinoni, L., Klebanoff, C. A. & Restifo, N. P. Paths to stemness: building the ultimate antitumour T cell. Nat Rev Cancer 12, 671-684, doi:10.1038/nrc3322 (2012).

272 Gattinoni, L. *et al.* Wnt signaling arrests effector T cell differentiation and generates CD8+ memory stem cells. Nat Med 15, 808-813, doi:10.1038/nm.1982 (2009).

273 Klebanoff, C. A. *et al.* Determinants of successful CD8+ T-cell adoptive immunotherapy for large established tumours in mice. Clin Cancer Res 17, 5343-5352, doi:10.1158/1078-0432.ccr-11-0503 (2011).

274 Hla, T. & Brinkmann, V. Sphingosine 1-phosphate (S1P): Physiology and the effects of S1P receptor modulation. Neurology 76, S3-8, doi:10.1212/WNL.0b013e31820d5ec1 (2011).

275 Scholzen, T. & Gerdes, J. The Ki-67 protein: from the known and the unknown. J Cell

Physiol 182, 311-322, doi:10.1002/(SICI)1097-4652(200003)182:3<311::AID-JCP1>3.0.CO;2-9 (2000).

276 Gierut, J. J., Jacks, T. E. & Haigis, K. M. Whole-mount X-Gal staining of mouse tissues. (2014).

277 Bierman, H. R. *et al.* Remissions in leukemia of childhood following acute infectious disease: staphylococcus and streptococcus, varicella, and feline panleukopenia. Cancer 6, 591-605, doi:10.1002/1097-0142(195305)6:3<591::aid-cncr2820060317>3.0.co;2-m (1953).

278 Moore, A. E. Viruses with oncolytic properties and their adaptation to tumours. Ann N Y Acad Sci 54, 945-952, doi:10.1111/j.1749-6632.1952.tb39969.x (1952).

279 Thorne, S. H. Immunotherapeutic potential of oncolytic vaccinia virus. Front Oncol 4, 155, doi:10.3389/fonc.2014.00155 (2014).

280 Contag, C. H. *et al.* Definition of an enhanced immune cell therapy in mice that can target stem-like lymphoma cells. Cancer Res 70, 9837-9845, doi:10.1158/0008-5472.CAN-10-2650 (2010).

281 Dai, P. *et al.* Intratumoural delivery of inactivated modified vaccinia virus Ankara (iMVA) induces systemic antitumour immunity via STING and Batf3-dependent dendritic cells. Sci Immunol 2, doi:10.1126/sciimmunol.aal1713 (2017).

282 Morel, P., Lin, L., Wiesehahn, G. & Corash, L. Photochemical inactivation of viruses and bacteriophage in plasma and plasma fractions. Blood Cells 18, 27-41; Discussion 41-22 (1992).

283 Tsung, K., Yim, J. H., Marti, W., Buller, R. M. & Norton, J. A. Gene expression and cytopathic effect of vaccinia virus inactivated by psoralen and long-wave UV light. J Virol 70, 165-171 (1996).

284 Veyer, D. L. *et al.* Analysis of the anti-apoptotic activity of four vaccinia virus proteins demonstrates that B13 is the most potent inhibitor in isolation and during viral infection. J Gen Virol 95, 2757-2768, doi:10.1099/vir.0.068833-0 (2014).

285 Postigo, A., Ramsden, A. E., Howell, M. & Way, M. Cytoplasmic ATR Activation Promotes Vaccinia Virus Genome Replication. Cell Rep 19, 1022-1032, doi:10.1016/j.celrep.2017.04.025 (2017).

286 Yadav, M. *et al.* Predicting immunogenic tumour mutations by combining mass

spectrometry and exome sequencing. Nature 515, 572-576, doi:10.1038/nature14001 (2014).

287 Yu, G. *et al.* GOSemSim: an R package for measuring semantic similarity among GO terms and gene products. Bioinformatics 26, 976-978, doi:10.1093/bioinformatics/btq064 (2010).

288 Sirbu, B. M. & Cortez, D. DNA damage response: three levels of DNA repair regulation. Cold Spring Harbor perspectives in biology 5, a012724-a012724, doi:10.1101/cshperspect.a012724 (2013).

289 Newman, A. M. *et al.* Determining cell type abundance and expression from bulk tissues with digital cytometry. Nat Biotechnol 37, 773-782, doi:10.1038/s41587-019-0114-2 (2019).

290 Love, M. I., Huber, W. & Anders, S. Moderated estimation of fold change and dispersion for RNA-seq data with DESeq2. Genome Biology 15, 550, doi:10.1186/s13059-014-0550-8 (2014).

291 Cox, D. R. Regression Models and Life-Tables. Journal of the Royal Statistical Society. Series B (Methodological) 34, 187-220 (1972).

292 Rosenberg, S. A., Restifo, N. P., Yang, J. C., Morgan, R. A. & Dudley, M. E. Adoptive cell transfer: a clinical path to effective cancer immunotherapy. Nat Rev Cancer 8, 299-308, doi:10.1038/nrc2355 (2008).

293 Rohaan, M. W., van den Berg, J. H., Kvistborg, P. & Haanen, J. B. A. G. Adoptive transfer of tumour-infiltrating lymphocytes in melanoma: a viable treatment option. Journal for ImmunoTherapy of Cancer 6, 102, doi:10.1186/s40425-018-0391-1 (2018).

294 Kaufman, H. L. & Bommareddy, P. K. Two roads for oncolytic immunotherapy development. J Immunother Cancer 7, 26, doi:10.1186/s40425-019-0515-2 (2019).

295 Li, L., Liu, S., Han, D., Tang, B. & Ma, J. Delivery and Biosafety of Oncolytic Virotherapy. Front Oncol 10, 475, doi:10.3389/fonc.2020.00475 (2020).

296 Davola, M. E. & Mossman, K. L. Oncolytic viruses: how “lytic” must they be for therapeutic efficacy? Oncoimmunology 8, e1581528, doi:10.1080/2162402X.2019.1596006 (2019).

297 Moss, B. Poxvirus DNA replication. Cold Spring Harb Perspect Biol 5, doi:10.1101/cshperspect.a010199 (2013).

298 Baldick, C. J., Jr. & Moss, B. Characterization and temporal regulation of mRNAs encoded

by vaccinia virus intermediate-stage genes. J Virol 67, 3515-3527, doi:10.1128/JVI.67.6.3515-3527.1993 (1993).

299 Broyles, S. S., Yuen, L., Shuman, S. & Moss, B. Purification of a factor required for transcription of vaccinia virus early genes. J Biol Chem 263, 10754-10760 (1988).

300 Broyles, S. S. & Fesler, B. S. Vaccinia virus gene encoding a component of the viral early transcription factor. J Virol 64, 1523-1529, doi:10.1128/JVI.64.4.1523-1529.1990 (1990).

301 Pearson, T. *et al.* Non-obese diabetic-recombination activating gene-1 (NOD-Rag1 null) interleukin (IL)-2 receptor common gamma chain (IL2r gamma null) null mice: a radioresistant model for human lymphohaematopoietic engraftment. Clin Exp Immunol 154, 270-284, doi:10.1111/j.1365-2249.2008.03753.x (2008).

302 Dhungel, P., Cantu, F. M., Molina, J. A. & Yang, Z. Vaccinia Virus as a Master of Host Shutoff Induction: Targeting Processes of the Central Dogma and Beyond. Pathogens 9, doi:10.3390/pathogens9050400 (2020).

303 Rice, A. P. & Roberts, B. E. Vaccinia virus induces cellular mRNA degradation. J Virol 47, 529-539, doi:10.1128/JVI.47.3.529-539.1983 (1983).

304 Bukowski, J. F., Woda, B. A., Habu, S., Okumura, K. & Welsh, R. M. Natural killer cell depletion enhances virus synthesis and virus-induced hepatitis in vivo. J Immunol 131, 1531-1538 (1983).

305 Natuk, R. J. & Welsh, R. M. Accumulation and chemotaxis of natural killer/large granular lymphocytes at sites of virus replication. J Immunol 138, 877-883 (1987).

306 Prlic, M., Gibbs, J. & Jameson, S. C. Characteristics of NK cell migration early after vaccinia infection. J Immunol 175, 2152-2157, doi:10.4049/jimmunol.175.4.2152 (2005).

307 Di Pilato, M. *et al.* NFκB activation by modified vaccinia virus as a novel strategy to enhance neutrophil migration and HIV-specific T-cell responses. Proceedings of the National Academy of Sciences 112, E1333 (2015).

308 Duffy, D. *et al.* Neutrophils transport antigen from the dermis to the bone marrow, initiating a source of memory CD8+ T cells. Immunity 37, 917-929, doi:10.1016/j.immuni.2012.07.015 (2012).

309 Chang, H. W., Watson, J. C. & Jacobs, B. L. The E3L gene of vaccinia virus encodes

an inhibitor of the interferon-induced, double-stranded RNA-dependent protein kinase. Proc Natl Acad Sci U S A 89, 4825-4829, doi:10.1073/pnas.89.11.4825 (1992).

310 Valentine, R. & Smith, G. L. Inhibition of the RNA polymerase III-mediated dsDNA-sensing pathway of innate immunity by vaccinia virus protein E3. J Gen Virol 91, 2221-2229, doi:10.1099/vir.0.021998-0 (2010).

311 Colamonici, O. R., Domanski, P., Sweitzer, S. M., Larner, A. & Buller, R. M. Vaccinia virus B18R gene encodes a type I interferon-binding protein that blocks interferon alpha transmembrane signaling. J Biol Chem 270, 15974-15978, doi:10.1074/jbc.270.27.15974 (1995).

312 Mehta, A. K., Gracias, D. T. & Croft, M. TNF activity and T cells. Cytokine 101, 14-18, doi:10.1016/j.cyto.2016.08.003 (2018).

313 Kim, E. Y. & Teh, H. S. TNF type 2 receptor (p75) lowers the threshold of T cell activation. J Immunol 167, 6812-6820, doi:10.4049/jimmunol.167.12.6812 (2001).

314 Yokota, S., Geppert, T. D. & Lipsky, P. E. Enhancement of antigen- and mitogen-induced human T lymphocyte proliferation by tumour necrosis factor-alpha. J Immunol 140, 531-536 (1988).

315 Kim, E. Y., Priatel, J. J., Teh, S. J. & Teh, H. S. TNF receptor type 2 (p75) functions as a costimulator for antigen-driven T cell responses in vivo. J Immunol 176, 1026-1035, doi:10.4049/jimmunol.176.2.1026 (2006).

316 Li, X., Yang, Y. & Ashwell, J. D. TNF-RII and c-IAP1 mediate ubiquitination and degradation of TRAF2. Nature 416, 345-347, doi:10.1038/416345a (2002).

317 Valencia, X. *et al.* TNF downmodulates the function of human CD4+CD25hi T-regulatory cells. Blood 108, 253-261, doi:10.1182/blood-2005-11-4567 (2006).

318 Zhang, Q. *et al.* TNF-alpha impairs differentiation and function of TGF-beta-induced Treg cells in autoimmune diseases through Akt and Smad3 signaling pathway. J Mol Cell Biol 5, 85-98, doi:10.1093/jmcb/mjs063 (2013).

319 Chen, X., Baumel, M., Mannel, D. N., Howard, O. M. & Oppenheim, J. J. Interaction of TNF with TNF receptor type 2 promotes expansion and function of mouse CD4+CD25+ T regulatory cells. J Immunol 179, 154-161, doi:10.4049/jimmunol.179.1.154 (2007).

320 Helleday, T., Petermann, E., Lundin, C., Hodgson, B. & Sharma, R. A. DNA repair

pathways as targets for cancer therapy. Nature Reviews Cancer 8, 193-204, doi:10.1038/nrc2342 (2008).

Appendix

Supplementary Table 1 | List of DEGs between P14 + VacVgp33 treated mice vs. P14 + VSVgp33 treated mice

Symbol	Gene name	Log_2FC	Adj. P Value
Tnfrsf11b	tumour necrosis factor receptor superfamily, member 11b (osteoprotegerin)	-1.34	0.001
S100a9	S100 calcium binding protein A9 (calgranulin B)	1.97	0.001
Apol10b	apolipoprotein L 10B	-1.26	0.001
Il1b	interleukin 1 beta	1.78	0.001
Ccl11	chemokine (C-C motif) ligand 11	-1.43	0.002
Chil1	chitinase-like 1	1.42	0.002
Ifitm1	interferon induced transmembrane protein 1	1.19	0.002
Crabp1	cellular retinoic acid binding protein I	1.11	0.002
Rab11fip1	RAB11 family interacting protein 1 (class I)	1.96	0.002
S100a8	S100 calcium binding protein A8 (calgranulin A)	1.96	0.002
Wfdc21	WAP four-disulfide core domain 21	1.63	0.002
Cacna1d	calcium channel, voltage-dependent, L type, alpha 1D subunit	1.15	0.002
Siglece	sialic acid binding Ig-like lectin E	1.41	0.002
Il1a	interleukin 1 alpha	2.02	0.002
Igsf6	immunoglobulin superfamily, member 6	1.90	0.002
Arg2	arginase type II	1.59	0.002
Atp6v0d2	ATPase, H+ transporting, lysosomal V0 subunit D2	-1.47	0.002
Sgk1	serum/glucocorticoid regulated kinase 1	1.05	0.002
Cmtm5	CKLF-like MARVEL transmembrane domain containing 5	-1.26	0.002
Cfp	complement factor properdin	1.26	0.002
Il23a	interleukin 23, alpha subunit p19	1.19	0.002
Cxcl2	chemokine (C-X-C motif) ligand 2	2.12	0.002
Ptgs2	prostaglandin-endoperoxide synthase 2	1.91	0.002
Mbp	myelin basic protein	-1.23	0.003
Cd38	CD38 antigen	1.84	0.003
Dnaic1	dynein, axonemal, intermediate chain 1	-1.16	0.003
Vamp5	vesicle-associated membrane protein 5	-1.26	0.003
Csf1r	colony stimulating factor 1 receptor	1.50	0.003
Mefv	Mediterranean fever	1.20	0.003
Aif1	allograft inflammatory factor 1	1.51	0.003
Casp12	caspase 12	-1.14	0.003
Nlrp3	NLR family, pyrin domain containing 3	1.77	0.003
Fpr1	formyl peptide receptor 1	2.90	0.003
Tlcd4	TLC domain containing 4	-1.10	0.003
C2	complement component 2 (within H-2S)	-1.20	0.003
Apol9a	apolipoprotein L 9a	-1.03	0.003
Rapgef4	Rap guanine nucleotide exchange factor (GEF) 4	-1.13	0.003
Fbxo36	F-box protein 36	-1.06	0.003
Gmfg	glia maturation factor, gamma	1.22	0.003
Apol9b	apolipoprotein L 9b	-1.02	0.003
Pla2g7	phospholipase A2, group VII (platelet-activating factor acetylhydrolase, plasma)	1.67	0.003

Symbol	Gene name	Log_2FC	Adj. P Value
Clec3b	C-type lectin domain family 3, member b	-1.47	0.003
Marco	macrophage receptor with collagenous structure	1.65	0.003
Trem1	triggering receptor expressed on myeloid cells 1	1.57	0.003
Chrdl1	chordin-like 1	-1.18	0.003
Ms4a4a	membrane-spanning 4-domains, subfamily A, member 4A	1.57	0.003
Ogn	osteoglycin	-1.08	0.003
Pilra	paired immunoglobin-like type 2 receptor alpha	1.44	0.003
Gstp2	glutathione S-transferase, pi 2	-1.07	0.003
Lyz1	lysozyme 1	1.04	0.003
Pilrb2	paired immunoglobin-like type 2 receptor beta 2	1.35	0.003
Nfkbia	nuclear factor of kappa light polypeptide gene enhancer in B cells inhibitor, alpha	1.27	0.003
Lrrtm2	leucine rich repeat transmembrane neuronal 2	-1.24	0.003
C5ar1	complement component 5a receptor 1	1.55	0.003
Blvrb	biliverdin reductase B (flavin reductase (NADPH))	1.05	0.003
G0s2	G0/G1 switch gene 2	1.18	0.004
Gm9733	predicted gene 9733	1.91	0.004
Mcemp1	mast cell expressed membrane protein 1	1.20	0.004
Cdh19	cadherin 19, type 2	-1.17	0.004
Mitf	melanogenesis associated transcription factor	-1.18	0.004
Ncf1	neutrophil cytosolic factor 1	1.28	0.004
Mrgpra2a	MAS-related GPR, member A2A	1.63	0.004
Aoah	acyloxyacyl hydrolase	1.24	0.004
Ly6i	lymphocyte antigen 6 complex, locus I	1.16	0.004
Ndst3	N-deacetylase/N-sulfotransferase (heparan glucosaminyl) 3	-1.21	0.004
Lyz2	lysozyme 2	1.26	0.004
Csf3r	colony stimulating factor 3 receptor (granulocyte)	1.18	0.004
Adgre1	adhesion G protein-coupled receptor E1	1.43	0.004
Hdc	histidine decarboxylase	1.26	0.004
Cyp2j6	cytochrome P450, family 2, subfamily j, polypeptide 6	-1.14	0.004
Cubn	cubilin (intrinsic factor-cobalamin receptor)	-1.02	0.004
Plbd1	phospholipase B domain containing 1	1.18	0.004
Ppp1r3b	protein phosphatase 1, regulatory subunit 3B	1.38	0.004
F13a1	coagulation factor XIII, A1 subunit	1.31	0.004
Pid1	phosphotyrosine interaction domain containing 1	1.65	0.004
Pla2g4c	phospholipase A2, group IVC (cytosolic, calcium-independent)	-1.07	0.004
Olfml1	olfactomedin-like 1	-1.44	0.004
Scn7a	sodium channel, voltage-gated, type VII, alpha	-1.21	0.004
Rassf4	Ras association (RalGDS/AF-6) domain family member 4	1.15	0.004
Tnfrsf1b	tumour necrosis factor receptor superfamily, member 1b	1.26	0.004
Clec4e	C-type lectin domain family 4, member e	1.62	0.004
Arg1	arginase, liver	1.83	0.004
Gstp1	glutathione S-transferase, pi 1	-1.00	0.004
Slc39a10	solute carrier family 39 (zinc transporter), member 10	-1.07	0.004

Symbol	Gene name	Log_2FC	Adj. P Value
Cacnb4	calcium channel, voltage-dependent, beta 4 subunit	-1.13	0.004
Lrguk	leucine-rich repeats and guanylate kinase domain containing	-1.04	0.004
Pi16	peptidase inhibitor 16	-1.38	0.005
Egln3	egl-9 family hypoxia-inducible factor 3	1.39	0.005
Dgat2	diacylglycerol O-acyltransferase 2	1.12	0.005
Retnla	resistin like alpha	-2.69	0.005
Dpt	dermatopontin	-1.01	0.005
Gnb4	guanine nucleotide binding protein (G protein), beta 4	-1.06	0.005
S100b	S100 protein, beta polypeptide, neural	-1.41	0.005
Enpp5	ectonucleotide pyrophosphatase/phosphodiesterase 5	-1.11	0.005
Akr1c14	aldo-keto reductase family 1, member C14	-1.23	0.005
Arl5c	ADP-ribosylation factor-like 5C	1.32	0.005
Akr1c18	aldo-keto reductase family 1, member C18	-1.70	0.005
Fkbp14	FK506 binding protein 14	-1.02	0.005
Grik2	glutamate receptor, ionotropic, kainate 2 (beta 2)	-1.42	0.005
Enc1	ectodermal-neural cortex 1	-1.02	0.005
Efcab7	EF-hand calcium binding domain 7	-1.07	0.005
Cmklr1	chemokine-like receptor 1	1.24	0.005
Traf1	TNF receptor-associated factor 1	1.47	0.005
Nkain1	Na+/K+ transporting ATPase interacting 1	-1.13	0.005
Gm5150	predicted gene 5150	1.51	0.005
Ikbke	inhibitor of kappaB kinase epsilon	1.15	0.005
Tyr	tyrosinase	-1.26	0.006
Cd14	CD14 antigen	1.33	0.006
Hpgd	hydroxyprostaglandin dehydrogenase 15 (NAD)	-1.32	0.006
Tlr1	toll-like receptor 1	1.28	0.006
Pfkfb3	6-phosphofructo-2-kinase/fructose-2,6-biphosphatase 3	1.18	0.006
Syk	spleen tyrosine kinase	1.00	0.006
Icam1	intercellular adhesion molecule 1	1.10	0.006
Lrg1	leucine-rich alpha-2-glycoprotein 1	1.35	0.006
Slc7a8	solute carrier family 7 (cationic amino acid transporter, y+ system), member 8	1.39	0.006
Spata13	spermatogenesis associated 13	1.08	0.006
Cd52	CD52 antigen	1.05	0.006
Itgam	integrin alpha M	1.08	0.006
Dkk3	dickkopf WNT signaling pathway inhibitor 3	-1.36	0.006
Calhm5	calcium homeostasis modulator family member 5	-1.00	0.006
Sfrp4	secreted frizzled-related protein 4	-1.39	0.007
Wfdc17	WAP four-disulfide core domain 17	1.42	0.007
Slc7a2	solute carrier family 7 (cationic amino acid transporter, y+ system), member 2	1.09	0.007
Gpr141	G protein-coupled receptor 141	1.73	0.007
Nfkbiz	nuclear factor of kappa light polypeptide gene enhancer in B cells inhibitor, zeta	1.50	0.007
Fgr	FGR proto-oncogene, Src family tyrosine kinase	1.17	0.007
Pianp	PILR alpha associated neural protein	-1.12	0.007

Symbol	Gene name	Log_2FC	Adj. P Value
Ncf4	neutrophil cytosolic factor 4	1.26	0.007
Ptprm	protein tyrosine phosphatase, receptor type, M	-1.09	0.007
Tarm1	T cell-interacting, activating receptor on myeloid cells 1	1.23	0.008
Cpa3	carboxypeptidase A3, mast cell	1.37	0.008
Eya1	EYA transcriptional coactivator and phosphatase 1	-1.05	0.008
Mxd1	MAX dimerization protein 1	1.02	0.008
Pik3cg	phosphatidylinositol-4,5-bisphosphate 3-kinase catalytic subunit gamma	1.17	0.008
Tex14	testis expressed gene 14	-1.08	0.008
Tinagl1	tubulointerstitial nephritis antigen-like 1	-1.06	0.008
Retnlg	resistin like gamma	1.53	0.008
Stfa2l1	stefin A2 like 1	1.63	0.008
E230029C05Rik	RIKEN cDNA E230029C05 gene	1.08	0.008
Mc1r	melanocortin 1 receptor	-1.37	0.008
Cd300e	CD300E molecule	1.49	0.008
Gsap	gamma-secretase activating protein	1.26	0.008
Il7	interleukin 7	-1.06	0.008
Tgfbi	transforming growth factor, beta induced	1.23	0.008
Irak3	interleukin-1 receptor-associated kinase 3	1.09	0.008
Cybb	cytochrome b-245, beta polypeptide	1.18	0.008
Sgms2	sphingomyelin synthase 2	1.46	0.008
Oca2	oculocutaneous albinism II	-1.41	0.008
Tnf	tumour necrosis factor	1.43	0.009
Aldh1a1	aldehyde dehydrogenase family 1, subfamily A1	-1.17	0.009
Rasgrp3	RAS, guanyl releasing protein 3	-1.11	0.009
Gjc3	gap junction protein, gamma 3	-1.43	0.009
Rab20	RAB20, member RAS oncogene family	1.01	0.009
Clec4a2	C-type lectin domain family 4, member a2	1.51	0.009
Car6	carbonic anhydrase 6	-1.04	0.009
Lrrc25	leucine rich repeat containing 25	1.30	0.009
Tagap	T cell activation Rho GTPase activating protein	1.12	0.009
Junb	jun B proto-oncogene	1.03	0.009
Cxcr2	chemokine (C-X-C motif) receptor 2	1.07	0.009
Mlph	melanophilin	-1.10	0.009
Dnajc22	DnaJ heat shock protein family (Hsp40) member C22	-1.35	0.009
Lst1	leukocyte specific transcript 1	1.06	0.009
Serpine1	serine (or cysteine) peptidase inhibitor, clade E, member 1	1.44	0.010
Chil3	chitinase-like 3	1.50	0.010
Apol6	apolipoprotein L 6	-1.22	0.010
Srxn1	sulfiredoxin 1 homolog (S. cerevisiae)	1.54	0.010
Dennd11	DENN domain containing 11	1.22	0.010
Glrb	glycine receptor, beta subunit	-1.06	0.010
Adam8	a disintegrin and metallopeptidase domain 8	1.12	0.010
Gm6377	predicted gene 6377	1.16	0.010

Symbol	Gene name	Log_2FC	Adj. P Value
Cited1	Cbp/p300-interacting transactivator with Glu/Asp-rich carboxy-terminal domain 1	-1.12	0.010
B3gnt5	UDP-GlcNAc:betaGal beta-1,3-N-acetylglucosaminyltransferase 5	1.21	0.010
Tnfaip3	tumour necrosis factor, alpha-induced protein 3	1.18	0.011
Il21r	interleukin 21 receptor	1.31	0.011
Pik3ap1	phosphoinositide-3-kinase adaptor protein 1	1.02	0.011
Gsta2	glutathione S-transferase, alpha 2 (Yc2)	-1.39	0.011
Ier5	immediate early response 5	1.09	0.011
Nos2	nitric oxide synthase 2, inducible	1.01	0.011
Clec4a1	C-type lectin domain family 4, member a1	1.18	0.012
Hck	hemopoietic cell kinase	1.17	0.012
Klra2	killer cell lectin-like receptor, subfamily A, member 2	1.25	0.012
Mlana	melan-A	-1.03	0.012
AB124611	cDNA sequence AB124611	1.14	0.012
Gpr65	G-protein coupled receptor 65	1.15	0.013
Htr7	5-hydroxytryptamine (serotonin) receptor 7	1.14	0.013
Enpp2	ectonucleotide pyrophosphatase/phosphodiesterase 2	-1.27	0.013
Ubl7	ubiquitin-like 7 (bone marrow stromal cell-derived)	-1.18	0.013
Adgre4	adhesion G protein-coupled receptor E4	1.04	0.014
Slc18b1	solute carrier family 18, subfamily B, member 1	-1.22	0.014
Ednrb	endothelin receptor type B	1.27	0.015
Nxpe5	neurexophilin and PC-esterase domain family, member 5	1.19	0.016
Acod1	aconitate decarboxylase 1	1.03	0.016
Ifitm6	interferon induced transmembrane protein 6	1.05	0.016
Fyb	FYN binding protein	1.02	0.017
Hcls1	hematopoietic cell specific Lyn substrate 1	1.01	0.017
Pira1	paired-Ig-like receptor A1	1.17	0.018
Tifab	TRAF-interacting protein with forkhead-associated domain, family member B	1.07	0.018
Chil4	chitinase-like 4	1.38	0.019
Msr1	macrophage scavenger receptor 1	1.07	0.019
Egr1	early growth response 1	1.08	0.020
Bace2	beta-site APP-cleaving enzyme 2	-1.19	0.020
Slc16a10	solute carrier family 16 (monocarboxylic acid transporters), member 10	1.18	0.020
Adap2	ArfGAP with dual PH domains 2	1.07	0.020
Clec4a3	C-type lectin domain family 4, member a3	1.00	0.021
Ets2	E26 avian leukemia oncogene 2, 3' domain	1.03	0.021
Mageb16	MAGE family member B16	-1.08	0.021
Tlr8	toll-like receptor 8	1.05	0.022
Nfkbid	nuclear factor of kappa light polypeptide gene enhancer in B cells inhibitor, delta	1.19	0.022
Lair1	leukocyte-associated Ig-like receptor 1	1.27	0.023
Clec12a	C-type lectin domain family 12, member a	1.08	0.023
B3galt1	UDP-Gal:betaGlcNAc beta 1,3-galactosyltransferase, polypeptide 1	-1.04	0.024
Btg2	BTG anti-proliferation factor 2	1.04	0.025
Hp	haptoglobin	1.20	0.026

Symbol	Gene name	Log_2FC	Adj. P Value
Mup1	major urinary protein 1	1.41	0.026
Ms4a7	membrane-spanning 4-domains, subfamily A, member 7	1.04	0.026
Stfa2	stefin A2	1.05	0.031
Cbr2	carbonyl reductase 2	1.06	0.032
Treml4	triggering receptor expressed on myeloid cells-like 4	1.04	0.035
Gpr84	G protein-coupled receptor 84	1.26	0.035
Spic	Spi-C transcription factor (Spi-1/PU.1 related)	1.29	0.037
Tspan10	tetraspanin 10	-1.11	0.040
Ptgds	prostaglandin D2 synthase (brain)	-1.08	0.040
A530064D06Rik	RIKEN cDNA A530064D06 gene	1.22	0.041

Supplementary Table 2 | List of DEGs between P14 + VacVgp33 treated mice vs. P14 treated mice

Symbol	Gene name	logFC	Adj. P Value
S100a9	S100 calcium binding protein A9 (calgranulin B)	4.943	0.000
S100a8	S100 calcium binding protein A8 (calgranulin A)	4.761	0.000
Il1f9	interleukin 1 family, member 9	4.575	0.000
Mrgpra2a	MAS-related GPR, member A2A	4.454	0.000
Cxcl2	chemokine (C-X-C motif) ligand 2	3.912	0.000
Stfa2l1	stefin A2 like 1	3.800	0.000
Fpr1	formyl peptide receptor 1	3.791	0.000
Lcn2	lipocalin 2	3.671	0.000
Slfn4	schlafen 4	3.570	0.000
Arg2	arginase type II	3.402	0.000
Retnlg	resistin like gamma	3.258	0.000
Il1a	interleukin 1 alpha	3.165	0.000
Cxcl5	chemokine (C-X-C motif) ligand 5	3.053	0.000
Cxcr2	chemokine (C-X-C motif) receptor 2	2.826	0.000
Serpinb2	serine (or cysteine) peptidase inhibitor, clade B, member 2	2.751	0.001
Chil1	chitinase-like 1	2.713	0.000
Stfa2	stefin A2	2.612	0.000
Trem1	triggering receptor expressed on myeloid cells 1	2.587	0.000
Cstdc4	cystatin domain containing 4	2.555	0.000
Saa3	serum amyloid A 3	2.547	0.000
Mmp8	matrix metallopeptidase 8	2.514	0.000
Siglece	sialic acid binding Ig-like lectin E	2.444	0.000
Cldn1	claudin 1	2.426	0.000
Il1b	interleukin 1 beta	2.399	0.000
Cd5l	CD5 antigen-like	2.391	0.003
Trim30c	tripartite motif-containing 30C	2.374	0.000
Nlrp3	NLR family, pyrin domain containing 3	2.329	0.000
Trim30b	tripartite motif-containing 30B	2.312	0.000
Cxcl13	chemokine (C-X-C motif) ligand 13	2.256	0.001
Hcar2	hydroxycarboxylic acid receptor 2	2.252	0.000
Ifit1bl2	interferon induced protein with tetratricopeptide repeats 1B like 2	2.247	0.000
Sgms2	sphingomyelin synthase 2	2.239	0.000
Tnfaip3	tumour necrosis factor, alpha-induced protein 3	2.216	0.000
Mmp9	matrix metallopeptidase 9	2.209	0.000
Mmp3	matrix metallopeptidase 3	2.200	0.000
Csta2	cystatin A family member 2	2.188	0.000
Cxcl1	chemokine (C-X-C motif) ligand 1	2.166	0.000
Nfkbiz	nuclear factor of kappa light polypeptide gene enhancer in B cells inhibitor, zeta	2.110	0.001
Irak3	interleukin-1 receptor-associated kinase 3	2.097	0.000
Ifit1bl1	interferon induced protein with tetratricpeptide repeats 1B like 1	2.094	0.001
Clec4e	C-type lectin domain family 4, member e	2.071	0.001

Symbol	Gene name	logFC	Adj. P Value
Selp	selectin, platelet	2.065	0.001
Acod1	aconitate decarboxylase 1	2.063	0.000
Nfkbia	nuclear factor of kappa light polypeptide gene enhancer in B cells inhibitor, alpha	2.059	0.000
Clec4d	C-type lectin domain family 4, member d	2.056	0.000
Gadd45b	growth arrest and DNA-damage-inducible 45 beta	2.049	0.000
Gm5150	predicted gene 5150	2.031	0.001
Tnf	tumour necrosis factor	1.986	0.001
Ccl4	chemokine (C-C motif) ligand 4	1.982	0.000
Samsn1	SAM domain, SH3 domain and nuclear localization signals, 1	1.964	0.002
Rnd1	Rho family GTPase 1	1.959	0.000
Spic	Spi-C transcription factor (Spi-1/PU.1 related)	1.954	0.003
Rrad	Ras-related associated with diabetes	1.950	0.001
Cd300e	CD300E molecule	1.939	0.001
Ccrl2	chemokine (C-C motif) receptor-like 2	1.918	0.000
Csf3r	colony stimulating factor 3 receptor (granulocyte)	1.908	0.000
Mxd1	MAX dimerization protein 1	1.878	0.000
Cxcl3	chemokine (C-X-C motif) ligand 3	1.876	0.002
Ccl3	chemokine (C-C motif) ligand 3	1.874	0.000
Lipg	lipase, endothelial	1.862	0.000
Ptges	prostaglandin E synthase	1.851	0.000
Ppp1r3b	protein phosphatase 1, regulatory subunit 3B	1.837	0.000
Ccl12	chemokine (C-C motif) ligand 12	1.827	0.002
Hdc	histidine decarboxylase	1.814	0.000
Ttc39c	tetratricopeptide repeat domain 39C	1.810	0.000
A530064D06Rik	RIKEN cDNA A530064D06 gene	1.804	0.004
Tagap	T cell activation Rho GTPase activating protein	1.795	0.000
Il1rl1	interleukin 1 receptor-like 1	1.777	0.001
Ms4a7	membrane-spanning 4-domains, subfamily A, member 7	1.775	0.001
Chil3	chitinase-like 3	1.768	0.002
Thbd	thrombomodulin	1.765	0.002
Hp	haptoglobin	1.762	0.002
Asprv1	aspartic peptidase, retroviral-like 1	1.751	0.000
Ednrb	endothelin receptor type B	1.750	0.002
Cd38	CD38 antigen	1.718	0.001
Cd24a	CD24a antigen	1.710	0.001
G0s2	G0/G1 switch gene 2	1.691	0.000
Il1r2	interleukin 1 receptor, type II	1.683	0.000
Ms4a4a	membrane-spanning 4-domains, subfamily A, member 4A	1.681	0.001
Chil4	chitinase-like 4	1.672	0.004
Ifitm6	interferon induced transmembrane protein 6	1.662	0.001
Rab11fip1	RAB11 family interacting protein 1 (class I)	1.653	0.001
Olr1	oxidized low density lipoprotein (lectin-like) receptor 1	1.648	0.002
Cd69	CD69 antigen	1.642	0.002

Symbol	Gene name	logFC	Adj. P Value
Mcemp1	mast cell expressed membrane protein 1	1.623	0.000
Wfdc21	WAP four-disulfide core domain 21	1.616	0.000
Cd14	CD14 antigen	1.596	0.001
Steap4	STEAP family member 4	1.593	0.000
Serpine1	serine (or cysteine) peptidase inhibitor, clade E, member 1	1.578	0.003
Slamf9	SLAM family member 9	1.555	0.001
Mefv	Mediterranean fever	1.549	0.000
Il1rn	interleukin 1 receptor antagonist	1.537	0.001
Egr1	early growth response 1	1.533	0.002
Cxcr1	chemokine (C-X-C motif) receptor 1	1.531	0.000
Tnfrsf1b	tumour necrosis factor receptor superfamily, member 1b	1.530	0.001
Thbs1	thrombospondin 1	1.521	0.002
Cd33	CD33 antigen	1.518	0.001
Slfn5	schlafen 5	1.517	0.001
Slc28a2	solute carrier family 28 (sodium-coupled nucleoside transporter), member 2	1.515	0.003
Tnfrsf23	tumour necrosis factor receptor superfamily, member 23	1.512	0.000
Dgat2	diacylglycerol O-acyltransferase 2	1.509	0.000
P2ry2	purinergic receptor P2Y, G-protein coupled 2	1.509	0.000
Ets2	E26 avian leukemia oncogene 2, 3' domain	1.508	0.002
Wfdc17	WAP four-disulfide core domain 17	1.506	0.002
Ier5	immediate early response 5	1.505	0.001
Tlr7	toll-like receptor 7	1.503	0.003
Sel1l3	sel-1 suppressor of lin-12-like 3 (C. elegans)	1.500	0.000
Ell2	elongation factor for RNA polymerase II 2	1.498	0.002
Prg4	proteoglycan 4 (megakaryocyte stimulating factor, articular superficial zone protein)	1.496	0.000
Pik3ap1	phosphoinositide-3-kinase adaptor protein 1	1.492	0.001
Smox	spermine oxidase	1.492	0.001
Ifi209	interferon activated gene 209	1.478	0.001
Ankrd1	ankyrin repeat domain 1 (cardiac muscle)	1.465	0.007
Fgf7	fibroblast growth factor 7	1.462	0.000
Zc3h12a	zinc finger CCCH type containing 12A	1.460	0.000
Clec4a3	C-type lectin domain family 4, member a3	1.459	0.002
Sell	selectin, lymphocyte	1.448	0.002
Gja1	gap junction protein, alpha 1	1.447	0.001
Il6	interleukin 6	1.441	0.003
Ifi27l2a	interferon, alpha-inducible protein 27 like 2A	1.441	0.000
Mustn1	musculoskeletal, embryonic nuclear protein 1	1.436	0.001
Dusp1	dual specificity phosphatase 1	1.431	0.002
Icam1	intercellular adhesion molecule 1	1.431	0.001
Gsap	gamma-secretase activating protein	1.430	0.002
Treml4	triggering receptor expressed on myeloid cells-like 4	1.429	0.005
Lox	lysyl oxidase	1.427	0.001
B430306N03Rik	RIKEN cDNA B430306N03 gene	1.425	0.001

Symbol	Gene name	logFC	Adj. P Value
Ccl7	chemokine (C-C motif) ligand 7	1.421	0.003
Adgre1	adhesion G protein-coupled receptor E1	1.413	0.002
Clec4a2	C-type lectin domain family 4, member a2	1.412	0.006
Traf1	TNF receptor-associated factor 1	1.399	0.003
Ifitm1	interferon induced transmembrane protein 1	1.396	0.000
Clec4a1	C-type lectin domain family 4, member a1	1.395	0.003
Htr2a	5-hydroxytryptamine (serotonin) receptor 2A	1.389	0.003
Csrnp1	cysteine-serine-rich nuclear protein 1	1.389	0.000
Oasl1	2'-5' oligoadenylate synthetase-like 1	1.385	0.002
Ptgs2	prostaglandin-endoperoxide synthase 2	1.385	0.003
Adgre4	adhesion G protein-coupled receptor E4	1.370	0.002
Ms4a6d	membrane-spanning 4-domains, subfamily A, member 6D	1.362	0.002
Pilrb1	paired immunoglobin-like type 2 receptor beta 1	1.359	0.000
Plek	pleckstrin	1.359	0.001
Car4	carbonic anhydrase 4	1.356	0.001
Ms4a4c	membrane-spanning 4-domains, subfamily A, member 4C	1.353	0.003
Clu	clusterin	1.353	0.001
Igsf6	immunoglobulin superfamily, member 6	1.352	0.003
Tlr1	toll-like receptor 1	1.351	0.002
Lrg1	leucine-rich alpha-2-glycoprotein 1	1.345	0.003
Pde4b	phosphodiesterase 4B, cAMP specific	1.337	0.001
Ifi213	interferon activated gene 213	1.335	0.002
Il1rap	interleukin 1 receptor accessory protein	1.334	0.000
Ncf4	neutrophil cytosolic factor 4	1.331	0.002
Btg2	BTG anti-proliferation factor 2	1.324	0.005
Sh2b2	SH2B adaptor protein 2	1.317	0.000
Slfn1	schlafen 1	1.317	0.002
Trim25	tripartite motif-containing 25	1.308	0.002
Vcan	versican	1.303	0.000
Adm	adrenomedullin	1.301	0.003
Il23a	interleukin 23, alpha subunit p19	1.299	0.000
Cd55b	CD55 molecule, decay accelerating factor for complement B	1.297	0.000
Vmn1r112	vomeronasal 1 receptor 112	1.286	0.020
Crabp1	cellular retinoic acid binding protein I	1.283	0.000
Rdh12	retinol dehydrogenase 12	1.279	0.005
Gm15319	predicted gene 15319	1.278	0.023
Gm6377	predicted gene 6377	1.272	0.003
Btbd35f22	BTB domain containing 35, family member 22	1.270	0.002
Abca1	ATP-binding cassette, sub-family A (ABC1), member 1	1.268	0.001
Ccr1	chemokine (C-C motif) receptor 1	1.264	0.005
Ncf1	neutrophil cytosolic factor 1	1.264	0.002
Fas	Fas (TNF receptor superfamily member 6)	1.264	0.001
Upp1	uridine phosphorylase 1	1.263	0.002

Symbol	Gene name	logFC	Adj. P Value
Dach1	dachshund family transcription factor 1	1.263	0.002
Nlrp12	NLR family, pyrin domain containing 12	1.263	0.003
Ifi214	interferon activated gene 214	1.257	0.005
P2ry13	purinergic receptor P2Y, G-protein coupled 13	1.255	0.002
Pilra	paired immunoglobin-like type 2 receptor alpha	1.255	0.002
Ggta1	glycoprotein galactosyltransferase alpha 1, 3	1.250	0.002
Ankrd2	ankyrin repeat domain 2 (stretch responsive muscle)	1.243	0.003
Lst1	leukocyte specific transcript 1	1.238	0.002
Ccl2	chemokine (C-C motif) ligand 2	1.237	0.002
Dmkn	dermokine	1.235	0.032
Btbd35f20	BTB domain containing 35, family member 20	1.232	0.040
Slfn2	schlafen 2	1.229	0.002
Rab20	RAB20, member RAS oncogene family	1.228	0.002
Slfn3	schlafen 3	1.227	0.004
Birc3	baculoviral IAP repeat-containing 3	1.227	0.001
Nfkbid	nuclear factor of kappa light polypeptide gene enhancer in B cells inhibitor, delta	1.227	0.011
Pf4	platelet factor 4	1.226	0.002
Egln3	egl-9 family hypoxia-inducible factor 3	1.221	0.004
Grem1	gremlin 1, DAN family BMP antagonist	1.221	0.005
Hsd11b1	hydroxysteroid 11-beta dehydrogenase 1	1.219	0.000
Chl1	cell adhesion molecule L1-like	1.218	0.003
Hilpda	hypoxia inducible lipid droplet associated	1.218	0.003
Tarm1	T cell-interacting, activating receptor on myeloid cells 1	1.215	0.003
Ms4a6c	membrane-spanning 4-domains, subfamily A, member 6C	1.215	0.007
Pilrb2	paired immunoglobin-like type 2 receptor beta 2	1.212	0.002
Psd4	pleckstrin and Sec7 domain containing 4	1.211	0.004
Slc7a11	solute carrier family 7 (cationic amino acid transporter, y+ system), member 11	1.208	0.004
Il13ra2	interleukin 13 receptor, alpha 2	1.208	0.001
Btbd35f12	BTB domain containing 35, family member 12	1.206	0.026
Btbd35f6	BTB domain containing 35, family member 6	1.203	0.017
Csf3	colony stimulating factor 3 (granulocyte)	1.200	0.002
Mmp27	matrix metallopeptidase 27	1.200	0.002
Slc16a10	solute carrier family 16 (monocarboxylic acid transporters), member 10	1.198	0.010
Eda2r	ectodysplasin A2 receptor	1.194	0.004
Ikbke	inhibitor of kappaB kinase epsilon	1.193	0.002
Cd55	CD55 molecule, decay accelerating factor for complement	1.192	0.001
Ifi208	interferon activated gene 208	1.190	0.004
Lrrc25	leucine rich repeat containing 25	1.189	0.007
Plk2	polo like kinase 2	1.178	0.007
Ciart	circadian associated repressor of transcription	1.177	0.002
Gpr141	G protein-coupled receptor 141	1.176	0.018
Gmfg	glia maturation factor, gamma	1.175	0.001
Ms4a6b	membrane-spanning 4-domains, subfamily A, member 6B	1.175	0.006

Symbol	Gene name	logFC	Adj. P Value
Tasl	TLR adaptor interacting with endolysosomal SLC15A4	1.171	0.007
Ifit1	interferon-induced protein with tetratricopeptide repeats 1	1.170	0.001
Tyrobp	TYRO protein tyrosine kinase binding protein	1.168	0.003
Tlr13	toll-like receptor 13	1.161	0.010
Il1r1	interleukin 1 receptor, type I	1.157	0.000
Ebi3	Epstein-Barr virus induced gene 3	1.154	0.003
Fam71f2	family with sequence similarity 71, member F2	1.153	0.012
Tlr9	toll-like receptor 9	1.152	0.010
Pgf	placental growth factor	1.149	0.002
Mmp10	matrix metallopeptidase 10	1.148	0.002
I830077J02Rik	RIKEN cDNA I830077J02 gene	1.142	0.010
Hck	hemopoietic cell kinase	1.137	0.007
Vmn1r119	vomeronasal 1 receptor 119	1.130	0.035
Btbd35f14	BTB domain containing 35, family member 14	1.127	0.035
Nrap	nebulin-related anchoring protein	1.127	0.001
Slc15a3	solute carrier family 15, member 3	1.125	0.002
Metrnl	meteorin, glial cell differentiation regulator-like	1.122	0.003
Tnc	tenascin C	1.122	0.001
Il1rl2	interleukin 1 receptor-like 2	1.121	0.003
Fcgr1	Fc receptor, IgG, high affinity I	1.119	0.004
Junb	jun B proto-oncogene	1.119	0.003
Hcls1	hematopoietic cell specific Lyn substrate 1	1.117	0.006
Trim30d	tripartite motif-containing 30D	1.116	0.002
Il18	interleukin 18	1.112	0.002
Ccl5	chemokine (C-C motif) ligand 5	1.110	0.002
Cd300ld	CD300 molecule like family member d	1.108	0.004
Aoah	acyloxyacyl hydrolase	1.107	0.003
Klra2	killer cell lectin-like receptor, subfamily A, member 2	1.105	0.011
Maff	v-maf musculoaponeurotic fibrosarcoma oncogene family, protein F (avian)	1.104	0.001
Tnfaip6	tumour necrosis factor alpha induced protein 6	1.100	0.012
Tlr6	toll-like receptor 6	1.091	0.005
Fbxl5	F-box and leucine-rich repeat protein 5	1.090	0.004
F5	coagulation factor V	1.081	0.001
C9orf72	C9orf72, member of C9orf72-SMCR8 complex	1.081	0.003
Cxcl11	chemokine (C-X-C motif) ligand 11	1.079	0.004
Spata13	spermatogenesis associated 13	1.079	0.003
Smim3	small integral membrane protein 3	1.078	0.009
Gm10471	predicted gene 10471	1.077	0.013
Serpinb1a	serine (or cysteine) peptidase inhibitor, clade B, member 1a	1.076	0.002
Ackr3	atypical chemokine receptor 3	1.075	0.001
B4galt6	UDP-Gal:betaGlcNAc beta 1,4-galactosyltransferase, polypeptide 6	1.074	0.003
Gpr84	G protein-coupled receptor 84	1.073	0.040
Tnfrsf26	tumour necrosis factor receptor superfamily, member 26	1.071	0.001

Symbol	Gene name	logFC	Adj. P Value
Tlr8	toll-like receptor 8	1.071	0.011
U90926	cDNA sequence U90926	1.070	0.001
Bcl2l11	BCL2-like 11 (apoptosis facilitator)	1.070	0.001
Slfn8	schlafen 8	1.069	0.001
C3ar1	complement component 3a receptor 1	1.068	0.010
Vav3	vav 3 oncogene	1.066	0.004
Il18rap	interleukin 18 receptor accessory protein	1.064	0.001
Rnf149	ring finger protein 149	1.062	0.001
Csrp3	cysteine and glycine-rich protein 3	1.057	0.005
Lyn	LYN proto-oncogene, Src family tyrosine kinase	1.057	0.005
Gm21671	predicted gene, 21671	1.055	0.011
Sema4d	sema domain, immunoglobulin domain (Ig), transmembrane domain (TM) and short cytoplasmic domain, (semaphorin) 4D	1.055	0.003
Ptafr	platelet-activating factor receptor	1.051	0.004
Ngf	nerve growth factor	1.051	0.009
Btbd35f5	BTB domain containing 35, family member 5	1.049	0.028
Adora2b	adenosine A2b receptor	1.048	0.005
C5ar1	complement component 5a receptor 1	1.047	0.008
Prkcb	protein kinase C, beta	1.046	0.001
Vmn1r127	vomeronasal 1 receptor 127	1.046	0.037
Syk	spleen tyrosine kinase	1.041	0.002
Ankrd23	ankyrin repeat domain 23	1.040	0.004
Nckap1l	NCK associated protein 1 like	1.034	0.003
Lcp2	lymphocyte cytosolic protein 2	1.032	0.010
Pfkfb3	6-phosphofructo-2-kinase/fructose-2,6-biphosphatase 3	1.029	0.005
Ddx60	DExD/H box helicase 60	1.029	0.000
Tlr2	toll-like receptor 2	1.026	0.004
Cd300lf	CD300 molecule like family member F	1.026	0.002
Lacc1	laccase domain containing 1	1.025	0.004
Treml2	triggering receptor expressed on myeloid cells-like 2	1.021	0.001
Vmn1r129	vomeronasal 1 receptor 129	1.019	0.014
Gm3500	predicted gene 3500	1.018	0.021
Vmn1r257	vomeronasal 1 receptor 257	1.017	0.027
Rbm47	RNA binding motif protein 47	1.016	0.022
Fgr	FGR proto-oncogene, Src family tyrosine kinase	1.016	0.006
Tfec	transcription factor EC	1.015	0.002
Lrrc2	leucine rich repeat containing 2	1.013	0.013
AI504432	expressed sequence AI504432	1.009	0.018
Gm8369	predicted gene 8369	1.007	0.004
Gpr65	G-protein coupled receptor 65	1.007	0.013
Dennd1l	DENN domain containing 1l	1.006	0.012
Sorl1	sortilin-related receptor, LDLR class A repeats-containing	1.006	0.002
Ifnz	interferon zeta	1.003	0.011
Rac2	Rac family small GTPase 2	1.002	0.002

Symbol	Gene name	logFC	Adj. P Value
Gm826	predicted gene 826	1.002	0.025
Slc43a3	solute carrier family 43, member 3	1.001	0.001
Stpg1	sperm tail PG rich repeat containing 1	-1.007	0.025
Cacnb4	calcium channel, voltage-dependent, beta 4 subunit	-1.007	0.003
Tinagl1	tubulointerstitial nephritis antigen-like 1	-1.007	0.005
Wdr46	WD repeat domain 46	-1.007	0.001
Ifi27	interferon, alpha-inducible protein 27	-1.007	0.035
Eogt	EGF domain-specific O-linked N-acetylglucosamine (GlcNAc) transferase	-1.009	0.003
Cdk1	cyclin-dependent kinase 1	-1.009	0.001
Efcab7	EF-hand calcium binding domain 7	-1.014	0.003
Cdk2	cyclin-dependent kinase 2	-1.016	0.002
Shmt2	serine hydroxymethyltransferase 2 (mitochondrial)	-1.019	0.001
Sytl2	synaptotagmin-like 2	-1.020	0.003
Epb41l4a	erythrocyte membrane protein band 4.1 like 4a	-1.023	0.008
S100a1	S100 calcium binding protein A1	-1.026	0.008
Dync2li1	dynein cytoplasmic 2 light intermediate chain 1	-1.027	0.003
Mlana	melan-A	-1.027	0.006
Ttc21b	tetratricopeptide repeat domain 21B	-1.027	0.001
Glrb	glycine receptor, beta subunit	-1.029	0.006
Tubb3	tubulin, beta 3 class III	-1.029	0.003
Ptprm	protein tyrosine phosphatase, receptor type, M	-1.029	0.004
Tesl1	testin LIM domain protein like 1	-1.034	0.006
G6pc3	glucose 6 phosphatase, catalytic, 3	-1.034	0.002
Gpm6a	glycoprotein m6a	-1.034	0.004
Scrn1	secernin 1	-1.039	0.005
Paqr6	progestin and adipoQ receptor family member VI	-1.040	0.001
Cadm1	cell adhesion molecule 1	-1.042	0.005
Rab38	RAB38, member RAS oncogene family	-1.044	0.004
Dennd5b	DENN/MADD domain containing 5B	-1.047	0.000
Elovl7	ELOVL family member 7, elongation of long chain fatty acids (yeast)	-1.047	0.006
Epb41l5	erythrocyte membrane protein band 4.1 like 5	-1.048	0.003
St3gal6	ST3 beta-galactoside alpha-2,3-sialyltransferase 6	-1.049	0.001
Ube2c	ubiquitin-conjugating enzyme E2C	-1.049	0.003
Lrguk	leucine-rich repeats and guanylate kinase domain containing	-1.050	0.002
Cenpv	centromere protein V	-1.050	0.010
Lpar5	lysophosphatidic acid receptor 5	-1.052	0.018
Slc44a3	solute carrier family 44, member 3	-1.053	0.004
Gjb2	gap junction protein, beta 2	-1.054	0.005
C2	complement component 2 (within H-2S)	-1.055	0.002
Tex2	testis expressed gene 2	-1.064	0.002
Chchd10	coiled-coil-helix-coiled-coil-helix domain containing 10	-1.064	0.001
Sox10	SRY (sex determining region Y)-box 10	-1.065	0.000
S100b	S100 protein, beta polypeptide, neural	-1.066	0.008

Symbol	Gene name	logFC	Adj. P Value
Mc1r	melanocortin 1 receptor	-1.069	0.011
Slc24a5	solute carrier family 24, member 5	-1.070	0.005
Prim1	DNA primase, p49 subunit	-1.070	0.002
Ano3	anoctamin 3	-1.072	0.003
Etl4	enhancer trap locus 4	-1.075	0.004
Chsy3	chondroitin sulfate synthase 3	-1.076	0.001
1700019D03Rik	RIKEN cDNA 1700019D03 gene	-1.078	0.005
Sox6	SRY (sex determining region Y)-box 6	-1.079	0.002
Tecr	trans-2,3-enoyl-CoA reductase	-1.079	0.002
Dip2c	disco interacting protein 2 homolog C	-1.081	0.002
Stox2	storkhead box 2	-1.082	0.001
Igsf11	immunoglobulin superfamily, member 11	-1.082	0.003
Fam53b	family with sequence similarity 53, member B	-1.083	0.002
Map7d2	MAP7 domain containing 2	-1.085	0.023
Slc7a1	solute carrier family 7 (cationic amino acid transporter, y+ system), member 1	-1.085	0.000
Syngr1	synaptogyrin 1	-1.087	0.003
Epha3	Eph receptor A3	-1.091	0.004
Sgip1	SH3-domain GRB2-like (endophilin) interacting protein 1	-1.092	0.003
Galm	galactose mutarotase	-1.094	0.001
Ciita	class II transactivator	-1.094	0.014
Fam174b	family with sequence similarity 174, member B	-1.103	0.003
Nckap5l	NCK-associated protein 5-like	-1.111	0.002
Tpmt	thiopurine methyltransferase	-1.112	0.007
Fanci	Fanconi anemia, complementation group I	-1.116	0.007
Mgll	monoglyceride lipase	-1.119	0.030
Ankfn1	ankyrin-repeat and fibronectin type III domain containing 1	-1.119	0.003
Syt9	synaptotagmin IX	-1.124	0.004
Sorbs3	sorbin and SH3 domain containing 3	-1.126	0.002
Gpr37	G protein-coupled receptor 37	-1.126	0.002
Slc24a4	solute carrier family 24 (sodium/potassium/calcium exchanger), member 4	-1.135	0.003
Cacna1a	calcium channel, voltage-dependent, P/Q type, alpha 1A subunit	-1.140	0.000
Car14	carbonic anhydrase 14	-1.141	0.004
Ica1	islet cell autoantigen 1	-1.144	0.002
Ldhb	lactate dehydrogenase B	-1.149	0.002
Cyp39a1	cytochrome P450, family 39, subfamily a, polypeptide 1	-1.154	0.004
Acot1	acyl-CoA thioesterase 1	-1.160	0.001
Insc	INSC spindle orientation adaptor protein	-1.168	0.003
Cyb5r2	cytochrome b5 reductase 2	-1.170	0.000
Pianp	PILR alpha associated neural protein	-1.175	0.002
Rasgrp3	RAS, guanyl releasing protein 3	-1.178	0.003
Slc7a5	solute carrier family 7 (cationic amino acid transporter, y+ system), member 5	-1.179	0.001
Apol6	apolipoprotein L 6	-1.185	0.005
H2-DMa	histocompatibility 2, class II, locus DMa	-1.188	0.004

Symbol	Gene name	logFC	Adj. P Value
Trpm1	transient receptor potential cation channel, subfamily M, member 1	-1.188	0.006
Cdca3	cell division cycle associated 3	-1.196	0.002
Tspan10	tetraspanin 10	-1.199	0.017
Ubl7	ubiquitin-like 7 (bone marrow stromal cell-derived)	-1.199	0.006
Rrm2	ribonucleotide reductase M2	-1.202	0.001
1110051M20Rik	RIKEN cDNA 1110051M20 gene	-1.217	0.018
Mras	muscle and microspikes RAS	-1.218	0.003
Kazn	kazrin, periplakin interacting protein	-1.226	0.001
Cdh19	cadherin 19, type 2	-1.228	0.001
Hsd17b7	hydroxysteroid (17-beta) dehydrogenase 7	-1.229	0.000
Mmp12	matrix metallopeptidase 12	-1.234	0.001
Dkk3	dickkopf WNT signaling pathway inhibitor 3	-1.237	0.004
Hcar1	hydrocarboxylic acid receptor 1	-1.241	0.016
Gjc3	gap junction protein, gamma 3	-1.247	0.008
Abhd6	abhydrolase domain containing 6	-1.253	0.002
Slc18b1	solute carrier family 18, subfamily B, member 1	-1.257	0.006
Gpr143	G protein-coupled receptor 143	-1.276	0.002
Tyr	tyrosinase	-1.276	0.002
Grik2	glutamate receptor, ionotropic, kainate 2 (beta 2)	-1.276	0.004
Gsta2	glutathione S-transferase, alpha 2 (Yc2)	-1.283	0.008
Gpr158	G protein-coupled receptor 158	-1.320	0.004
Cdk15	cyclin-dependent kinase 15	-1.333	0.001
Mlph	melanophilin	-1.334	0.002
Fndc3c1	fibronectin type III domain containing 3C1	-1.348	0.001
Rspo3	R-spondin 3	-1.354	0.005
Mgl2	macrophage galactose N-acetyl-galactosamine specific lectin 2	-1.389	0.002
Dnajc22	DnaJ heat shock protein family (Hsp40) member C22	-1.427	0.004
Atp6v0d2	ATPase, H+ transporting, lysosomal V0 subunit D2	-1.435	0.001
Smpd1	sphingomyelin phosphodiesterase 1, acid lysosomal	-1.437	0.004
Oca2	oculocutaneous albinism II	-1.478	0.003
Ankfn1	ankyrin-repeat and fibronectin type III domain containing 1	-1.480	0.002
Ptgds	prostaglandin D2 synthase (brain)	-1.516	0.005
Prph	peripherin	-1.616	0.001
Cited1	Cbp/p300-interacting transactivator with Glu/Asp-rich carboxy-terminal domain 1	-1.664	0.001
Bace2	beta-site APP-cleaving enzyme 2	-1.679	0.002
Lyve1	lymphatic vessel endothelial hyaluronan receptor 1	-1.937	0.001
Retnla	resistin like alpha	-2.905	0.002

Supplementary Table 3 | List of DEGs between P14 + VSVgp33 treated mice vs. P14 treated mice

Symbol	Gene name	logFC	Adj. P Value
Il1f9	interleukin 1 family, member 9	4.026	0.000
S100a9	S100 calcium binding protein A9 (calgranulin B)	2.975	0.000
Prg4	proteoglycan 4 (megakaryocyte stimulating factor, articular superficial zone protein)	1.753	0.000
Chac1	ChaC, cation transport regulator 1	-1.340	0.000
Cxcl5	chemokine (C-X-C motif) ligand 5	2.411	0.000
S100a8	S100 calcium binding protein A8 (calgranulin A)	2.798	0.000
Cyb5r2	cytochrome b5 reductase 2	-1.279	0.000
Mrgpra2a	MAS-related GPR, member A2A	2.823	0.000
Cd34	CD34 antigen	1.437	0.000
Trib3	tribbles pseudokinase 3	-1.211	0.000
Trim30c	tripartite motif-containing 30C	2.705	0.000
Steap4	STEAP family member 4	1.321	0.000
Cd55b	CD55 molecule, decay accelerating factor for complement B	1.626	0.000
Slfn4	schlafen 4	2.859	0.000
Cd55	CD55 molecule, decay accelerating factor for complement	1.620	0.000
Ccl22	chemokine (C-C motif) ligand 22	-1.511	0.000
Sel1l3	sel-1 suppressor of lin-12-like 3 (C. elegans)	1.470	0.000
Cstdc4	cystatin domain containing 4	2.216	0.000
Ifit3b	interferon-induced protein with tetratricopeptide repeats 3B	1.043	0.000
Ccl11	chemokine (C-C motif) ligand 11	1.570	0.000
Ms4a4d	membrane-spanning 4-domains, subfamily A, member 4D	1.219	0.000
Gfpt2	glutamine fructose-6-phosphate transaminase 2	1.641	0.000
Csta2	cystatin A family member 2	1.875	0.000
Trim30b	tripartite motif-containing 30B	1.699	0.000
Rnd1	Rho family GTPase 1	1.598	0.000
Slc1a4	solute carrier family 1 (glutamate/neutral amino acid transporter), member 4	-1.449	0.000
Herpud1	homocysteine-inducible, endoplasmic reticulum stress-inducible, ubiquitin-like domain member 1	-1.071	0.000
Ifi44	interferon-induced protein 44	1.096	0.000
Hcar2	hydroxycarboxylic acid receptor 2	1.761	0.001
Kcnab1	potassium voltage-gated channel, shaker-related subfamily, beta member 1	1.112	0.001
Lpar4	lysophosphatidic acid receptor 4	1.033	0.001
Il1rl1	interleukin 1 receptor-like 1	2.163	0.001
Mmp2	matrix metallopeptidase 2	1.225	0.001
Hsd11b1	hydroxysteroid 11-beta dehydrogenase 1	1.194	0.001
Arg2	arginase type II	1.816	0.001
Shmt2	serine hydroxymethyltransferase 2 (mitochondrial)	-1.268	0.001
Slc43a3	solute carrier family 43, member 3	1.181	0.001
Slc7a1	solute carrier family 7 (cationic amino acid transporter, y+ system), member 1	-1.060	0.001
Ackr3	atypical chemokine receptor 3	1.389	0.001
Dcn	decorin	1.169	0.001
Ccl5	chemokine (C-C motif) ligand 5	1.621	0.001

Symbol	Gene name	logFC	Adj. P Value
Cxcl13	chemokine (C-X-C motif) ligand 13	2.793	0.001
Il1rap	interleukin 1 receptor accessory protein	1.067	0.001
Mmp3	matrix metallopeptidase 3	1.709	0.001
Nrap	nebulin-related anchoring protein	1.262	0.001
Ddx60	DExD/H box helicase 60	1.031	0.001
Cxcr2	chemokine (C-X-C motif) receptor 2	1.751	0.001
Epha7	Eph receptor A7	-1.162	0.001
Csf1	colony stimulating factor 1 (macrophage)	1.043	0.001
Chil1	chitinase-like 1	1.288	0.001
Ifit1bl2	interferon induced protein with tetratricopeptide repeats 1B like 2	2.093	0.001
Spp1	secreted phosphoprotein 1	1.240	0.002
Fgf7	fibroblast growth factor 7	1.292	0.002
Hpgd	hydroxyprostaglandin dehydrogenase 15 (NAD)	1.820	0.002
Rsad2	radical S-adenosyl methionine domain containing 2	1.135	0.002
Mmp9	matrix metallopeptidase 9	1.578	0.002
Mmp8	matrix metallopeptidase 8	2.278	0.002
Cxcl1	chemokine (C-X-C motif) ligand 1	1.775	0.002
Mmp27	matrix metallopeptidase 27	1.418	0.003
Lcn2	lipocalin 2	2.884	0.003
Efemp1	epidermal growth factor-containing fibulin-like extracellular matrix protein 1	1.798	0.003
Pi16	peptidase inhibitor 16	1.667	0.003
Ifit1	interferon-induced protein with tetratricopeptide repeats 1	1.287	0.003
Mmp12	matrix metallopeptidase 12	-1.187	0.003
Cxcr1	chemokine (C-X-C motif) receptor 1	1.317	0.003
Ifit1bl1	interferon induced protein with tetratricpeptide repeats 1B like 1	2.315	0.003
Apod	apolipoprotein D	1.427	0.003
Csprs	component of Sp100-rs	1.209	0.003
Rab15	RAB15, member RAS oncogene family	1.380	0.003
Cldn1	claudin 1	2.149	0.003
Ccl2	chemokine (C-C motif) ligand 2	1.402	0.003
Oas2	2'-5' oligoadenylate synthetase 2	1.026	0.003
Cxcl11	chemokine (C-X-C motif) ligand 11	1.495	0.003
Slc39a10	solute carrier family 39 (zinc transporter), member 10	1.232	0.003
Stfa2l1	stefin A2 like 1	2.168	0.003
Adamts5	a disintegrin-like and metallopeptidase (reprolysin type) with thrombospondin type 1 motif, 5 (aggrecanase-2)	1.376	0.004
Lipg	lipase, endothelial	1.344	0.004
Gzma	granzyme A	1.431	0.004
Ly6i	lymphocyte antigen 6 complex, locus I	-1.238	0.004
Ogn	osteoglycin	1.094	0.004
Cmpk2	cytidine monophosphate (UMP-CMP) kinase 2, mitochondrial	1.129	0.004
Il1rl2	interleukin 1 receptor-like 2	1.369	0.005
Lbp	lipopolysaccharide binding protein	1.240	0.005
Tnfrsf23	tumour necrosis factor receptor superfamily, member 23	1.144	0.005

Symbol	Gene name	logFC	Adj. P Value
Ltbp1	latent transforming growth factor beta binding protein 1	1.038	0.005
Mx1	MX dynamin-like GTPase 1	1.045	0.005
U90926	cDNA sequence U90926	1.079	0.005
Sqle	squalene epoxidase	-1.144	0.005
Serpinb1a	serine (or cysteine) peptidase inhibitor, clade B, member 1a	1.078	0.006
Cxcl2	chemokine (C-X-C motif) ligand 2	1.789	0.006
Marco	macrophage receptor with collagenous structure	-1.553	0.006
Ifi207	interferon activated gene 207	1.033	0.006
Akr1c18	aldo-keto reductase family 1, member C18	1.812	0.007
Slfn8	schlafen 8	1.015	0.007
Lyve1	lymphatic vessel endothelial hyaluronan receptor 1	-1.577	0.007
Gadd45b	growth arrest and DNA-damage-inducible 45 beta	1.103	0.007
Saa3	serum amyloid A 3	1.644	0.007
Adgrg2	adhesion G protein-coupled receptor G2	1.036	0.008
Ch25h	cholesterol 25-hydroxylase	1.039	0.008
Slc24a4	solute carrier family 24 (sodium/potassium/calcium exchanger), member 4	-1.240	0.009
Pla1a	phospholipase A1 member A	1.039	0.009
Siglece	sialic acid binding Ig-like lectin E	1.039	0.009
Retnlg	resistin like gamma	1.724	0.009
Htr2a	5-hydroxytryptamine (serotonin) receptor 2A	1.541	0.010
Prph	peripherin	-1.270	0.010
Lgi2	leucine-rich repeat LGI family, member 2	1.158	0.010
Il1rn	interleukin 1 receptor antagonist	1.157	0.011
Tek	TEK receptor tyrosine kinase	1.366	0.011
Fgf2	fibroblast growth factor 2	1.011	0.012
Ccl7	chemokine (C-C motif) ligand 7	1.456	0.012
Mustn1	musculoskeletal, embryonic nuclear protein 1	1.225	0.012
Slamf9	SLAM family member 9	1.219	0.013
Rrad	Ras-related associated with diabetes	1.593	0.013
Ptges	prostaglandin E synthase	1.159	0.013
Ccl4	chemokine (C-C motif) ligand 4	1.045	0.014
Stfa2	stefin A2	1.559	0.014
Scn7a	sodium channel, voltage-gated, type VII, alpha	1.081	0.014
Trim30d	tripartite motif-containing 30D	1.063	0.015
Lvrn	laeverin	1.120	0.015
Scara5	scavenger receptor class A, member 5	1.075	0.015
H2-Ab1	histocompatibility 2, class II antigen A, beta 1	-1.167	0.015
Car2	carbonic anhydrase 2	1.081	0.016
Cd24a	CD24a antigen	1.157	0.018
Dhrs9	dehydrogenase/reductase (SDR family) member 9	1.155	0.019
Cxcl14	chemokine (C-X-C motif) ligand 14	-1.019	0.019
Tmem45a	transmembrane protein 45a	1.018	0.019
Ttc39c	tetratricopeptide repeat domain 39C	1.108	0.019

Symbol	Gene name	logFC	Adj. P Value
Clec4d	C-type lectin domain family 4, member d	1.300	0.020
Ccl3	chemokine (C-C motif) ligand 3	1.074	0.021
Arg1	arginase, liver	-1.511	0.021
Clu	clusterin	1.004	0.021
Ankrd2	ankyrin repeat domain 2 (stretch responsive muscle)	1.182	0.022
Ngf	nerve growth factor	1.227	0.023
Cdca3	cell division cycle associated 3	-1.022	0.023
Des	desmin	1.007	0.024
Mest	mesoderm specific transcript	-1.050	0.024
Serpinb2	serine (or cysteine) peptidase inhibitor, clade B, member 2	2.003	0.025
Eda2r	ectodysplasin A2 receptor	1.135	0.026
Mexis	macrophage expressed LXRa(NR1H3)-dependent amplifier of Abca1 transcription lncRNA	1.106	0.027
Myoz2	myozenin 2	1.261	0.027
Tmod4	tropomodulin 4	1.022	0.028
Irak3	interleukin-1 receptor-associated kinase 3	1.007	0.028
Slfn5	schlafen 5	1.003	0.029
Csrp3	cysteine and glycine-rich protein 3	1.026	0.030
Ifi213	interferon activated gene 213	1.040	0.030
Ifi209	interferon activated gene 209	1.053	0.030
Klhl41	kelch-like 41	1.130	0.035
Mgl2	macrophage galactose N-acetyl-galactosamine specific lectin 2	-1.076	0.037
Thbd	thrombomodulin	1.247	0.038
Lrrc2	leucine rich repeat containing 2	1.136	0.039
Ccrl2	chemokine (C-C motif) receptor-like 2	1.027	0.039
Il1a	interleukin 1 alpha	1.148	0.039
Tmem100	transmembrane protein 100	1.236	0.042
Ifi208	interferon activated gene 208	1.017	0.042
Trem1	triggering receptor expressed on myeloid cells 1	1.016	0.045
Acod1	aconitate decarboxylase 1	1.029	0.048
Ankrd1	ankyrin repeat domain 1 (cardiac muscle)	1.372	0.048
Tnfaip6	tumour necrosis factor alpha induced protein 6	1.174	0.048